ANALYSIS OF CORONAVIRUS NONSTRUCTURAL PROTEINS IN VIRUS-INDUCED MEMBRANE MODIFICATIONS

By

Dia Chenelle Beachboard

Dissertation

Submitted to the Faculty of the

Graduate School of Vanderbilt University

in partial fulfillment of the requirements

for the degree of

DOCTOR OF PHILOSOPHY

in

Microbiology and Immunology

May 2015

Nashville, Tennessee

Approved:

Earl Ruley, Ph.D.

Sebastian Joyce, Ph.D.

Anne Kenworthy, Ph.D.

Andrew Link, Ph.D.

Matthew Tyska, Ph.D.

Mark Denison, M.D.

To the individuals who inspired me to pursue this journey.

ACKNOWLEDGEMENTS

I have spent time thinking about my inspirations for pursuing a doctoral degree in science and there have been several people throughout my life who in some way contributed to this journey. First, as a child, my parent encouraged me to read nonfiction books and though my readings about primates, I discovered Jane Goodall and Dian Fossey. These two women inspired me to want to be a scientist. Next, I used to spend summers in Oak Ridge with my grandparents. When it was raining, they would drop my sisters and I off at the American Museum of Science and Energy. During the hours I spent at the science museum, I developed my passion for scientific knowledge. Much later, during undergraduate studies, there were several professors that helped me decide that I wanted to study microbes. Dr. Sandra Daniel introduced me to the world of microbiology. Dr. Tim Sparer taught me virology and inspired me to become a virologist. Dr. Pamela Small and Dr. Heather Williamson Jordan introduced me to research science. Dr. Small along with the members of her lab, Heather, Samantha Wirth, and Lydia Mosi all supported me and encouraged me to pursue graduate school. Finally, Mark Denison, my graduate mentor who has trained me to be a virologist. To all of these people, I am immensely grateful.

Denison Lab – I would like to thank all members of the Denison lab that overlapped with me – Clint, Xiaotao, Nicole, Megan, Brett, Erica, Michelle, Lindsay, Chris, Lance, and Wayne. You all made my graduate school experience fun and exciting. You all provided me with help and ideas for my project. I would also like to thank former members of the lab, Mark Gadlage and Jen Sparks who built the foundation for my dissertation project. I would also like to thanks the students who worked with me on various aspects my

projects: Nicole Diggins, Nelly Grigorian, Jordan Anderson-Daniels, and Javier Galdon-Armero.

More specifically, I would like to thank Mark, my mentor. I really appreciate that you took me in even though you had just gotten two new students in the lab. I really appreciate your enthusiasm for science. You are always there to celebrate with me when things were going well and encourage me when science is not working or not working the way I anticipated. You have taught me so much about science and communication.

Dermody and Williams Labs – Thank you Terry and John for your great advice and questions about my project. I would like to thank all members of the Dermody and Williams labs. You all provided great advice for my project, as well as reagents. Additionally, I appreciate your friendship over the years. I will miss our lunches together.

Committee Members – I would like to thank all the members of my committee, Earl Ruley, Sebastian Joyce, Anne Kenworthy, Andy Link, and Matt Tyska. You all provided me with great advice and suggestions throughout my training.

Department of Pathology, Microbiology and Immunology, Division of Pediatrics Infectious Disease and the Elizabeth Lamb Center – I would like to thank all members of these programs that have helped and encouraged me along the way. In particular, I would like to thank Chris Aiken. As the Director of Graduate Studies, you helped me though a rough time during graduate school when I was transitioning between labs. You also always ask me great questions and give me advice about my project. Part of Chapter

IV of this dissertation originated with you asking me during one of my Research In Progress seminars “Is it loss of glycosylation or just mutations within nsp4 that cause the aberrant DMVs?” I was not able to answer the question at the time, but I went back to lab and figured it out.

Additionally, I would like to thank the administrators; specifically, Jean Tidwell, Lorie Franklin, and Janet Shelton for helping me register for classes, file paper work for my committee meetings and exams and arranged my travel. I would also like to thank the Immunobiology of Blood and Vascular Systems training grant for financial support.

Cell Imaging Shared Resource – I would like to thank the CISR for all of their help with imaging and image analysis. In particular, I would like to thank Sean Schaffer for help with confocal microscopy and Mary Dawes with help on fluorescence, confocal, and electron microscopy. I would also like to specially thank Janice Williams who worked with me to get the beautiful electron microscopy images I present in this dissertation.

Friends and Family- Lastly, I would like to thank my friends and family who have supported me throughout graduate school. I would like to thank my parents, sisters, nieces, and nephews for your support. Thank you for not giving me too hard of a time missing functions because science needs me. I would like to specially say thank you to Rachel. You were very encouraging and supportive of me throughout graduate school. I appreciate that you always let me come visit you in Knoxville after my committee meetings to get away from science, clear my head, and relax.

TABLE OF CONTENTS

LIST OF TABLES

Table Page

LIST OF FIGURES

Figure Page

LIST OF ABBREVIATIONS

3CLpro, 3C-like protease (nsp5)

[^{35}S]-met/-cys, [^{35}S]-methionine/cysteine radiolabel

ACE2, Angiotensin-converting enzyme 2

ActD, actinomycin D

BHK, baby hamster kidney cells

BMM, bone marrow derived macrophages

CEACAM 1, Carcinoembryonic antigen-related cell adhesion molecule 1

CM, convoluted membranes

CPE, cytopathic effect

CoV, coronavirus

DBT, murine delayed brain tumor cells

DFCP1, Double FYVE-containing protein 1

DGM, double glycosylation mutant

DMV, double membrane vesicle

DPP4, dipeptidyl peptidase 4

E, envelope proteins

EDEM1, ER degradation enhancer mannosidase alpha-like 1

EM, electron microscopy

EndoH, endoglycosidase H

ER, endoplasmic reticulum

EOP, efficiency of plating

ERAD, ER associated degradation

ERGIC, ER-Golgi intermediate compartment

EU, 5-ethynyl uridine

FFL, firefly luciferase

FIP, feline infectious peritonitis

HCoV, human coronavirus

H p.e., hours post electroporation

H p.i. hours post infection

IBV, infectious bronchitis virus

IFN, interferon

IP, immunoprecipitation

M, membrane protein

MEF, mouse embryonic fibroblasts

MERS, Middle East respiratory syndrome

MHV, murine hepatitis virus

MHVR, MHV receptor

MG3, MHV GFP-nsp3 fusion virus

MOI, multiplicity of infection

N, nucleocapsid

Nsp, nonstructural protein

Nt, nucleotide

Nsp3C, C-terminal domain of nsp3

ORF, open reading frame

OS9, osteosarcoma amplified 9

P0, passage 0

PDH, pyruvate dehydrogenase

PEDV, porcine epidemic diarrhea virus

PLP, papain-like protease (nsp3)

pp, polyprotein

PRRSV, porcine reproductive and respiratory syndrome virus

RLU, relative light units

SARS, sever acute respiratory syndrome

S, spike

TGEV, transmissible gastroenteritis virus

TM, transmembrane

ts, temperature-sensitive

WT, wildtype

CHAPTER I: BACKGROUND AND LITERATURE REVIEW

Introduction

Positive-sense single stranded RNA ((+) ssRNA) viruses cause diseases of humans, animals, plants, and invertebrates. Some examples of (+) ssRNA viruses that cause significant human disease are Chikungunya virus, Hepatitis C virus, MERS-coronavirus, poliovirus, and West Nile virus. RNA viruses have the potential for rapid adaptation and change (Cleri et al., 2010; WHO, 2014a). Among the (+) ssRNA viruses, the coronaviruses (CoVs) in the order Nidovirales have unique capabilities for adaptation and have caused severe disease in humans and animals with economic importance. Currently, there are five circulating human coronaviruses that cause upper and lower respiratory tract infections, including the ongoing outbreak of the novel human virus, MERS-CoV (WHO, 2014a).

Coronaviruses share several common key features with other (+) ssRNA viruses. They replicate in the host cell cytoplasm, where their (+) ssRNA message-sense genomes are translated into one or more large polyproteins that are subsequently cleaved by viral and/or cellular proteases into intermediate and mature functional proteins. (+) ssRNA viruses replicate in association with virus modified host membranes (Miller and Krijnse-Locker, 2008). These viruses face multiple challenges when replicating in the cytoplasm since host and viral factors required for replication need to be recruited and maintained at the site of replication and the virus can be exposed to the host immune response. (+) ssRNA viruses replicate via dsRNA intermediates, which if exposed to pattern recognition receptors in the cytoplasm would result in cellular responses detrimental to

virus replication. One approach by which positive-sense RNA viruses circumvent these challenges is by replicating on or within modified cytoplasmic membranes. Characterized (+) ssRNA viruses induce two major forms of membrane modifications. The first type of modification is the invagination of cytosolic membranes, with replication occurring within the pocket that is connected to the cytoplasm via a pore. The second type of membrane modifications are closed membrane structures including single and double membrane vesicles and tubules using host cytosolic membranes (Miller and Krijnse-Locker, 2008).

The membrane source has been identified for several virus-induced membrane modifications. Rubella virus and semliki forest virus use late endosome/lysosome membranes (Kujala et al., 2001; Magliano et al., 1998); Flock house viruses utilize the outer mitochondrial membrane (Kopek et al., 2007); Hepatitis C virus, poliovirus, dengue virus, West Nile virus and severe acute respiratory syndrome coronavirus (SARS-CoV) use endoplasmic reticulum (ER) membranes (Belov et al., 2006; Gillespie et al., 2010; Knoops et al., 2008a; Romero-Brey et al., 2012; Schneider et al., 2014; Welsch et al., 2009); and Kunjin virus modifies Golgi complex membranes (Westaway et al., 1997). The membrane modifications form the sites of viral replication and are required for efficient viral replication and optimal virus yield. My work has focused on coronavirus-induced membrane modifications, and the role of the CoV nonstructural protein 4 (nsp4) in the formation and regulation of the coronavirus induced double membrane vesicles (DMVs). When I began this work, it was known that nsp4 is required for viral replication and that mutations within nsp4 alter virus replication, RNA synthesis and DMV morphology (Gadlage et al., 2009; Sparks et al., 2007). It also had been reported that

specific mutations in nsp4 resulted in a novel temperature sensitive (ts) phenotype associated with changes in protein and replication complex localization. However, the determinants of nsp4 functions in DMV formation and stability had not been carefully studied. This dissertation describes experiments that I have performed to demonstrate that: 1) the nsp4-N258T mutant virus is not temperature-sensitive and has normal cellular localization (Chapter II) contrary to reports in the literature; 2) amino acid residues E226 and E227 within nsp4 are important for nsp4 structure and/or function and viral replication (Chapter III); 3) mutations across nsp4 alter DMV morphology and DMV number. Loss of nsp4 glycosylation is associated with reduced viral fitness (Chapter IV); 4) nsp4 is glycosylated co-translationally and exists as previously unrecognized nsp4-5 and nsp4-5-6 precursors (Chapter V); and 5) residues within the transmembrane domain of nsp3 are important for viral replication (Chapter VI). Finally, I have shown the localization of the MERS-CoV replication complex proteins to perinuclear cytoplasmic foci similar to that of SARS-CoV and MHV (Chapter VII).

Coronavirus Disease

Coronaviruses infect a broad range of hosts, from birds, to whales, to humans (ICTV, 2013; Masters, 2006). There are coronaviruses that affect the farming industry by causing disease in cows (Bovine CoV), pigs (porcine epidemic diarrhea virus, PEDV; transmissible gastroenteritis virus, TGEV) and chickens (infectious bronchitis virus, IBV). Currently there is an outbreak of PEDV in pigs in the U.S. that has high mortality rates of 80-100% in piglets (Mole, 2013). Feline CoV causes mild disease in cats; however, a spontaneous mutation in feline CoV leads to feline infectious peritonitis (FIP), which results in high mortality (Borschensky and Reinacher, 2014; Vennema et al.,

1998). In humans, there are six known human coronaviruses that cause upper and lower respiratory infections: severe acute respiratory syndrome coronavirus (SARS-CoV), HCoV-HKU1, HCoV-OC43, HCoV-229E, HCoV-NL63, and Middle East respiratory syndrome coronavirus (MERS-CoV). Recently, both SARS-CoV and MERS-CoV emerged as zoonotic infections that cause significant disease.

In 2002, SARS-CoV emerged in the Guangdong province in China, causing acute respiratory distress syndrome. It rapidly spread to 29 countries, infected approximately 8,000 individuals, and resulted in about 10% mortality (Cleri et al., 2010). Recently, a SARS-CoV like virus was isolated from a Chinese horseshoe bat that shared 99.9% sequence identity with SARS-CoV and uses the same receptor as SARS-CoV (Ge et al., 2014). This demonstrates that SARS-like viruses are circulating in bats and have the potential to cross into the human population and cause disease.

In 2012, MERS-CoV emerged in the Middle East and has spread to 21 countries with the majority of cases in Saudi Arabia (WHO, 2014b). The virus is still circulating in the Middle East and in December of 2014 there were 941 cases including 347 deaths (WHO, 2014a). This virus is thought to be endemic in camels since at least 1992 (Alagaili et al., 2014) and is likely transmitted between humans and camels. It is currently not clear how this is occurring but very high percentages of camels are seropositive for MERS-CoV antibodies (Alagaili et al., 2014). In one case, virus was isolated from a man who died of MERS and his camel who suffered from rhinorrhea. The viruses isolated from the man and camel were identical (Azhar et al., 2014). This strongly suggests that the virus is transmitted between camels and humans; however, there are cases that have no clear connection to camels suggesting that the virus has multiple

sources for transmission into humans. There is also human-to-human spread with a high rate of nosocomial infections. Currently, there are no vaccines or effective antivirals against these viruses. The SARS-CoV and MERS-CoV outbreaks highlight the potential of coronaviruses to emerge and cause disease in humans. They also highlight the need to understand coronavirus replication so better targets for therapeutics can be developed.

Murine hepatitis virus (MHV) is a natural pathogen in mice and also used extensively in laboratories as a BSL-2 model of coronavirus infection. Different strains of MHV cause different disease pathogenesis and infect the brain, liver, and lung (Weiss and Leibowitz, 2011). The MHV reverse genetics system developed and used in our laboratory is the MHV-A59 strain and will subsequently be called WT MHV (Yount et al., 2002). Neurovirulent strains of MHV cause encephalomyelitits with extensive demyelination and hepatovirulent stains cause hepatitis. MHV-A59 causes mild disease that is both neurovirulent and hepatovirulent (Weiss and Leibowitz, 2011).

Coronavirus Genome Organization

The coronavirus genome is a positive-strand RNA molecule of 26 to 32 kb that contains a 5' cap and 3' poly-A tail (Masters, 2006). CoVs encode from 7-15 genes, open reading frame (ORF) 1a/1ab encodes the 16 replicase nonstructural proteins (nsps 1-16). Downstream ORFs encode structural and accessory proteins (MHV shown in Figure I.1) involved in virus structure, entry, virulence, and immune evasion. The structural proteins include, spike (S), envelope (E), membrane (M), and nucleocapsid (N) (Figure I.2). ORF1a and ORF1b are connected by a minus one ribosomal frameshift allowing for translation of the fusion polyprotein. The nsps are cleaved by 2-3 viral proteases, PLP1/2 within nsp3 or 3CLpro nsp5 (Masters, 2006).

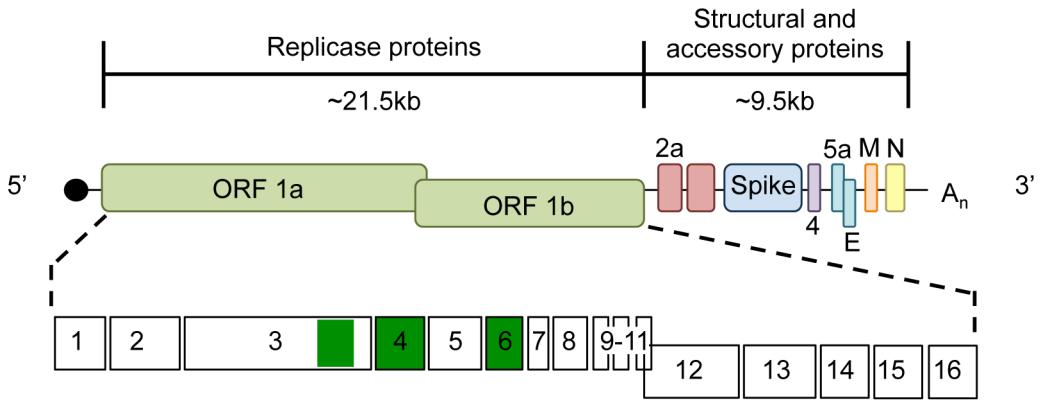

Figure I.1: MHV genome organization.

Schematic of the coronavirus genome with the 5' cap and 3' poly A tail. ORF 1a/b encodes the nonstructural proteins (nsp1-16) that function in viral replication. The downstream ORFs (ORF 2-7) encode the structural and accessory proteins. The nsps with transmembrane domains are highlighted in green.

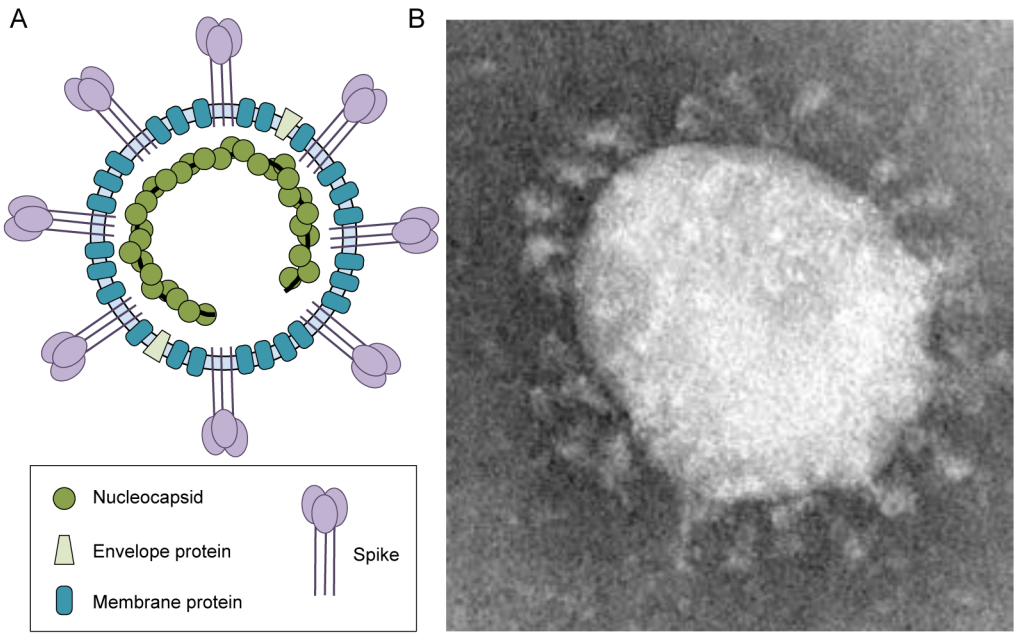

Figure I.2: Virion structure.

(A) Schematic of a coronavirus virion. The virion contains spike, membrane, and envelope proteins on the surface, with RNA encapsidated by nucleocapsid on the interior. **(B)** EM of a coronavirus showing spike proteins projecting from the surface (CDC, Public Health Image Library).

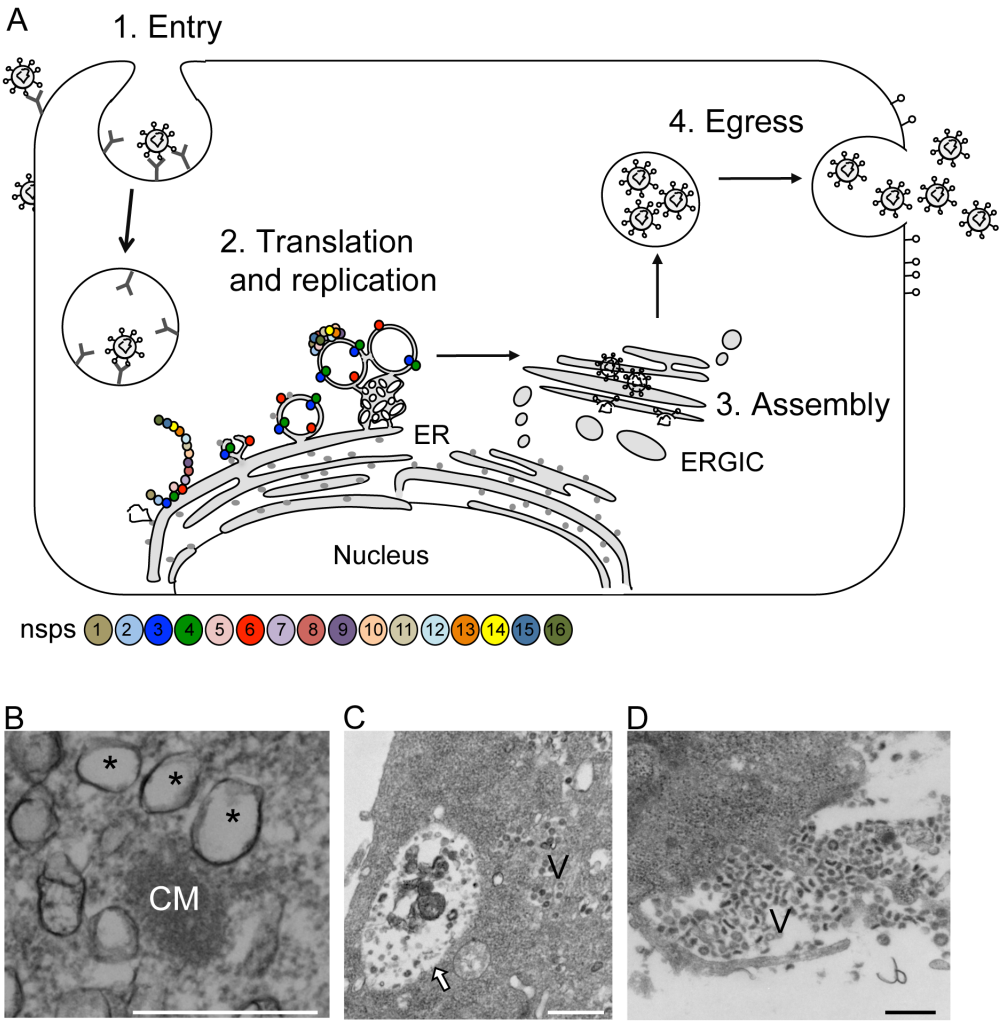

Figure I.3: Coronavirus lifecycle.

(**A**) The virus attaches to the viral receptor and enters the cell by either receptor mediated endocytosis or direct fusion to the plasma membrane (1). The genome is directly translated into a large polyprotein containing the replicase proteins, the polyprotein is cleaved to form mature proteins, replication complexes form and replication begins (2). The genome and structural proteins are assembled into virions at the ER-GIC (3) and are released in a non-lytic fashion via the secretory pathway (4). (**B**) EM of DMVs (*) and convoluted membranes (CM). (**C**) EM showing the assembled virions (V) in the cytoplasm and within a virion containing vesicle (arrow). (**D**) EM showing virions being released from the cell. (B-D) Scale bars are 500 nm. Beachboard, unpublished.

Coronavirus lifecycle

The coronavirus lifecycle begins with the attachment of spike protein to the host cell receptor and spike-mediated viral fusion with the host membrane. The receptors for several coronaviruses have been identified: SARS-CoV uses angiotensin-converting enzyme 2 (ACE2) (Li et al., 2003); MHV uses carcinoembryonic antigen-related cell adhesion molecule 1 (CEACAM1) (Hemmila et al., 2004); and MERS-CoV uses dipeptidyl peptidase-4 (DPP4) (Raj et al., 2013). The virus enters the cell via either receptor-mediated endocytosis or through direct fusion with the plasma membrane (Hansen et al., 1998; Hofmann et al., 2004; Nomura et al., 2004; Simmons et al., 2004; Sturman et al., 1990; Weismiller et al., 1990; Yang et al., 2004).

The details of viral replication once the genome is released into the cytoplasm have not been clarified. However, I have generated a model for CoV-induced membrane modifications based on what is known and predicted to occur. The model starts with the genome binding to the ribosome and ORF1 is translated into polyprotein (pp)1a and pp1ab (Figure I.3A). Work presented in Chapter V will demonstrate that the polyprotein is inserted into the membrane co-translationally. Then pp1ab is processed into 16 nonstructural proteins (nsps1-16) (functions listed in Table I.1) by up to three virally encoded proteases, papain-like protease 1/2 (PLP1/2, nsp3) and 3C-like protease (3CLpro, nsp5) (Baker et al., 1993; Y. Lu et al., 1995). Next, double membrane vesicles are induced at the ER membranes by nsp3, nsp4, and nsp6 (Angelini et al., 2013). The mechanism of DMV formation and the host proteins and processes required for their formation remain unknown. Next, replication complexes form at membrane modifications and viral replication begins with localization of viral nsps to both DMVs

and CM (Bost et al., 2000; Brockway et al., 2003; Gosert et al., 2002; Knoops et al., 2008b; Snijder et al., 2006; Sparks et al., 2007; van der Meer et al., 1999). A replication complex is formed to generate genomic and subgenomic RNAs. The complex is likely composed of the polymerase (nsp12), the helicase (nsp13), the primase (nsp8), ssRNA binding proteins (nsp7 and nsp9), the 3'-5'exoribonuclease (nsp14) and nsp10 which enhances the activity of nsp14 (Bonilla et al., 1994; Brayton et al., 1982; Brockway et al., 2003; Deming et al., 2007; Dennis and Brian, 1982; Gorbalenya et al., 1989; Imbert et al., 2006; Lee et al., 1991; Smith and Denison, 2013). In order to evade immune detection, CoVs use nsp14 and nsp16 to cap the viral transcripts (Y. Chen et al., 2009; Decroly et al., 2008). During genomic replication, minus sense RNA is synthesized, resulting in dsRNA intermediates. Electron tomography has demonstrated that dsRNA is localized to the interior of DMVs (Knoops et al., 2008a). Since the interior of the DMV is a closed structure, it has been proposed that it acts as a depot for dsRNA but is not the site of viral replication. The structural and accessory genes are generated through subgenomic RNA synthesis using transcription-regulating sequences (Perlman and Netland, 2009). The structural proteins and genomic RNA are transported to the ER-GIC where virion assembly occurs and the lipid envelope is acquired. For MHV, virions are packaged into large vesicles at the Golgi complex and secreted from the cell in a non-lytic fashion (Figure I.3C) (Klumperman et al., 1994). For some CoVs, the fusogenic spike protein is transported to the plasma membrane during viral egress and induces the fusion of infected cells with neighboring cell, forming multinucleated giant cells (syncytia). This syncytia formation is a hallmark of MHV infection in tissue culture.

Table I.1:Function of CoV nonstructural proteins.

1	Promotes host mRNA degradation; host cell translation shutoff	(Kamitani et al., 2006; Tanaka et al., 2012)
2	Unknown	
3	Protease, DMV formation, deubiquitination, ADP-1’’-phosphatase	(Angelini et al., 2013; Barretto et al., 2005; Ratia et al., 2006; Saikatendu et al., 2005)
4	DMV formation	(Angelini et al., 2013; Gadlage et al., 2009)
5	Cysteine protease	(Y. Lu et al., 1995)
6	DMV formation	(Angelini et al., 2013)
7	Involved in RNA synthesis	(Deming et al., 2007)
8	Primase, Involved in RNA synthesis	(Deming et al., 2007; Imbert et al., 2006)
9	Involved in RNA synthesis	(Deming et al., 2007)
10	Involved in RNA synthesis	(Deming et al., 2007)
11	Unknown	
12	RNA dependent RNA polymerase	(Bonilla et al., 1994; Brayton et al., 1982; Brockway et al., 2003; Dennis and Brian, 1982; Gorbalenya et al., 1989; Lee et al., 1991)
13	Helicase	(Ivanov et al., 2004b; Ivanov and Ziebuhr, 2004; Seybert et al., 2000)
14	Exonuclease, N7 Methyltransferase	(Y. Chen et al., 2009; Eckerle et al., 2007)
15	Endonuclease	(Ivanov et al., 2004a)
16	2’-O-ribose methyltransferase	(Decroly et al., 2008)

Coronaviruses induce ER membrane modifications to form DMVs and CM

Over the course of my graduate career, much has been learned about CoV-induced membrane modifications. Initially, it was known that CoV induce the formation of DMVs and convoluted membranes (Gosert et al., 2002; Knoops et al., 2008b). It was also known that the nonstructural proteins tested colocalize by immunofluorescence at perinuclear foci that were thought to be the membrane modifications (Bost et al., 2000; Brockway et al., 2003; Gosert et al., 2002; Knoops et al., 2008b; Snijder et al., 2006;

Ulasli et al., 2010; van der Meer et al., 1999). Several studies tried to determine the membrane source of DMVs. Our lab used a fractionation approach to demonstrate that MHV nsp1, nsp13, N and viral RNA fractionate with NADPH cytochrome C reductase activity, a marker of ER membranes (Sims et al., 2000). The late endosome was implicated as the membrane source of DMVs because nsp8 and nsp12 co-localized with lysosomal-associated membrane protein 2 (LAMP2) (van der Meer et al., 1999). Two studies tested the requirement for the early secretory system and found that viral replication is dependent on Golgi-specific brefeldin A-resistance guanine nucleotide exchange factor 1 (GBF1)-mediated ADP-ribosylation factor 1 (Arf1) activation (Verheije et al., 2008) and nsp3 co-localizes with the ER marker protein disulfide isomerase (PDI), and an ER translocon, sec61α (Knoops et al., 2009).

The 3D structure of SARS-CoV DMVs has been determined by electron tomography. In the study, Knoops *et al.* identified a reticulovesicular network that is composed of DMVs, convoluted membranes and ER The DMVs are contiguous with the CM and ER though their outer membrane (Figure I.3 and Figure I.4) (Knoops et al., 2008b).. Additionally, they determined the subcellular localization of several nsps and dsRNA by immunoEM. Nsp3, nsp5 and nsp8 localized to CM and nsp8 and dsRNA localize to DMVs. The dsRNA specifically localized to the interior of the DMVs. Additional studies have identified that nsp2, nsp3, nsp4, nsp5, and nsp8 localize to both the DMVs and CM, but nsp13 localizes to DMVs only (Snijder et al., 2006; Ulasli et al., 2010). Based on these data, Knoops *et al.* hypothesized that the DMVs are the site of viral replication and CM are the site of polyprotein processing, allowing for spatial separation of the two processes. However, the spatial separation would only occur at later

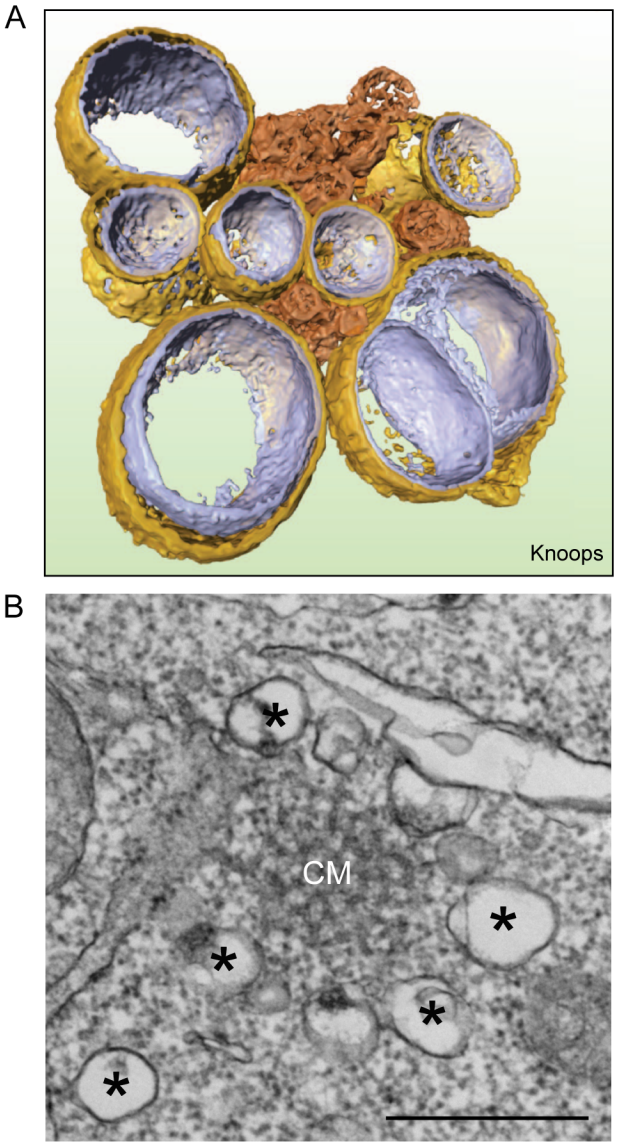

Figure I.4: Coronavirus-induced membrane modifications.
(**A**) 3D reconstruction of convoluted membranes and double membrane vesicles generated by electron tomography (Knoops *et al.*, 2008). DMV outer membrane is gold, DMV inner membrane is purple and convoluted membranes are copper. (**B**) EM of convoluted membranes (CM) surrounded by DMVs (*). Scale is 500 nm.

time points post infection since DMVs form before CM, and polyprotein processing occurs very early during infection (Ulasli et al., 2010). Next, to determine the temporal formation of membrane modifications, Ulasli et al. performed an EM time course of MHV-infected cells. This study identified several additional membrane modifications including tubules that contain E protein, cubic membrane structures that contain S protein, and large virion containing vesicles (Ulasli et al., 2010). This, in combination with the recent report from the Denison lab that demonstrates that CoVs induce plasma membrane modifications via macropinocytosis (Freeman et al., 2014b), highlight the extent to which CoVs modify host membranes. The EM time course determined that DMVs are present as early as 2 h p.i. Convoluted membranes form after DMVs and can be visualized as early as 3 h p.i. Virions can be seen at 5 h p.i. and are visualized in large vesicles at 6 h p.i. Tubules were visualized at 6 h p.i. and cubic membrane structures were visualized at 9 h p.i. The EM time course was performed at an MOI of 100 PFU/cell (Ulasli et al., 2010); therefore, the rare membrane modifications were more readily visualized than at a lower MOI of 5 PFU/cell that I used for my experiments in chapter IV. During my EM experiments, I was not able to visualize tubules or cubic membrane structures (Chapter IV).

Recently, Megan Culler Freeman, a former graduate student in the Denison lab, demonstrated that CoVs induce plasma membrane modification by inducing macropinocytosis. Macropinocytosis begins between 4 and 6 h p.i. and continues throughout infection. Macropinocytosis is initiated by spike protein directly or indirectly signaling through EGFR at the cell surface (Freeman et al., 2014b). During this process, large membrane protrusions occur at the plasma membrane that sample the extracellular

milieu by internalizing these contents inside large vesicles. I have visualized large cytoplasmic vesicle that are consistent in size with macropinosomes by EM.

Host cell processes implicated in CoV-induced membrane modifications

Since DMVs look very similar to autophagosomes morphologically, Erik Prentice, a former graduate student in the Denison lab, tested the requirement of autophagy for MHV replication (pathway depicted in Figure I.5). In DBT cells, nsp8 and nucleocapsid but not membrane protein colocalize with light chain 3 (LC3). MHV-infected cells have increased protein degradation during a long-lived protein degradation assay that could not be inhibited by the addition of the autophagy inhibitor 3-methyladenine. Next, APG5$^{-/-}$ cells were tested for viral infection and DMV formation. APG5$^{-/-}$ cells infected with MHV exhibited an approximately 1000 to 5000-fold reduction in viral yield and lacked DMVs. The APG5$^{-/-}$ cells displayed large vesicles surrounded by swollen ER membranes and structures with loosely approximated second membranes that are similar to early autophagosomes (Prentice, 2003). Subsequently, it was determined that MHV replicates indistinguishably in WT bone marrow derived macrophages (BMM) and ATG5$^{-/-}$ BMMs (Zhao et al., 2007). This suggests that the requirement for components of the autophagy pathway for MHV membrane modification may be cell type-dependent.

Infectious bronchitis virus (IBV) nsp6 has been shown to induce autophagy through an omegasome intermediate at the ER membrane (Cottam et al., 2011). In the study, when vero cells were transiently transfected with IBV nsp6, LC3 relocalized to punctate cytoplasmic foci, which was prevented when Atg5 was depleted. Double FYVE-

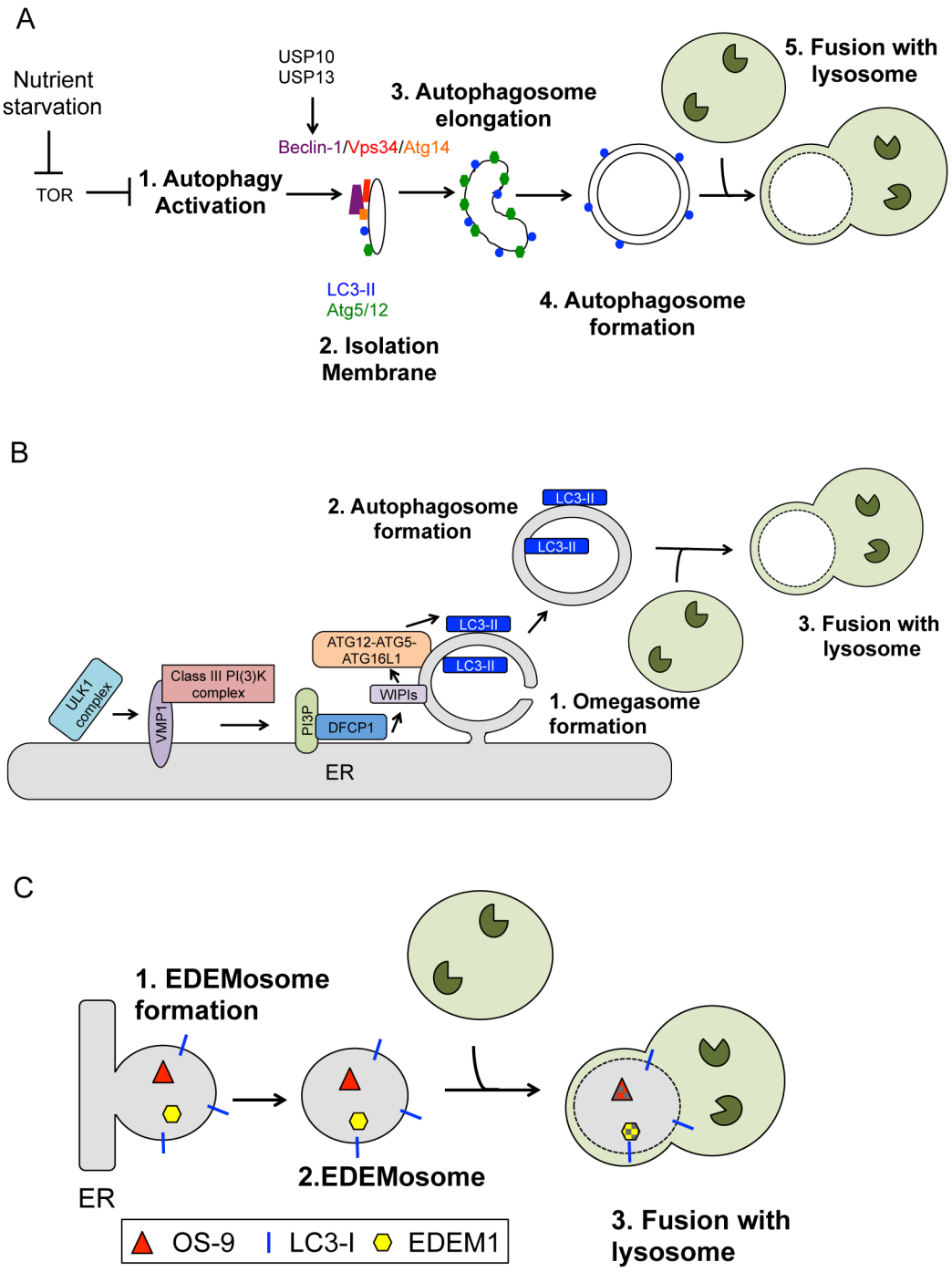

Figure I.5: Pathways implicated in DMV formation.
(**A**) Schematic of autophagosome formation. (**B**) Schematic of autophagosome formation through an omegasome intermediate. (**C**) Schematic of EDEMosome formation.

containing protein 1 (DFCP1), a marker for omegasomes (pathway depicted in Figure I.5), expression increased and localized to punctate foci. This demonstrated that nsp6-induced autophagosomes form through an omegasome intermediate. IBV-nsp6 does not get incorporated into the autophagosome, which later matures and fuses with the lysosome. Lastly, MHV, SARS-CoV, and porcine reproductive and respiratory syndrome virus (PRRSV)- nsp6 induced the relocalization LC3 into punctate foci (Cottam et al., 2011). This data suggests that CoV nsp6 induces autophagosome formation.

Recently, Reggiori *et al.* tested the requirements for autophagy. In the study, they determined that Atg7 is not required for MHV replication or replication complex formation in mouse embryonic fibroblasts (MEFs) (Reggiori et al., 2010). Atg7 is an E1-like ubiquitin ligase, required during the phagophore elongation step, which contributes to the conversion of LC3-I into LC3-II. $Atg7^{-/-}$ MEF cells still produced DMV. However, the DMVs do not appear to be closed and are shaped similar to a major sector (pacman). Next, they demonstrated that LC3-I, but not LC3-II, colocalized with nsp2/3 at the replication complex. The ER-associated degradation (ERAD) tuning pathway contains LC3-I positive vesicles (pathway depicted in Figure I.5). In order to test the requirement of ERAD for DMV formation, both Hela cells and MEF cells were analyzed for colocalization of two ERAD markers, ER degradation enhancer mannosidase alpha-like 1 (EDEM1) and osteosarcoma amplified 9 (OS9), with replication complexes. Both EDEM1 and OS9 colocalize with dsRNA in MHV infected cells. Lastly, when LC3 was depleted, viral replication was decreased by 80%. The authors conclude that MHV co-opts the ERAD tuning pathway for DMV formation (Reggiori et al., 2010). The host cell process(es) required for DMV formation remains a controversial topic within the field. It

is unknown which process(es) are actually required and whether the same process(es) are required for all CoVs.

Viral proteins required for membrane modifications

Until recently, it was not known which viral protein induced DMV formation. Angelini *et al.* demonstrated that SARS-CoV nsp3, nsp4, and nsp6 are necessary and sufficient for DMV formation (Angelini et al., 2013). In these experiments, nsp3, nsp4 and nsp6 were over-expressed individually or in combinations. While each protein individually altered host cytoplasmic membranes, all three proteins were required for DMV formation. Nsp3 alone causes membrane proliferation; nsp6 alone induces single membrane vesicles; nsp3 and nsp4 together have the capacity to pair membranes; and nsp3, nsp4, and nsp6 together form DMVs (Angelini et al., 2013). The data suggests that nsp6 mediates vesicle formation and interactions of nsp3 with nsp4 pairs membranes in order to generate a double membrane vesicle.

Collectively, the data discussed above lead to a model for CoV replication complex formation (Figure I.3A). I hypothesize that nsp3 and nsp4 interact across the lipid bilayers of ER derived membranes and that nsp6 induces the vesicle formation to form DMVs. During this processes, a membranous network is formed that contains DMVs, convoluted membranes, and ER. It is unclear where on the DMV the replication complexes form. However, a protease protection assay demonstrated that nsp2 is located on the cytosolic side of the reticulovesicular network (Hagemeijer et al., 2010). Based on protease protection assays, the predicted topology of nsp3, nsp4, and nsp6, and data presented in Chapter V, replication likely occurs on the external surface of DMVs.

Recently, *Al-Mulla et al.* suggested that DMVs are not important for viral fitness (Al-Mulla et al., 2014). In the study, the authors analyzed a panel of temperature-sensitive (ts) mutants for DMV size, total numbers, and fitness. The authors concluded that there was no disadvantage to producing DMVs with smaller diameter or producing fewer DMVs (Al-Mulla et al., 2014). However, the authors did not test mutations in the transmembrane domain of nsp3, nsp4, or nsp6. In Chapter IV, I confirmed their results with mutations in nsp4 that alter the morphology and number of DMVs.

Nonstructural protein 4

Nsp4 is an integral membrane protein. The MHV and SARS-CoV nsp4 contain four predicted transmembrane domains (TM1-4) all of which span the ER membrane (Oostra et al., 2008; 2007; Sparks et al., 2007) (Figure I.6). Deletion of the MHV nsp4 coding sequence did not allow recovery of recombinant virus, suggesting that nsp4 is required for viral replication (Sparks et al., 2007). Additionally, when nsp4 domain deletion viruses were generated, TM4 and the C terminal 10 kDa of nsp4 were dispensable for virus replication, but not TM1-3 (Sparks et al., 2007). Charge-to-alanine mutagenesis identified residues within nsp4 that have variable effects on viral replication, suggesting that some of these residues are critical for nsp4 structure, function, and/or viral replication (Sparks et al., 2007).

Glycosylation of nsp4 is a conserved feature, although the location and number of glycosylation sites varies among CoVs (Figure I.7). MHV nsp4 contains two N-linked glycosylation sites in nsp4 loop 1 (Figure I.6). Both sites have been demonstrated to be glycosylated *in vitro* and during infection (Clementz et al., 2008; Gadlage et al., 2009). When the glycosylation sites were removed by introduction of asparagine-to-alanine

substitutions, the viruses exhibited delayed replication kinetics and RNA synthesis, as well as, aberrant DMV formation (Gadlage et al., 2009). This was the first evidence that nsp4 may be critical for DMV formation.

Nonstructural proteins 3 and 6

Nsp3 is a large multifunctional protein, with at least four distinct domains: 1) an acidic (Ac) domain which is enriched in glutamic acid residues, 2) the X domain with ADP-1’’-phosphasatase activity, 3) one or two papain-like protease domains (PLP1 and PLP2), and 4) a transmembrane domain that spans the membrane twice. Additionally SARS-CoV nsp3 contains a SARS-specific unique domain. Interestingly, PLP2 has been shown to also have deubiquitylation activity in both SARS-CoV and MHV (Barretto et al., 2005; Lindner et al., 2005; Zheng et al., 2008).

The topology of nsp3 was determined. While nsp3 contains five predicted transmembrane domains, only two span the membrane (Figure I.6) (Oostra et al., 2008). Nsp3 has been demonstrated to interact with several replicase proteins and nucleocapsid, suggesting that it may act as a scaffolding protein that maintains the replication complex at the membrane (Imbert et al., 2008).

Nsp6 is a transmembrane protein that contains seven predicted transmembrane domains, six of which actually span the membrane (Figure I.6) (Baliji et al., 2009; Oostra et al., 2008). Additionally, nsp6 induces autophagosomes and single membrane vesicles (Angelini et al., 2013; Cottam et al., 2011). K22, a small molecule inhibitor of coronavirus replication, inhibit membrane modifications (Lundin et al., 2014). K22 resistance mutations were identified within nsp6 that resulted in aberrant DMV formation

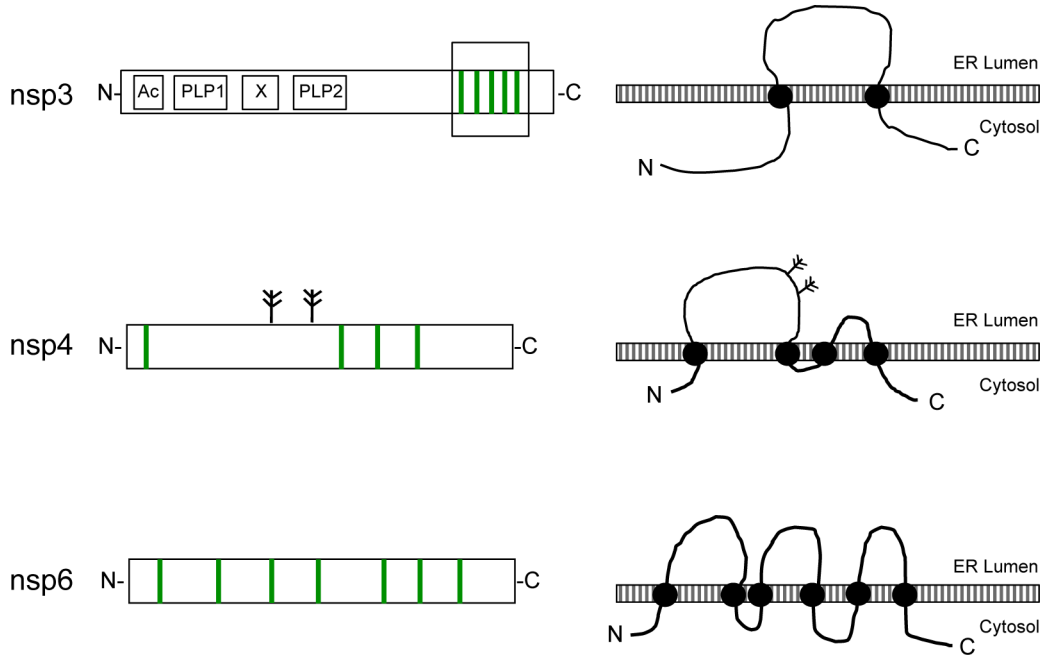

Figure I.6: Topology of MHV nsp3, nsp4, and nsp6.

Linear schematics (left) and topology (right) of nsp3, nsp4 and nsp6. Nsp3 is a large multifunctional protein with multiple domains shown. The region boxed is the transmembrane domain that is shown in the topology diagram below. Nsp3 contains five predicted transmembrane domains and two span the membrane. Nsp4 contains 4 transmembrane domains that span the lipid bilayer. Additionally, nsp4 contains two glycosylation sites within the large luminal loop. Nsp6 contains seven predicted transmembrane domains and six span the membrane.

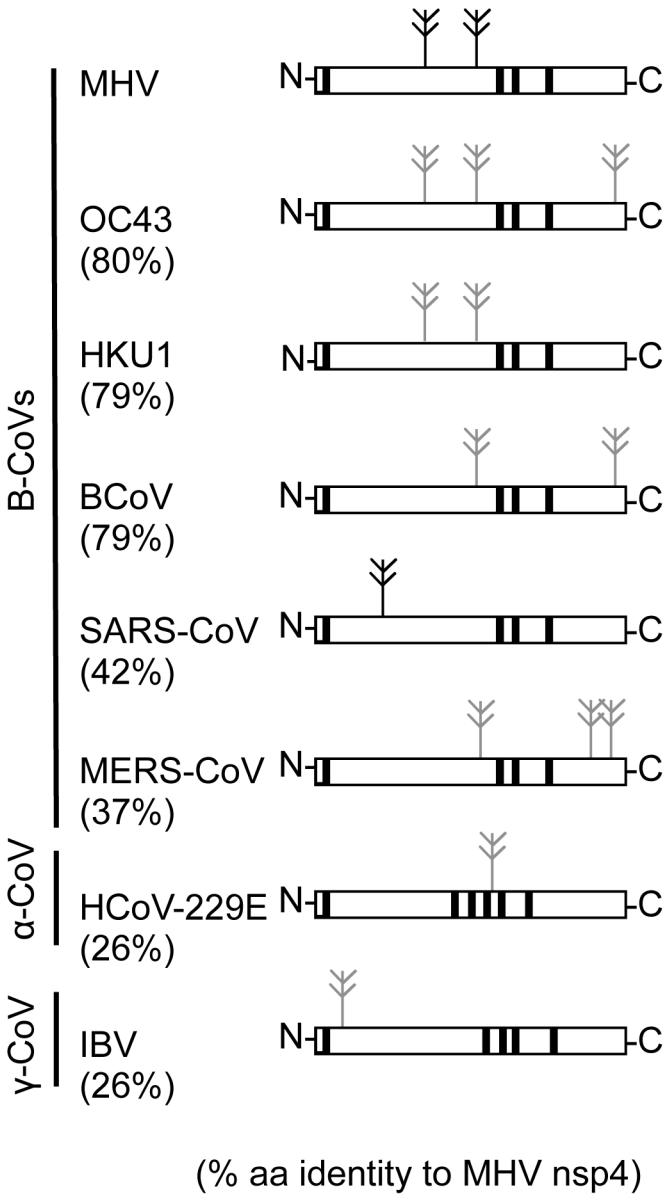

Figure I.7: Glycosylation of coronavirus nsp4 is conserved.
Glycosylation is a conserved feature of nsp4. Shown above are the confirmed (black) or predicted (grey) glycosylation sites within several coronavirus nsp4 proteins. The percent amino acid identity compared to MHV is shown in parentheses.

similar to what is seen with the nsp4 glycosylation mutants (Gadlage et al., 2009; Lundin et al., 2014). These data demonstrate that nsp6 is required for formation or maintenance of DMVs. Interestingly K22 does not impact autophagosome formation suggesting that the reduction in DMVs is independent of autophagy.

Nonstructural Proteins 3, 4, and 6 induce membrane modifications

Equine arteritis virus (EAV), an arterivirus in the Nidovirus family, encodes two membrane proteins (nsp2 and nsp3) that are homologous to CoV nsp3 and nsp4. When nsp2 and nsp3 are co-expressed in cells, induce DMVs similar to those produced during infection (Snijder et al., 2001). This data provided the first suggestion that nsp3, nsp4, and possibly nsp6

would be necessary and sufficient for coronavirus DMV formation. Historically, nsp3, nsp4 and nsp6 have been difficult to express in bacteria and mammalian cells by our lab and others (personal communication). However, two separate labs have now expressed nsp3, nsp4, and nsp6 from MHV (de Haan lab) and SARS-CoV (Buchmeier lab).

Hagemeijer *et al.* expressed MHV nsp3C (C-terminus only), nsp4 and nsp6 and analyzed the localization within cells (Hagemeijer et al., 2011). Individually, all three proteins localize to the ER but upon co-expression, nsp3C and nsp4 interacted and relocalized into distinct foci within the ER. The interaction of nsp3 and nsp4 is likely occurring through the luminal loop of nsp3 and loop 1 of nsp4 (Hagemeijer et al., 2014). Additionally, the study demonstrated that nsp4 interacts with nsp3C, nsp4, and nsp6 by co-immunoprecipitation, protein complementation and yeast-2-hybrid (Hagemeijer et al., 2011). Co-expression of nsp3C- and nsp4- paired ER membranes but did not form DMVs

or convoluted membranes (Hagemeijer et al., 2014). As described above, SARS-CoV nsp3, nsp4, and nsp6 are necessary for DMV formation (Angelini et al., 2013).

Summary

When I started this project, it was known that nsp3, nsp4, and nsp6 are transmembrane proteins and the topology of each protein had been determined *in vitro* (Baliji et al., 2009; Oostra et al., 2008; 2007). It was also known that nsp4 is indispensible for viral replication (Sparks et al., 2007). A putative temperature sensitive mutation was identified in nsp4 that was thought to mislocalize replication complexes to the mitochondria (Clementz et al., 2008). Mutations in nsp4 were associated with several replication phenotypes that range from WT-like to a 4 h delay in exponential replication with a 1000-fold reduction in peak viral titer (Sparks et al., 2007). Nsp4 is N-linked glycosylated at two sites within loop 1 of nsp4 (Clementz et al., 2008; Gadlage et al., 2009; Oostra et al., 2008; 2007). Mutations that remove the glycosylation sites resulted in aberrant DMV formation (Gadlage et al., 2009). In Chapter II, I sought to test the mechanism of mis-localization of the replication complex to the mitochondria. I demonstrated that the putative nsp4 ts mutation, N258T, is not ts and does not alter the localization of the replication complex at either 30°C or 40°C. In Chapter III, I demonstrated that position E226 of nsp4 is important for nsp4 function in viral replication. In Chapter IV, I analyzed mutations within nsp4 for aberrant DMV formation and tested whether DMV morphology and numbers alter virus fitness. I determined that mutations across nsp4 alter DMV morphology and number. Additionally, I demonstrated that loss of nsp4 glycosylation is associated with a fitness cost to the virus. These data suggest that the structure of nsp4 is required for proper DMV formation and that the

double membrane of the DMV is maintained by interactions between nsp4 and viral and/or cellular proteins. In Chapter V, I determined that nsp4 is glycosylated as an nsp4-10 polyprotein and identified two previously unknown polyprotein precursors, nsp4-5 and nsp4-5-6. In Chapter VI, I introduced charge-to-alanine substitutions into nsp3 and identified mutations that result in delayed viral replication. In Chapter VII, I determined the localization of MERS-CoV replicase proteins to perinuclear cytoplasmic foci. My work contributes to the understanding of how DMVs are formed and their role in viral fitness.

CHAPTER II: MURINE HEPATITIS VIRUS NSP4 N258T MUTANTS ARE NOT TEMPERATURE-SENSITIVE

Introduction

Coronaviruses, like other RNA viruses, induce modifications of cytoplasmic membranes in order to form replication complexes, as sites of viral RNA synthesis. Three of the coronavirus-encoded replicase non-structural proteins - nsp3, nsp4 and nsp6 - contain membrane-spanning domains and are thought to be essential for cytoplasmic membrane modifications (Baliji et al., 2009; Imbert et al., 2008; Kanjanahaluethai et al., 2007; Oostra et al., 2008). The topology of nsp4 in membranes has been described and nsp4 has been shown to localize to replication complexes (Gadlage et al., 2009; Hagemeijer et al., 2011; Oostra et al., 2007). Mutations in nsp4 of murine hepatitis virus (MHV) decrease viral RNA synthesis and viral replication, and modification of glycosylation sites within the first luminal loop of nsp4, alters the electron micrograph morphology of virus-induced double membrane vesicles (DMVs) (Gadlage et al., 2009; Sparks et al., 2007).

Sawicki *et al.* analyzed a known temperature sensitive mutant of MHV, Alb ts6, by sequence and reversion analysis. They identified within the nsp4 coding region an A$\underline{A}_{9494}$T-to-A$\underline{C}_{9494}$T nucleotide (nt) change resulting in an Asn258Thr (N258T) substitution as the putative ts mutation (Sawicki et al., 2005; Sturman et al., 1987). Clementz *et al.* engineered the N258T substitution in recombinant MHV using a two nt change A$\underline{AT}_{9494\text{-}9495}$-to-A$\underline{CA}_{9494\text{-}9495}$. The resulting virus, Alb ts6 icv, was reported to be ts at 39.5^{o}C, and to demonstrate altered distribution of nsp4 in the infected murine delayed brain tumor cell, colocalizing with protein markers for the mitochondria. It was

concluded that nsp4 and particularly residue N258 is important for membrane localization (Clementz et al., 2008). Subsequently, Sparks *et al.* sequenced an Alb ts6 isolate and found four non-synonymous mutations in the complete genome sequence that did not include the previously reported N258T substitution, but instead identified a Val148Ala (V148A) substitution in nsp5 (3CLpro), which was ultimately confirmed by reverse genetics and complete genome sequencing to be responsible for the ts phenotype (Sparks et al., 2008). Xiaotao Lu, a coauthor on the publication associated with this chapter (Appendix A) (Beachboard et al., 2013), generated the viruses used in this study and all experiments presented in this chapter were performed by me.

Recovery of mutant viruses containing all N258T codon variants

We sought to reconcile these disparate results, using our established reverse genetic system (Yount et al., 2002) to engineer $N258T_{ACA}$ into the same WT-MHV-A59 isogenic background as reported by Clementz *et al.* (Clementz et al., 2008). The introduced mutations would require a two nt change for primary reversion to Asn (Figure II.1). The $N258T_{ACA}$ virus was recovered at 30^{o}C and two rounds of plaque purification were performed prior to expansion and determination of the genome sequence from nt 10 to 31334 by the di-deoxy (Sanger) approach. The A<u>AT</u> to A<u>CA</u> change was confirmed and no other changes from the cloned isogenic genome sequence were identified. In order to measure temperature sensitivity, efficiency of plating (EOP) is calculated as the titer at the non-permissive temperature (40^{o}C) divided by the titer at the permissive temperature (30^{o}C). When WT and $N258T_{ACA}$ viruses were compared for EOP, $N258T_{ACA}$ demonstrated an EOP similar to WT, and without a ts phenotype (Figure II.1).

The finding that N258T$_{ACA}$ was not ts by EOP lead us to the questions: why our engineered mutant virus was different than the one reported by Clementz *et al.*; whether there were additional changes in their virus that lead to the observed phenotypes; and if the phenotype was codon-specific. Therefore, we engineered viruses containing the T$_{ACC}$, T$_{ACG}$ and T$_{ACT}$ codon variants. All three Thr258 codon variant viruses, N258T$_{ACA}$, N258T$_{ACC}$, and N258T$_{ACT}$, were recovered at 30^{o}C. Sanger sequencing of the complete nsp4 sequence confirmed the presence of the introduced mutations and no additional mutations were identified.

N258T codon variant viruses exhibit defects in viral replication

All codon variant N258T viruses were tested for temperature-sensitivity by plaque assay in murine DBT cells at the permissive (30^{o}C) and non-permissive (40^{o}C) temperatures and EOP was calculated (Figure II.1). Wild-type (WT) virus had an EOP of 0.79 demonstrating that there is no replication impairment at 40^{o}C. As a ts control, the EOP of nsp5 tsV148A, was performed in parallel and calculated to be 1.4 x10^{-5} confirming the ts phenotype. All four codon variant viruses had WT-like EOPs (0.52 – 2.10) indicating that they are not impaired for replication at 40^{o}C, inconsistent with a ts phenotype (Figure II.1). Because plaque replication and numbers are only a measure of fitness and temperature sensitivity, we next compared replication kinetics of the mutant viruses at 30^{o}C. DBT cells were infected at an MOI of 0.1 PFU/cell and supernatant was sampled at 0.6, 2, 4, 6, 8, 10, 12, 16, 24, and 28 h p.i. for plaque assay (Figure II.1). At 30^{o}C, all four codon mutants had indistinguishable replication characteristics and achieved peak titers similar to WT at 28 h p.i. However, between 8 and 24 h p.i., the codon mutant viruses exhibited a lag in exponential replication with a 0.5 to 1 log

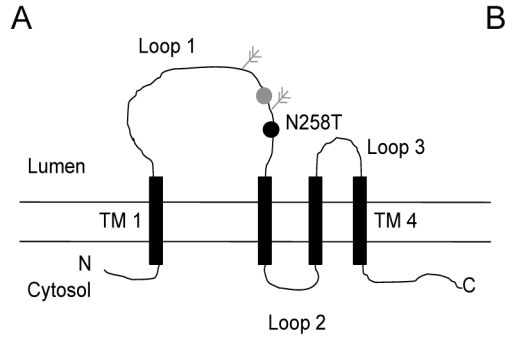

B

Virus	Titer at:		EOP (40/30)
	30°C	40°C	
WT $N258_{AAT}$	1.2×10^9	9.3×10^8	0.79
[1]$N258T_{ACA}$	5.4×10^7	2.8×10^7	0.52
$N258T_{ACC}$	4.6×10^7	3.5×10^7	0.77
$N258T_{ACG}$	4.3×10^7	3.7×10^7	0.88
[2]$N258T_{ACT}$	1.2×10^7	2.3×10^7	2.10
V148A	1.3×10^8	1.9×10^3	1.4×10^{-5}

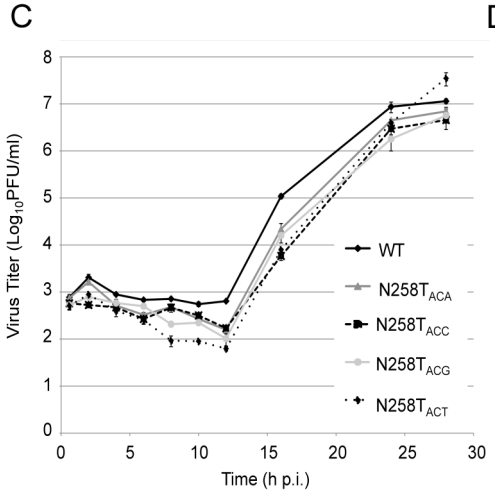

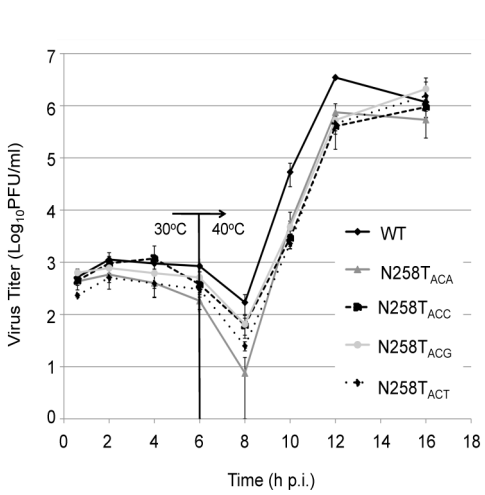

Figure II.1: Analysis of nsp4 N258T codon variant mutants of MHV.
(**A**) Proposed topology of MHV nsp4. Nsp4 has 4 membrane-spanning region (TM1 to 4, black rectangles) and 3 loop regions (loop 1-3). Previously reported mutations in loop one are indicated as the grey double-headed arrows (glycosylation sites) and the grey dot (E226A/E227A) (Gadlage et al., 2010; Sparks et al., 2007). The N258T (AAT to ACX at nt positions 9493 to 9495) substitution is shown as a black dot. (**B**) Titers were determined by plaque assay in DBT-9 cells at 30°C and 40°C. EOP was calculated as the titer at 40°C divided by the titer at 30°C. Titers represent the average titer of two independent experiments. [1]Codon variant previously reported by Clementz *et al.*(Clementz et al., 2008), [2] Codon variant previously reported by Sawicki *et al.* (Sawicki et al., 2005). (**C**) DBT cells were infected at an MOI of 0.1 PFU/cell with the indicated viruses and incubated at 30°C for 28 h and titers were determined by plaque assay. Error bars represent the standard error of the mean of two independent plaque assays done in duplicate. (**D**) DBT cells were infected at an MOI of 0.1 PFU/cell with the indicated viruses and incubated at 30°C with a temperature shift to 40 °C at 6 h p.i. and titers were determined by plaque assay. Error bars represent the standard error of the mean of two independent plaque assays done in duplicate.

decrease in viral titers during this phase, consistent with a stable replication defect and likely decreased fitness compared with WT (Figure II.1). We then tested replication following a temperature shift from 30°C to 40°C at 6 h p.i., with supernatants sampled at 0.6, 2, 4, 6, 8, 10, 12, and 16 h p.i. WT virus replication kinetics demonstrated an initial decrease in titer immediately following the temperature shift, but recovered quickly, and achieved peak titers by 12 h p.i. All four codon mutants replicated indistinguishably from each other, and achieved WT-like peak titers at 16 h p.i. Similar to replication at 30°C, between 8 and 16 h p.i., the codon mutants exhibited a lag in exponential replication and decreased viral titers compared to WT (Figure II.1). These data demonstrate that while the N258T substitution within nsp4 exhibited impairment in replication, it did not confer temperature-sensitivity, contrary to what has been previously reported.

N258T nsp4 localizes to the replication complex

The $N258T_{ACA}$ virus reported by Clementz *et al.* was concluded to have altered localization of nsp4 to mitochondrial membranes at 39.5°C (Clementz et al., 2008). To determine the localization of our mutant nsp4 proteins, DBT cells were infected with WT, $N258T_{ACA}$, $N258T_{ACC}$, $N258T_{ACG}$, and $N258T_{ACT}$ on glass coverslips at an MOI of 5 PFU/cell for 16 h at 30°C or for 7 h at 40°C (Figure II.2). Infected cells were then fixed and permeabilized with methanol, immunostained with antibodies specific to nsp4 and nsp8 or pyruvate dehydrogenase (PDH), a mitochondrial matrix protein. Cells were imaged using a Zeiss LSM510 confocal microscope.

At both 30°C and 40°C, for WT and $N258T_{ACA}$, nsp4 and nsp8 extensively colocalized to punctate perinuclear foci (Figure II.2). In contrast, both WT and mutant viruses display non-colocalization of nsp4 and PDH. Nsp4

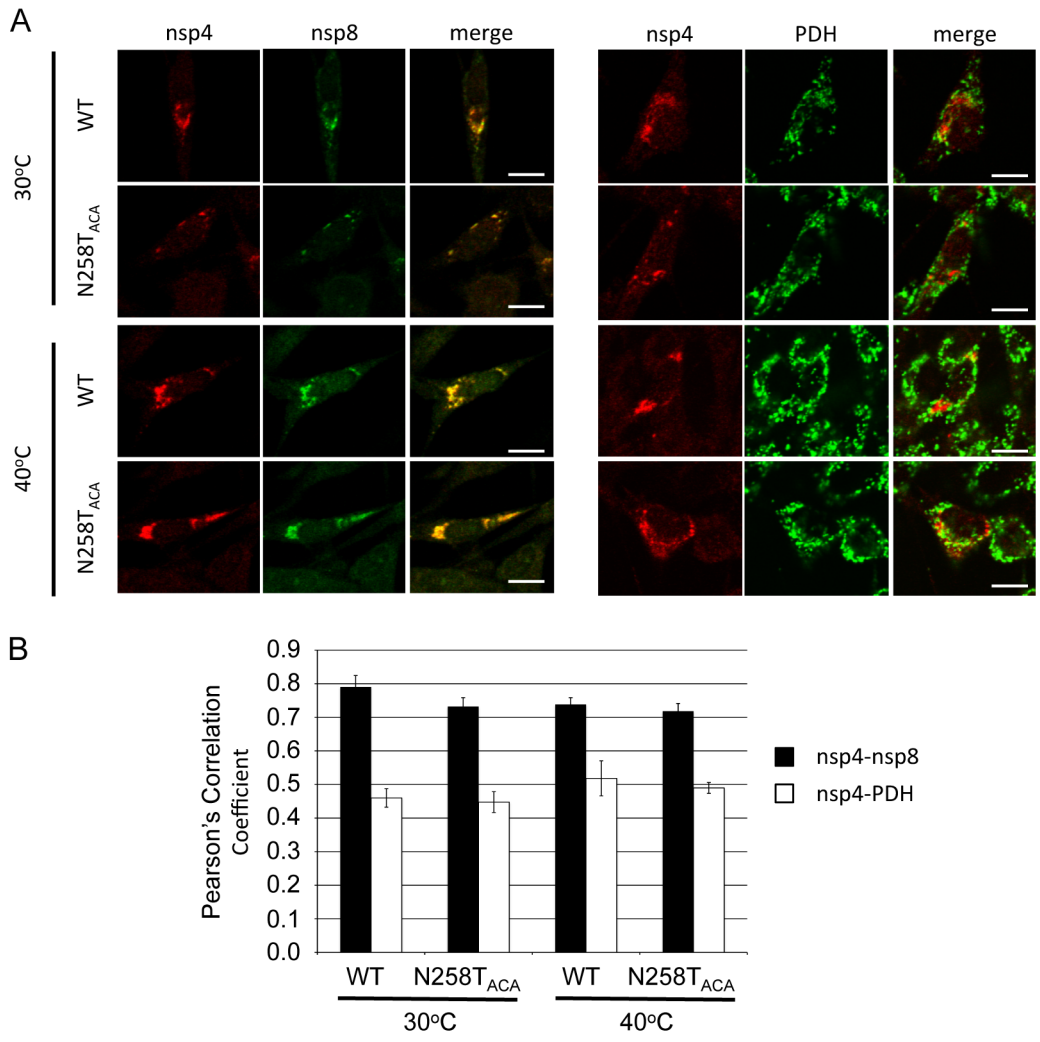

Figure II.2: nsp4 N258T$_{ACA}$ codon variant localizes to the replication complex. (**A**)DBT-9 cells were infected at an MOI of 5 PFU/cell for 16 h at 30°C or 7 h at 40°C. Cells were fixed in methanol, probed for nsp4 (red) and nsp8 (green) or PDH (green) and imaged on a Zeiss LSM510 confocal microscope. Yellow pixels represent colocalization of overlapping red and green pixels. The scale bar in the bottom right corner of merged images represents 10µm. (**B**) Pearson's correlation coefficient was calculated for nsp4-nsp8 or nsp4-PDH for both WT and N258T$_{ACA}$ at 30°C and 40°C (n=5). Nsp4-nsp8 colocalization was significantly higher than nsp4-PDH ($p < 0.002$) as measured by Student's t test. Error bars represent standard deviation.

localized to punctate perinuclear foci, whereas PDH localized to foci dispersed throughout the cytoplasm that were adjacent to but distinct from nsp4 foci. Within the same fields of view, there were infected cells that had not formed syncytia as well as syncytial cells and the pattern of colocalization were consistent between both sets of infected cells as well as within a z-stack. In order to quantify colocalization, Pearson's correlation coefficient was calculated using the JACoP plugin for ImageJ (Bolte and Cordelières, 2006; Schneider et al., 2014). To avoid bias, colocalization was quantified for the entire field and the entire z-stack of five images per condition. At both 30^{o}C and 40^{o}C, WT and N258T$_{ACA}$ nsp4 and nsp8 had Pearson's correlation coefficients of between 0.71 and 0.79, consistent with colocalization. Nsp4 and PDH displayed Pearson's correlation coefficients of 0.45 to 0.52 ($p < .002$) demonstrating non-colocalization (Figure II.2). These results demonstrate that the nsp4 N258T substitution did not result in altered localization of nsp4 to the mitochondria at either 30^{o}C or 40^{o}C.

Discussion

Our results demonstrate that the nsp4 N258T substitution is not responsible for either the ts phenotype, or for the altered localization of nsp4 to the mitochondria reported by Clementz *et al*. Although the nsp4 N258T codon variant viruses were not ts, they displayed decreased titers and delayed replication, demonstrating that N258 or loop 1 of nsp4 is likely important for viral replication. Interestingly, this residue is highly conserved among beta-coronaviruses, including bovine coronavirus, human coronavirus OC43 and SARS-CoV as an aspartic acid, with MHV being the exception. The conservation of this residue suggests that it may be important. Our lab has previously reported two nsp4 mutant viruses, with mutations located in luminal loop 1. Nsp4

contains two glycosylation sites at N176 and N237 (Figure II.1), that when substituted with alanine, demonstrate delayed replication and decreased viral titers similar to those of nsp4 N258T, as well as altered DMV formation (Gadlage et al., 2009). The nsp4 E226A/E227A mutant virus is debilitated for replication and viral RNA synthesis (Sparks et al., 2007). Together, these mutations suggest that loop 1 of nsp4 is important for viral replication, RNA synthesis, and the formation of DMVs.

We are unable to explain the results reported by Clementz *et al*. because the virus was not available for direct comparison. However, our EOP results were confirmed by the Baker lab (personal communication). The reverse genetics system uses seven cDNA fragments that are ligated and used for transcription of genomic RNA that is then electroporated into cells for virus recovery. There is the possibility that mutations arose during amplification or transcription of the cloned fragments. Our lab and the Baker lab have the same original source for the cDNA fragments. In order to account for changes during amplification, we obtained all seven cDNA fragments from the Baker lab and attempts to recover virus were unsuccessful. We sequenced the cDNA fragment containing nsp4 and identified the $N258T_{ACA}$ substitution, as well as a single nucleotide deletion at nt 8582 that resulted in a possible stop codon (UGA at nt 8644 to 8646). The virus reported by Clementz *et al.* was difficult to recover (personal communication), leading to the possibility of multiple adaptive changes. The virus was not available for sequencing; therefore, we cannot test for additional mutations. The experiments in this study were performed in MHV-A59, and it is important to consider polymorphisms within different strains of the virus when analyzing the importance of specific residues. The results of our study strongly suggest that sequencing of the entire genome of mutant

coronaviruses derived from the reverse genetics approach may be necessary. Several studies have documented mutations that arise during the process of mutagenesis or propagation of cDNA clones, as well as adaptive mutations that may occur in genes not thought to have any relationship. We demonstrated that the original MHV infectious clone had WT-like replication in culture, but was attenuated *in vivo* (Sperry et al., 2005). Complete genome sequencing found mutations in other fragments that arose during propagation of the clones that were confirmed to be responsible for the attenuating phenotype. Hurst et al. showed that impairment in MHV replication by mutations in the nucleocapsid gene resulted in compensating second-site mutations in the replicase nsp3 protein (Hurst et al., 2010). Thus coronaviruses may have unexpected linked functions or epistatic relationships that might be missed by partial sequencing. Fortunately, the cost and time of genome sequencing is rapidly improving. Establishment and availability of validated primer sets may allow for more rapid sequencing in a 96 well format or by deep sequencing, further reducing cost and time associated with complete genome analysis, and may identify novel and important new relationships among coronavirus proteins.

CHAPTER III: REVERSION ANALYSIS OF MHV NSP4 E226A/E227A

Introduction

Positive-sense RNA viruses replicate on modified host cytosolic membranes (Miller and Krijnse-Locker, 2008). Coronavirus non-structural proteins (nsps) 3, 4, and 6 induce rearrangement of ER membranes to form a network composed of double membrane vesicles and convoluted membranes that remain contiguous with the ER (Knoops et al., 2008b). These membrane modifications are the site of viral replication (Miller and Krijnse-Locker, 2008). In addition to their role in membrane modifications, it is thought that nsp3, nsp4, and nsp6 anchor the replication complex to the membrane. Studies have tested interactions among the nsps by yeast-2-hybrid and mammalian-2-hybrid and determined that nsp3 interacts with several nsps. The data suggests that nsp3 may act as a scaffolding protein (Brunn et al., 2007; Imbert et al., 2008; Pan et al., 2008). Nsp4 has been demonstrated to form heterotypic interactions with nsp3 and nsp6, as well as, homotypic interactions (Hagemeijer et al., 2011).

A previous study demonstrated that nsp4-E226A/E227A is severely debilitated for viral replication, exhibiting a 1000-fold reduction in peak viral titers and a 4 h delay in exponential replication when tested at an MOI of 0.01 (Sparks et al., 2007). We hypothesized that this mutation disrupted critical interactions between nsp4 and another viral protein that are required for efficient viral replication. In order to test this hypothesis, I performed reversion analysis on the E226A/E227A virus by passaging the virus seven times and analyzing for the presence of additional mutations. Nelly Grigorian assisted with the genome sequencing of the E226A/E227A P5 virus. All other experiments and data analysis were performed by me.

Results

Passaging of the nsp4 E226A/E227A mutant virus

To test for compensatory mutations, E226A/E227A was blindly passaged in murine delayed brain tumor cells seven times (P1 to P7) and the supernatant from each passage was collected and used to infect cells for TRIzol RNA extraction. Each passage was sequenced across nsp4 to determine whether the engineered mutation was maintained. The mutation was maintained from P1 to P3. At P4, there was a mixed population containing both the E226A/E227A and a primary psuedorevertant at position 226 (A226D) that resulted from a single nucleotide mutation (GCC to GAC). By P5, the A226D was fixed in the population and was retained in all further passages. For each passage, titers were determined by plaque assay and plaque size was calculated (Figure III.1). During the passage series, there was a trend of increased titer with each passage. However, there was an approximately 2.5-fold increase in titers at P3 that corresponds to and 3-fold increase in plaque size. At P5, there was an approximately 10-fold increase in titer, which correlated to the fixation of the A226D substitution in the population.

Genome Sequencing of E226A/E227A P5 virus identified four mutations

In order to determine whether any additional mutation(s) arose during the passage series, the P5 virus population was sequenced across the genome. P5 was chosen based on the increase in titer at this passage. Two rounds of plaque purification were performed on the P5 virus and RNA was isolated in TRIzol. Subsequently, the genome was sequenced as 15 overlapping amplicons. Sequencing of nt 12 – 31335 revealed three mutations in addition to the A226D/A227: (nt changes are noted at the genomic location

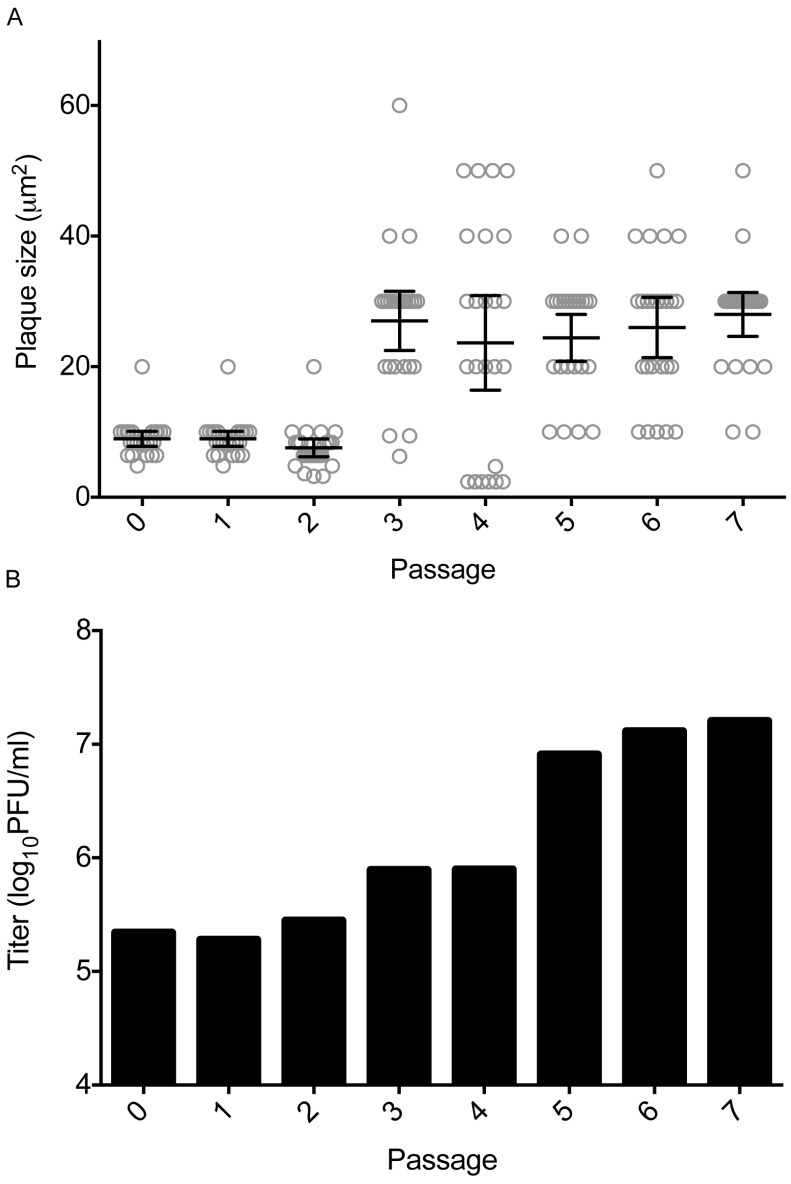

Figure III.1: Passage of the E226A/E227A virus increased plaque size and titer. (A) The total area of individual plaques was measure using ImageJ software. Each circle represents a plaque that was measured and lines represent the mean with 95% confidence intervals indicated. (B) Viral titer for each passage was determined by plaque assay.

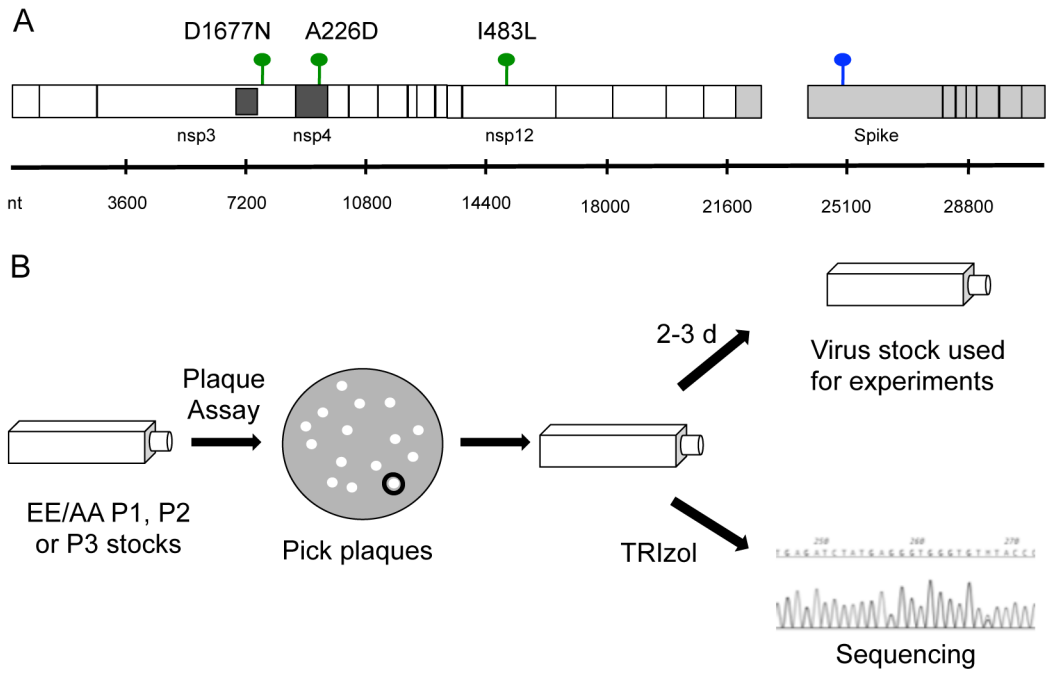

C

Virus Nomenclature	Nsp3 (D1677N)	Nsp4 (E226A/E227A)	Nsp12 (I483L)
WT	D	EE	I
EE/AA	D	AA	I
EE/AA +3	N	AA	I
EE/AA +12	D	AA	L
EE/AA +3/12	N	AA	L

Figure III.2: Genome sequencing of the P5 virus and isolation of biological revertants.

(A) The genome of the P5 virus was sequenced and 3 non-synonymous (green) and 1 synonymous (blue) mutations were identified. (B) Biological revertants were plaque isolated, and amplified for viral stocks and sequencing. (C) Nomenclature of of the biological revertants and which mutations they contain.

and amino acid changes are listed by position within the protein) a $\underline{G}_{7737}$AT to $\underline{A}_{7737}$AT mutation (D1677N) in nsp3, a $\underline{A}_{15026}$TA to $\underline{C}_{15026}$TA mutation (I483L) in nsp12 and a TG$\underline{C}_{25080}$ to TG$\underline{T}_{25080}$ mutation (C348C) in spike (Figure III.2). To determine when the mutations arose, the P1 to P4 viruses were sequenced across the nsp3, nsp12, and spike and analyzed for the presence of the mutations. The $\underline{G}_{7737}$AT to $\underline{A}_{7737}$AT (D1677N, nsp3) mutation arose during the first passage as a mixed population and became fixed in the population at P5. The $\underline{A}_{15026}$TA to $\underline{C}_{15026}$TA (I483L, nsp12) mutation arose during P1 as a mixed population and became fixed in the population at P3. The TG$\underline{C}_{25080}$ to TG$\underline{T}_{25080}$ (C348C, Spike) mutation arose during P5. This data suggests that the mutations within nsp3 or nsp12 may account for the increase titer.

Isolation of biological revertants

In order to specifically test the contribution of the D1677N (nsp3) and I483L (nsp12) substitutions to the partial reversion phenotype (Figure III.2B), I isolated eachbiological revertant in the background of E226A/E227A. Three plaques were isolated from each passage of P1 to P3. I chose these passages to exclude the A226D psuedoreversion. Plaques were expanded and sequenced across the region of nsp3, nsp4, nsp12 and spike. Four viruses were isolated, including: the nsp3 D1677N reversion (EE/AA+3), the nsp12 I483L (EE/AA+12) reversion, or both the nsp3 D1677N and the nsp12 I483L (EE/AA+3/12) reversions in combination, and the nsp4 E226A/E227A original substitution (Figure III.2C).

Biological revertants replicate similar to E226A/E227A

To determine whether these mutations effect viral replication, murine DBT cells were infected with WT, EE/AA, EE/AA+3, EE/AA+12 or EE/AA+3/12 at an MOI of 0.1

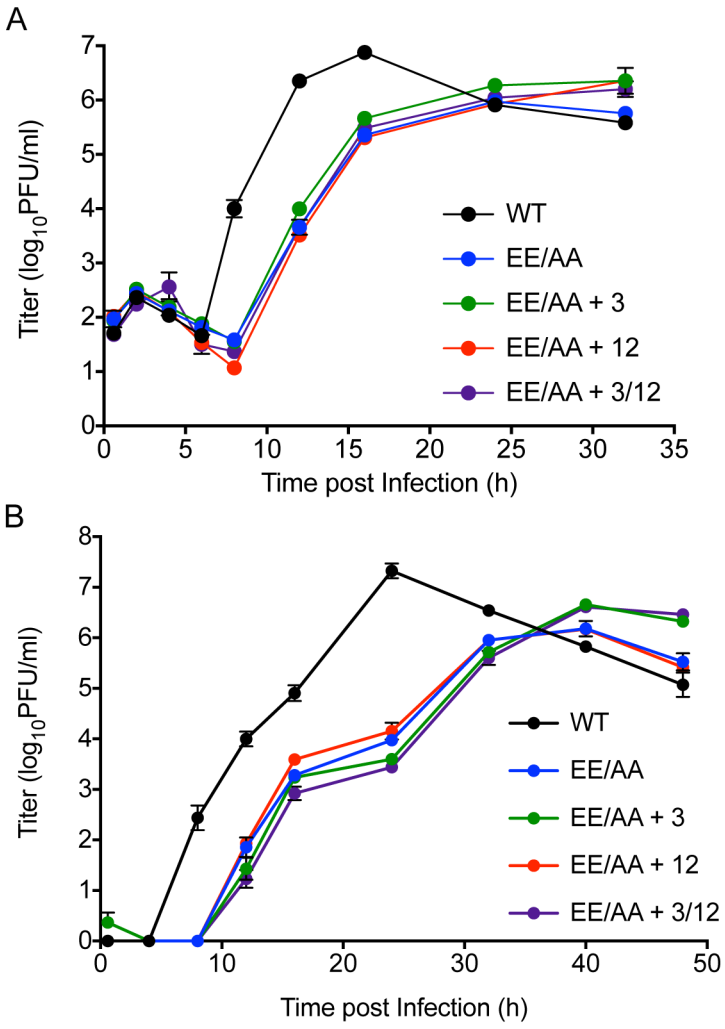

Figure III.3: Replication of the biological revertants.
DBT cells were infected with indicated plaque purified viruses at an MOI of 0.1 PFU/cell (**A**) or 0.001 PFU/cell (**B**) for up to 48 h. Supernatants were sampled at times indicated and titered by plaque assay. Error bars represent SEM of 3 replicates plated in duplicate.

PFU/cell, supernatants were sampled over a 32 h time course, and titers were determined by plaque assay (Figure III.3A). WT virus reached peak titers of about $1x10^7$ PFU/ml at 16 h p.i. All mutant viruses exhibited an approximately 2 h delay in exponential replication and achieved peak titers that were 10-fold decreased compared to WT. The E226A/E227A plaque isolated virus exhibited increased peak titers compared to the viral stock. These data support the conclusion that the additional mutations in nsp3 and nsp12 do not increase viral replication and may decrease viral replication when the population is analyzed.

In order to determine whether the viruses exhibited altered replication during multiple cycles of replication, DBT cells were infected with the indicated viruses at an MOI of 0.001 PFU/cell, supernatants were sampled, and titered by plaque assay (Figure III.3B). WT virus started exponential replication between 4-8 h p.i. and plateaued from 12-16 h p.i., then finally achieved peak titers by 24 h p.i. Replication kinetics were similar for each mutant, with delayed exponential replication. The viruses achieved peak titers that were 10-fold decreased from WT between 36- 42 h p.i. It was also noted that between 24-32 h p.i.; plaque size for all mutant viruses increased to WT-like size, suggesting that there may have been additional mutations that arose late during infection. However, plaques were not isolated for sequencing. Even at a low MOI, I was unable to determine differences in viral replication. This confirms that these mutations do not alter virus replication and suggests that the E226D psuedorevertant is responsible for the increased titer.

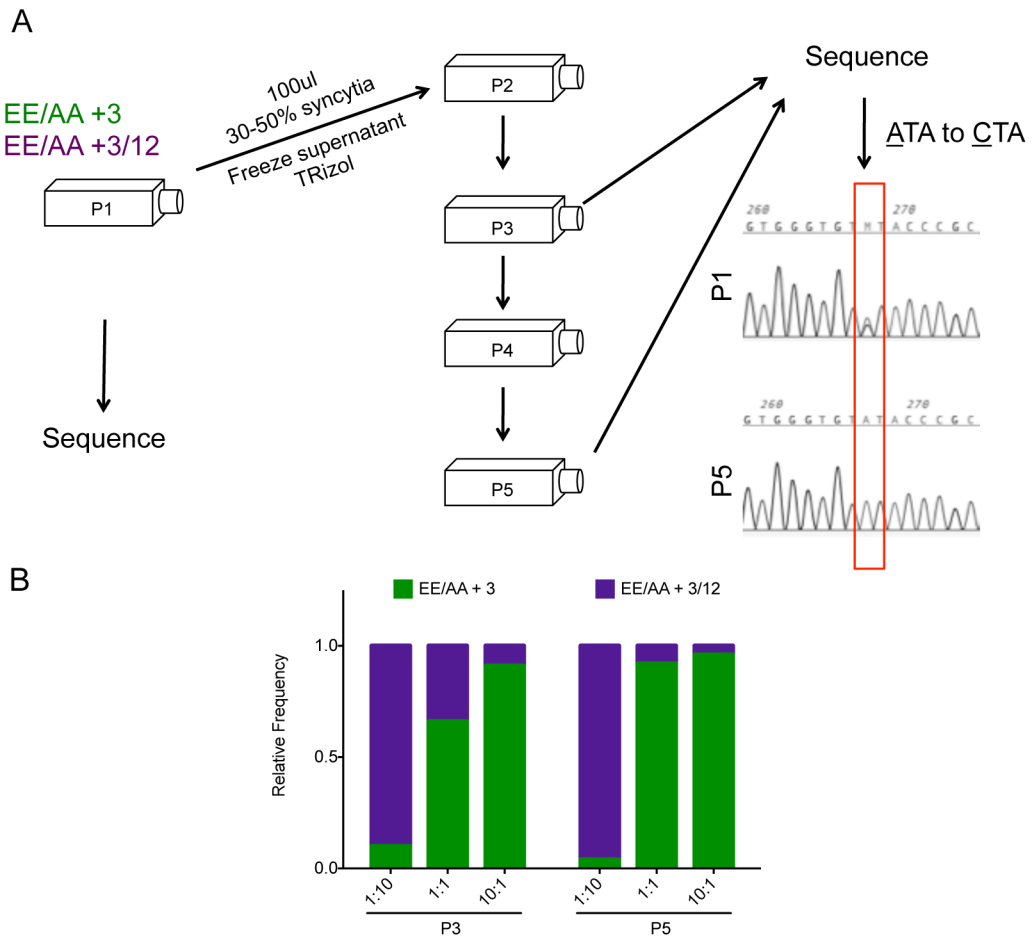

Figure III.4: Competition of EE/AA+3 and EE/AA+3/12.
DBT cells were co-infected with the EE/AA+3 and EE/AA+3/12 at a total MOI of 0.1 PFU/cell at ratios of 1:10, 1:1 or 10:1. Viruses were passaged 5 times and sequenced across the nsp12 region at P3 and P5. Relative frequency was determined by calculating area under the peak of the residue on the electropherogram, A (EE/AA+3) or C (EE/AA+3/12).

EE/AA + 3 outcompetes EE/AA + 3/12

In order to test if there was an advantage to a double mutation (nsp3 + nsp12) over the single mutation (nsp3), DBT cells were co-infected at a total MOI of 0.01 PFU/cell. Cells were infected at 1:1, 1:10 and 10:1 ratios (nsp3 only:nsp3/nsp12) and passaged 5 times. At each passage, supernatants were collected for passaging and the cell monolayers were harvested in TRIzol for RNA extraction. At passages 1, 3, and 5 the region of nsp12 containing the mutation was amplified and sequenced. Peaks on the electropherograms were analyzed to determine the ratio of nsp3 (ATA) only to nsp3/nsp12 mutant (CTA) (Figure III.4). When infected at a 1:10 or a 10:1 ratio, the virus that was given the initial advantage outcompetes the other virus as expected. However, for the 1:1 infection, the nsp3 only revertant progressively outcompetes the double mutant and is 90% of the population at P5. This suggests that the nsp12 mutation exhibits a neutral or negative impact on viral fitness.

The A226D/E227A virus exhibited a 10-fold increase in replication titers

Since the mutations in nsp3 and nsp12 had no apparent effect on viral replication, I next characterized the P5 virus. In order to determine if the A226D pseudoreversion was responsible for the increase in viral replication, I tested the P5 virus. DBT cells were infected at an MOI of 1 PFU/cell with WT, P1 and P5 viruses. Supernatants were collected over a 28 h time course. Titers were then determined by plaque assay (Figure III.5). WT virus began exponential replication between 6 and 8 h p.i. and achieved peak titer at 16h p.i. The P1 virus began exponential replication between 8 and 12 h p.i. and reached peak titers at 24 h p.i. The P1 peak titer were ~500-1000 fold decreased compared to WT. The P5 virus maintains the replication delay exhibited by the P1 virus

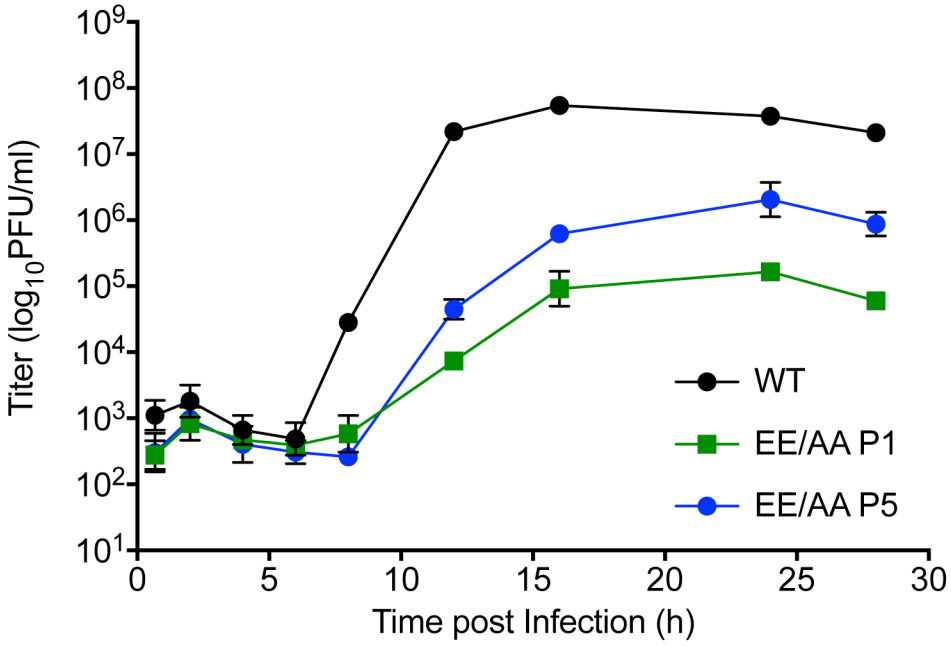

Figure III.5: Replication kinetics of the P1 and P5 of the E226A/E227A. DBT cells were infected with WT, P1 or P5 virus at an MOI of 0.1 PFU/ml. Supernatants were sampled over 28 h and titered by plaque assay. Error bars represent the SEM of three replicates plated in duplicate.

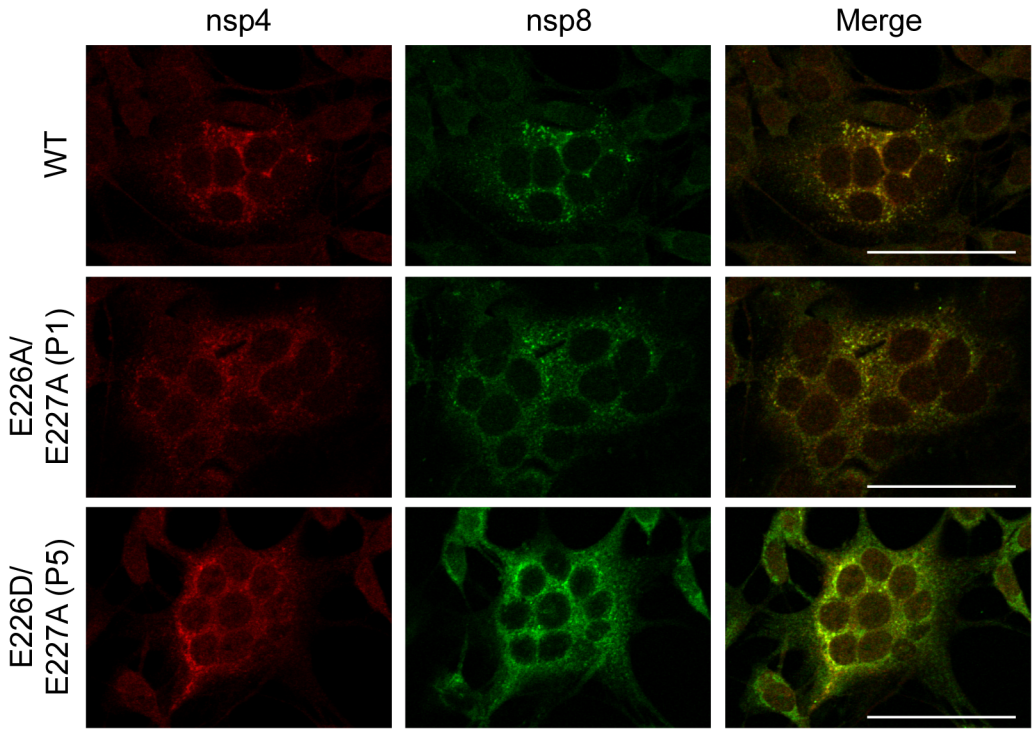

Figure III.6: Localization of nsp4.

DBT cells were infected with WT, P1 or P5 at an MOI of 0.1 PFU/cell. At 8 h p.i., cells were fixed and permeablized with methanol, stained with antibodies where indicated, and imaged by confocal microscopy. Scale bar represents 20 μm.

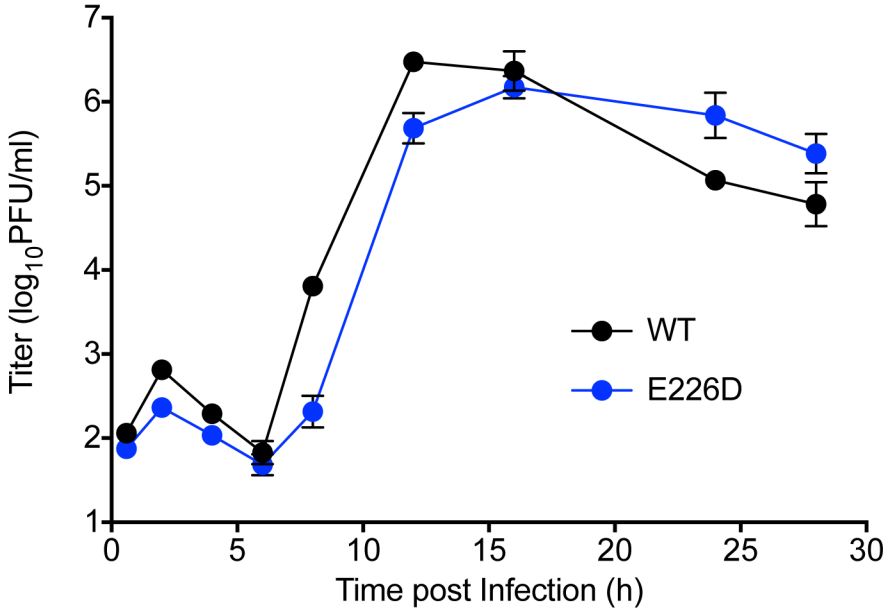

Figure III.7: Replication kinetics of E226D.
DBT cells were infected with WT or E226D at an MOI of 1 PFU/ml. Supernatants were sampled over 24h and titered by plaque assay. Error bars represent the SEM of three replicates plated in duplicate.

and starts exponential replication between 8 and 12 h p.i. with peak titers at 24 h p.i. However, the P5 virus had an intermediate peak titer that is 50-100 fold decreased compared to WT but 10-fold increased compared to P1. These data suggest that the A226D is responsible for the increased viral replication; however, we cannot rule out the possibility of a synergistic effect of multiple mutations. In order to address this possibility, I attempted to engineer the E226D/E227A substitution into the cloned isogenic background; however, I was only able to recover E226D, the double mutant was not recovered.

E226A/E227A nsp4 localizes to the replication complex

In order to determine whether the original substitution and the pseudorevertant display altered localization of nsp4, DBT cells on glass coverslips were infected at an MOI of 0.1 PFU/cell (Figure III.6). At 10 h p.i., cells were fixed in methanol, stained with antibodies specific to nsp4 and nsp8 and imaged using a Zeiss LSM510 confocal microscope. For WT, E226A/E227A (P1) and E226D/E227A (P5) infected cells, nsp4 and nsp8 are localized to perinuclear foci and demonstrated extensive colocalization. The signal appeared to be reduced in the E226A/E227A (P1) virus infected cells suggesting that protein expression was decreased. The data suggests that these residues may be critical for proper folding and expression of the protein or that the E226A/E227A nsp4 protein is rapidly degraded.

E226D exhibited delayed viral replication

We were unsuccessful at cloning the E226D/E227A substitutions; however, I was able engineer several E226X substitutions into the MHV infectious clone (MHVic) B fragment (Table III.1). Five substitutions were introduced but only the E226D virus was

recovered. In order to analyze viral replication, DBT cells were infected with WT or E226D viruses, supernatants were sampled over 24 h, and titers were determined by plaque assay (Figure III.7). WT began exponential replication between 6 and 8 h p.i. and achieved peak titer at 12 h p.i. E226D exhibited a two-hour delay in exponential replication and achieved WT-like titer at 16 h p.i. This suggested that even single conservative changes within nsp4 can alter the timing of viral replication.

Table III.1: E226X virus recovery.

Substitution	Virus Recovered
E226D	Yes
E226G	No
E226L	No
E226S	No
E226W	No

Summary and Future Directions

I concluded based on the above results that the mutations within nsp3 and nsp12 are not responsible for the increase in viral replication demonstrated by the E226D/E227A (P5) virus. It is unclear based on these results what the role of these mutations may be. However, it is possible that the mutations outside nsp4 function at the quasispecies level and thus effects cannot be detected in the plaque isolates. We have seen precedent for this type of effect with studies of an nsp3 PLP1 knock out virus that produces dominant interfering particles. However, when clones were picked there was loss of the dominant interfering particles (Xiaotao Lu, unpublished data), which may have allowed for the increase in peak titer for the plaque isolated virus. Alternatively, the mutations may have arisen as random mutations during passage.

Together these data show that the E226 and E227 residues are critical for nsp4 structure/ function. Future studies should continue to passage the virus for subsequent passages to determine if the E227A residue also pseudoreverts to E227D or if there are additional mutations outside of nsp4 that allow for WT-like replication. Based on the data presented in this chapter, I would anticipate that upon subsequent passaging the A227 will pseudorevert to an A227D and this will restore the peak viral titer. Several mutations within nsp4 have been demonstrated to exhibit delayed exponential replication; therefore, I would anticipate that the E227D mutations would also maintain the delayed exponential replication. Based on data presented in Chapter IV, I would a anticipate that the E226D mutant would produce aberrant DMVs and produce less DMV than WT virus. I hypothesize that mutations within nsp4 alter the structure and/or function of nsp4, leading to a delay in DMV formation, and downstream replication. Further studies will need to be performed in order to determine the cause of the delayed exponential replication. Experiments described in this chapter were not further pursued because the virus pseudoreverted, suggesting that the E226 and E227 residues important for the structure of nsp4 and may not be useful for identifying mutations outside of nsp4.

CHAPTER IV: MUTATIONS IN MURINE HEPATITIS VIRUS NSP4 ALTER VIRUS FITNESS AND MEMBRANE MORPHOLOGY

Introduction

RNA viruses modify host cytoplasmic membranes during the formation of viral replication complexes (Miller and Krijnse-Locker, 2008). Coronaviruses (CoVs) induce substantial membrane rearrangements, including a reticulovesicular network composed of two types of membrane modifications, double membrane vesicles (DMVs) and convoluted membranes (CM). The reticulovesicular network is contiguous with the ER membranes and is the site of viral RNA synthesis (Knoops et al., 2008a). CoV genomes, which are 26-32kb, encode two replicase/transcriptase ORFS 1a and 1b which are translated into the polyproteins 1a and 1ab incorporating nonstructural proteins 1-16 (nsps 1-16). The replicase polyproteins are cleaved by virus-encoded proteases within nsp3 (PLP1/2) and nsp5 (3CLpro). All nsps tested to date colocalize by immunoelectron microscopy to DMVs and/or CM and by immunofluorescence at probable sites of viral RNA synthesis (Angelini et al., 2013; Bost et al., 2000; Brockway et al., 2003; Gadlage et al., 2009; Gosert et al., 2002; Knoops et al., 2008a; Miller and Krijnse-Locker, 2008; Snijder et al., 2006; Sparks et al., 2007; Ulasli et al., 2010; van der Meer et al., 1999).

Nonstructural proteins 3, 4, and 6 are integral membrane proteins. The topology has been determined *in vitro* for both Severe Acute Respiratory Syndrome-CoV (SARS-CoV) and murine hepatitis virus (MHV) (Clementz et al., 2008; Gosert et al., 2002; Knoops et al., 2008a; Oostra et al., 2008). Nsp3, 4, and 6 contain two, four, and six transmembrane domains, respectively (Baliji et al., 2009; Kanjanahaluethai et al., 2007; Oostra et al., 2007; 2006). SARS-CoV nsp3, nsp4, and nsp6 are necessary and sufficient

for double membrane vesicle formation. When expressed alone, nsp3 causes membrane proliferation and the membranes accumulate into disordered membrane bodies that appear as clustered membranes. Single expression of nsp6 induces single membrane vesicles of unknown origin. When co-expressed, nsp3 and nsp4 together have the capacity to pair membranes. All three proteins are required for formation of DMVs (Angelini et al., 2013). I hypothesize that interactions among these proteins mediate membrane modifications. Hagemeijer *et al.* demonstrated that MHV nsp4 forms homotypic and heterotypic interactions with the transmembrane domain of nsp3 and nsp6 by immunoprecipitation and protein complementation assays (Hagemeijer et al., 2011). The region of nsp4 that interacts with nsp3 and nsp6, as well as the regions of these proteins required for membrane modifications, remain unknown.

Nsp4 contains four transmembrane domains and three loop regions. Loops 1 and 3 are ER-luminal, whereas loop 2 and the N- and C-termini are cytosolic (Oostra et al., 2008; 2007). Nsp4 is predicted to be required for replication as demonstrated by the inability to recover a virus with an nsp4 deletion (Sparks et al., 2007). Deletion of transmembrane 4 (TM4) and truncation of the C-terminus of nsp4 allows recovery of viable mutants. However, these viruses have altered viral replication and RNA synthesis (Sparks et al., 2007). Additionally, charge-to-alanine mutagenesis of nsp4 identified viral mutants having a range of replicative capacity, ranging from WT-like replication to delayed exponential replication with 3 $\log_{10}$ reduction in peak viral titers (Sparks et al., 2007).

The MHV nsp4 protein is N-linked glycosylated at two asparagine residues (N176 and N237) within loop 1 as demonstrated by EndoH sensitivity (Clementz et al., 2008;

Gadlage et al., 2009; Oostra et al., 2008). Glycosylation has many functions including protein folding, sorting, and trafficking (Helenius and Aebi, 2004). SARS-CoV nsp4 also has been demonstrated to be glycosylated *in vitro* at an atypical glycosylation site N_{131}IC (Oostra et al., 2008). All coronavirus nsp4 proteins tested to date contain at least one predicted glycosylation site. However, the location and number of the glycosylation sites varies (Figure I.7). Our lab previously generated an MHV nsp4 mutant lacking both glycosylation sites (N176A/N237A), referred to as DGM (double glycosylation mutant). The DGM virus exhibited delayed exponential replication, a reduction in RNA synthesis, and aberrant DMVs (Gadlage et al., 2009). These observations suggested a direct link between the capacity of the virus to induce stable DMVs and virus fitness. However, the relationship of DMV size and number to virus fitness has been questioned (Al-Mulla et al., 2014). Since nsp4 is directly involved in DMV formation, we tested the role of DGM and other mutations across nsp4 on the stability and number of DMVs. Additionally, we determined the fitness of these viruses over multiple passages as compared to wildtype and DGM. Our data demonstrate that mutations across nsp4 domains, in addition to glycosylation mutants, result in alterations of DMV morphology and number, and that loss of nsp4 glycosylation is clearly associated with fitness cost when directly competed. Jordan Anderson-Daniels, a coauthor on the publication associated with this chapter (Beachboard et al., 2014) (Appendix B), helped engineer Nx(S/T) mutations into the MHV B or C frag. Javier Galdon-Armero assisted with tunicamycin experiments. I performed all other experiments and analyzed all the results.

Results

DGM-FFL replicates indistinguishably from DGM

First, I sought to determine if aberrant DMVs were the result of loss of nsp4 glycosylation or due to mutations within nsp4. I wanted to test whether chemical inhibition of glycosylation would result in aberrant DMV formation. In order to test the effects of tunicamycin on viral replication, a firefly luciferase (FFL) reporter virus was engineered. Previously, a WT- FFL virus was generated with FFL fused to nsp2 (Freeman et al., 2014a). I generated the DGM virus in the background of WT-FFL (Figure IV.1). The virus was engineered using the MHV reverse genetics system. The FFL was inserted into the A fragment and the DGM mutations were introduced into nsp4 in the B fragment. The DGM-FFL virus was recovered and sequenced across FFL and nsp4 to ensure no additional mutations arose during virus recovery. FFL was intact and the DGM mutations were present. No additional mutations were identified in the two regions amplified.

To ensure that the addition of FFL did not effect viral replication, DBT cells were infected with WT, WT-FFL, DGM or DGM-FFL viruses at and MOI of 1 PFU/cell and supernatants were sampled over a 24 h time course (Figure IV.1). Viral titer at each time point was determined by plaque assay. WT and WT-FFL virus began exponential replication between 6 and 8 h p.i. and achieved peak viral tier at 12 h p.i. DGM exhibited a 2 h delay in exponential replication and achieved WT-like peak viral titer at 16 h p.i. The DGM-FFL virus replicated indistinguishably from the DGM virus. These data indicate that fusion of FFL to nsp2 had no effect on viral replication.

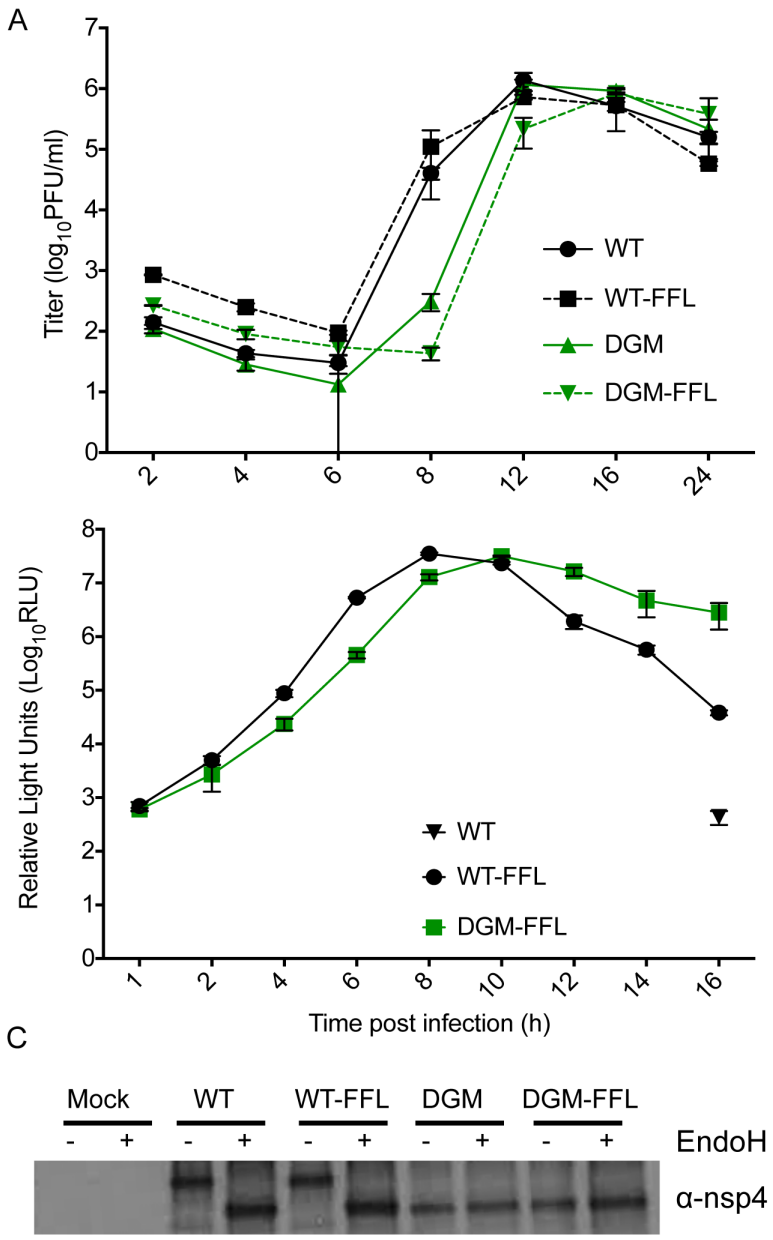

Figure IV.1 : Replication and expression of DGM-FFL

(**A**) DBT cells were infected with indicated viruses at an MOI of 1 PFU/cell, supernatants were sampled from 0-24h p.i., and titered by plaque assay. Error bars represent the SEM of three replicates plated in duplicate. (**B**) DBT cells were infected with indicated viruses at an MOI of 1 PFU/cell. At time points from 0-16 h p.i., cells were harvested in reporter lysis buffer and luciferase activity was assessed. Error bars represent the SEM of 3 replicates. (**C**) DBT cells were infected with indicated viruses at an MOI of 10 PFU/ cell for 4 h before starving in -Cys/-Met media supplemented with ActD. From 5-7 h p.i., cells were radiolabeled with [^{35}S]-Cys/-Met. nsp4 was immunoprecipitated and treated in the presence or absence of EndoH, and resolved by SDS-PAGE.

DGM-FFL produces luciferase with delayed kinetics compared to WT-FFL

To determine the luciferase production of the DGM-FFL virus, DBT cells were infected with WT, WT-FFL or DGM-FFL viruses for 16 h and cells were harvested and tested for luciferase activity (Figure IV.1). Luciferase activity could be detected as early as 2 h p.i. and peaks at 8 h p.i. for WT-FFL virus. The DGM-FFL virus produces luciferase with similar kinetics as WT-FFL but with a 2 h delay in peak luciferase expression. This demonstrates that the DGM-FFL virus is a sensitive tool for evaluation of viral replication.

DGM-FFL is not glycosylated

In order to demonstrate that the DGM-FFL nsp4 protein was not glycosylated, DBT cells were infected with WT, WT-FFL, DGM and DGM-FFL at an MOI of 10 PFU/cell. Cells were then radiolabeled with [^{35}S]-Met/-Cys and lysates were immunoprecipitated for nsp4. Samples were treated in the presence or absence of EndoH before proteins were resolved by SDS-PAGE and imaged by autoradiography. WT and WT-FFL nsp4 migrated at 44kDa in the absence of endoH and then exhibit a mobility shift to 39kDa in the presence of endoH. Both DGM- and DGM-FFL nsp4 migrated at 39kDa in both the presence and absence of endoH, indicating that the nsp4 proteins are not glycosylated.

Tunicamycin is tolerated by DBT cells

To test cytotoxicity of tunicamycin, DBT cells were treated with concentrations of tunicamycin that ranged from 0-1 μg/ml. Cells were then tested for viability using the CellTiterGlo assay (Figure IV.2). Cell viability was normalized to untreated control cells.

At least 80% of cells were viable for each concentration of tunicamycin tested. I conclude that tunicamycin is not toxic to cells at the concentrations used for these studies.

Tunicamycin inhibits nsp4 glycosylation

To test whether tunicamycin effectively inhibited glycosylation at 0.1 to 1 μg/ml concentrations, nsp4 glycosylation was analyzed (Figure IV.2). DBT cells were infected with WT virus at an MOI of 10 PFU/cell, radiolabeled with [^{35}S]-Met/-Cys, and cell lysates were harvested. Lysates were then immunoprecipitated with antibodies specific to nsp4. As a positive control for loss of glycosylation, a WT sample was treated in the presence or absence of EndoH. All samples were resolved by SDS-PAGE electrophoresis. At 0.1 μg/ml of tunicamycin, there were bands indicative of 0, 1, and 2 glycans, suggesting that tunicamycin is partially effective at this concentration. At both 0.5 and 1 μg/ml, there was complete inhibition of nsp4 glycosylation. For all subsequent experiments, 0.5μg/ml tunicamycin was used because this was the minimum effective dose tested.

Tunicamycin inhibits viral replication

To test the effect of tunicamycin on viral replication, DBT cells were infected with WT/WT-FFL or DGM/DGM-FFL viruses for 10 h and cells were harvested for analysis of luciferase activity or RNA synthesis and supernatants were collected to calculate titers (Figure IV.2). Luciferase activity was used to determine viral replication. Both viruses exhibited decreased luciferase compared to DMSO controls. However, the DGM-FFL virus was decreased compared to WT-FFL in the presence of tunicamycin. A similar effect was demonstrated with RNA synthesis where the DGM exhibited further decreased RNA synthesis compared to WT treated with tunicamycin. The data suggests

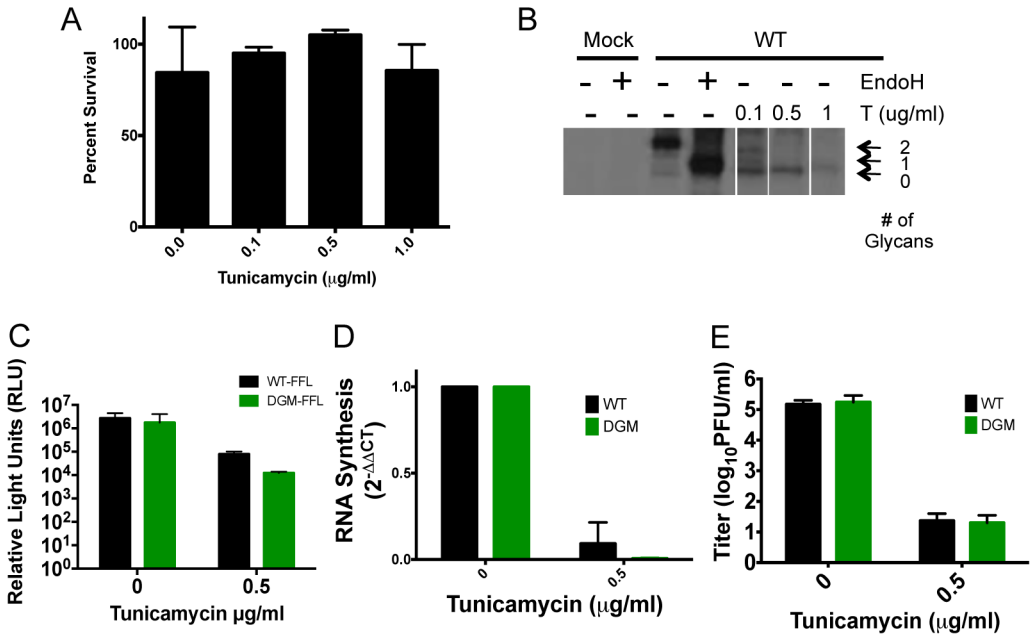

Figure IV.2: Effects of tunicamycin on viral replication.

(**A**) DBT cells were treated with increasing concentrations of tunicamycin in DMSO. At 24h p.t., cells were harvested and tested for viability using the CellTiter Glo Assay. (**B**) DBT cells were infected with WT virus at an MOI of 10 PFU/cell and treated with tunicamycin (T) for 4h before starving in -Cys/-Met media supplemented with ActD, and radiolabeled from 5-7h p.i. with [^{35}S]-Cys/-Met. As a control, nsp4 was immunoprecipitated and treated in the presence or absence of Endo and bands were resolved by SDS-PAGE. (**C-E**) Cells were infected with WT-FFL or DGM-FFL at an MOI of 1 PFU/cell and treated with 0.5 μg/ml tunicamycin from 0-2 h p.i. At 10 hp.i., cells were harvested in reporter lysis buffer and analyzed for luminescence (**C**), harvested in trizol for RNA extraction and qRT-PCR (**D**), or supernatants were collected and titered by plaque assay (**E**).

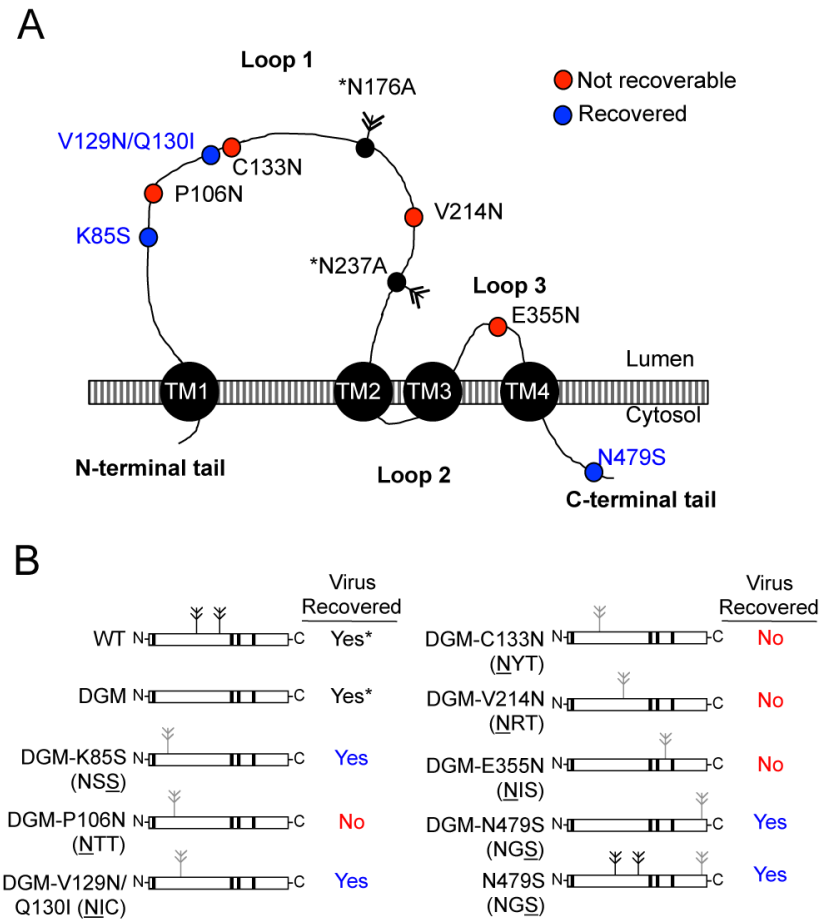

Figure IV.3: Engineering nsp4 mutants.

(A) Proposed topology of nsp4: nsp4 has 4 transmembrane regions (TM1-4, black circles) and three loops (loop 1-3). Mutations in nsp4 tested in this study are shown on the diagram. Red circles represent non-viable mutations, blue circles represent viable viruses that were recovered in this study. The double-headed arrows represent native glycosylation sites within MHV-nsp4. **(B)** nsp4 mutants were engineered with alternate NXS/T sites (grey double-headed arrows) in the DGM background. The location of the introduced NXS/T sequons (grey double-headed arrows) are shown. Virus nomenclature is listed with the introduced NXS/T site shown below. * Indicates previously recovered viruses (11, 19).

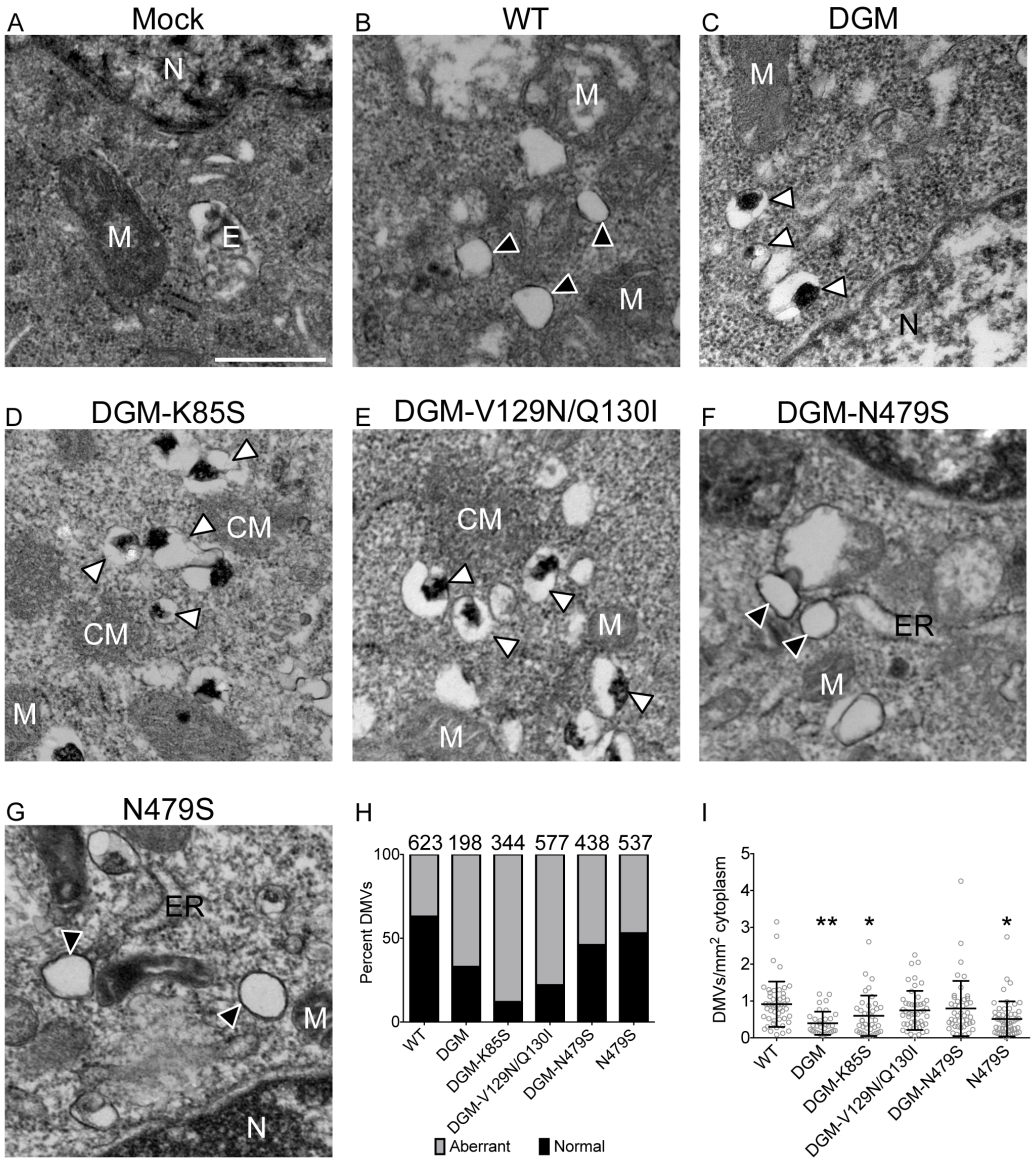

Figure IV.4: Electron microscopic analysis of alternate Nx(S/T) sequon mutants. **(A-F)** DBT cells were mock-infected **(A)** or infected with WT **(B)**, DGM **(C)**, DGM-K85S **(D)**, DGM-V129N/Q130I **(E),** DGM-N479S **(F)** or N479S **(G)** viruses at an MOI of 5 PFU/cell for 8h before being fixed in 2% gluteraldehyde and processed for TEM. Black arrowheads denote normal DMVs, the white arrowheads represent aberrant DMVs. CM, convoluted membranes; N, nucleus; M, mitochondrion; E, endosome. Scale bar is 500 nm. **(H)** Normal and aberrant DMVs were calculated for each virus. Percent of total DMVs that are normal are shown in black and the percentage of DMVs that are aberrant is shown in grey. The total number of DMVs analyzed is shown above each bar. **(I)** The number of DMVs per area of cytoplasm were calculated and shown on the graph. Each circle represents and individual field and the bars show the mean ± standard deviation. The Kruskal-Wallis test was used to analyze for significant differences in number of DMVs per area of cytoplasm. * ($p = 0.008$) and ** ($p < 0.0001$) indicate statistical difference compared to WT.

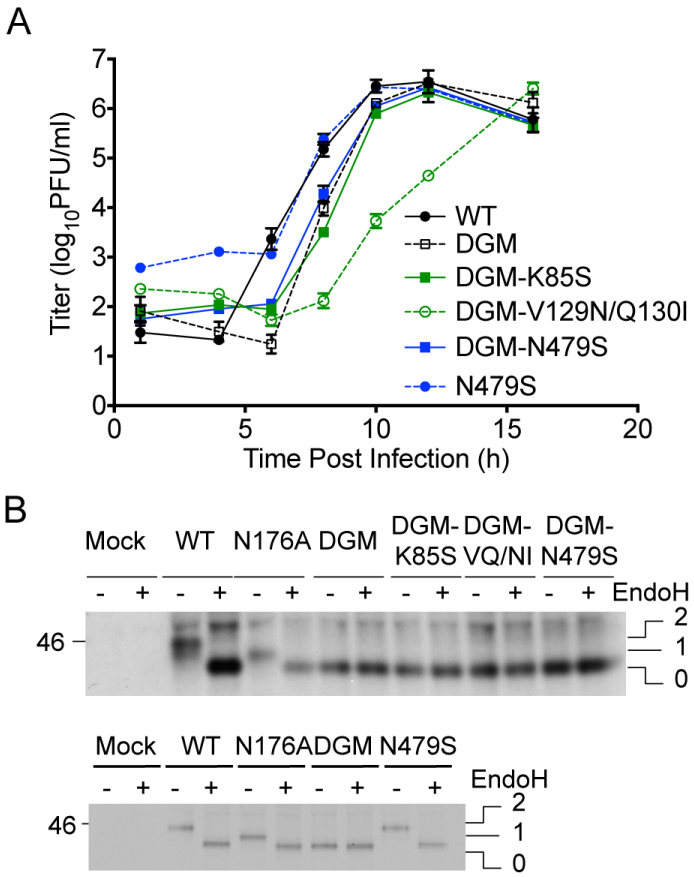

Figure IV.5: Replication kinetics and glycosylation of alternate Nx(S/T) sequon viruses.

(A) DBT cells were infected with indicated viruses at an MOI of 1 PFU/cell. Supernatants were sampled form 0 to 16 h p.i. and titered by plaque assay. Error bars represent the SEM of three replicates plated in duplicate. **(B)** DBT cells were infected with indicated viruses at an MOI of 10 PFU/cell. At 4 h p.i., cells were starved in -Met/-Cys DMEM and treated with ActD for 1 h before radiolabel with [^{35}S]-Met/-Cys. At 7h p.i., lysates were harvested and immunoprecipitated with antibodies specific for nsp4 and treated in the presence or absence of EndoH. Proteins were resolved by SDS-PAGE. n≥2. DGM-VQ/NI, DGM-V129N/Q130I.

that tunicamycin has an independent effect on viral replication. It is possible that there are cellular or other viral proteins that are required for replication that contain glycosylation sites. Additionally, there was a significant impact on virus titer when cells were treated with tunicamycin. The decrease in viral titer is consistent with the literature that demonstrated that the spike protein requires glycosylation for function (Rottier et al., 1981). These data suggest that the secreted virus is not infectious. Based on these results, further EM experiments were not pursued because it would be difficult to distinguish the effects of loss of nsp4 glycosylation from loss of glycosylation on other proteins required for DMV formation and the defect in viral replication.

Mutations across nsp4 impair DMV morphology and numbers.

In order to test whether nsp4 glycosylation regulates proper DMV formation independent of its position in the protein, we engineered mutations to introduce a glycosylation sequon, Nx(S/T) at different locations in the nsp4-DGM (double glycosylation mutant (N176A/N237A)) background (Figure IV.3). Two viruses were engineered to insert predicted glycosylation sites from other coronaviruses; V129N/Q130I is the glycosylation sequon of SARS-CoV, and the sequon introduced by N479S is present in both HCoV-OC43 and Bovine CoV (BoCV). All other mutations were inserted near highly conserved asparagine, serine or threonine residues to introduce the new Nx(S/T) sequons (Figure IV.3). Both strategies have successfully been used to introduce glycosylation sites into other proteins (Chang et al., 1994; Hresko et al., 1994; Popov et al., 1997; Vagin et al., 2005). We recovered three mutants in the DGM background and one in the WT background; viruses that contain Nx(S/T) mutations from other coronaviruses (DGM-V129N/Q130I and DGM-N479S), as well as one that was

introduced after a conserved asparagine (DGM-K85S). Additionally, N479S was recovered in the WT-nsp4 background. Recovered viruses were sequenced across nsp3 through nsp6 and found to contain no additional mutations. Recovery of all other engineered genomes were attempted at least three times with no signs of virus-induced CPE.

To determine whether the mutations that introduce potential alternate glycosylation sequons restored proper DMV morphology, murine delayed brain tumor (DBT) cells were infected with WT or nsp4 mutant viruses and analyzed for membrane changes by TEM (Figure IV.4). Mock-infected cells exhibited regular cellular architecture and normal organelles. WT-infected cells displayed swollen ER and Golgi, as well as the presence of several virus-induced structures including DMVs, convoluted membranes (CM), and vesicles containing newly-formed virions (Figure IV.4). The DMVs in WT-infected cells have membranes containing two lipid bilayers in close proximity to one another. Similarly, DGM-infected cells have swollen ER and Golgi but the DMVs are aberrant. Aberrant DMVs in this study are defined as having inner membranes that are separated, or collapsed away from the outer membrane. The degree of inner membrane collapse varied. However, the majority of aberrant DMVs inner membranes were completely collapsed and appeared as an electron dense structure at one side of the vesicle. This is in contrast to the DMV artifacts with spider web-like content seen with standard EM of SARS-CoV infected cells (Snijder et al., 2006). All DMVs considered normal in this study have both lipid-bilayers intact and contain no spider web-like contents. Each of the viruses that contain engineered Nx(S/T) sequons exhibited aberrant DMVs similar to the DGM virus. The number of normal and aberrant DMVs

was calculated for each virus. DGM-K85S- and DGM-V129N/Q130I-infected cells produced increased numbers of aberrant DMVs (88% and 78% respectively) compared to DGM (67%) (Figure IV.4 and Table IV.1). Cells infected with DGM-N479S and N479S produced fewer aberrant DMVs (54% and 53% respectively) than DGM, but more aberrant DMVs than WT (37%). Next, the number of DMVs per area cytoplasm was calculated to determine whether the differences in total number of DMVs counted per sample correspond to differences in total numbers of DMVs (Figure IV.4). DGM, DGM-K85S and N479S had significantly decreased number of DMVs compared to WT (Figure IV.4). The differences in total numbers of DMVs may be due to direct effects of

Table IV.1: Quantification of normal and aberrant DMVs.

Virus	Total DMVs	Normal DMVs	Aberrant DMVs (percentage)
WT	623	393	230 (37%)
DGM	198	65	133 (67%)
DGM-K85S	344	40	304 (88%)
DGM-V129I/Q130I	577	126	451 (78%)
DGM- N479S	438	202	236 (54%)
K44A/D47A	308	101	207 (67%)
E226A/E227A	326	96	230 (71%)
N258T	412	128	284 (69%)
N479S	587	310	277 (53%)

mutations in nsp4 or may reflect differences in the degree of viral replication occurring. These data demonstrate that inserting additional mutations within loop 1 of nsp4 exacerbates the aberrant DMV formation associated with the DGM phenotype. Additionally, these data demonstrate that mutations within the C-terminus of nsp4 cause aberrant DMVs independent of mutations within loop 1.

Nsp4 Nx(S/T) sequons do not complement defects in replication or nsp4 glycosylation.

Next we sought to determine whether the viruses with aberrant DMVs were associated with altered replication kinetics. DBT cells were mock-infected or infected with viruses at an MOI of 1 PFU/cell. At indicated times, supernatants were sampled and titered by plaque assay (Figure IV.5). WT virus began exponential replication between 4-6 h p.i. and achieved peak titer at 10 h p.i. The DGM virus replicated with delayed kinetics, began exponential replication between 6-8 h p.i., and achieved WT-like peak titer at 12 h p.i. N479S replicated indistinguishably from WT, and the DGM-K85S and DGM-N479S viruses replicated indistinguishably from the parental DGM virus. The DGM-V129N/Q130I mutant displayed delayed exponential replication and peak titer compared with both WT and the parental DGM virus.

These data suggested that glycosylation at alternate residues did not complement the replication delay of DGM. Alternatively, these nsp4 proteins were not glycosylated. To determine the glycosylation status of the mutant nsp4 proteins, virus-infected cells were radiolabeled, and the cell lysates were immunoprecipitated with antibodies specific for nsp4 followed by treatment with EndoH to remove N-linked glycans (Figure IV.5). WT nsp4 migrated at 44kDa in the absence of EndoH, and displayed a mobility shift to 39kDa following EndoH treatment, indicative of the removal of two glycans. The N176A virus is glycosylated at one site (42kDa) and DGM lacks glycosylation and migrated at 39kDa. In contrast, all of the alternate Nx(S/T) mutant viruses in the DGM background migrated at 39kDa regardless of EndoH treatment, indicating that the mutant nsp4 proteins were not glycosylated. The N479S nsp4 protein migrated at 44kDa in absence of

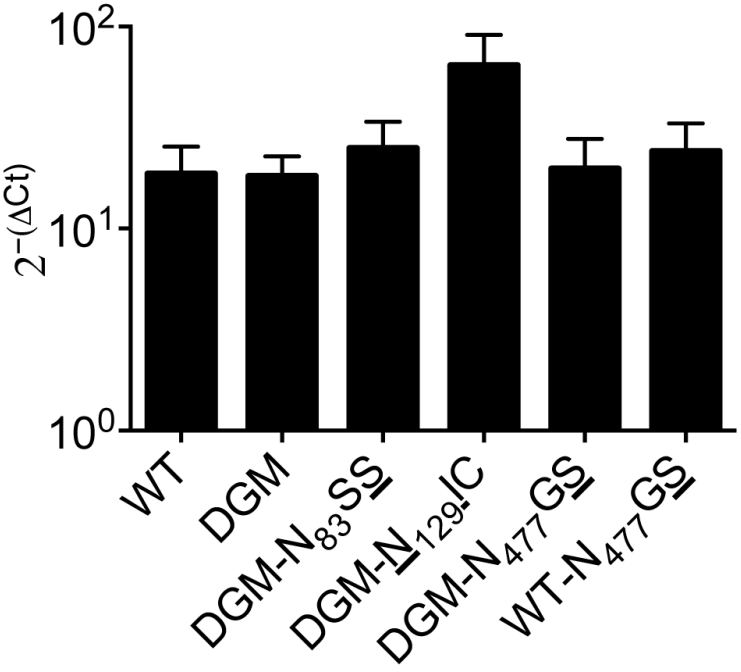

Figure IV.6: RNA Synthesis of nsp4 Nx(S/T) mutants.

DBT cells were infected with indicated viruses at an MOI of 1 PFU/cell for 10 h. Cells were then harvested in TRIzol and genomic RNA was extracted. Genomic RNA levels were determined by qRT-PCR using primers specific to Orf1a. RNA levels were normalized using $2^{-\Delta Ct}$ to endogenous GAPDH expression. Mean values ± S.E.M. are shown, n≥3. Values are not significantly different from WT using the Kruskal-Wallis test.

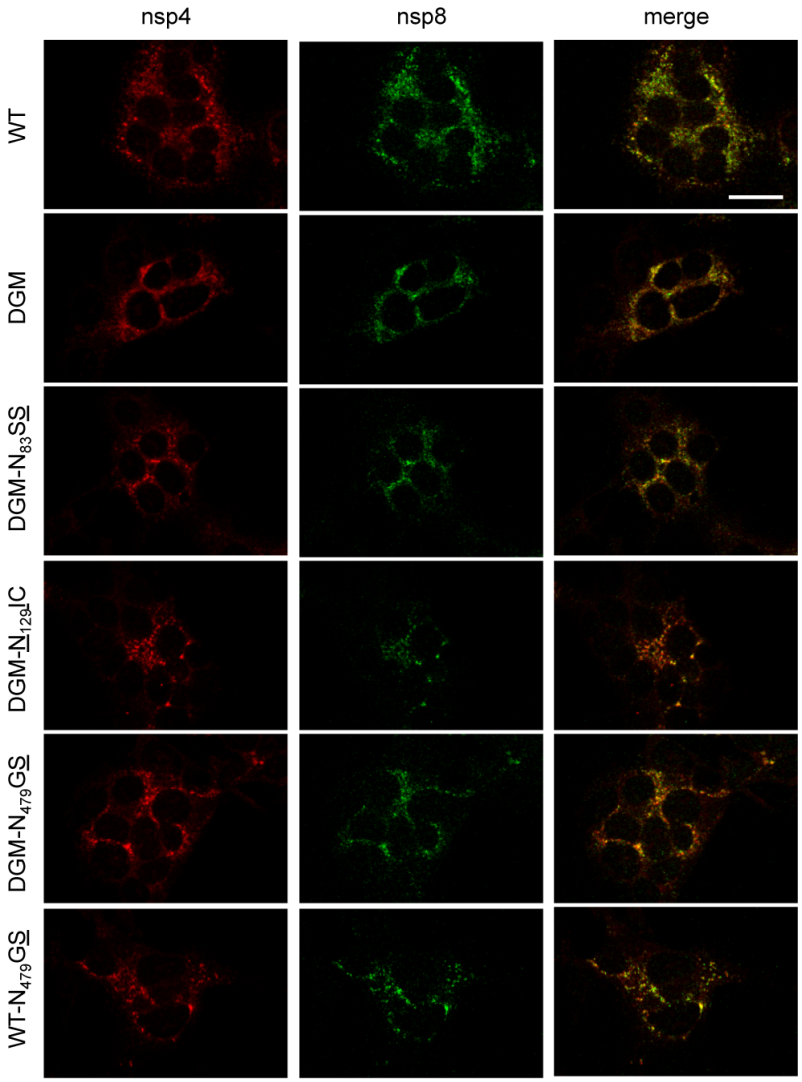

Figure IV.7: Immunofluorescence of nsp4 Nx(S/T) mutants.

DBT cells w were infected with indicated viruses at an MOI of 5 PFU/cell for 6.5 h. Cells were then fixed in 100% methanol and stained with antibodies specific for nsp4 (red) and nsp8 (green). Yellow pixels represent colocalization of red and green pixels. Scale bar represents 20μm.

EndoH and shifted to 39kDa in the presence of EndoH, suggesting that this nsp4 protein is glycosylated at the native glycosylation sites only. While we can draw no conclusions from inability to recover virus mutants, we did observe that all recovered viruses did not confer glycosylation at the introduced sequon, whereas compared with a large number of mutations that are tolerated in nsp4, several attempted new Nx(S/T) sequons in loop 1 could not be recovered after multiple attempts. The results led us to consider the possibility that sequons capable of glycosylation may not be tolerated in loop 1.

Nsp4 Nx(S/T) mutants have WT-like RNA synthesis.

Since the differences in total DMV numbers demonstrated by EM may reflect overall differences in viral replication, next we assessed the RNA synthesis capacity of these viruses. DBT cells were infected at an MOI of 1 PFU/cell for 10 h. Total cellular RNA was harvested in TRIzol and qRT-PCR performed to amplify nsp10 and GAPDH. All viruses have RNA synthesis levels indistinguishable form WT (Figure IV.6). It is likely that similar to replication kinetics, if time points were taken, there would have been a delay in RNA synthesis. This data suggests that the viruses have no significant decrease in viral replication at 10 h p.i. and that aberrant DMVs are capable of supporting RNA synthesis.

Nsp4 Nx(S/T) mutants localize to the replication complex.

In order to determine whether differences in total numbers of DMVs corresponds to differences in replication complex formation and overall protein levels, DBT cells on coverslips were infected with WT or the nsp4 Nx(S/T) viruses at an MOI of 5 PFU/cell for 6.5 h (Figure IV.7). Cells were then fixed in methanol and stained with antibodies specific to nsp4 and nsp8, a marker for the replication complex. In WT-infected cells,

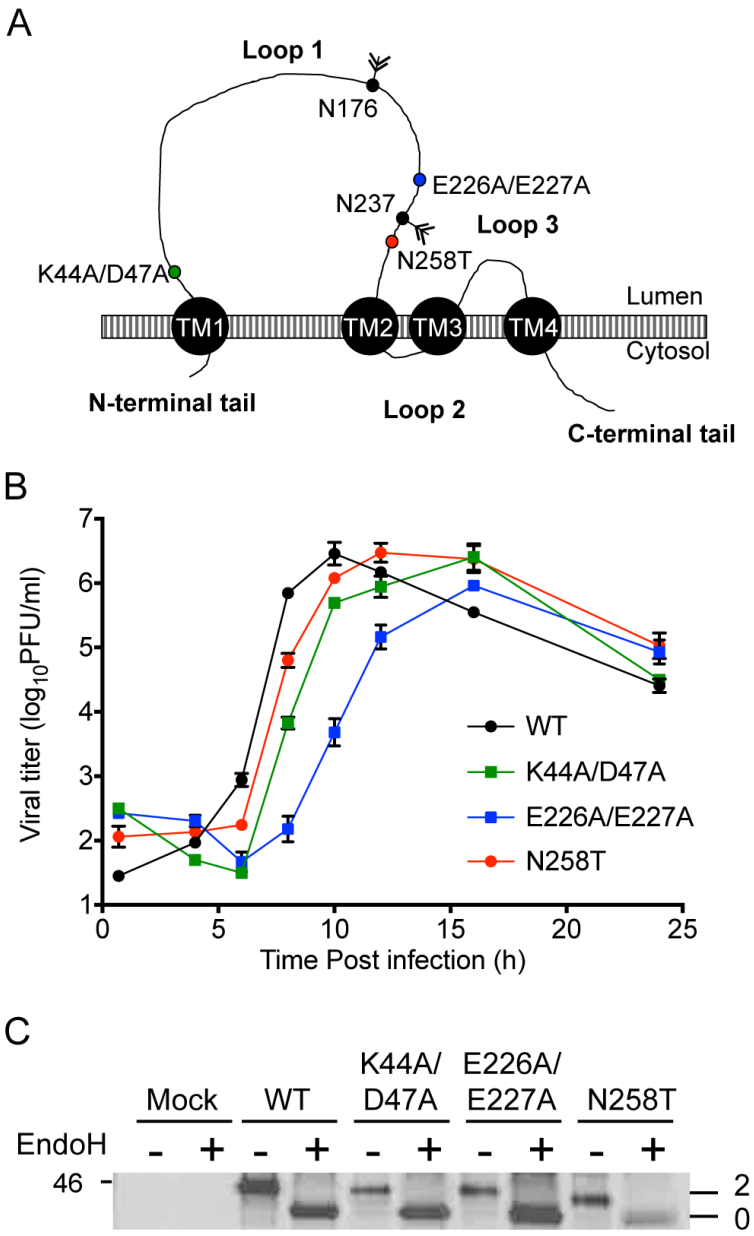

Figure IV.8: Replication and glycosylation of nsp4 mutants.

(A) Schematic of nsp4 showing the location of the nsp4 mutations. **(B)** DBT cells were infected with indicated viruses at an MOI of 1 PFU/ml for 24 h. At indicated time points, supernatants were sampled and titered by plaque assay. Error bars represent the SEM of three replicates plated in duplicate. **(C)** DBT cells were infected with indicated viruses at an MOI of 10 PFU/cell. Cells were starved with -Cys/-Met DMEM in presence of ActD for 1h prior to radiolabel with [^{35}S]-Cys/-Met for 2h before lysates were harvested. Lysates were immunoprecipitated with antibodies specific to nsp4 in the presence or absence of EndoH and proteins were resolved by SDS-PAGE. n≥2

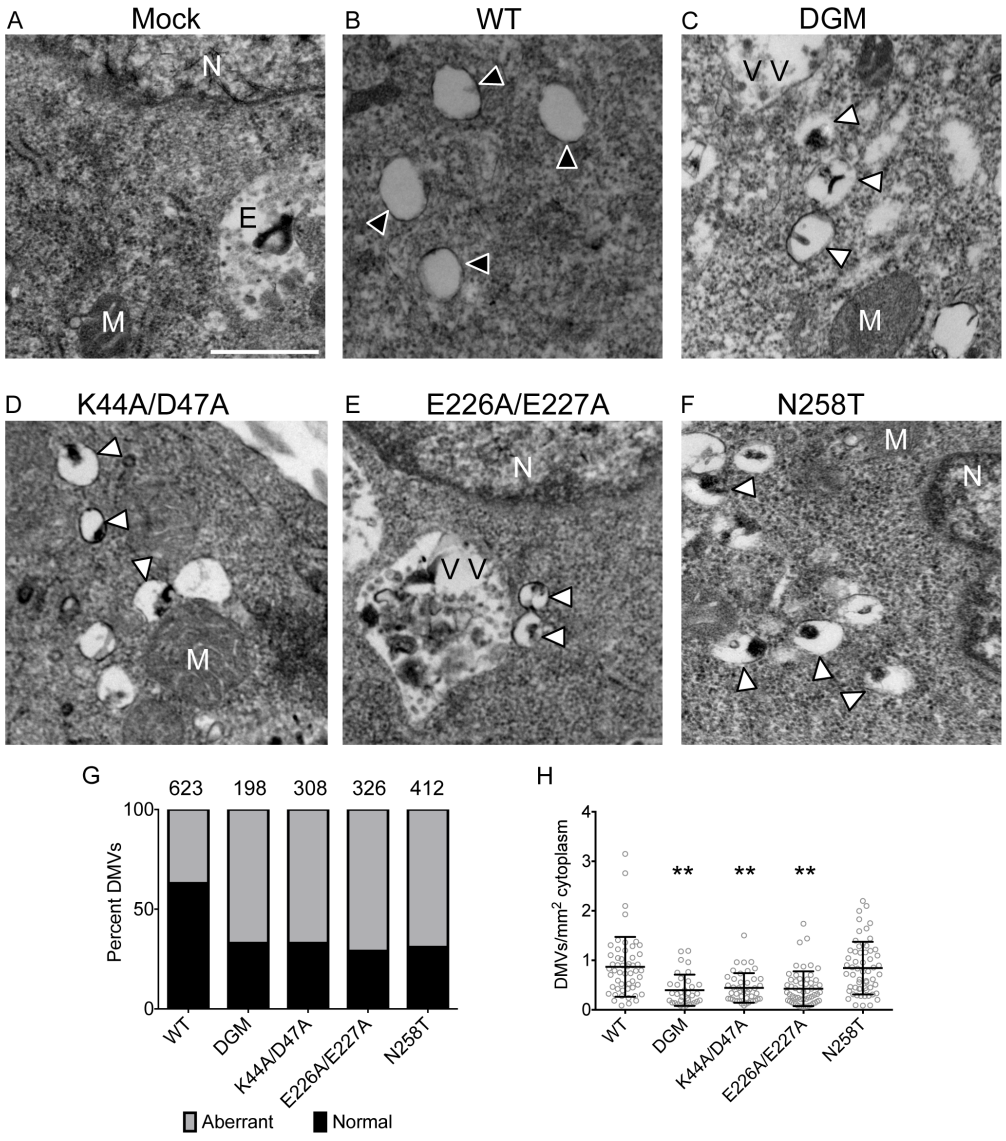

Figure IV.9: EM of nsp4 mutant-infected cells.

(A-F) DBT cells were mock infected **(A)** or infected with WT **(B)**, DGM **(C)**, K44A/D47A **(D)**, E226A/E227A **(E)**, or N258T **(F)** viruses for 8 h before fixation in 2% gluteraldehyde and processed for TEM. Black arrowheads are normal DMVs and white arrowheads are aberrant DMVs. CM, convoluted membranes; N, nucleus; M; mitochondrion. **(G)** Normal and aberrant DMVs were calculated and shown as percentage of total DMVs. Normal DMVs are shown in black and aberrant DMVs are shown in grey. The total number of DMVs analyzed is shown above the bar. **(H)** Total number of DMVs per area of cytoplasm was calculated. Circles represent the number of DMVs per area of cytoplasm for a single field. Bars represent the mean ± standard deviation. The Kruskal-Wallis test was used to analyze for significant differences in number of DMVs per area of cytoplasm. * ($p = 0.008$) and ** ($p < 0.0001$) indicate statistical difference compared to WT.

nsp4 and nsp8 colocalize at punctate perinuclear foci. All mutant nsp4 protein extensively colocalize with nsp8 at perinuclear foci. This data demonstrates that the Nx(S/T) mutant nsp4 proteins localize to the replication complex. Additionally, there is no apparent correlation between aberrant DMV formation and the level of replication complex formation or protein expression. Collectively, the RNA synthesis and immunofluorescence data indicate that the difference in total numbers of DMVs does not reflect overall replication or protein expression within these infected cells.

Substitutions in nsp4 loop1 alter replication kinetics and DMV morphology independent from glycosylation status.

Having demonstrated that mutations in nsp4 loop 1 exacerbate aberrant DMV morphology associated with the DGM phenotype, we tested whether any mutation in nsp4 loop 1, independent of glycosylation potential, impacted replication and DMV morphology/numbers. Nsp4 loop 1 mutants previously reported from our lab were tested (Figure IV.8): K44A/D47A (VUJS11), E226A/E227A (VUJS17), and N258T (Beachboard et al., 2013; Sparks et al., 2007). In contrast to WT MHV-A59, all three mutant viruses exhibited a range of replication defects. The N258T mutant was minimally delayed but achieved WT-like titers. The K44A/D47A mutant showed an increase in the delayed exponential replication and decreased peak titer. The E226A/E227A mutant showed a significant delay but achieved WT like peak titer (Figure IV.8). We then tested the glycosylation status of the mutant nsp4 proteins by radiolabel and immunoprecipitation. All nsp4 loop 1 mutant nsp4 proteins migrated at 44kDa in absence of EndoH and at 39kDa in the presence of EndoH. These results show that all tested nsp4 loop 1 mutants are glycosylated at both native asparagine residues. Thus the

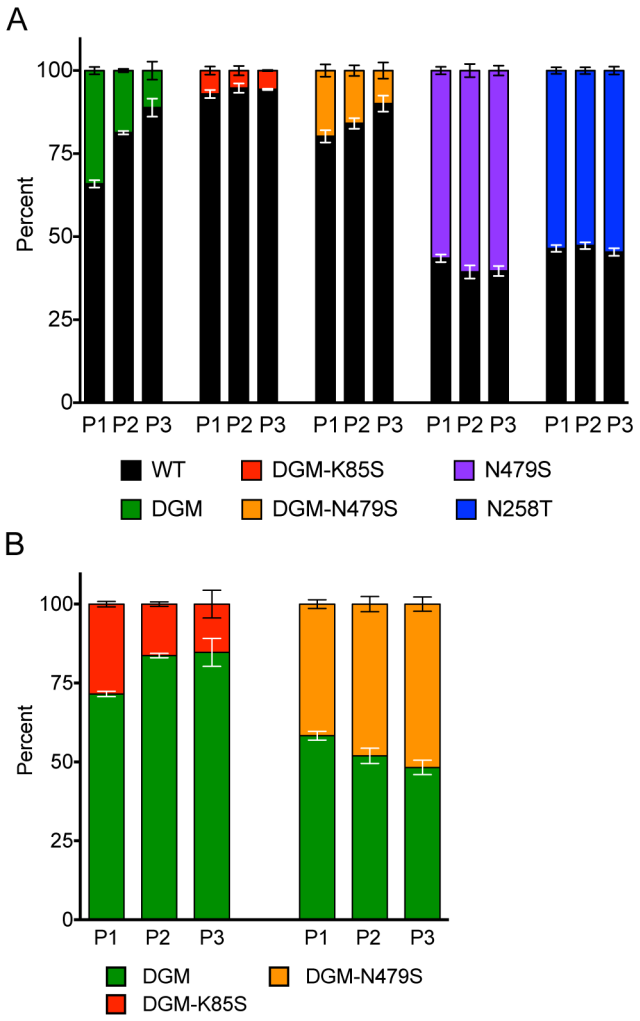

Figure IV.10: Competition Assay of nsp4 mutants.

DBT cells were infected with indicated pairs of viruses at a total MOI of 0.1 PFU/cell at a 1:1 ratio. When cells were at least 50% involved in cytopathic effect, supernatants were collected and cell monolayers were harvested in TRIzol. Supernatants were used for subsequent passage for a total of three passages. Total RNA was extracted and nsp4 amplicons were generated by RT-PCR and sequenced. For residues of interest, area under the peak was calculated using MacVector 13. Then the percentage of nucleotides of virus A to virus B was calculated and plotted on the graph. Error bars represent SEM, n≥2.

observed replication defects were not due to changes in glycosylation status of the protein. Finally, we examined the DMV morphology and numbers in mutant virus infected cells (Figure IV.9 and Table IV.1). Similar to the N479S mutation alone, each of the nsp4 mutant virus-infected cells produced aberrant DMVs. The percentage of aberrant DMVs was calculated for each virus and was increased compared to WT. All of the loop 1 mutant viruses produced numbers of aberrant DMVs similar to the DGM mutant. Infection with K44A/D47A and E226A/E227A also resulted in significantly fewer DMVs than WT virus. In contrast, N258T produced similar number of DMVs to WT. Thus, our results indicate that in addition to mutations that affect glycosylation of nsp4, substitutions at other locations in nsp4 loop 1 result in altered DMV morphology.

Loss of nsp4 glycosylation results in decreased virus fitness.

We next tested the effect of nsp4 mutations on virus competitive fitness. In order to test the fitness of nsp4 mutant viruses compared to WT or DGM, DBT cells were co-infected at a ratio of 1:1 and passaged three times at 37°C (Figure IV.10A). The N258T and N479S viruses competed equally with WT and were maintained ~50 percent of the population. In contrast, viruses lacking glycosylation of nsp4 exhibited profoundly decreased fitness compared to WT and were ~10 percent of the population at passage three. We next competed DGM-K85S and DGM-N479S with DGM, to test the effects of additional mutations within the DGM virus on fitness (Figure IV.10B). When K85S was introduced into DGM-nsp4 loop 1 (DGM-K85S), virus fitness was further deceased relative to DGM. However, DGM-N479S competed equally with DGM and each remained approximately 50 percent of the population. The results suggest that the decrease in fitness of DGM-N479S compared to WT is likely due to the DGM phenotype

and that the N479S mutation does not alter virus fitness. Collectively these data demonstrate that loss of nsp4 glycosylation is associated with a substantial decrease in virus fitness that can then be further decreased by introduction of additional mutations into the DGM-nsp4 loop 1.

Discussion

The role of host cytoplasmic membrane modifications in coronavirus replication and fitness is a subject of increasing investigation and interest for understanding replication, pathogenesis, and a target for broad-spectrum inhibition of coronavirus infection. Recently, nsp3, nsp4, and nsp6 have been shown to mediate membrane modifications during individual and co-expression in cells (Angelini et al., 2013). Recent studies with a novel inhibitor have shown that drugs targeting coronavirus membrane modifications are associated with profoundly impaired replication (Lundin et al., 2014). Studies have shown that nsp4 is necessary for DMV formation and that mutations at nsp4 glycosylation sites result in aberrant DMVs (Angelini et al., 2013; Gadlage et al., 2009). In this study, I show that mutations across nsp4, independently or in combination with mutations that abolish glycosylation, cause or exacerbate defects in DMV formation. Further I show that loss of nsp4 glycosylation is associated with a substantial fitness cost.

Intact nsp4 is required for proper DMV morphology.

We previously reported that mutations in nsp4 loop 1 were important for efficient RNA synthesis (Sparks et al., 2007). We also described glycosylation of nsp4 at N-linked glycosylation sites in loop one and the negative effect on DMV formation by elimination of these sites (Gadlage et al., 2009). Our current results indicate multiple residues and domains within nsp4, including the C-terminal non-TM domain, impact DMV

morphology, rather than glycosylation alone. In addition, mutations in other regions of nsp4 loop 1 exacerbated changes in membrane structures of the DGM virus. Angelini *et al.* demonstrated that when co-expressed, nsp3 and nsp4 have the capacity to pair membranes (Angelini et al., 2013). Nsp3 and nsp4 likely interact across the DMV lipid bilayer to hold both membranes in close proximity. In this model, any perturbation of the nsp3-nsp4 interaction would result in separations of the inner and outer membranes. Our present results support that it is possible to dysregulate nsp4 functions in DMV formation by mutations at several locations in nsp4 loop 1, as well as, other locations including the C-terminal 10 kDa region, that is not predicted to be luminal or transmembrane. Since the mutation in the C-terminus induced aberrant DMV formation, this would suggest that the nsp4 C-terminus also is involved in DMV formation or stability after formation. We previously have demonstrated the nsp4 C-terminal 10 kDa portion of the protein is dispensable for viral replication in culture (Sparks et al., 2007). The crystal structure of the C-terminus of nsp4 for MHV A59 and Feline CoV have been determined and are structurally conserved (Manolaridis et al., 2009; Xu et al., 2009). The N479S residue maps to a surface exposed loop in the MHV A59 C-terminus crystal structure (Figure IV.11). The DMV morphology phenotype was the same between N479S and DGM-N479S, even though the viruses exhibit differences in replication kinetics (Figure IV.4 and Figure IV.5). This suggests that even mutations that do not effect viral replication can alter DMV morphology and numbers. Our data, in combination with other studies suggests that DMV presence and not morphology is critical for efficient viral replication (Lundin et al., 2014; Prentice, 2003).

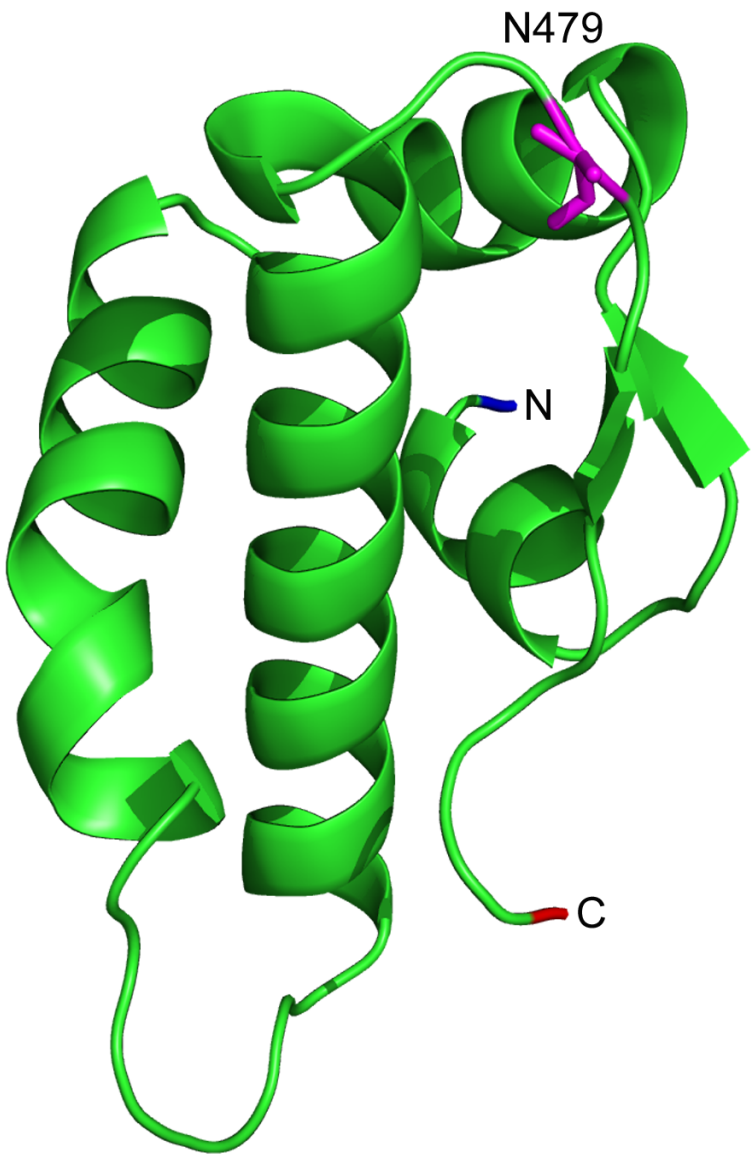

Figure IV.11: Structure of the MHV-nsp4 C-terminus.
The crystal structure of the c-terminus of MHV-nsp4 is shown (PDB:3VC8). N-terminal portion of the protein is blue and the C-terminus is in red. Highlighted in pink is the N479 residue that is located in a surface exposed loop.

Membrane modifications and virus fitness

All published studies to date are similar in demonstrating that disruption of "normal" DMV formation is not necessarily lethal to virus replication, and likely represents an evolutionarily optimized process for maximum organization of replication components (Al-Mulla et al., 2014; Gadlage et al., 2009; Lundin et al., 2014; Prentice, 2003). However, the directly attributable role of DMVs in virus replication and fitness has recently been called into question by a study by Al-Mulla *et al*. which used temperature-sensitive (ts) mutants in multiple replicase proteins to study the relationship of DMV size and number to virus fitness (Al-Mulla et al., 2014). In our study, we tested whether mutations within nsp4, one of the proteins directly involved in DMV formation and stability, affect DMV morphology and viral fitness. Our results support the conclusions of Al-Mulla *et al.* by demonstrating that alterations in DMV morphology and total numbers are not associated with a fitness cost compared to WT virus (WT versus N258T or N479S; Figure IV.10). Previously we observed that mutation of the nsp4 glycosylation sites alter DMV morphology and the current study extends the result by demonstrating that loss of nsp4 glycosylation is associated with a substantial fitness cost. We cannot conclude that the decreased fitness is due to changes in DMV morphology or numbers because mutations across nsp4 that do not alter virus fitness cause aberrant DMVs and decreased numbers regardless of location.

The relationship DMVs to viral replication remains complex. Multiple mutations in nsp4, particularly loop 1, have significant affects on viral replication. Additionally, a small molecule inhibitor was identified that prevents coronavirus DMV formation likely by targeting nsp6 (Lundin et al., 2014). The inhibitor profoundly knocked down virus

replication demonstrating that DMVs are linked to virus replication. The mechanisms of DMV formation and how the small molecule inhibits DMV formation remain unknown. Understanding how viruses induce membrane modifications and form replication complexes will help better design antivirals to target this process. This work emphasizes the role of nsp4 loop 1 in the proper formation of DMVs and identifies nsp4 glycosylation as putative targets for antiviral therapy.

CHAPTER V: CORONAVIRUS NSP4 IS PRESENT AS NSP4-5 AND NSP4-NSP5-NSP6 POLYPROTEIN INTERMEDIATES

Introduction

CoV genomes, which are 26-32kb in length, encode two replicase ORFS 1a and 1b which are translated into the polyproteins 1a and 1ab and incorporate nonstructural proteins 1-16 (nsps 1-16) (Figure V.1). The replicase polyproteins are cleaved by virus-encoded proteases within nsp3 (PLP1/2) and nsp5 (3CLpro). The nsp5 protease is responsible for 11 cleavage events that liberate nsp4 through nsp16 (Y. Lu et al., 1995). Biochemical studies have demonstrated that nsp5 requires dimerization for activity. To form a mature dimer, nsp5 must be cleaved from the polyprotein (S. Chen et al., 2007; Shi et al., 2008). Based on *in vitro* data, it is predicted that nsp5 autocleaves from the polyprotein first (S. Chen et al., 2010), which would result in mature nsp4, nsp5, and potential nsp6-nsp10/nsp16 precursors. Nsp5 exists as two known polyprotein precursors, nsp4-10 (p150) and nsp7-10 (Deming et al., 2007; Kanjanahaluethai and Baker, 2001).

While preforming immunoprecipitation experiments described in Chapter IV, I identified two bands, in addition to nsp4, that migrated differently in the presence of EndoH. Experiments described in this chapter are aimed at the identification of the 68kDa and 88kDA bands as an nsp4-nsp5 and an nsp4-nsp5-nsp6 precursors, respectively. I performed all experiments described in this chapter.

Results

Nsp4 is glycosylated in intermediate processed polyprotein precursors.

MHV nsp4 exists in a nsp4-10 precursor (Kanjanahaluethai and Baker, 2001). Proteolytic cleavage between nsp4 and nsp5 has been proposed to be the first nsp5-

mediated processing event, arguing that nsp4 exists only as an nsp4-10 precursor or mature nsp4 (S. Chen et al., 2010; Kanjanahaluethai and Baker, 2001). Since nsp4 likely interacts with nsp3 and nsp6, we sought to determine whether nsp4 is present in other intermediate forms, and whether nsp4 is inserted in the ER lumen before, during, or after processing from the polyprotein. To answer this question, we determined the glycosylation state of nsp4 in cells infected with WT MHV-A59 and with engineered mutants lacking both the N176 and N237 glycosylation sites (referred to as Double Glycosylation Mutants or DGM) (Gadlage et al., 2009) by the mobility shift associated with loss of glycosylation following treatment with endoglycosidase H (EndoH) (Figure V.2). As previously reported, mature WT nsp4 showed a large mobility shift when treated with EndoH, consistent with the loss of two N-linked glycans (Gadlage et al., 2009). In contrast, both EndoH-treated and -untreated DGM nsp4 migrated with a similar mobility, suggesting no change in glycosylation status following EndoH treatment. In addition to mature nsp4 and the nsp4-10 precursor, two previously unknown proteins were detected by nsp4-specific antibodies (Figure V.2A). The first band that was identified shifted from 68kDa to 62kDa in the presence of EndoH in WT-infected cells. This band migrated at 62kDa for DGM-infected cell lysates in both the presence and absence of EndoH. Both the lack of a mobility shift following EndoH treatment of the DGM lysates and the apparent molecular weight of 68kDa

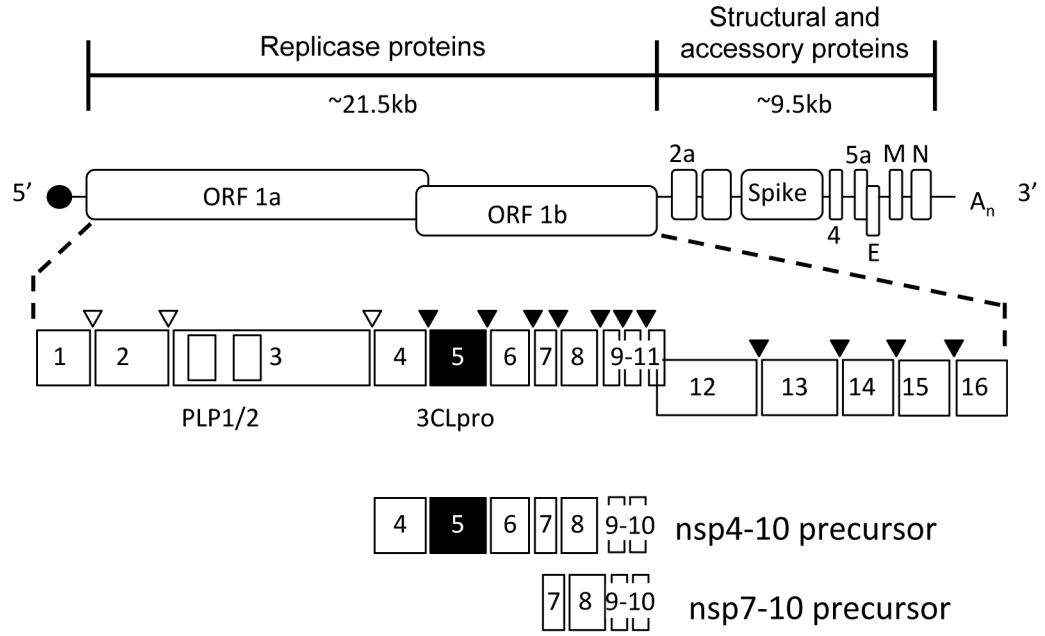

Figure V.1: CoV genome organization and polyprotein processing.
Schematic of the MHV genome. The MHV genome contains seven genes. The replicase gene encodes 16 nonstructural proteins that are translated into a large polyprotein that is cleaved by the virally encoded proteases, nsp3 and nsp5. Below are the two known polyprotein precursors, nsp4-10 and nsp7-10.

suggested that this band was an nsp4-5 precursor. To test this, we immunoprecipitated proteins with antibodies specific to nsp5 in the presence and absence of EndoH, resulting in detection of both the 68 and 62kDa bands (Figure V.2B), confirming that the 68kDa protein represents a previously unidentified nsp4-5 precursor protein. Additionally, nsp4- and nsp5-specific antibodies detected a protein in WT-infected cells that migrated at 88 kDa but shifted to 81 kDa in the presence of EndoH, consistent with an nsp4-5-6 precursor. Though nsp6-specific antibodies were not available to directly test this, there is no other possible combination of proteins containing both nsp4-5 that could account for this protein size. Both nsp4- and nsp5-specific antibodies consistently detected a visible mobility shift of the known 150 kDa nsp4-10 precursor band in WT-infected cells treated with EndoH. In agreement with the inclusion of nsp4 in the nsp4-5 and nsp4-5-6 precursors, EndoH treatment of immunoprecipitated proteins following infection with DGM did not result in a mobility shift. Collectively, these data demonstrate that nsp4 is glycosylated as a polyprotein precursor and suggest that the nsp4-10 precursor is inserted into ER lumen before polyprotein processing. These data also demonstrate that subsequent processing results in both nsp4-5-6 and nsp4-5 intermediates, in addition to mature nsp4. These results also differ from *in vitro* biochemical assays by showing that in the context of virus infection, the cleavage at nsp4-5 cleavage site is not always the first activity of nsp5 (S. Chen et al., 2010). Our results are the first to suggest that nsp5 may be functioning as a precursor still linked to membrane inserted nsp4 and nsp6.

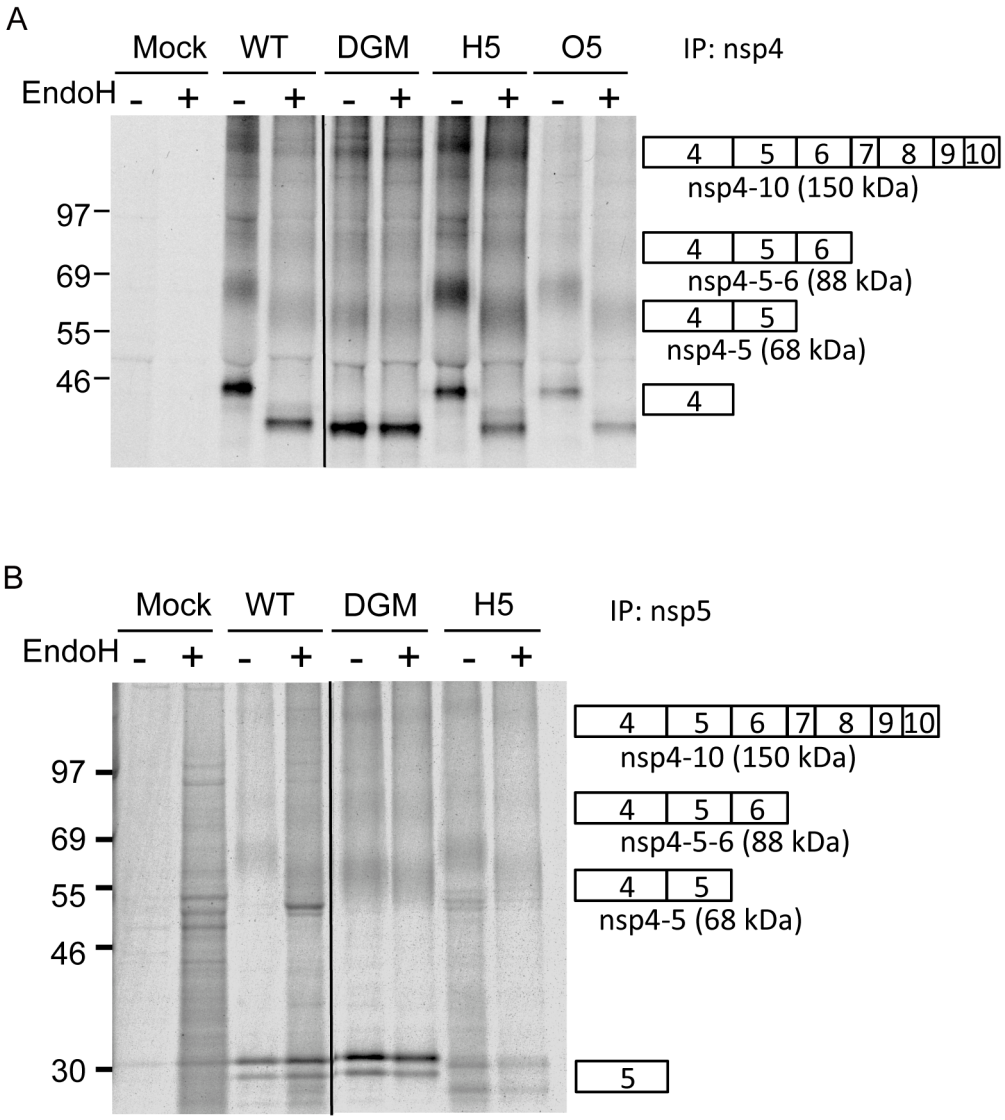

Figure V.2.: CoV nsp4 exists as nsp4-5 and nsp4-5-6 precursors.
DBT cells were infected with indicated viruses at an MOI of 10 PFU/cell. At 4 h p.i., cells were starved in -Met/-Cys DMEM and treated with ActD for 1 h before radiolabel with [^{35}S]-Met/-Cys. At 7h p.i., lysates were harvested and immunoprecipitated with antibodies specific for nsp4 **(A)** or nsp5 **(B)** in the presence or absence of EndoH. Proteins were resolved by SDS-PAGE. n≥2. The vertical line indicates where irrelevant lanes were removed from the gel.

HKU1 and OC43 nsp5 chimeras produces the nsp4-nsp5 and nsp4-nsp5-nsp6 precursors

Previous studies by Chris Stobart, a former graduate student in the Denison lab, demonstrated that HKU1 and OC43 nsp5 could be exchanged into the MHV background virus instead of native MHV-nsp5. Those viruses, H5 (MHV-HKU1-nsp5) and O5 (MHV-OC43-nsp5) replicate similar to WT-MHV but have decrease competitive fitness when compared to WT-MHV (Stobart et al., 2013). To test whether these chimeric viruses were capable of producing the nsp4-nsp5 and nsp4-nsp5-nsp6precursors, H5 and O5 were radiolabeled with [^{35}S]-met/-cys and immunoprecipitated with antibodies specific for nsp4 (Figure V.2, last 4 lanes in A and last 2 lanes in B). When nsp4 was immunoprecipitated, both the 68kDa and 88kDa bands were identified for both H5 and O5. These bands shifted to a lower molecular weight in the presence of EndoH, demonstrating that nsp4 glycosylation is intact. The antibody specific to MHV-nsp5 was cross-reactive to the HKU1 nsp5 but not OC43 nsp5. As a result, I was unable to identify precursors in the O5 infected cells using the MHV nsp5 antibody. The MHV-nsp4 antibody did pull down the 68kDa precursor and the 88kDa precursor demonstrating the H5 and O5 proteases produce the same precursors as WT-MHV.

Discussion

Nsp4 intermediate precursors are inserted in membranes and glycosylated.

In our studies to analyze glycosylation mutants of nsp4 during replication, an unexpected outcome was the detection of two, previously unknown nsp4 intermediate precursors consistent with nsp4-nsp5 (nsp4-5) and nsp4-nsp5-nsp6 (nsp4-6). The use of the glycosylation mutants and treatment with EndoH, along with immunoprecipitation by

antibodies specific for nsp4 and nsp5, showed that in addition to previously identified nsp4-10 (Kanjanahaluethai and Baker, 2001), nsp4 is detectable and glycosylated as a precursor nsp4-5 and nsp4-5-6. EndoH treatment allowed for identification of these precursors among a complicated pattern of immunoprecipitated proteins based on the mobility shift. Glycosylation of these precursors, including nsp4-10 indicates that the precursors are associated with the ER and that the nsp4 loop 1 is ER luminal. This is the first virological data to confirm that the maturing polyprotein is inserted into membranes cotranslationally. The results support the conclusion that nsp4 and nsp6 are inserted into the ER or DMV membrane and nsp5, and nsp7-10 are cytoplasmic. The result does not allow conclusions about whether this is occurring within or on the outside of DMVs. However, the early association of nsp4-10 would suggest the possibility of interactions of the polyprotein with viral and cellular factors prior to formation and closure of DMVs.

Polyprotein processing order and timing

Our results also raise an interesting question regarding the order and timing of processing of nsp4-10. The current model for nsp5-mediated cleavage, based on *in vitro* studies, suggests that nsp5 autocleaves at the nsp4-5 cleavage site first. This cleavage allows for dimerization of nsp5 which is required for subsequent cleavage events, including the nsp5-nsp6 cleavage (S. Chen et al., 2010). This model suggests that nsp5 cleaves the nsp4-5 cleavage site first, the nsp5-6 cleavage site second, and then cleaves subsequent sites. However, these studies were performed *in vitro* and not in the context of a full-length polyprotein. Our identification of the nsp4-5 and nsp4-5-6 precursors suggests that the order of cleavage may be different during infection. Our approach will let us compare the pattern of processing with the timing of glycosylation to better

understand how nsp5 functions during virus replication and possibly regulates protein interactions involved in membrane modifications.

CHAPTER VI: CHARGE-TO-ALANINE MUTAGENESIS OF MHV NSP3

Introduction

CoVs induce membrane modifications in order to establish replication complexes. CoVs rearrange ER membranes to form a reticulovesicular network composed on double membrane vesicles (DMVs) and convoluted membranes that are contiguous with the ER through the outer membrane (Knoops et al., 2008a). The CoV genome encodes 16 replicase non-structural proteins (nsp1-16). Three of these proteins (nsp3, nsp4, and nsp6) are integral membrane proteins (Baliji et al., 2009; Gosert et al., 2002; Oostra et al., 2008; 2007; Sparks et al., 2007) are required for membrane rearrangements (Angelini et al., 2013). Several studies have demonstrated that nsp4 is required for viral replication and proper DMV formation (Gadlage et al., 2009; Sparks et al., 2007) (Chapter II, III, IV). However, no study has analyzed mutations within nsp3 to identify residues critical for DMV morphology. Nsp3 is a 210kDa multifunctional protein. It contains several domains and activities including: papain-like protease domain(s), deubiquitinating activity, ADP-ribose-1”-monophpsphatase activity, and a transmembrane domain (Barretto et al., 2005; Ratia et al., 2006; Saikatendu et al., 2005). The topology of the transmembrane domain has been determined *in vitro* and contains two regions that span the membrane, forming one luminal loop with the N- and C-termini in the cytosol (Oostra et al., 2007). The goal of the experiments in this chapter was to identify residues within the nsp3 transmembrane domain critical for membrane modifications. Nicole Diggins assisted in engineering the nsp3 mutations into the MHV B fragment. All virus recoveries, experiments described, and data analyses were performed by me.

Results

Nsp3 charge-to-alanine mutants exhibit delayed viral replication

Charged residues frequently mediate protein-protein interactions. Charge-to-alanine mutagenesis of nsp4 identified residues within nsp4 that are important for viral replication (Sparks et al., 2007) and DMV morphology (Beachboard et al., 2014). To identify critical residues of nsp3 required for viral replication, the nsp3 transmembrane domain sequence was analyzed for the presence of charged residues. Six charge-to-alanine substitutions were introduced into the transmembrane domain region of nsp3 (Figure VI.1). Viruses were assembled using the MHV reverse genetics system and electroporated into baby hamster kidney (BHK) cells overlaid onto murine DBT cells. Cells were monitored for cytopathic effect (syncytia formation) over at least 72 h. Five viruses were recovered that contain mutations spanning the luminal loop and C-terminal region of the transmembrane domain of nsp3. The virus that was unrecoverable was attempted twice.

To determine the replication capacity of these mutant viruses, DBT cells were infected at an MOI of 1 PFU/cell with the indicated viruses, supernatants were sampled over 28 h, and titers were determined by plaque assay (Figure VI.2). WT virus began exponential replication between 6 and 8 h p.i. and achieved peak viral titers at 12h p.i. Each of the nsp3 mutants exhibited an approximate 2 h delay in exponential replication. All viruses achieved peak viral titer at 16 h p.i. except D1507A which achieved peak titers at 24 h p.i., approximately 12 later than WT. This delay in exponential replication is a characteristic of several CoV mutants. Since nsp3 is involved in the induction of membrane modifications required for replication complex formation, it is

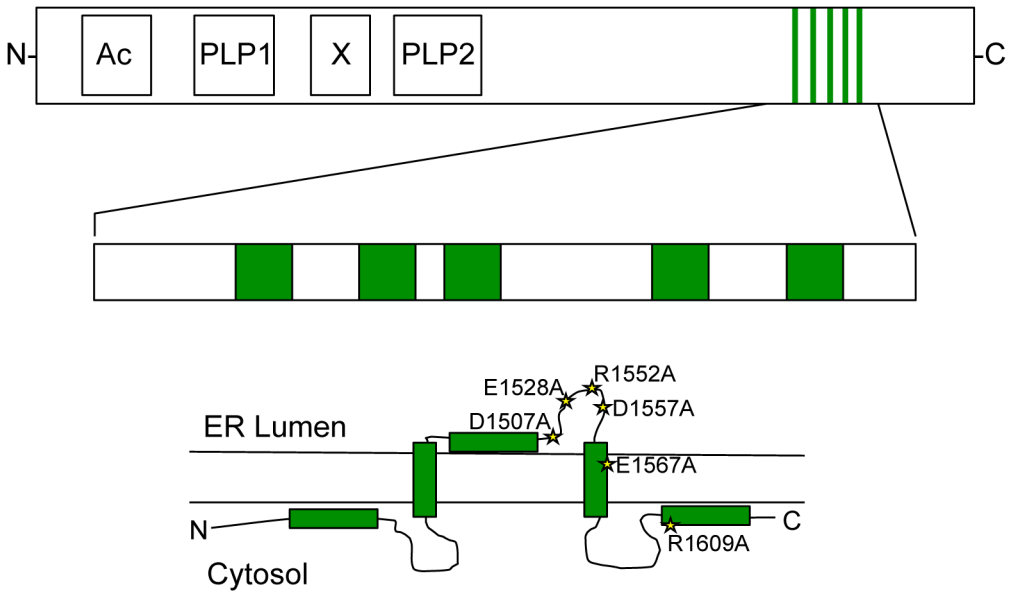

Figure VI.1: Nsp3 schematic and mutagenesis.

(**A**) Schematic of nsp3 with the domains labeled. The transmembrane domain of nsp3 is zoomed with the predicted transmembranes shown in green. (**B**) Topology of nsp3 (Oostra et al., 2007) with the location of the nsp3 charge-to-alanine mutations shown in yellow stars.

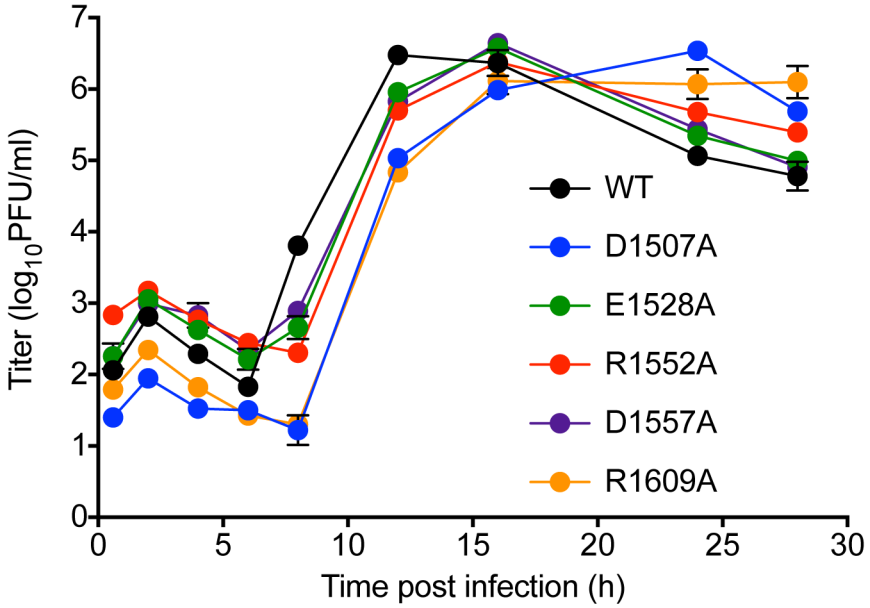

Figure VI.2: Replication kinetics of the nsp3 charge-to-alanine mutants. DBT cells were infected with indicated viruses at an MOI of 1 PFU/cell. Supernatants were sampled at indicated time points and titer was determined by plaque assay. Error bars represent the SEM of three replicates plated in duplicate.

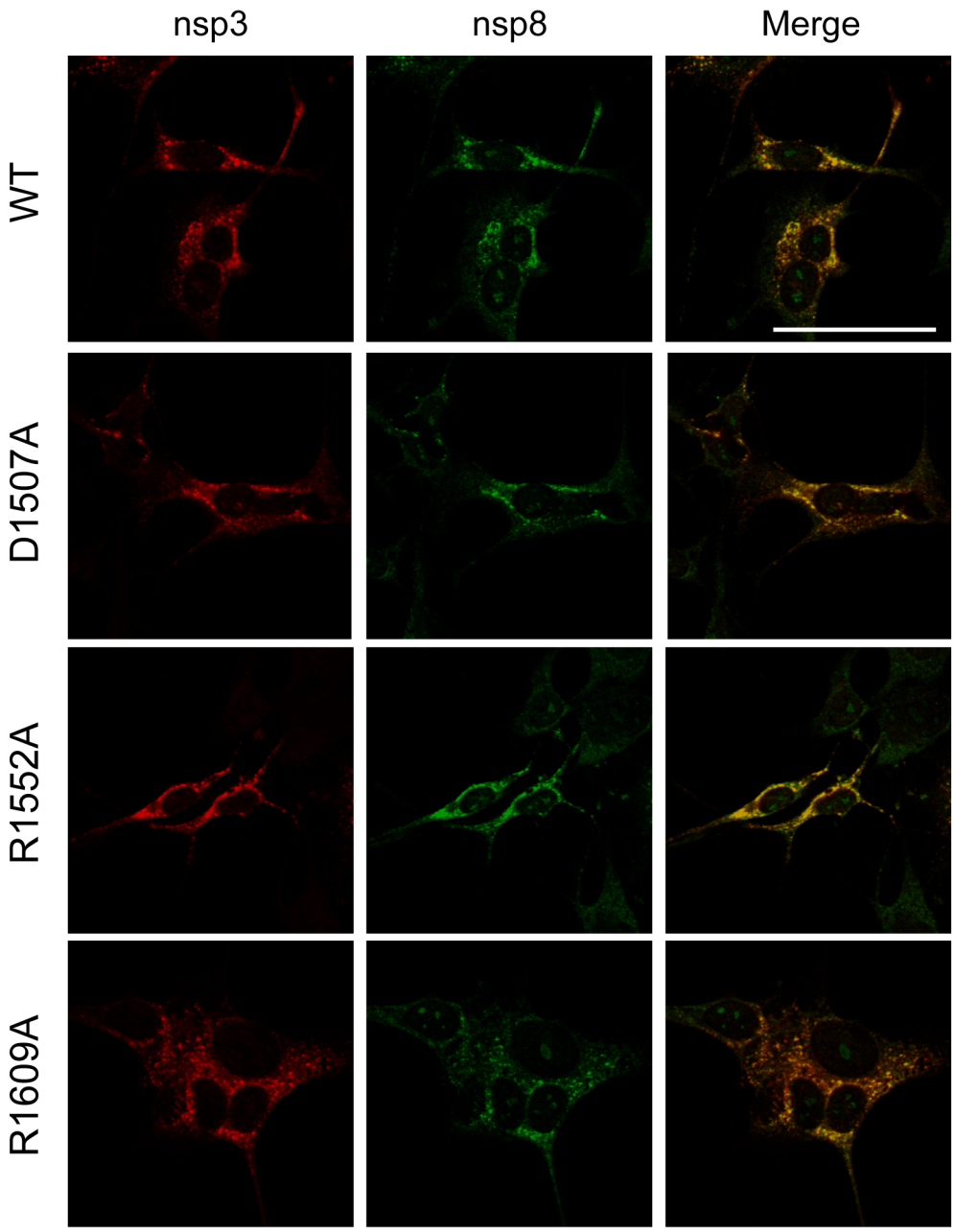

Figure VI.3:Localization of nsp3.

DBT cells were infected with the indicated viruses at an MOI of 5 PFU/cells for 8 h. Cells were fixed with MeOH and stained with antibodies specific to nsp3 and nsp8. Yellow pixels in the merged images represent colocalization. Scale bar represents 50μm.

hypothesized that the delay in replication is due to delayed membrane modifications or replication complex formation. However, additional experiments will need to be performed to test this hypothesis.

Nsp3 mutants localize to the replication complex

To determine the localization of nsp3 in mutant virus-infected cells, DBT cells on glass coverslips were mock infected or infected with WT, D1507A, R1552A, or R1609A nsp3 viruses for 8 h at an MOI of 5 PFU/cell. Cells were then stained with antibodies specific to nsp3 and nsp8 (a marker of the replication complex). Nsp3 and nsp8 extensively colocalize to cytosolic perinuclear foci in WT-infected cells (Figure VI.3). Each of the nsp3 mutant viruses displayed extensive colocalization between nsp3 and nsp8. These data suggest that nsp3 is appropriately localized to the replication complex. Additionally, the level of expression of both nsp3 and nsp8 visually appear to be similar between WT and mutant infected cells, suggesting that the expression of nsp3 at 8 h p.i. is not altered.

Summary and Future Directions

These data demonstrate that charged residues of the transmembrane region of nsp3 may be critical for timing of viral replication. Likely, mutations in nsp3 alter the timing of DMV formation and subsequent RNA synthesis and virion release. However, these mutations could effect other nsp3 functions through long-distance communication networks. Our lab has identified a network of long-distance communication within the nsp5 protease (Stobart et al., 2012). It would be necessary to test the effect of these mutations on protease activity and ADP-ribose-1'-monophosphatase activity to determine off-target effects of the mutations. The entire nsp3 protein is required to induce

membrane modifications, suggesting that the N-terminal region of the protein is involved and it is not just the transmembrane region. Since nsp3 is such a large protein and has several enzymatic functions, it is possible that one of these upstream functions is critical for interaction with host proteins that are required for DMV formation.

My work (Chapter IV) has demonstrated that mutation within nsp4 cause aberrant DMV formation. Lundin et al. determined that mutations in nsp6 alter DMV morphology (Lundin et al., 2014). It will be interesting to test these nsp3 mutant viruses and determine whether mutations within the transmembrane domain region of nsp3 also alter total number and morphology of DMVs.

CHAPTER VII: VISUALIZING MERS-CORONAVIRUS REPLICATION COMPLEXES

Introduction

In June 2012, Middle East respiratory syndrome coronavirus (MERS-CoV) was isolated from a man with acute pneumonia and renal failure in Saudi Arabia (Zaki et al., 2012). The number of MERS cases has increased to 835 with 301 deaths by October 2014 (WHO, 2014b). Most cases have occurred on the Arabian Peninsula, or are associated with travel to the Middle East. MERS-CoV RNA has also been detected in dromedary camels, Nycteris bats, Pipistrellus bats, and Taphozous bats (Annan et al., 2013; Memish et al., 2013; Meyer et al., 2014; Reusken et al., 2013). Serological evidence suggests that MERS-CoV has been circulating in camels since at least 1992 (Alagaili et al., 2014; Zaki et al., 2012). Person-person transmission of MERS-CoV has also been confirmed, though at this time it is less communicable than Severe Acute Respiratory Syndrome CoV (SARS-CoV). In addition, MERS-CoV has a higher case fatality rate than that of SARS-CoV (WHO, 2014a). With two pandemics within a decade, CoVs have proven their capacity to emerge as new human pathogens, highlighting the necessity for understanding viral replication in order to design effective therapeutics.

The MERS-CoV genome is organized similarly to all other CoV genomes (Figure VII.1). The genome is approximately 30 kb with a 5’ cap and 3’ poly A tail. The first two thirds of the genome encodes the replicase gene, while the remainder encodes the structural and accessory proteins (Scobey et al., 2013). Translation of the replicase gene results in a large polyprotein that is proteolytically cleaved by two viral proteases, PLpro

(nsp3) and 3CLpro (nsp5), to form 16 nonstructural proteins (nsp1-16) (Kilianski et al., 2013). For other CoVs, like SARS-CoV and murine hepatitis virus (MHV), the replicase proteins colocalize to punctate perinuclear foci that are associated with modified ER membranes (Bost et al., 2000; Brockway et al., 2003; Gosert et al., 2002; Knoops et al., 2008b; Snijder et al., 2006; Ulasli et al., 2010). MHV and SARS-CoV replication complexes exclude most cellular markers but partially colocalize with the ER proteins PDI and Sec61α (Knoops et al., 2009). The structural proteins localize to the ERGIC where virus assembly occurs (Sims et al., 2000). It is not known whether MERS-CoV replication complexes are similar to other CoV replication complexes.

The Denison lab generated antibodies that allow for testing of immune evasion, viral inhibition and viral replication. Nsp1 has been shown to be involved in host mRNA degradation, host translation shutoff, and inhibition of interferon signaling (Kamitani et al., 2006; Narayanan et al., 2008; Wathelet et al., 2007; Züst et al., 2007). Nsp5 is the main viral protease that is responsible for 11 polyprotein cleavage events that are required for the formation of mature proteins (X. Lu et al., 1996). Recently, nsp5 has become a target for coronavirus inhibition (Agnihothram et al., 2014; Ghosh et al., 2008; Kilianski et al., 2013). Nsp8 is a primase that has been extensively used as a marker for the replication complex (Deming et al., 2007; Imbert et al., 2006). Nsp9 is a single-stranded RNA binding protein that is required for viral replication (Deming et al., 2007).

In this study, I sought to investigate the structure and formation of MERS-CoV replication complexes. First, antibodies specific to MERS-CoV nsp1, nsp5, nsp8 and nsp9 were generated. The antibodies are specific for MERS-CoV antigen by immunofluorescence. Further, the replicase proteins colocalize with one another at

regions of the host cell cytoplasm that are enriched in ER membranes. Additionally, I determined that the MERS-CoV nsp5 antibody cross-reacts with MHV antigen, the MHV nsp10 antibody cross-reacts with MERS-CoV antigen, and the SARS-CoV nsp5 and nsp9 antibodies cross-react with MERS-CoV antigen. Because MERS-CoV has recently emerged and has a high case fatality rate, it is important to better understand its replication strategies such that they might be effectively targeted for therapeutic intervention. Prior to the work described in this chapter, Clint Smih and Xiaotao Lu generated MERS-CoV proteins, which were used to generate antibodies at Cocalico Inc. Clint Smith and Michelle Becker performed all the MERS-CoV and SARS-CoV infections and Megan Culler Freeman generated Figure VII.2. I performed all other experiments and data analysis for this chapter.

Results

Detection of MERS-CoV replicase proteins by immunofluorescence.

In order to test the antibodies for use in immunofluorescence assays, WHO-Vero cells on glass coverslips were mock infected or infected with MERS-CoV at an MOI of 1 PFU/cell for 24h. Cells were then fixed in methanol and stained with pre-immune sera or antibodies directed at nsp1, nsp5, nsp8, and nsp9 and imaged by widefield microscopy (Figure VII.2). Widefield microscopy was used for these experiments such that the background in the entire field could be discerned, instead of only the background within a z-slice. Infected WHO-Vero cells stained with pre-immune sera or mock-infected cells stained with immune sera demonstrated low-level, diffuse background fluorescence in all cells. WHO-Vero cells infected with MERS-CoV and stained with antibodies directed toward nsp1, nsp5, nsp8, and nsp9 demonstrated a punctate cytoplasmic pattern

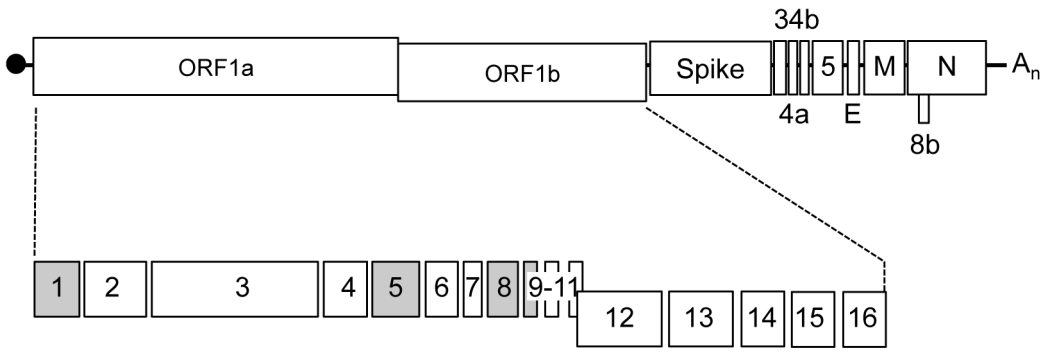

Figure VII.1: MERS-CoV genome organization.
Genome organization of MERS-CoV. ORF1ab is translated into 16 nonstructural proteins (nsp1-16). Proteins to which antibodies were generated are shown in grey.

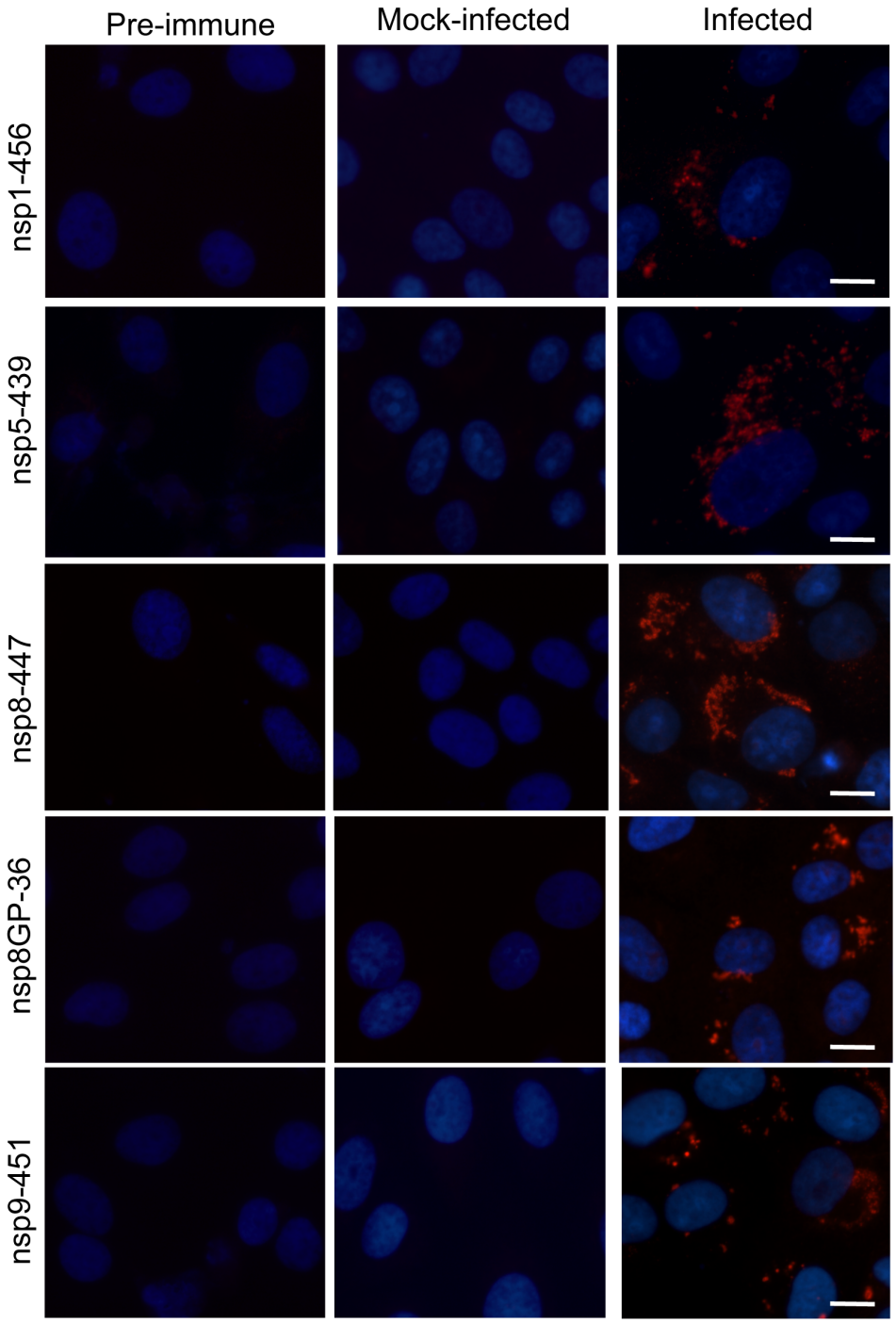

Figure VII.2: Specific labeling of MERS-CoV nsps.
WHO-Vero cells were mock-infected or infected with WT MERS-CoV at an MOI of 1 PFU/cell. At 24 h p.i. cells were fixed, stained with antibodies or pre-immune serum as indicated (α-nsp1, α-nsp5, α-nsp8, or α-nsp9) and secondary antibodies labeled with Alexa 546 and imaged by widefield microscopy. Nuclei are stained by DAPI. Scale bar represents 20μm. Images by Megan Culler Freeman.

of localization that often formed a partial ring around the nucleus. Each of the antibodies demonstrated very low background signal in contrast to the bright signal visualized in infected cells. These data in combination with dot blots (Xiaotao Lu, unpublished) demonstrate that the antibodies are specific to MERS-CoV proteins within infected cells.

MERS-CoV replication proteins localize foci proximal to ER membranes.

Having demonstrated that the localization of viral proteins was similar to MHV and SARS-CoV, we next sought to determine whether MERS-CoV replicase proteins colocalize with ER, Golgi, mitochondria or actin, co-immunostaining was performed (Figure VII.3). First, in order to determine whether MERS-CoV replicase proteins colocalize with ER markers, MERS-CoV infected cells on glass coverslips were co-stained for each nsp and protein disulfide isomerase (PDI), an ER protein. All nsps localized to regions of the cell that are in close proximity to ER membranes. Additionally, both nsp8 and nsp9 demonstrate partial colocalization with PDI, similar to SARS-CoV nsp3 (Knoops et al., 2009). Previous studies have demonstrated that some nsps relocalize at late time points to the site of viral assembly (Bost et al., 2000), in order to test whether MERS-CoV nsps localize to the Golgi, we tested co-localization of each nsp with N-acetyl-D-glucosamine and sialic acid residues (WGA). Nsp foci were distinct from the Golgi. These data demonstrate that at the time point tested, the replicase proteins are distinct from the sites of virus assembly at the Golgi. Further testing will be need to be performed in order to determine whether the replicase protein relocalize to the sites of assembly and to confirm the ERGIC as the site of assembly.

Next, in order to determine whether other organelle markers were excluded from replication complexes, we analyzed colocalization of the nsps with mitochondria using

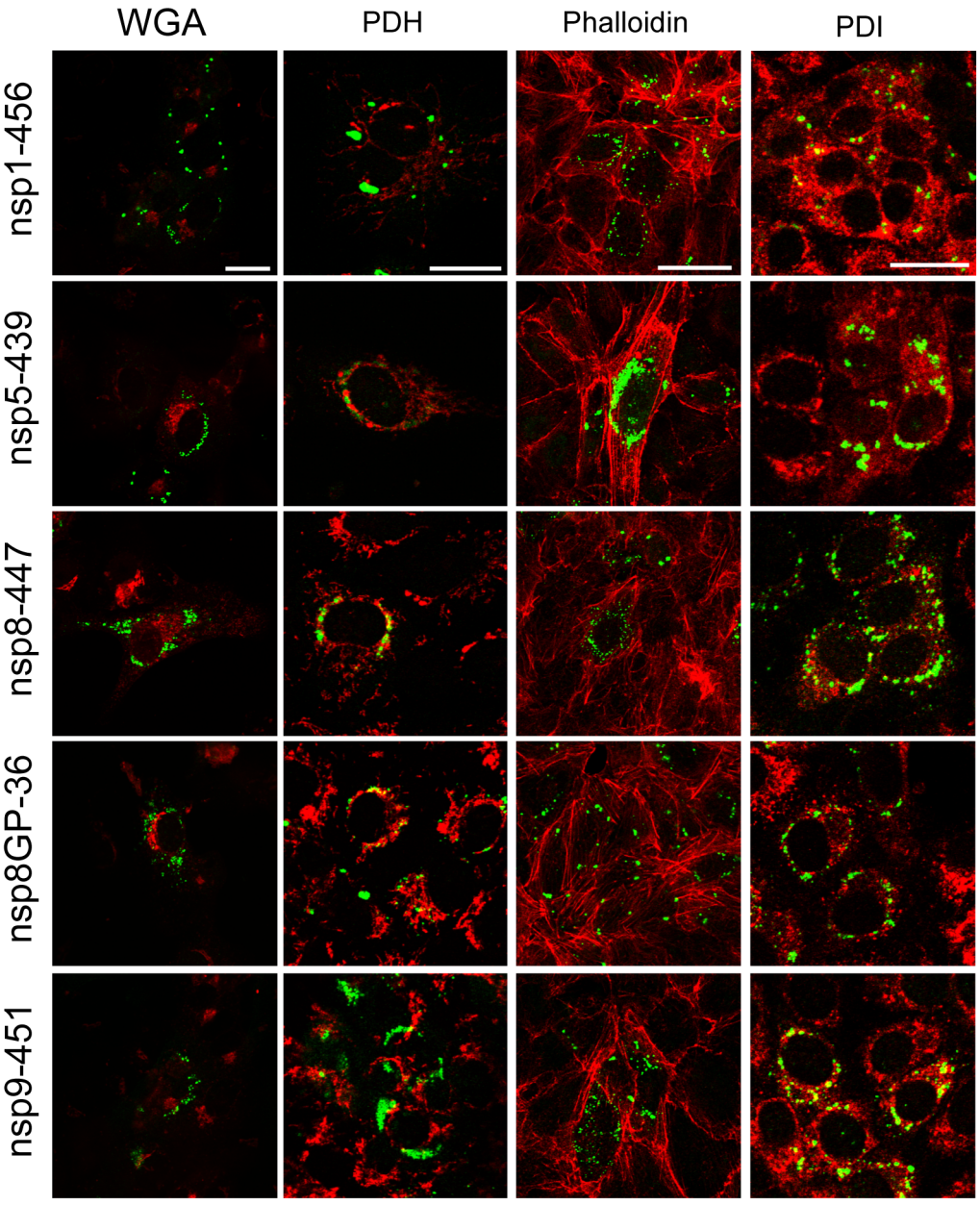

Figure VII.3: MERS-CoV nsps localizes to regions of the cell enriched in ER membranes.

WHO-Vero or Vero cells were infected with WT MERS-CoV at an MOI of 1 PFU/cell. At 24 h p.i. cells were fixed, stained with antibodies as indicated and secondary antibodies labeled with Alexa 546 or 488. Cells were imaged by confocal microscopy. Scale bar represents 20μm.

the mitochondrial protein, pyruvate dehydrogenase (PDH). Nsp1, nsp5, and nsp9 show no colocalization with PDH (Figure VII.3). There was partial colocalization of nsp8 and mitochondria but it was only at the periphery of distinct foci, suggesting that the two compartments may be in close proximity (Figure VII.3). Additionally, to test for colocalization with the actin cytoskeleton, F-actin was labeled with phallodin. All nsp foci were distinct from actin cytoskeleton. Collectively, these data suggest that MERS-CoV forms replication complexes that are similar to other beta-CoVs.

Replicase proteins colocalize at perinuclear foci.

Huh7 cells form robust infection and distinctive CPE, including syncytia formation. Colocalization of replicase proteins was determined in both WHO-Vero and Huh7 cells. WHO-Vero or Huh7 cells were infected with MERS-CoV at an MOI of 0.1 PFU/cell for 24h. Cells were then stained with antibodies specific to MERS-CoVnsp8 and nsp1 (Figure VII.4), nsp5 (Figure VII.5), or nsp9 (Figure VII.6). Representative images of both single nuclei cells and syncytia (Huh7 cells only) are shown for each antibody. Nsp1, nsp5 and nsp9 extensively colocalize with nsp8 at perinuclear foci in both cell types and in single nuclei and multiple nuclei cells (Figure VII.4, Figure VII.5, and Figure VII.6). The staining pattern looked similar to what is seen for MHV- or SARS-CoV- infected cells (Angelini et al., 2013; Bost et al., 2000; Brockway et al., 2003; Gadlage et al., 2009; Knoops et al., 2008b; Sparks et al., 2007; van der Meer et al., 1999). This suggests that MERS-CoV replication complexes are formed similar to those of SARS-CoV and MHV.

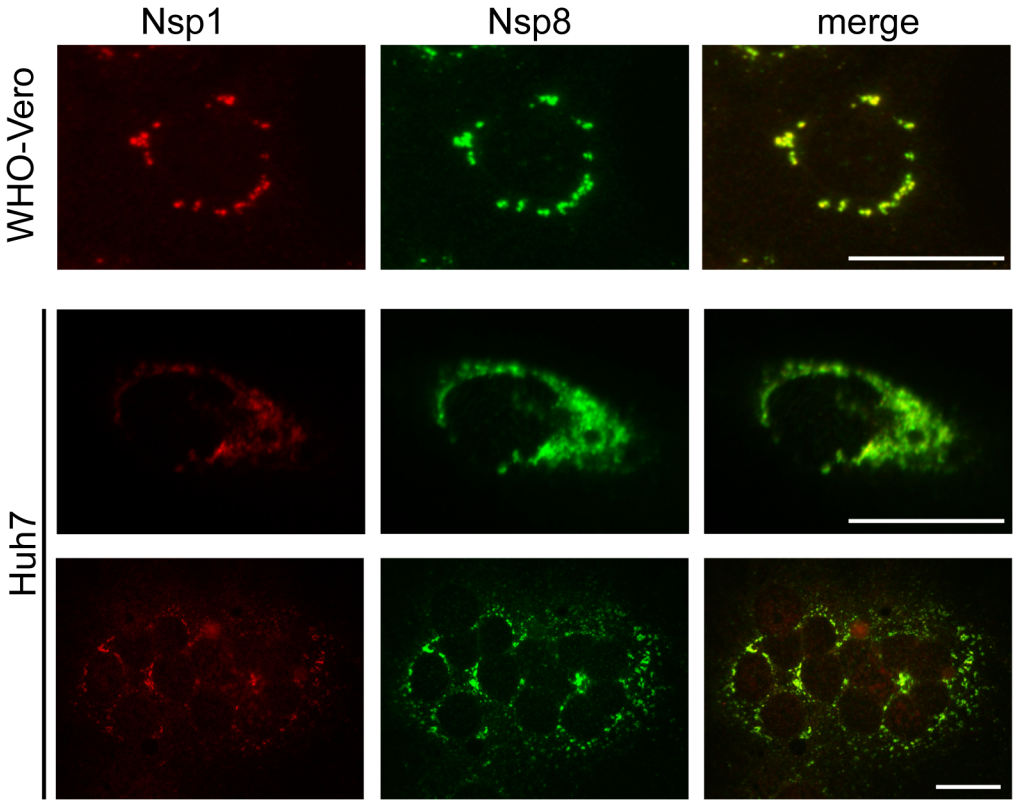

Figure VII.4: Colocalization of nsp1 and nsp8.

WHO-Vero or Huh& cells were infected with MERS-CoV at an MOI of 1 PFU/cell for 24 h before fixation in methanol. Cells were then stained with antibodies specific to viral nsp1 (red) and nsp8 (green). Scale bar represents 20 μm.

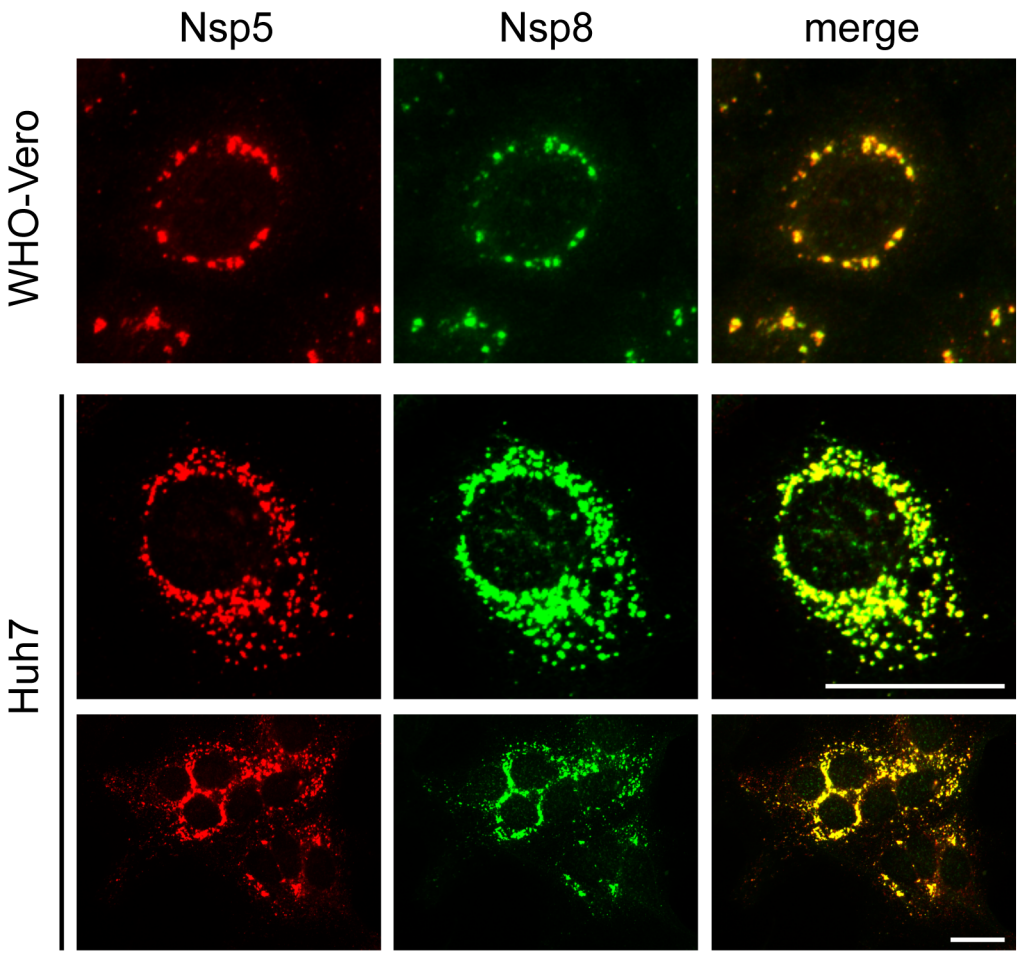

Figure VII.5: Colocalization of nsp5 and nsp8.
WHO-Vero or Huh& cells were infected with MERS-CoV at an MOI of 1 PFU/cell for 24 h before fixation in methanol. Cells were then stained with antibodies specific to viral nsp5 (red) and nsp8 (green). Scale bar represents 20 μm.

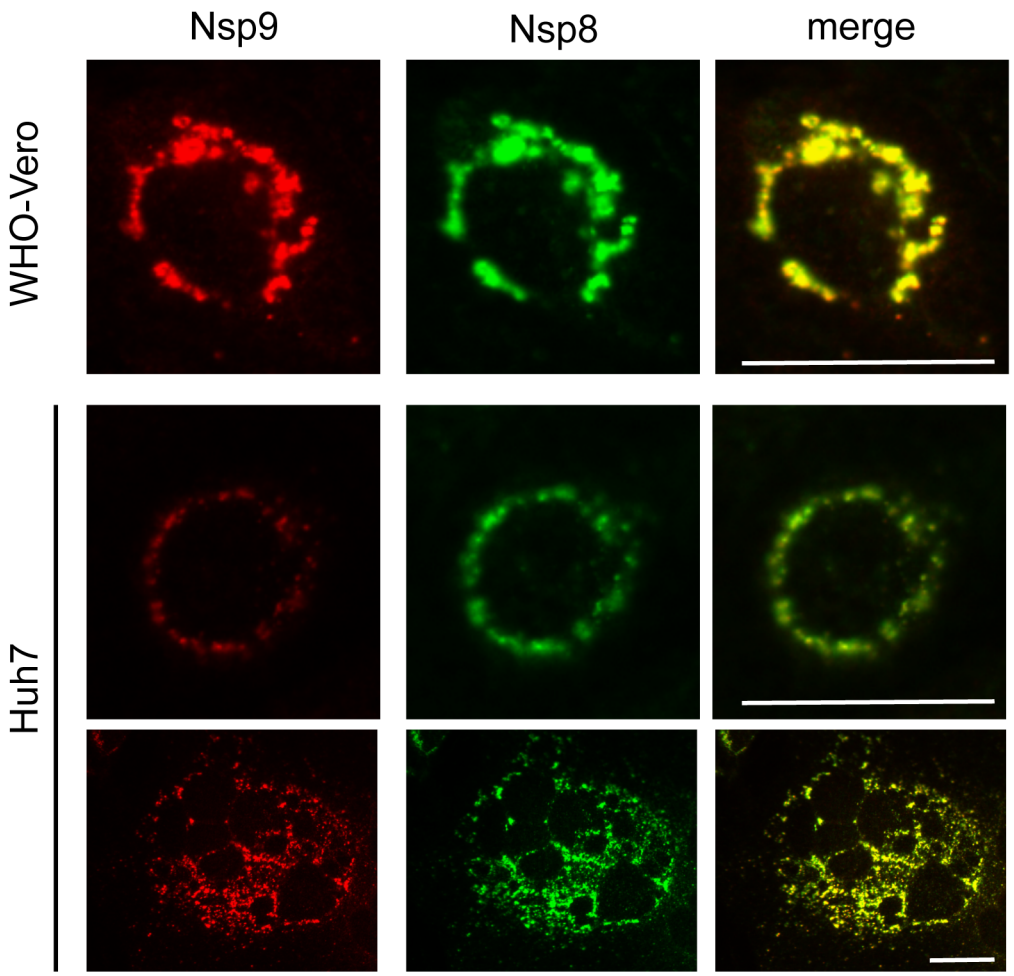

Figure VII.6: Colocalization of nsp8 and nsp9.
WHO-Vero or Huh& cells were infected with MERS-CoV at an MOI of 1 PFU/cell for 24 h before fixation in methanol. Cells were then stained with antibodies specific to viral nsp9 (red) and nsp8 (green). Scale bar represents 20 μm.

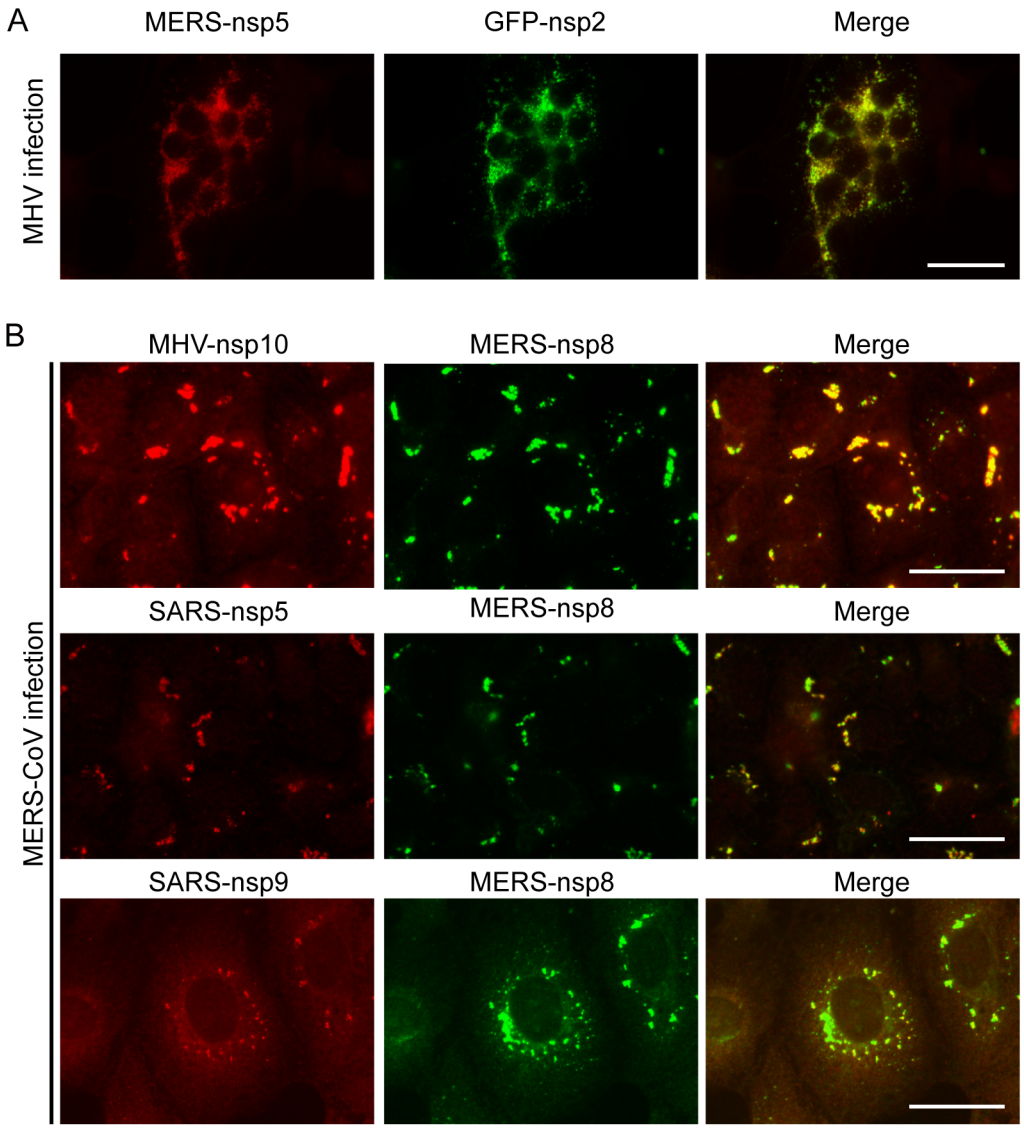

Figure VII.7: Cross-reactivity of MERS-CoV, SARS-CoV, and MHV antibodies. (**A**) DBT cells were infected with MHV-GFP-nsp2 at an MOI of 5 PFU/cell for 7h. Cells were then fixed in methanol and stained with MERS-CoV nsp5 antibodies. (**B**) WHO-Vero cells were infected with MERS-CoV at an MOI of 1 PFU/cell for 24h, followed by fixation in methanol. Cells were then stained with antibodies directed MERS-CoV nsp8 (green) to identify infected cells and MHV or SARS-CoV proteins (red).

MERS nsp5 antibody is cross-reactive with MHV nsp5

Next we sought to test whether the antibodies generated were cross-reactive with SARS-CoV or MHV proteins. DBT cells were infected with MHV-GFP (Freeman et al., 2014a) at an MOI of 5 PFU/cell for 6 h. Cells were fixed in methanol and stained with antibodies specific to MERS-CoV nsp1, nsp5, nsp8, and nsp9. For MHV-infected cells, the nsp1, nsp8, and nsp9 antibodies demonstrated no cross-reactivity with MHV proteins (data not shown). However, the MERS-CoV-nsp5 antibody did cross react with MHV nsp5 (Figure VII.7). The signal detected with the MERS-CoV nsp5 antibody extensively co-localized with GFP-nsp2 at the MHV replication complex. The results demonstrated that MHV nsp5 can be detected by the MERS-CoV antibody.

SARS-CoV and MHV protein antibodies cross-react with MERS-CoV infected cells

There are several MERS-CoV proteins that cannot be visualized because of lack of reagents. In order to determine whether MHV or SARS-CoV antibodies cross react with MERS-CoV proteins, WHO-Vero cells were infected with MERS-CoV at an MOI of 1 PFU/cell for 24 h before fixation in methanol. Cells were then stained with antibodies specific to SARS-CoV nsp1, nsp2, nsp3, nsp4, nsp5, nsp8, nsp9, or nsp10 and to MHV nsp1, nsp2, nsp3, nsp4, nsp5, nsp8, nsp9, nsp10, or nsp12. Additionally, to identify MERS-CoV replication complexes, cells were stained with the MERS-CoV guinea pig nsp8 antibody. The majority of the antibodies were not cross-reactive with MERS-CoV infected cells (data not shown); however, the MHV nsp5 and SARS-CoV nsp5 and nsp9 antibodies cross-reacted with MERS-CoV infected cells (Figure VII.7). The signal from the MHV or SARS-CoV antibodies extensively colocalize with MERS-

CoV nsp8 labeled replication complexes. This demonstrates that MHV and SARS-CoV nsp5 and SARS-CoV nsp9 antibodies are cross-reactive with MERS-CoV proteins.

Discussion

MERS-CoV is an important infectious agent with severe consequences to human health (WHO, 2014a). In this work, I have tested these antbodies to determine that they are highly specific and robust for use in immunofluorescence studies. MERS-CoV nsps localize to punctate perinuclear foci, as is seen for other coronaviruses. Each nsp tested colocalizes with nsp8, a marker of the replication complex. The nsps localize to cytosolic areas that are enriched in ER membranes, but do not coloclalize with markers for actin, the Golgi network, or mitochondria. Additionally, we have identified cross-reactive MERS-CoV, SARS-CoV and MHV antibodies.

MERS-CoV replication complexes

Previous studies have determined that all nsps tested localize to the replication complex by immunofluorescence for both SARS-CoV and MHV (Bost et al., 2000; Brockway et al., 2003; Gosert et al., 2002; Knoops et al., 2008b; Prentice et al., 2004; Snijder et al., 2006; Ulasli et al., 2010). It has also been determined that cellular proteins are excluded from the coronavirus replication complex. Studies have demonstrated partial co-localization with PDI, Sec61α, LC3-I, OS-9 and EDEM-1 (Knoops et al., 2009; Reggiori et al., 2010). We determined that MERS-CoV formed similar replication complexes. Nsp3, nsp5, and nsp9 colocalize with nsp8 at perinuclear cytoplasmic foci that are in close proximity to ER membranes. Colocalization at the replication complex was tested in two cell types, WHO-Vero cells and Huh7 cells. The viral proteins formed perinuclear foci in both cells types, although there appeared to be an increase in number

of foci in Huh7 cells. This difference likely indicates an increase in the amount of viral replication in these cells.

Cross-reactive antibodies

With the emergence of a new pathogen, there are few tools and reagents to study the pathogen. We tested cross-reactivity of the antibodies to see whether our MHV and SARS-CoV reagents can be used for studying MERS-CoV. This will also test the conservation of protein structure. We found that the SARS-CoV nsp5 antibody is cross-reactive for MERS-CoV. Additionally, the MERS-CoV nsp5 antibody is cross-reactive with MHV nsp5, although the MHV nsp5 antibody did not recognize MERS-CoV nsp5. MERS-CoV nsp5 have about 50% amino acid identity with both MHV and SARS-CoV nsp5. Therefore, the capacity of these nsp5 antibodies to cross-react suggests that the antibodies are recognizing a conserved structural feature of the protein rather than specific sequences. Additionally the SARS-CoV nsp9 antibody cross-reacted with MERS-CoV but the MERS-CoV nsp9 antibody was not cross-reactive. This suggests that the MERS-CoV antibody may be recognizing specific amino acids that are not conserved across the viruses or is binding to a unique region of MERS-CoV nsp9. Importantly, I identified an MHV antibody that recognizes a MERS-CoV protein for which we currently do not have antibodies. The MHV nsp10 antibody was cross-reactive for MERS-CoV, which allows for the use of the antibody for studying MERS-nsp10. Nsp10 has been demonstrated to act as a cofactor for the nsp14 exonuclease and the nsp16 2'-O-methyltransferase. Therefore, the antibody could be used in studies of MERS-CoV replication fidelity.

Significance and utility.

I have demonstrated in this work that the antibodies generated against MERS-CoV nonstructural proteins are specific and robust. Antibodies generated in this study will be valuable resources for studying MERS-CoV evasion of the host immune response, testing the efficacy of nsp5 inhibitors, and evaluating viral replication.

CHAPTER VIII: SUMMARY AND FUTURE DIRECTIONS

Introduction

When I began working in the Denison lab, several things were known about nsp4 and its role in DMV formation. First, nsp4 is an integral membrane protein and the topology of both MHV nsp4 and SARS-CoV nsp4 had been determined *in vitro* (Baliji et al., 2009; Oostra et al., 2008; 2007). Next, it had been demonstrated that nsp4 was required for MHV replication (Sparks et al., 2007). Several nsp4 mutants had been identified with a range of replication phenotypes, from WT-like to a four-hour delay in exponential replication with a 1000-fold reduction in peak viral yield (Sparks et al., 2007). Additionally, we had determined that nsp4 was N-linked glycosylated at two residues within loop 1 of the protein. Viruses containing mutations that disrupted the glycosylation sites within nsp4 produced aberrant DMVs, where the inner membrane of the DMV appeared to have collapsed (Gadlage et al., 2009).

There were several unanswered questions at the time I began my research: 1) On which membrane do replication complexes form within the DMV?, 2) How do DMVs form and which viral proteins mediate this process?, 3) Is the *in vitro* topology accurate in the context of a DMV?, 4) Is aberrant DMV formation specifically due to loss of nsp4 glycosylation?, and 5) Are aberrant DMVs associated with a fitness cost to the virus?

My work has contributed to the understanding of these questions. First, Chapter V of this dissertation strongly suggests that replication complexes form on the outer membrane of the DMV. I determined that nsp4 is inserted into the membrane as a polyprotein. Since the N- and C-termini of the membrane proteins are cytosolic, the remainder of the replicase proteins localize to the cytosolic surface of the DMV.

Additionally, the majority of DMVs in the nsp4 mutant-infected cells are aberrant. However, the virus still ultimately achieves WT-like viral yield and RNA synthesis levels, suggesting that the replication complexes are intact and that the DMVs are functional. If replication occurred on the inner membrane of the DMV, it is unlikely that that the aberrant DMVs would be functional. Second, Angelini et al. demonstrated that nsp3, nsp4, and nsp6 are required for membrane modifications (Angelini et al., 2013). Third, while we have not fully tested the topology of nsp4 during virus infection, we know that loop 1 is luminal, consistent with *in vitro* data, since it becomes glycosylated during infection. Fourth, I have determined that mutations across nsp4 result in aberrant DMV formation. Additionally, viruses containing mutations within nsp6 produce aberrant DMVs (Lundin et al., 2014). Finally, there is not a fitness cost associated with aberrant DMV or decreased total DMVs. However, there is a fitness cost associated with the loss of nsp4 glycosylation.

Several questions still remain about the role of nsp4 in membrane modifications. What is the mechanism of DMV formation? What is the mechanism of aberrant DMV formation? Can coronavirus membrane modifications be targeted *in vivo* using small molecule inhibitors? Future studies described here propose experiments to address these questions.

Future Directions

Mechanism of DMV formation

Virus-induced membrane modifications have been studied extensively for several positive-sense RNA viruses. The structures of the membrane modifications have been determined though EM and electron tomography. These methods have identified two

major types of membrane modifications. First, there are modifications that form invaginations of host cytoplasmic membranes and are connected to the cytoplasm through a pore, e.g. Flock House Virus (Kopek et al., 2012), Infectious Bronchitis Virus (Maier et al., 2013), Semiliki forest virus (Spuul et al., 2010). Second, there are membrane modifications that form closed vesicles with single or double lipid bilayers, e.g. SARS-CoV (Knoops et al., 2008b), Poliovirus (Belov et al., 2011), and Hepatitis C Virus (Romero-Brey et al., 2012). The viral proteins required for membrane modifications have been identified by overexpression of individual or combinations of viral proteins in cells. These experiments identified that nsp3, nsp4, and nsp6 are required for coronavirus DMV formation (Angelini et al., 2013), NS4B is required for Hepatitis C virus membranous web formation (Egger et al., 2002), and proteins 2C and 2BC are required for Poliovirus vesicle formation (Cho et al., 1994). For some viruses, lipid and protein constituents of the replication organelles have been identified. Phosphatidylinositol-4-phosphate is enriched in Coxsackievirus B3, Poliovirus, and Hepatitis C virus replication organelles and binds the polymerase of all three viruses (Hsu et al., 2010). Tomato bushy stunt tombusvirus utilizes several endosomal sorting complexes required for transport (ESCRT) proteins for the formation of its replication complex (Barajas et al., 2009). LC3-I is required for MHV replication complexes (Reggiori et al., 2010). However, the mechanism of how the membrane modifications are formed is not well understood. Experiments described below will elucidate the mechanism of DMV formation.

Which host proteins are required for DMV formation?

Several studies have tried to determine host factors and pathways involved coronavirus DMV formation. Autophagy (Maier and Britton, 2012; Prentice, 2003), ERAD tuning (Bernasconi et al., 2012; Reggiori et al., 2010; 2011) and the secretory pathway (Knoops et al., 2009) have been implicated based on colocalization of proteins from these pathways with nsps and testing the effects of loss of the protein on viral replication and DMV formation. This is a topic of debate within the field because multiple studies have found different results based on the virus and experimental approach. In order to identify the host factors required for membrane modifications, it would be necessary to determine the lipid and protein composition of the DMVs. Our lab has previously isolated DMVs though ball-bearing homogenization and differential centrifugation with GFP- nsp3 and DiD labeled vesicles (Sunny Lee, unpublished data). Preliminary mass spectrometry data identified several cellular proteins that localize to the DMV. Proteins identified need to be validated for their requirement in DMV formation by depletion of the proteins and testing for viral replication and DMV formation and then complementing the protein back to determine if that restores DMV formation. Lipids can also be identified within these purified vesicles. This data could then be used in an *in vitro* assay to identify the mechanism of DMV formation.

How do nsp3, nsp4, and nsp6 induce DMV formation?

In order to test the mechanism of membrane modifications, one would need an *in vitro* system with giant unilamellar vesicles. The proteins could then be incorporated into the giant unilamellar vesicles and assessed for the capacity to induce membrane curvature and form DMVs. The cellular protein(s) identified above could also be used in the *in*

vitro system to determine if the proteins play a direct role in membrane curvature and DMV formation.

Where do replication complexes form on DMVs?

Previous work has determined that nsp2 is located on the cytosolic surface by membrane protection assays using digitonin and proteinase K (Hagemeijer et al., 2010). In order to test the localization of the C-terminus of nsp4 and the N-terminus of GFP-nsp3 (MG3 virus) (Freeman et al., 2014a), one could perform digitonin and proteinase K treatments assays. I anticipate that nsp3 and nsp4 localize to both membranes of the DMV and that there would be protein signal when cells were treated with digitonin and proteinase K.

ImmunoEM studies have been limited in the capacity to identify where within a DMV the replication complex forms. Because of the fixation methods required for immunolabeling, the DMVs appear as hollow structures (Ulasli et al., 2010). We have been able to identify whether or not proteins localize to DMV, but not to which membrane surface they localize. Aberrant DMVs may allow the resolution to identify whether nsps localize to the inner or outer membrane of a DMV. Because the separation of the membranes, we should be able to identify which proteins localize to the outer membrane of the DMV and which proteins localize to the inner membrane. I would anticipate that the replication complex forms on the cytosolic side of the outer membrane. Based on the predicted topology of nsp3, nsp4, and nsp6, all the remaining proteins should localized to the cytosolic surface. Additionally, this would maintain access to the ribosome for translation. It is likely that the replication machinery forms a tight complex at the membrane to prevent protein diffusion into the cytoplasm.

Models of Coronavirus Aberrant DMV Formation

Hagemeijer *et al.* demonstrated that MHV nsp4 is involved in homotypic interactions and heterotypic interactions with nsp3C (the C-terminal portion of nsp3 including the transmembrane region) and nsp6 (Hagemeijer et al., 2011). They also demonstrated that co-expression of nsp3C and nsp4 resulted in re-localization of these proteins to punctate foci. Since it has been demonstrated that nsp3 and nsp4 pair membranes, it is likely that nsp3C and nsp4 interact across two lipid bilayers to maintain them in close proximity and cause the re-localization of the proteins upon co-expression. Currently, it is not known which domains of nsp3, nsp4, and nsp6 are required for their interactions. It is also not known whether nsp3, nsp4, and nsp6 need to be in their mature cleaved form to induce-membrane modifications or if the polyprotein precursors are capable of inducing membrane modifications. Overall, there is very little knowledge of how membrane modifications are initiated. However, we can model what happens based on end points that have been determined experimentally.

Based on the single and co-expression experiments with SARS-CoV nsp3, nsp4, and nsp6, it is likely that nsp6 initiates vesicle formation. Since nsp3 and nsp4 pair membranes, it is likely that these proteins make an otherwise single membrane vesicle into a double membrane vesicle. I have generated three models for how aberrant DMVs form (Figure VIII.1). First, nsp4 could be degraded and not available at the DMV for interactions that maintain the two lipid bilayers in close proximity. In this model, mutations within nsp4 would alter the confirmation of the protein in such a way that it may activate the unfolded protein response or get degraded in some other manner. However, immunofluorescence and immunoprecipitation data (Figure IV.7 and

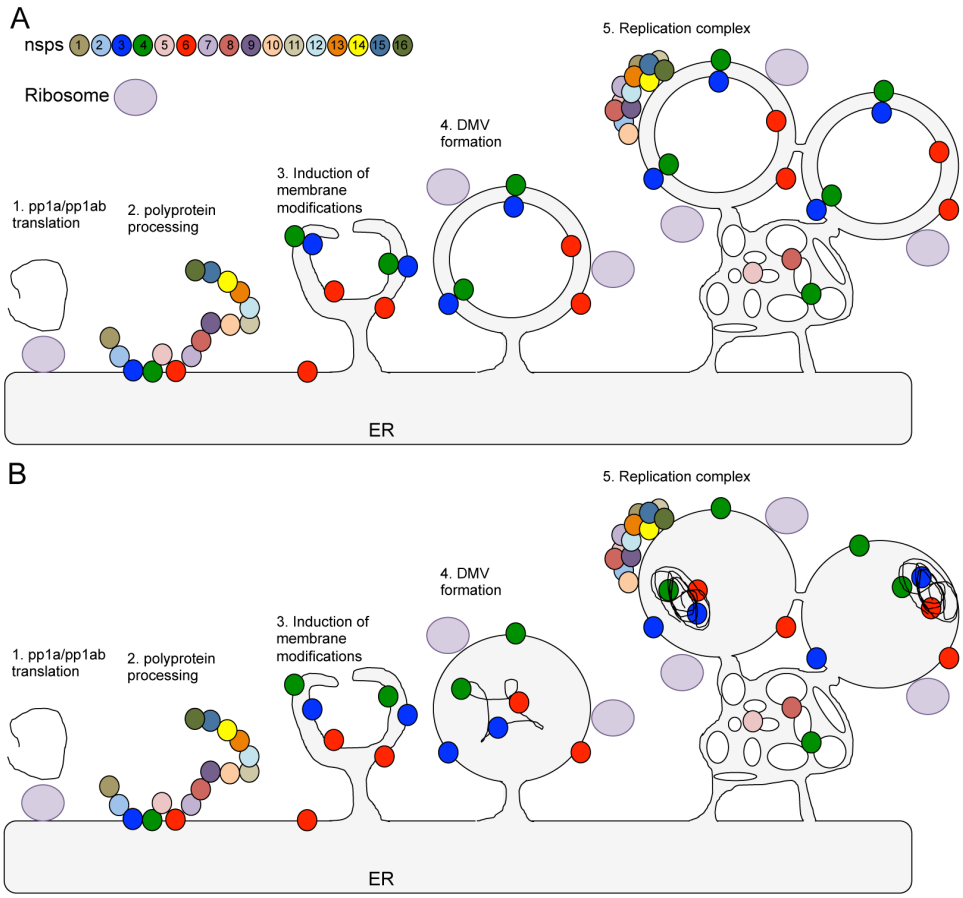
A
nsps 1 2 3 4 5 6 7 8 9 10 11 12 13 14 15 16
Ribosome
1. pp1a/pp1ab translation
2. polyprotein processing
3. Induction of membrane modifications
4. DMV formation
5. Replication complex
ER
B
1. pp1a/pp1ab translation
2. polyprotein processing
3. Induction of membrane modifications
4. DMV formation
5. Replication complex
ER

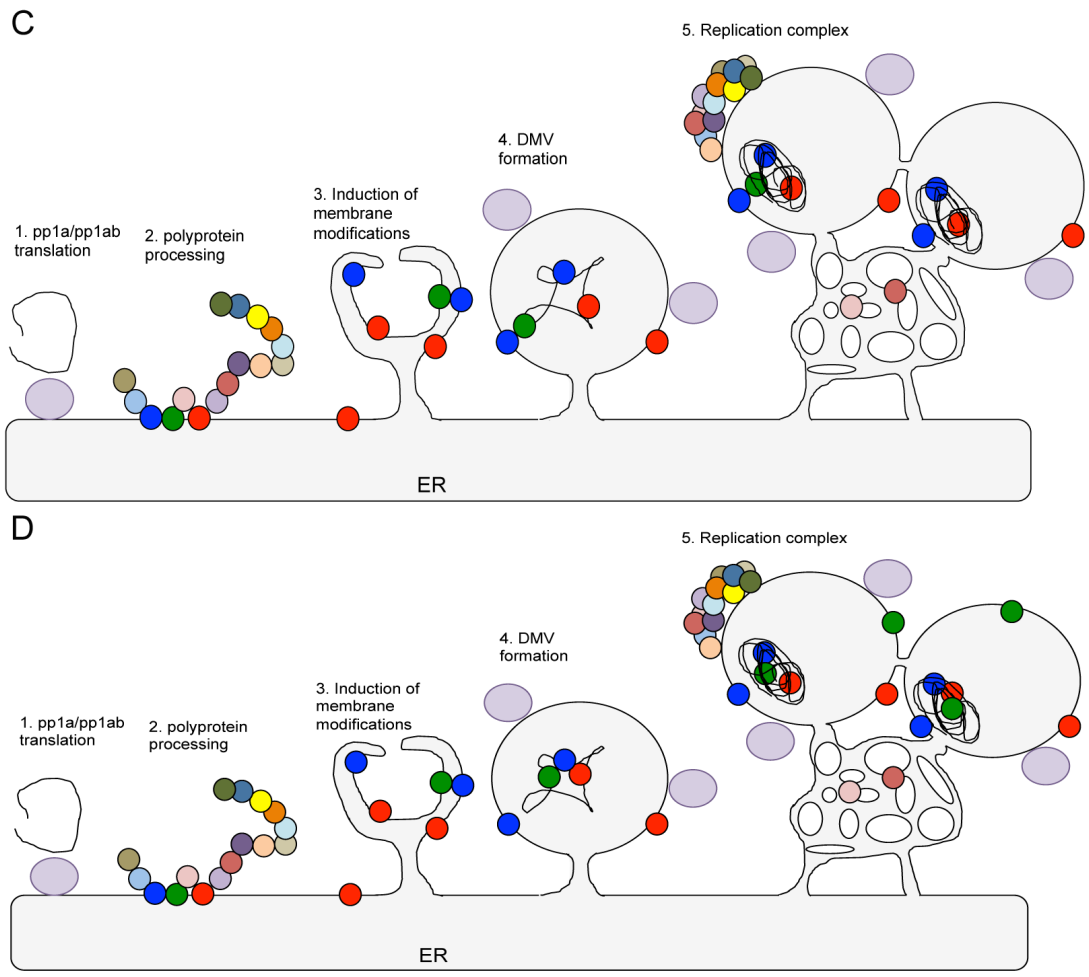

Figure VIII.1: Models for aberrant DMV formation.

(**A**) Model for the formation of normal DMVs. The replicase polyprotein is translated by the ribosome into a large polyprotein that is inserted into the membrane and subsequently cleaved by viral proteases to form mature proteins. Nsp3, nsp4, and nsp6 induce the formation of DMVs with two lipid bilayers in close proximity and convoluted membranes. (**B**) The process begins the as described in A; however, nsp4 is no longer capable of interacting across the lipid bilayer to maintain them in close proximity. (**C**) The process begins as in A except nsp4 is rapidly degraded. Loss of nsp4 results in decreased or lack of interactions to maintain the bilayers in close proximity. (**D**) The process begins as in A but inner bilayer proteins aggregate and collapse the inner membrane.

Figure IV.5) suggests that the protein expression is similar between the nsp4 mutants and WT. The second model involves equal expression of nsp4, however, nsp4 is no longer capable to mediate interactions with nsp3 or another host or viral protein to pair the two membranes of the DMV, resulting in collapse. In this model, DMVs would be initiated, but nsp4 would not interact across the lipid bilayer and maintain the membrane in close proximity. A third possible mechanism is that the proteins within the inner membrane on the DMV aggregate and collapse the membrane. DMVs would initiate similar to WT DMVs, likely with nsp4 interacting with all the appropriate partners to pair the membranes of the DMV. Then once formed, the proteins within the inner membrane interact amongst themselves, likely though the N- or C-termini for clustering and then via loops to mediate collapse. It is also possible that these proposed models are acting in concert, where the mutations alter the confirmation in a way that disrupts membrane-pairing interactions and causes the protein to be degraded at a faster rate than normal and then the remaining proteins interact through other regions of the protein causing aggregation and membrane collapse. Additionally we cannot rule out the possibility that mutations in nsp4 alter DMV maintenance rather than formation. Experiments described below will test how aberrant DMVs are formed.

Do mutant nsp4 protein interact with nsp3 or nsp6?

In order to test the model of whether mutations within nsp4 disrupt interactions with nsp3, co-immunoprecipitations would need to be performed. This is difficult in infected cells because the virus forms polyprotein precursors and numerous proteins are pulled down by immunoprecipitation. Therefore, it would be best to test interactions *in vitro*. In order to test for interactions, it is necessary to generate expression constructs of

MHV nsp3, nsp4, and nsp6. We have SARS-CoV nsp4 and nsp6 constructs that contain C-terminal fusions to either HA or GFP in a modified pCAGGS plasmid (gift from Matt Friedman) (Table VIII.1). Additionally, I received the SARS-CoV nsp3, nsp4, and nsp6 constructs from Michael Buchmeier's lab (UC Irvine). The SARS-CoV nsp3 construct has HA and biotin tags and nsp4 and nsp6 contain HA and FLAG tags. However, not all the mutations I tested in MHV nsp4 were conserved in SARS-CoV; therefore, it is necessary to test the mutations in the context of MHV. I have attempted to generate an MHV nsp4 construct. I used to constructs from Matt Friedman as a backbone, using restriction enzymes to remove the insert and ligating in the MHV nsp4. I was able to successfully engineer WT nsp4 and several mutant nsp4 proteins into the pCAGGS backbones with both GFP and HA (Table VIII.2). However, I was never successful at expressing these proteins. I tried at least two different transfection reagents (lipofectamine and PEI) at several ratios of DNA: transfection reagent and over a time course. This may be due to toxicity associated with the nsp4 protein. It would also be important to clone the MHV nsp3 and nsp6 constructs in order to test the interactions. The de Haan lab has contructs to express MHV nsp3 (c-terminal region), nsp4, and nsp6 using a recombinant Vaccinia virus encoding bacteriophage T7 RNA polymerase expression system (Hagemeijer et al., 2011). It may be possible to acquire the expression system from the de Haan lab; however, during my time in graduate school, they were direct competitors. Additionally, the loop regions of nsp3, nsp4 and nsp6 could be tested for interactions if the whole protein cannot be expressed.

Based on the EM quantification, it would be most interesting to test WT vs. WT, WT vs. DGM-K85S, and DGM- K85S vs. DGM- K85S for homotypic interactions.

Specifically, I would test DGM- K85S because this mutant produced almost 90% aberrant DMVs. Angelini *et al.* demonstrated that nsp3 and nsp4 pair membranes and Hagemeijer *et al.* demonstrated that coexpression of nsp3 and nsp4 results in their relocization to foci suggesting interactions. Therefore, I would test whether the co-expression of nsp3 with WT versus mutant nsp4 maintain the capacity to relocalize

Table VIII.1: Expression constructs for nsp3, nsp4, and nsp6.

Expression construct	Virus background	Source	Expression*
pCAGGS-nsp4-HA	SARS-CoV	Frieman	Yes
pCAGGS-nsp4-GFP	SARS-CoV	Frieman	Yes
pCAGGS-nsp6-HA	SARS-CoV	Frieman	Yes
pCAGGS-nsp6-GFP	SARS-CoV	Frieman	Yes
pCAGGS-nsp3-biotin-HA	SARS-CoV	Buchmeier	No
pCAGGS-nsp4-HA-FLAG	SARS-CoV	Buchmeier	Yes
pCAGGS-nsp6-HA-FLAG	SARS-CoV	Buchmeier	Yes

*In my hands.

Table VIII.2: MHV nsp4 expression constructs.

Expression construct	Tags
pCAGGS-MHV-nsp4	HA, GFP
pCAGGS-MHV-nsp4-DGM	HA, GFP
pCAGGS-MHV-nsp4-E226A/E227A	HA, GFP
pCAGGS-MHV-nsp4-DGM-K85S	HA, GFP
pCAGGS-MHV-nsp4-DGM-N479S	HA

nsp3 and nsp4 into foci. If the mutant protein no longer relocalized with nsp3, it would suggest that the two proteins could no longer interact and pair membranes. Cells co-transfected with either mutant nsp4 and WT nsp3 or mutant nsp4 with WT nsp6 could be harvested and tested for protein interactions by co-IP. I anticipate that the mutant nsp4 proteins will not interact with WT nsp3 and WT nsp6 or have reduced interactions.

Are Aberrant DMVs functional?

Future studies will need to determine whether aberrant DMVs are functional. My RNA synthesis **(**Figure IV.6) and viral yield (Figure IV.5 and Figure IV.8) data suggest that aberrant DMVs are functional although this is indirect evidence. It is likely that the aberrant DMVs are functional since the DGM-K85S virus only produces 12% normal DMVs and ultimately achieves WT-like titer. One could use Click-it technology with 5-ethynyl uridine (EU) to directly label newly synthesized RNA. EU is incorporated into the newly synthesized RNA and can then be detected using Click chemistry and azide-derivitized fluorophores. Infected cells can then be immunostained for EU and nsp4, to determine if all the nsp4 positive foci produce RNA. The de Haan lab has successfully labeled MHV RNA using this system. They also tested colocalization of EU labeled RNA with dsRNA, BrdU and several nsps to demonstrate that newly synthesized RNA are labeled (Hagemeijer, 2012). If the nsp4 foci colocalize with EU labeling, it would suggest that nsp4 positive vesicles produce viral RNA. Since recent reports have demonstrated that membrane modifications can be antiviral targets, understanding how much membrane derangement is required to prevent efficient viral replication will inform inhibitor design.

Do nsp3 mutants produce aberrant DMVs?

A recent report has identified that two mutations within HCoV-229E-nsp6 result in aberrant DMVs similar to the ones we reported (Gadlage et al., 2009; Lundin et al., 2014). This demonstrates that altering nsp4 or nsp6 results in aberrant DMVs. It is likely that mutations within nsp3 also cause aberrant DMV formation. In Chapter VI of this dissertation, I generated several nsp3 charge-to-alanine mutations within the transmembrane region that could be tested for aberrant DMV formation. It has been demonstrated that the entire nsp3 protein is required for DMV formation and that N-terminal truncated forms of nsp3 cannot form DMVs (Angelini et al., 2013; Hagemeijer et al., 2014). Therefore, it would be interesting to test mutations outside of the transmembrane domain that do not impact the other functions of nsp3 for DMV morphology. I would anticipate that mutations within N-terminal region and the transmembrane domain of nsp3 would result in aberrant DMV formation.

Targeting membrane modifications for therapeutics

Recently, virus-induced membrane modifications have become targets for small molecule inhibition. In the Hepatitis C virus field, this has been studied extensively and daclatasvir is the lead compound. Studies have demonstrated that daclatasvir targets NS5A, a viral phosphoprotein that is necessary for membranous web formation (Lee et al., 2011). The inhibitors block the hyperphosorylation of NS5A and disrupt the NS5A-PI4KIIIα complex that is required for maintaining the appropriate concentrations of PI4P and cholesterol within the membranous web (replication complex) (Reghellin et al., 2014). In untreated cells, NS5A localizes to cytoplasmic foci that are scattered throughout the cytoplasm. It is thought that NS5A inhibitors work by sequestering NS5A

to lipid droplets or another location within the cytoplasm and preventing replication complex formation (Reghellin et al., 2014; Targett-Adams et al., 2011).

A small molecule inhibitor (K22) was identified that targets coronavirus membrane modifications. K22 reduced HCoV-229E replication 10,000-fold and when EM was performed, there were no DMVs (Lundin et al., 2014). Additionally, K22 inhibited MHV, FCoV, SARS-CoV, IBV, and MERS-CoV by 2-5 $\log_{10}$ reductions, with the greatest activity against MERS-CoV, FCoV and IBV. Resistance mutations in nsp6 produced aberrant DMVs that decrease viral fitness. It would be important to test for additional compounds that target CoV membrane modifications and test K22 *in vivo*.

Can membrane modifications be targeted in vivo?

Since K22 effectively inhibited SARS-CoV, it would be interesting to test for efficacy in mice. There is a mouse-adapted SARS-CoV strain that has been used extensively by the Baric lab (Day et al., 2009). Mice would be infected with the virus and treated with K22 or vehicle control and monitored for weight loss as a correlate of disease and then viral titers in the lung determined. I would anticipate that mice treated with K22 would not show signs of weight loss and would have minimal replication within the lung, resulting in decreased lung titers. It is possible that the virus will develop resistance to the compound and may replicate; therefore, it would be necessary to sequence the genomes or minimally the transmembrane proteins of virus isolated from the lungs of K22 infected mice.

Are resistance mutants attenuated in vivo?

Nsp5 is one of the main targets for coronavirus inhibition by small molecules. Dang et al. reported resistance mutations to CE-5, a chloropyridyl ester that targets the

nsp5 active site (Deng et al., 2014). When the resistance mutations were reengineered into the isogenic background, the virus was attenuated *in vivo*. It would be interesting to test the K22 resistance mutants *in vivo* for resistance and attenuation. I hypothesize that the virus would be attenuated because it produces aberrant DMVs.

Significance and application of research

The recent emergence of two novel zoonotic CoVs highlights potential for CoVs to emerge into the human population and cause significant disease. Currently there are no known therapeutics or vaccines for coronaviruses. It is necessary to further understand the determinants of viral replication in order to design therapeutics and vaccine candidates. Recently, it has been demonstrated that small molecule compounds that block membrane modifications inhibit both CoVs and Hepatitis C virus (Guedj et al., 2013; Lee et al., 2011; Lundin et al., 2014; Targett-Adams et al., 2011). My work has contributed to the understanding of how CoV membrane modifications can be altered and demonstrates that inner membrane collapse is not enough to alter virus fitness. Small molecules will need to be identified that alter the morphology of both membranes of the DMVs. Additionally, it has not yet been tested how broadly reactive the membrane modification inhibitors are against various viral families. Several viruses, including coronaviruses, use ER membranes to form DMVs. The question remains if viruses use the same membrane source to form similar membranous structures, would the same inhibitors be effective against both viruses? Therefore, understanding how viruses induce membrane modifications may lead to the design of broadly reactive antivirals.

CHAPTER IX: MATERIALS AND METHODS

WT virus, cells and antibodies

Recombinant MHV A59 (GenBank accession number AY910861) virus was used as a WT control viruses for all experiments. DGM, VUJS11 (K44A/D47A), VUJS17 (E226A/E227A) and N258T were previously described (Beachboard et al., 2013; Gadlage et al., 2009; Sparks et al., 2007). Delayed brain tumor (DBT) cells and baby hamster kidney (BHK) cells were grown in Dulbecco's modified Eagle medium (DMEM; Gibco) supplemented with 10% fetal bovine serum, 1% HEPES, 1% penicillin/streptomycin and 0.1% Amphotericin B (complete DMEM). Media for the BHK-MHV receptor (MHVR) cells was supplemented with G418 (Mediatech) at 0.8mg/ml to maintain selection of MHVR. Rabbit polyclonal antibodies were used for biochemical studies and immunofluorescence directed at the viral proteins, nsp3 (VU164) (Graham et al., 2005), nsp4 (VU158) (Sparks et al., 2007), and nsp8 (VU123) (Bost et al., 2001).

Mutagenesis

In order to introduce substitutions into nsp3 or nsp4, the MHV reverse genetics system was used. Briefly, the MHV genome is divided into seven plasmids, the transmembrane domain of nsp3 is in pCR-XL-pSMART B and nsp4 spans two of these plasmids (pCR-XL-pSMART B and pCR-XL-pSMART C). Nucleotides 8721 to 9555 of the MHV-A59 clone are located in fragment B, and nucleotides 9556-10208 are in fragment C. Substitutions were introduced into the B or C fragment by PCR mutagenesis using Quick Change (Stratagene), and the primers listed in (Table IX.1, Table IX.2, and Table IX.3).

Table IX.1: Mutagenesis primers for nsp4 E226X.

Primer name	Sequence	Template	Purpose
E226D sense	GGTTTATGT**GAC**GAGGCCGAGG	B	Mutagenesis for E226D
E226D antisense	CCTCGGC**GTC**CTCACATAAACC	B	Mutagenesis for E226D
E226G sense	GGTTTATGT**GGT**GAGGCCGAGG	B	Mutagenesis for E226G
E226G antisense	CCTCGGCCTC**CCA**ACATAAACC	B	Mutagenesis for E226G
E226S sense	GGTTTATGT**TCC**GAGGCCGAGG	B	Mutagenesis for E226S
E226S antisense	CCTCGGCCTC**GGA**ACATAAACC	B	Mutagenesis for E226S
E226V sense	GGTTTATGT**GTC**GAGGCCGAGG	B	Mutagenesis for E226V
E226V antisense	CCTCGGCCTC**CAG**ACATAAACC	B	Mutagenesis for E226V

E226V mutagenesis resulted in the E226L substitution. E226G mutagenesis resulted in E226G and E226W.

Table IX.2: Mutagenesis primers for Nx(S/T) mutants

Primer Name	Sequence	Purpose
K88S sense	5'-CCGCAACTCT**TTC**GCTTGTCCTG-3'	Mutagenesis for N_{86}S<u>S</u>
K88S antisense	5'-CAGGACAAGC**GGA**AGAGTTGCGG-3'	Mutagenesis for N_{86}S<u>S</u>
V129N sense	5'-CTACTGATAGC**AAC**CAGTGTTACACGC-3'	Mutagenesis for <u>N_{129}</u>QC
V129N antisense	5'-GCGTGTAACACTG**GTT**GCTATCAGTAG-3'	Mutagenesis for <u>N_{129}</u>QC
Q130I sense	5'-CTACTGATAGCAAC**ATA**TGTTACACGC-3'	Mutagenesis for <u>N_{129}I</u>C
Q130I antisense	5'-GCGTGTAACA**TAT**GTTGCTATCAGTAG-3'	Mutagenesis for <u>N_{129}I</u>C
C133N sense	5'-GATAGCGTGCAG**AAC**TACACGCCAC-3'	Mutagenesis for <u>N_{133}</u>YT
C133N antisense	5'-GTGGCGTGTA**GTT**CTGCACGCTAG-3'	Mutagenesis for <u>N_{133}</u>YT
L155N sense	5'-GTTGTCATCC**AAC**TGTACTATGC-3'	Mutagenesis for <u>N_{155}</u>CT
L155N antisense	5'-GCATAGTACA**GTT**GGATGACAAC-3'	Mutagenesis for <u>N_{155}</u>CT
V214N sense	5'-GTGCGTGTT**AAC**CGCACTCGC-3'	Mutagenesis for <u>N_{214}</u>RT
V214N antisense	5'-GCGAGTGCG**GTT**AACACGCAC-3'	Mutagenesis for <u>N_{214}</u>RT
E355N sense	5'-CAACACTTAT**ATT**CGAAGGG-3'	Mutagenesis for <u>N_{355}</u>IS
E355N antisense	5'-CCCTTCG**AAT**ATAAGTGTTG-3'	Mutagenesis for <u>N_{355}</u>IS
N479S sense	5'-CATAATAATGGT**TCC**GATGTTCTC-3'	Mutagenesis for N_{477}G<u>S</u>
N479S antisense	5'-GAGAACATC**GGA**ACCATTATTATG-3'	Mutagenesis for N_{477}G<u>S</u>

Bold letters denote nucleotides used to introduce mutations and underlined letters denote amino acid changes.

Table IX.3: Mutagenesis primers for the nsp3 charge-to-alanine mutants.

Primer name	Sequence	Purpose
D1507A sense	CCATCTGT**GCG**TTCTACCAG	Mutagenesis for D1507A
D1507A antisense	CTGGTAGAA**CGC**ACAGATGG	Mutagenesis for D1507A
E1528A sense	GGTATGT**GCC**CTATGCTTCTC	Mutagenesis for E1528A
E1528A antisense	GAGAAGCATAG**GGC**ACATACC	Mutagenesis for E1528A
R1552A sense	GTAGAT**GCC**CGTTTGTCCTTTG	Mutagenesis for R1552A
R1552A antisense	CAAAGGACAAACG**GGC**ATCTAC	Mutagenesis for R1552A
D1557A sense	GTTTGTCCTTT**GCG**TATATTAG	Mutagenesis for D1557A
D1557A antisense	CTAATATA**CGC**AAAGGACAAACG	Mutagenesis for D1557A
E1567A sense	GTAGTT**GCC**CTTGTAATCGG	Mutagenesis for E1567A
E1567A antisense	CCGATTACAAG**GGC**AACTAC	Mutagenesis for E1567A
R1609A sense	GGAGTGCT**GCC**TTGTTTGTG	Mutagenesis for R1609A
R1609A antisense	CACAAACAA**GGC**AGCACTCC	Mutagenesis for R1609A

Bold is the codon change.

Changes to the manufacturer's protocol include the use of PFU turbo and the following PCR conditions: initial denaturation at 95°C for 2 min, followed by 16 cycles of denaturation at 95°C for 30 sec, annealing at temperatures dependent on the primers for 1 min, and extension for 10 min at 72°C. All B and C fragment plasmids containing mutations in nsp3 or nsp4 were sequenced to ensure that PCR amplification did not introduce additional changes in the coding region.

Virus Recovery

Viruses containing the nsp3 or nsp4 mutations were generated using the reverse genetics system for MHV-A59 described by Yount *et al.* (Yount et al., 2002) and modified by Denison *et al*. (Denison et al., 2004) and Sparks *et al.* (Sparks et al., 2007) (Figure IX.1). The DGM-FFL virus was generated using fragments A and B from previously published viruses, WT-FFL (Freeman et al., 2014a) and DGM (Gadlage et al., 2009). Briefly, the MHV-A59 genome is divided into seven cDNA fragments, which were digested using the appropriate restriction enzymes. These digested fragments were then ligated at 16 °C overnight before the DNA was purified, *in vitro* transcribed and electroporated into BHK-MHVR cells along with N gene transcripts. Electroporated cells were co-cultured with DBT cells and incubated at 37 °C until cytopathic effects were seen. The cytopathic effect see in MHV-infected cells is the formation of multinucleated giant cells (syncytia formation). The virus produced from electroporated cells (passage 0 [P0]) was passaged onto uninfected DBT cells to generate a P1 stock virus that was used for all experiments. The P0 virus was sequenced across the nsp3 transmembrane domain, FFL, or nsp4 gene to ensure that no additional mutations were present. If the *in vitro*

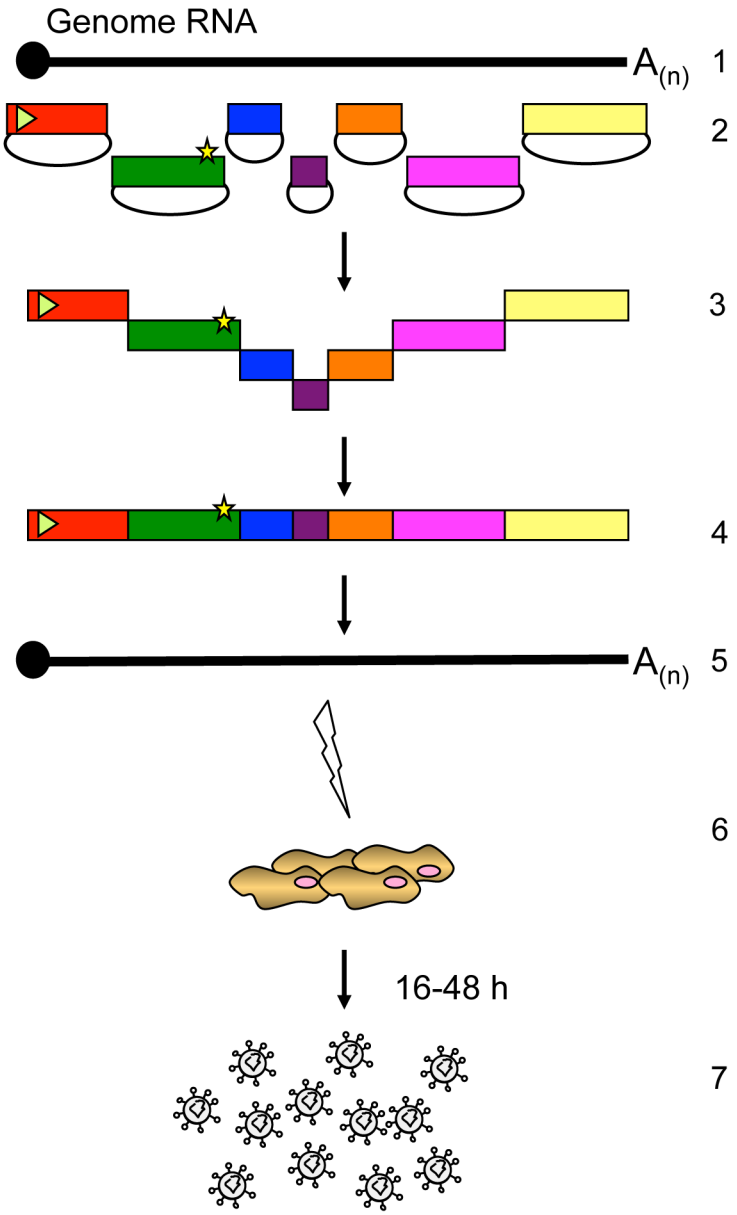

Figure IX.1: MHV reverse genetics system.
The RNA genome (1) is divided into seven cDNA fragments (2). To engineer mutant viruses, the mutation (star) is introduced into the corresponding fragment. CDNA fragments are digested with specific restriction enzymes (3) and ligated together (4). The ligation product is then *in vitro* transcribed (5) and electroporated into permissive cells. Virus can be harvested from the supernatant between 16- 48h post electroporation (7). Adapted from J. Sparks.

transcribed genome did not produce virus on the first attempt, virus assembly was attempted at least two additional times.

Viral passage and isolation of biological revertants

E226A/E227A was passaged blindly seven times (P1-7). Cells were subjected to one round of freeze thaw when they were at least 80% involved in syncytia and 25-100µl of supernatant was used to infect cell for the subsequent passage. After seven passages, viruses were titered by plaque assay and the area of 25 plaques per passage was calculated using ImageJ software (Schneider et al., 2014). Plaque assays were performed on the P1-P3 viruses, as previously described (Kim et al., 1995). Then plaques were isolated an resuspended in gel saline solution and amplified for viral stocks as well as for sequencing.

RT-PCR and sequencing

Total intracellular RNA was isolated using TRIzol (Invitrogen) and the manufacturer's protocol. Viral RNA was then reverse transcribed using Superscript III (Invitrogen) and random hexamers (Roche). The FFL coding sequence with overlaps into nsp1 and nsp2 was amplified using primers complementary to 596 to 613 (sense, nsp1) and 1867 to1883 (antisense, nsp2). The nsp4 coding sequences was amplified by PCR using primers complementary to 8339 to 8335 (sense) and 10345 to 10361 (antisense). The nsp3 transmembrane domain coding sequences was amplified by PCR using primers complementary to 6698 to 6715 (sense) and 7737 to 754 (antisense). The FFL, nsp3, or nsp4 amplicons generated were directly Sanger sequenced to analyze retention of the engineered mutations and absence of additional mutations. For genome sequencing, 15 overlapping amplicons that span the complete genome were generated by PCR and

sequenced directly using Sanger sequencing. Genome amplicons were aligned to the parent virus using MacVector and analyzed for additional mutations.

qRT-PCR

Total intracellular RNA was extracted in TRIzol (Invitrogen) using the manufacturers protocol. Viral RNA (1 μg) was then reverse transcribed using Superscript III (Invitrogen) and random hexamers (Roche). qRT-PCR was performed as previously described (Smith et al., 2013). Briefly, qPCR was performed on the RT product using the Applied Biosciences 7500 Real-Time PCR System with Power SYBR Green PCR Master Mix (Life Technologies). Values were normalized to glyceraldehyde-3-phosphate dehydrogenase (GAPDH).

Viral replication Assay

DBT cells were infected with either WT or mutant viruses at an MOI of 1 PFU/cell and absorbed for 30 min. Cells were then washed twice with PBS, media was replaced, and cells were incubated at 37°C. Supernatants were sampled from 30 min to 24 h post infection (p.i.) and viral titers were determined by plaque assay, as previously described (Kim et al., 1995).

Radiolabel of viral proteins and protein immunoprecipitations

DBT cells were infected at an MOI of 10 PFU/cell or mock infected. At 4 h p.i., the medium was replaced with DMEM that lacks cysteine and methionine and supplemented with 20 μg/ml actinomycin D (ActD; Sigma). At 5 h p.i., [^{35}S]-Methionine/-Cysteine ([^{35}S]-Met/-Cys) was added to the cells and monitored for CPE. When cells were 90-100% involved in CPE, lysates were harvested in lysis buffer (1% NP-40, 0.5% sodium deoxycholate, 150 mM NaCl, and 50 mM Tris, pH 8.0). Lysates

were centrifuged at 6,000 x g for 3 min to remove nuclei. Viral proteins were immunoprecipitated in a total volume of 1ml with 0.6 mg of Protein A-Sepharose beads (Sigma), 200ul lysate, 1:200 dilution of polyclonal nsp4 antisera, and a protease inhibitor cocktail (Roche) in lysis buffer. After an overnight incubation, immunoprecipitated proteins were pelleted by centrifugation at 12,000 x g for 1 min. Protein-bead conjugates were then washed in low salt lysis buffer (lysis buffer with 150mM NaCl), high salt lysis buffer (Lysis buffer with 1M NaCl) and low salt lysis buffer. Samples were then resuspended in 2x SDS protein sample buffer, heated to 70°C for 10 min. For Endoglycosidase H (EndoH; Sigma) treatment, EndoH was added to the supernatant according to manufacturer's protocol and incubated at 37°C for 3h. Proteins were resolved by SDS-PAGE gel electrophoresis on 4-12% Bis-Tris polyacrylamide gels (Invitrogen) and imaged by autoradiography. A full range rainbow ladder (GE Healthcare) and ^{14}C ladder (PerkinElmer LAS) were used as molecular weight standards.

MHV mutants immunofluorescence assay

DBT cells on glass coverslips were mock-infected or infected with WT or nsp4 mutant viruses. At 7 h p.i., medium was aspirated and cells were fixed in 100% methanol at -20°C. Cells were then rehydrated in PBS for 10 min and blocked in PBS containing 5% bovine serum albumin. For indirect immunofluorescence, cell were incubated with nsp3 or nsp4 in wash solution (1% bovine serum albumin and 0.05% NP40 in PBS) containing 2% normal goat serum for 45 min. Cells were then washed 3 times for 5 min each in wash solution. Cells were then incubated with goat anti-rabbit Alexa 488 at 1:1000 for 30 min at room temperature. Anti-nsp8 directly conjugated to Alexa-546 was used for direct immunofluorescence, as previously described (Gadlage et al., 2009). Cells

were incubated with anti-nsp8 at 1:200 dilution for 30 min at room temperature. Cells were then washed three times in wash solution for 5 min each before a final wash in PBS for 30 min. PBS was then aspirated and replaced with distilled water. Coverslips were mounted to glass slides using aquapolymount (Polysciences) and visualized using a Ziess LSM 510 META Inverted confocal microscope with a 40X oil immersion lens. Images were merged and processed using Adobe Photoshop CS5.

MERS-CoV immunofluorescence

WHO-Vero cells grown to 60% confluency on 12-mm glass coverslips were infected with MERS-CoV at an MOI of 1 PFU/cell for the time designated. Viral studies with MERS-CoV were preformed in a BSL-3 laboratory using protocols reviewed and approved by the Institutional Biosafety Committee of Vanderbilt University and the Centers for Disease Control for the safe study and maintenance of MERS-CoV. Medium was aspirated from cells, and cells were fixed and permeablized in methanol at -20^{o}C overnight. Materials were removed from the BSL-3 in accordance with established protocols. Staining was performed as described above. MERS-CoV α-nsp1, nsp5, nsp8, and nsp9 were used at a 1:250 dilution. Goat α-rabbit, mouse, or guinea pig-AlexaFluors 488 (1:1000) or 546 (1:2000 Invitrogen Molecular Probes) were used as secondary antibodies. For cellular markers, PDI and WGA were used at a 1:500 dilution and PDH was used at a 1:1000 dilution and phallodin was used at a 1:40 dilution. Goat α-mouse antibodies were used as secondary antibodies for PDI and PDH. Cells were visualized by widefield immunofluoresnce microscopy on a Nikon Eclipse TE-2000S, or by confocal immunofluorescence microscopy on a Zeiss LSM 510 laser scanning confocal microscope at 488 and 543nm with a 40X oil immersion lens. Images were processed and

assembled using Nikon Elements, ImageJ, and Adobe Photoshop CS5 (12.0.4). All images were processed side-by-side with mock images.

Cell viability assay

DBT cells were plated into 96-well plates at 1 x 10^4 cells/well. At 24h, cells were treated with increasing concentrations of tunicamycin in 0.5% DMSO or cells were treated with 0.5% DMSO for 24h. Cells were then processed for CellTiter-Glo using manufacturers protocol. Briefly, the plate was equilibrated to room temperature for 30 min, and equal volume of CellTiter-Glo reagent was added for 2 min with shaking and 10 min without shaking and then luminescence was measure on the Veritas luminometer (Turner BioSystems).

Luciferase reporter assay

DBT cells in 6-well plates were infected with WT, WT-FFL, or DGM-FFL at an MOI of 1 PFU/cell and incubated at 37°C. At 40 min p.i., media was aspirated to remove inoculum, cells were washed once with PBS, and supplemented with media. At time points indicated, cells were lysed in Reporter Lysis Buffer (Promega), and subjected frozen at -80°C. Following freeze-thaw, lysates were vortexed and centrifuged briefly at top speed, and supernatants transferred to new tubes. To measure luciferase activity, 20 µL of lysate per sample was added to a well of an opaque 96-well plate. Plates were loaded onto a Veritas luminometer (Turner BioSystems) and the automatic injector was used to add 100 µl of reconstituted Luciferase Assay Reagent (Promega) to each well as the samples were being read, 5 s per well, 0 s delay.

Optimization of transmission electron microscopy

In Chapter III, I sought to test the effects of the E226A/E227A mutations on DMV formation. Due to low viral titers, I infected DBT cells at and MOI of 0.1 PFU/cell with WT, the double glycosylation mutant (DGM) or E226A/E227A viruses (Figure IX.2). At 6, 9, and 12 h p.i., cells were fixed in 2% gluteraldehyde and processed for TEM. Mock-infected cells have normal organelles. WT, DGM and E226A/E227A all exhibited signs of infection, including membrane whirls and virion containing vesicles. However, no DMVs or convoluted membranes were visualized. It is possible that DMVs were not visualized because of the use of a low MOI.

Next, in order to optimize visualization of DMVs by EM, an EM time course was performed at a high MOI of 5 PFU/cell using WT virus (Figure IX.3). At 4, 6 and 8 h p.i., WT-infected cells displayed signs of infection, including swollen ER and Golgi complex, DMVs, convoluted membranes, and virions often contained in vesicles. While DMVs and convoluted membranes were present at all time points, they were best visualized at 8 h p.i. I recommend based on these result concentrating low titer viruses to get an MOI of 5 PFU/cell for EM studies.

Transmission Electron Microscopy

DBT cells were mock infected or infected with WT or nsp4 glycosylation mutant viruses at an MOI of 5 PFU/cell in 3 60-mm dishes per sample and incubated at 37°C. At 8 h p.i., medium was aspirated, and cells were washed once with PBS. The cells were then fixed in 2% glutaraldehyde for 10 minutes, scraped off the dishes, and pelleted. The initial 2% glutaraldehyde was aspirated, fresh 2% glutaraldehyde was added to the fixed cells for 1 h, aspirated, and fresh glutaraldehyde was added to the fixed cells for

overnight incubation at 4°C. Cells were washed three times in PBS, transferred to 1% osmium tetroxide in diH_2O for 1 h, and washed three times in diH_2O. Cells were stained *en bloc* in 1% aqueous uranyl acetate for 1 h, and washed three times in diH_2O. Dehydration of cells was carried out gradually using graded series of ethanol and increasing the times each remained in solution, starting with 30%, followed by 50%, 70%, 95%, and finally absolute ethanol. Propylene oxide was used as a transitional solvent to replace the dehydration solution. Cells were transferred to a 1:1 PolyEmbed 812:propylene oxide mixture for 1 hour and then placed in pure PolyEmbed 812 for four exchanges over 36 hours. Pure resin specimens were then transferred into capsules containing fresh resin and finally placed into an oven overnight to polymerize. Ultra-thin serial sections (50-60 nm) from polymerized blocks were obtained using a Leica UCT Ultracut microtome (Leica Microsystems, Vienna, Austria), transferred to formvar-coated slot grids, and examined using a Phillips/FEI T-12 TEM (FEI Company, Hillsboro, OR) equipped with an ATM XR41-S side mounted 2K x 2K CCD camera (Advanced Microscopy Techniques Corp., Woburn, MA). DMVs were categorized as either normal or aberrant (inner membrane appears collapsed). For statistical analysis, the area of cytoplasm was calculated using ImageJ software (Schneider et al., 2014) and the number of DMVs per area of cytoplasm was determined. The Kruskall-Wallis test was used to determine statistical significance of DMVs per area among the viruses.

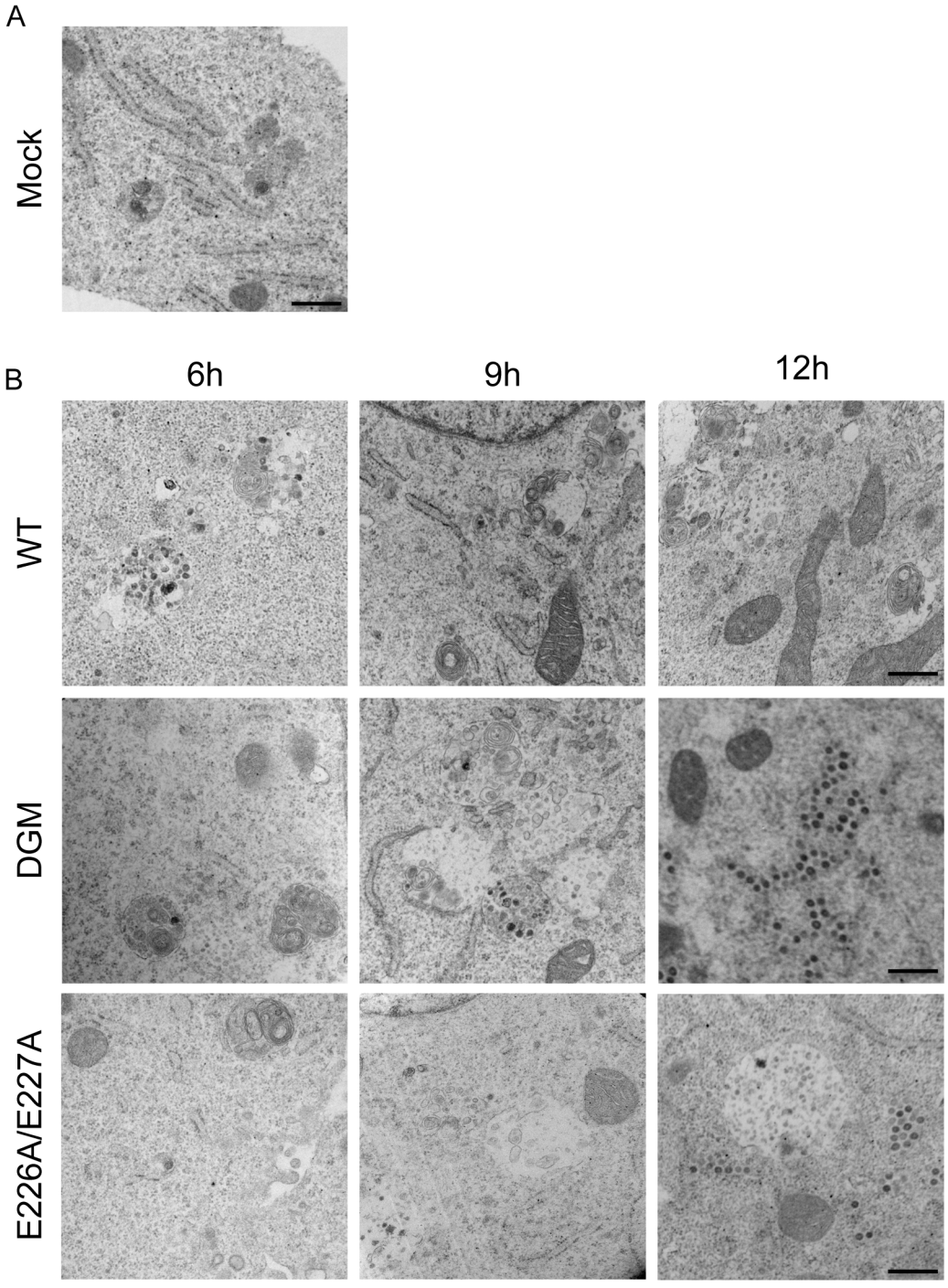

Figure IX.2: EM of E226A/E227A infected cells.

(A) DBT cells were mock infected and fixed in 2% gluteraldehyde and processed for TEM. **(B)** DBT cells were infected with WT, DGM or E226A/E227A at an MOI of 0.1 for indicated times and then fixed in 2% gluteraldehyde and processed for TEM. Scale bars represent 500nm.

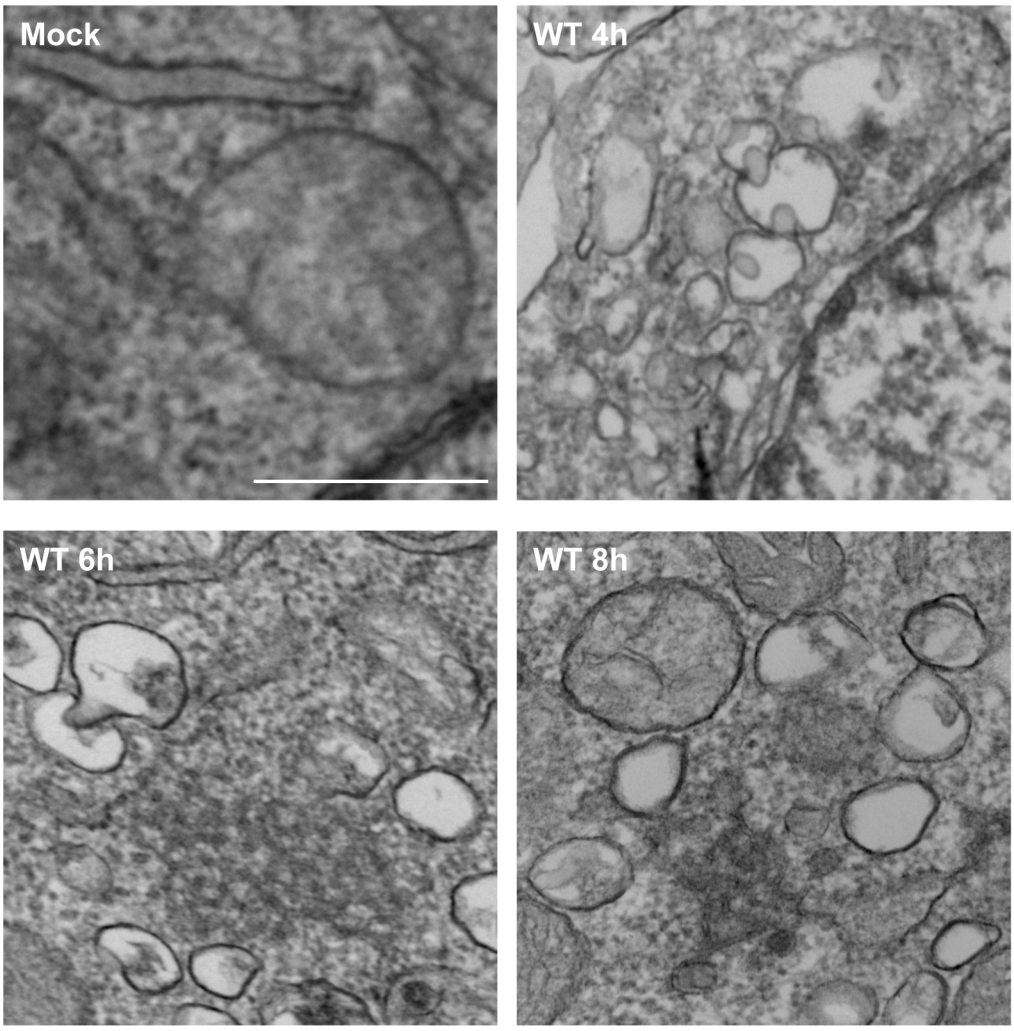

Figure IX.3: EM time course.

DBT cells were mock infected or infected with WT virus at an MOI of 5 PFU/cell and cells were fixed in 2% gluteraldehyde at 4, 6 or 8 h p.i. and processed for TEM. The scale for all images is the same and the scale bar represents 500 nm.

APPENDIX A: MURINE HEPATITIS VIRUS NSP4 N258T MUTATIONS ARE NOT TEMPERATURE-SENSITIVE

Virology 435 (2013) 210–213

Contents lists available at SciVerse ScienceDirect

Virology

journal homepage: www.elsevier.com/locate/yviro

Rapid Communication

Murine hepatitis virus nsp4 N258T mutants are not temperature-sensitive

Dia C. Beachboard [a], Xiaotao Lu [b], Susan C. Baker [c], Mark R. Denison [a,b,*]

[a] Department of Pathology, Microbiology and Immunology, Vanderbilt University Medical Center, 1161 21st Avenue South, Nashville, TN 37232, USA
[b] Department of Pediatrics, Vanderbilt University Medical Center, 1161 21st Avenue South, Nashville, TN 37232, USA
[c] Department of Microbiology and Immunology, Loyola University Chicago Stritch School of Medicine, 2160 South First Avenue, Maywood, IL 60153, USA

ARTICLE INFO

Article history:
Received 13 August 2012
Returned to author for revisions
15 September 2012
Accepted 1 October 2012
Available online 23 October 2012

Keywords:
Coronavirus
Murine hepatitis virus
Replication
Non-structural protein 4
nsp4
Temperature-sensitive mutants
Cell biology

ABSTRACT

Coronavirus replicase nsp4 is critical for virus-induced membrane modifications. An nsp4 mutant (N258T) of murine hepatitis virus (MHV) has been reported to be temperature-sensitive (ts) and to alter membrane targeting. We engineered and recovered all four possible codon variants of N258T in the cloned MHV-A59 background. All mutant viruses demonstrated impaired replication compared to wildtype MHV, but no nsp4 N258T mutant virus was ts, and all variants colocalized with viral protein markers for replication complexes, but not with markers for mitochondria. This study emphasizes that complete genome sequencing may be necessary, even with directed and confirmed reverse genetic mutants.

The study

Coronaviruses, like other RNA viruses, induce modifications of cytoplasmic membranes in order to form replication complexes, as sites of viral RNA synthesis. Three of the coronavirus-encoded replicase non-structural proteins, nsps3, 4 and 6, contain membrane-spanning domains and are thought to be essential for cytoplasmic membrane modifications (Baliji et al., 2009; Imbert et al., 2008; Kanjanahaluethai et al., 2007; Oostra et al., 2008). The topology of nsp4 in membranes has been described and nsp4 has been shown to localize to replication complexes (Gadlage et al., 2010; Hagemeijer et al., 2011; Oostra et al., 2007). Mutations in nsp4 of murine hepatitis virus (MHV) decrease viral RNA synthesis and viral growth, and modification of glycosylation sites within the first luminal loop of nsp4, alters the electron micrograph morphology of virus-induced double-membrane vesicles (DMVs) (Gadlage et al., 2010; Sparks et al., 2007).

Sawicki et al. analyzed a known temperature-sensitive(ts) mutant of MHV, Alb ts6, by sequence and reversion analysis. They identified within the nsp4 coding region an A$\underline{A}_{9494}$T-to-A $\underline{C}_{9494}$T nucleotide (nt) change resulting in an Asn258Thr (N258T) substitution as the putative ts mutation (Sawicki et al., 2005; Sturman et al., 1987). Clementz et al. engineered the N258T substitution in recombinant MHV using a two nt change A$\underline{AT}_{9494–9495}$-to-A$\underline{CA}_{9494–9495}$. The resulting virus, Alb ts6 icv, was reported to be ts at 39.5 °C, and to demonstrate altered distribution of nsp4 in the infected cell, colocalizing with protein markers for the mitochondria. It was concluded that nsp4, and particularly residue N258, is important for membrane localization (Clementz et al., 2008). Subsequently, Sparks et al. (2008) sequenced an Alb ts6 isolate and found four non-synonymous mutations in the complete genome sequence that did not include the previously reported N258T substitution, but instead identified a Val148Ala (V148A) substitution in nsp5 (3CLpro), which was ultimately confirmed by reverse genetics and complete genome sequencing to be responsible for the ts phenotype.

We sought to reconcile these disparate results, using our established reverse genetic system (Yount et al., 2002) to engineer $N258T_{ACA}$ into the same wildtype (WT)-MHV-A59 isogenic background as reported by Clementz et al. (2008). The introduced mutations would require a two nt change for primary reversion to Asn (Fig. 1). The $N258T_{ACA}$ virus was recovered at 30 °C and two rounds of plaque purification were performed prior to expansion and determination of the genome sequence from nt 10 to 31334 by the di-deoxy (Sanger) approach. The $\underline{AT}$ to $\underline{CA}$ change was confirmed and no other changes from the cloned isogenic genome sequence were identified. In order to measure temperature sensitivity, efficiency of plating (EOP) is calculated as the titer at the non-

* Corresponding author at: Department of Pediatrics, Vanderbilt University Medical Center, D6217 MCN, 1161 21st Avenue South, Nashville, TN 37232-2581, USA. Fax: +1 615 343 9723.
E-mail address: mark.denison@vanderbilt.edu (M.R. Denison).

0042-6822/$ - see front matter © 2012 Elsevier Inc. All rights reserved.
http://dx.doi.org/10.1016/j.virol.2012.10.001

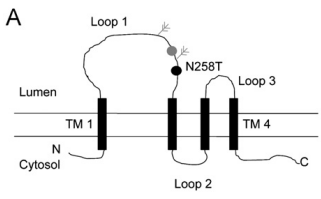

B

Virus	Titer at:		EOP (40/30)
	30°C	40°C	
WT $N258_{AAT}$	1.2×10^9	9.3×10^8	0.79
[1]$N258T_{ACA}$	5.4×10^7	2.8×10^7	0.52
$N258T_{ACC}$	4.6×10^7	3.5×10^7	0.77
$N258T_{ACG}$	4.3×10^7	3.7×10^7	0.88
[2]$N258T_{ACT}$	1.2×10^7	2.3×10^7	2.10
V148A	1.3×10^8	1.9×10^3	1.4×10^{-5}

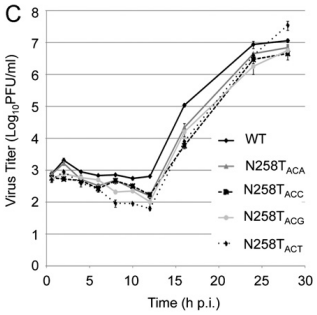

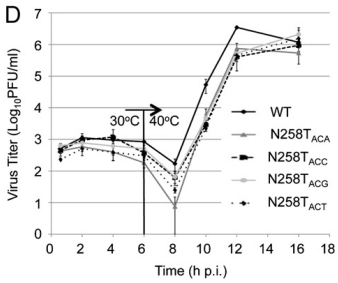

Fig. 1. Analysis of nsp4 N258T codon variant mutants of MHV. (A) Proposed topology of MHV nsp4: nsp4 has 4 membrane-spanning regions (TM1–4, black rectangles) and three loop regions (loop 1–3). Previously reported mutations in loop 1 are indicated as the gray double-headed arrows (glycosylation sites) and a gray dot (E226A/E227A) (Gadlage et al., 2010; Sparks et al., 2007). The N258T (AAT to ACX at nt positions 9493–9495) substitution is shown as a black dot. (B) Titers were determined by plaque assay in DBT cells at 30 °C and 40 °C. EOP was calculated as the titer at 40 °C divided by the titer at 30 °C. Titers represent the average titer of two independent experiments. [1] Codon variant previously reported by Clementz et al. (2008), [2] Codon variant previously reported by Sawicki et al. (2005). (C) DBT cells were infected at an MOI of 0.1 PFU/cell with the indicated viruses and incubated at 30 °C for 28 h and titers were determined by plaque assay. Error bars represent the standard error of the mean of two independent plaque assays done in duplicate. (D) DBT cells were infected at an MOI of 0.1 PFU/cell with the indicated viruses and incubated at 30 °C with a temperature shift to 40 °C at 6 h p.i. and titers were determined by plaque assay. Error bars represent the standard error of the mean of two independent plaque assays done in duplicate.

permissive temperature (40 °C) divided by the titer at the permissive temperature (30 °C). When WT and $N258T_{ACA}$ viruses were compared for EOP, $N258T_{ACA}$ demonstrated an EOP similar to WT, and without a ts phenotype (Fig. 1).

The finding that $N258T_{ACA}$ was not ts by EOP lead us to the questions: why our engineered mutant virus was different than the one reported by Clementz et al.; whether there were additional changes in their virus that led to the observed phenotypes; and if the phenotype was codon-specific . Therefore, we engineered viruses containing the T_{ACC}, T_{ACG} and T_{ACT} codon variants. All three Thr258 codon variant viruses, $N258T_{ACA}$, $N258T_{ACC}$, and $N258T_{ACT}$, were recovered at 30 °C. Sanger sequencing of the complete nsp4 domain confirmed the introduced mutations and no additional mutations were identified.

All codon variant N258T viruses were tested for temperature-sensitivity by plaque assay in murine DBT cells at the permissive (30 °C) and non-permissive (40 °C) temperatures and EOP was calculated (Fig. 1). WT virus had an EOP of 0.79 demonstrating that there is no growth impairment at 40 °C. As a ts control, the EOP of nsp5 tsV148A, was performed in parallel and calculated to be 1.4×10^{-5}, confirming the ts phenotype. All four codon variant viruses had WT-like EOPs (0.52–2.10) indicating that they are not impaired for growth at 40 °C, inconsistent with a ts phenotype (Fig. 1). Because plaque growth and numbers are only a measure of fitness and temperature sensitivity, we next compared growth of the mutant viruses at 30 °C. DBT cells were infected at an MOI of 0.1 PFU/cell and supernatant was sampled at 0.6, 2, 4, 6, 8, 10, 12, 16, 24, and 28 h p.i. for plaque assay (Fig. 1). At 30 °C, all four codon mutants had indistinguishable growth characteristics and achieved peak titers similar to WT at 28 h p.i. However, between 8 and 24 h p.i., the codon mutant viruses exhibited a lag in exponential growth with a 0.5 to 1 log 10 decrease in viral titers during this phase, consistent with a stable replication defect and likely decreased fitness compared with WT (Fig. 1).

We then tested growth following a temperature shift from 30 °C to 40 °C at 6 h p.i., with supernatants sampled at 0.6, 2, 4, 6, 8, 10, 12, and 16 h p.i. WT virus growth kinetics demonstrated an initial decrease in titer immediately following the temperature shift, but recovered quickly, and achieved peak titers by 12 h p.i. All four codon mutants grew indistinguishably from each other, and achieved WT-like peak titers at 16 h p.i. Similar to growth at 30 °C, between 8 and 16 h p.i., the codon mutants exhibited a lag in exponential growth and decreased viral titers compared to WT (Fig. 1). These data demonstrate that while the N258T substitution within nsp4 exhibited impairment in growth, it did not confer temperature-sensitivity, contrary to what has been previously reported.

The $N258T_{ACA}$ virus reported by Clementz et al. (2008). was concluded to have altered localization of nsp4 to mitochondrial membranes at 39.5 °C. To determine the localization of our mutant nsp4 proteins, DBT cells were infected with WT, $N258T_{ACA}$, $N258T_{ACC}$, $N258T_{ACG}$, and $N258T_{ACT}$ on glass coverslips at an MOI of 5 PFU/cell for 16 h at 30 °C or for 7 h at 40 °C (Fig. 2). Infected cells were then fixed and permeabilized with methanol, immunostained with antibodies specific to nsp4 and nsp8 or pyruvate dehydrogenase (PDH), a mitochondrial matrix protein. Cells were imaged using a Zeiss LSM510 confocal microscope.

At both 30 °C and 40 °C, for WT and all N258T codon substitutions, nsp4 and nsp8 extensively colocalized to punctate perinuclear foci (Fig. 2 and data not shown). In contrast, both WT and

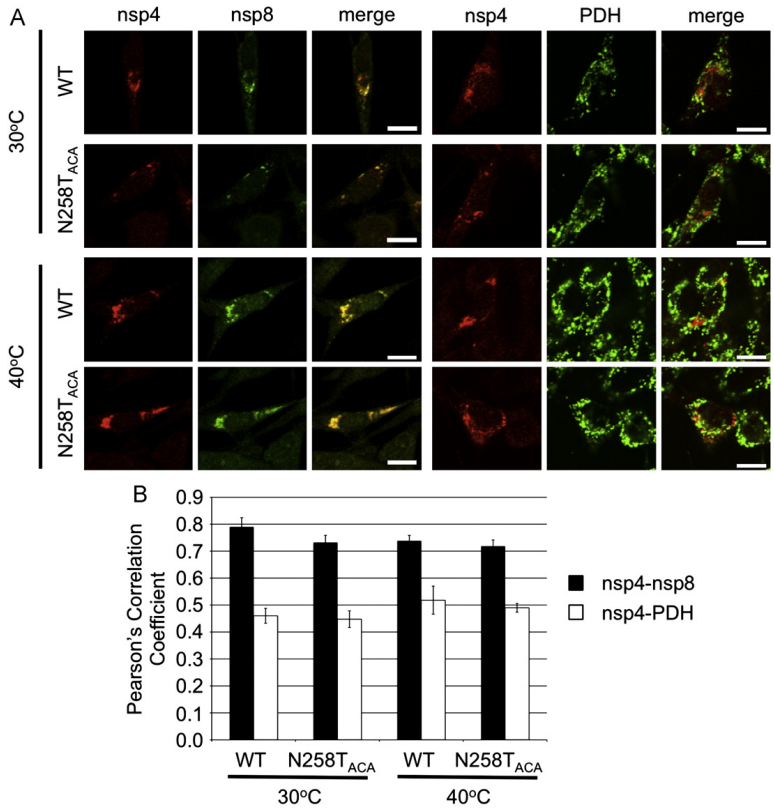

Fig. 2. (A) Nsp4 N258T$_{ACA}$ codon variant localizes to the replication complex. DBT cells were infected at an MOI of 5 PFU/cell for 16 h at 30 °C or 7 h at 40 °C. Cells were fixed in methanol, probed for nsp4 (red) and nsp8 (green) or PDH (green) and imaged on a Zeiss LSM510 confocal microscope. Yellow pixels represent colocalization of overlapping red and green pixels. The scale bar in the bottom right corner of merged images represents 10 μm. (B) Pearson's correlation coefficient was calculated for nsp4-nsp8 or nsp4-PDH for both WT and N258T$_{ACA}$ at 30 °C and 40 °C ($n=5$). Error bars represent standard deviation.

mutant viruses display non-colocalization of nsp4 and PDH. Nsp4 localized to punctate perinuclear foci, whereas PDH localized to foci dispersed throughout the cytoplasm that were adjacent to but distinct from nsp4 foci. Within the same fields of view, there were infected cells that had not formed syncytia as well as syncytial cells and the pattern of colocalization were consistent between both sets of infected cells as well as within a z-stack . In order to quantify colocalization, Pearson's correlation coefficient was calculated using the JACoP plugin for ImageJ (Bolte and Cordelieres, 2006; Schneider et al., 2012). To avoid bias, colocalization was quantified for the entire field and the entire z-stack of five images per condition. At both 30 °C and 40 °C, WT and N258T$_{ACA}$ nsp4 and nsp8 had Pearson's correlation coefficients of between 0.71 and 0.79, respectively, consistent with colocalization. Nsp4 and PDH displayed Pearson's correlation coefficients of 0.45 to 0.52 ($p<.002$), respectively, demonstrating non-colocalization (Fig. 2). These results demonstrate that the nsp4 N258T substitution did not result in altered localization of nsp4 to the mitochondria at either 30 °C or 40 °C.

Conclusions

Our results demonstrate that the nsp4 N258T substitution is not responsible for either the ts phenotype, or for the altered localization of nsp4 to the mitochondria reported by Clementz et al. Although the nsp4 N258T codon variant viruses were not ts, they displayed decreased titers and delayed growth, demonstrating that N258 or loop 1 of nsp4 is likely important for replication. Interestingly, this residue is highly conserved among beta-coronaviruses, including bovine coronavirus, human coronavirus OC43 and SARS-CoV as an aspartic acid, with MHV being the exception. The conservation of this residue suggests that it may be important. Our lab has previously reported two nsp4 mutant viruses, with mutations located in luminal loop 1. Nsp4 contains two glycosylation sites at N176 and N237 (Fig. 1), that when substituted with alanine, demonstrate delayed growth and decreased viral titers similar to those of nsp4 N258T, as well as altered DMV formation (Gadlage et al., 2010). The nsp4 E226A/E227A mutant virus (Fig. 1) is debilitated for growth and viral RNA synthesis (Sparks et al.,

2007). Together, these mutations suggest that loop 1 of nsp4 is important for viral replication, RNA synthesis, and formation of DMVs.

We are unable to explain the results reported by Clementz et al. because the virus was not available for direct comparison. However, our EOP results were confirmed by the Baker lab (data not shown). The reverse genetics system uses seven cDNA fragments that are ligated for transcription of genomic RNA that is then electroporated into cells for virus recovery. There is the possibility that mutations arose during amplification or transcription of the cloned fragments. Our lab and the Baker lab have the same original source for the cDNA fragments. In order to account for changes during amplification, we obtained all seven cDNA fragments from the Baker lab and attempts to recover virus were unsuccessful. We sequenced the cDNA fragment containing nsp4 and identified the $N258T_{ACA}$ substitution, as well as a single nucleotide deletion at nt 8582 that resulted in a possible stop codon (UGA at nt 8644 to 8646). The virus reported by Clementz et al. was difficult to recover (personal communication), leading to the possibility of multiple adaptive changes. The virus was not available for sequencing; therefore, we could not test for additional mutations. The experiments in this study were performed in MHV-A59, and it is important to consider polymorphisms within different strains of virus when analyzing the importance of specific residues. The results of our study strongly suggest that sequencing of the entire genome of mutant coronaviruses derived from the reverse genetics approach may be necessary. Several studies have documented mutations that arise during the process of mutagenesis or propagation of cDNA clones, as well as adaptive mutations that may occur in genes not thought to have any relationship. We demonstrated that the original MHV infectious clone had WT-like replication in culture, but was attenuated in vivo (Sperry et al., 2005). Complete genome sequencing found mutations in other fragments that arose during propagation of the clones that were confirmed to be responsible for the attenuating phenotype. Hurst et al. (2010) showed that impairment in MHV replication by mutations in the nucleocapsid gene resulted in compensating second-site mutations in the replicase protein nsp3. Thus coronaviruses may have unexpected linked functions or epistatic relationships that might be missed by partial sequencing. Fortunately, the cost and time of genome sequencing is rapidly improving. Establishment and availability of validated primer sets may allow for more rapid sequencing in a 96 well format or by deep sequencing, further reducing the cost and time associated with complete genome analysis, and may identify novel and important new relationships among coronavirus proteins.

Acknowledgments

This work was supported by Public Health Service award RO1 AI50083 (M.R.D.) from the National Institute of Allergy and Infectious Disease. D.C.B. was supported by Immunobiology of Blood and Vascular Systems through the Vanderbilt University School of Medecine (T32HL697659). This work was also supported by the Elizabeth B. Lamb Center for Pediatric Research.

References

Baliji, S., Cammer, S.A., Sobral, B., Baker, S.C., 2009. Detection of nonstructural protein 6 in murine coronavirus-infected cells and analysis of the transmembrane topology by using bioinformatics and molecular approaches. J. Virol. 83, 6957–6962.

Bolte, S., Cordelieres, F.P., 2006. A guided tour into subcellular colocalization analysis in light microscopy. J. Microsc. 224, 213–232.

Clementz, M.A., Kanjanahaluethai, A., O'Brien, T.E., Baker, S.C., 2008. Mutation in murine coronavirus replication protein nsp4 alters assembly of double membrane vesicles. Virology 375, 118–129.

Gadlage, M.J., Sparks, J.S., Beachboard, D.C., Cox, R.G., Doyle, J.D., Stobart, C.C., Denison, M.R., 2010. Murine hepatitis virus nonstructural protein 4 regulates virus-induced membrane modifications and replication complex function. J. Virol. 84, 280–290.

Hagemeijer, M.C., Ulasli, M., Vonk, A., Reggiori, F., Rottier, P.J., de Haan, C.A., 2011. Mobility and interactions of the coronavirus nonstructural protein 4. J. Virol. 85, 4572–4577.

Hurst, K.R., Ye, R., Goebel, S.J., Jayaraman, P., Masters, P.S., 2010. An interaction between the nucleocapsid protein and a component of the replicase–transcriptase complex is crucial for the infectivity of coronavirus genomic RNA. J. Virol. 84, 10276–10288.

Imbert, I., Snijder, E.J., Dimitrova, M., Guillemot, J.C., Lecine, P., Canard, B., 2008. The SARS-Coronavirus PLnc domain of nsp3 as a replication/transcription scaffolding protein. Virus Res. 133, 136–148.

Kanjanahaluethai, A., Chen, Z., Jukneliene, D., Baker, S.C., 2007. Membrane topology of murine coronavirus replicase nonstructural protein 3. Virology 361, 391–401.

Oostra, M., Hagemeijer, M.C., van Gent, M., Bekker, C.P., te Lintelo, E.G., Rottier, P.J., de Haan, C.A., 2008. Topology and membrane anchoring of the coronavirus replication complex: not all hydrophobic domains of nsp3 and nsp6 are membrane spanning. J. Virol. 82, 12392–12405.

Oostra, M., te Lintelo, E.G., Deijs, M., Verheije, M.H., Rottier, P.J., de Haan, C.A., 2007. Localization and membrane topology of coronavirus nonstructural protein 4: involvement of the early secretory pathway in replication. J. Virol. 81, 12323–12336.

Sawicki, S.G., Sawicki, D.L., Younker, D., Meyer, Y., Thiel, V., Stokes, H., Siddell, S.G., 2005. Functional and genetic analysis of coronavirus replicase–transcriptase proteins. PLoS Pathog. 1, e39.

Schneider, C.A., Rasband, W.S., Eliceiri, K.W., 2012. NIH image to imageJ: 25 years of image analysis. Nat. methods 9, 671–675.

Sparks, J.S., Donaldson, E.F., Lu, X., Baric, R.S., Denison, M.R., 2008. A novel mutation in murine hepatitis virus nsp5, the viral 3C-like proteinase, causes temperature-sensitive defects in viral growth and protein processing. J. Virol. 82, 5999–6008.

Sparks, J.S., Lu, X., Denison, M.R., 2007. Genetic analysis of Murine hepatitis virus nsp4 in virus replication. J. Virol. 81, 12554–12563.

Sperry, S.M., Kazi, L., Graham, R.L., Baric, R.S., Weiss, S.R., Denison, M.R., 2005. Single-amino-acid substitutions in open reading frame (ORF) 1b-nsp14 and ORF 2a proteins of the coronavirus mouse hepatitis virus are attenuating in mice. J. Virol. 79, 3391–3400.

Sturman, L.S., Eastwood, C., Frana, M.F., Duchala, C., Baker, F., Ricard, C.S., Sawicki, S.G., Holmes, K.V., 1987. Temperature-sensitive mutants of MHV-A59. Adv. Exp. Med. Biol. 218, 159–168.

Yount, B., Denison, M.R., Weiss, S.R., Baric, R.S., 2002. Systematic assembly of a full-length infectious cDNA of mouse hepatitis virus strain A59. J. Virol. 76, 11065–11078.

APPENDIX B: MUTATIONS ACROSS MURINE HEPATITIS VIRUS NSP4 ALTER VIRUS FITNESS AND MEMBRANE MODIFICATIONS

JVI Journals.ASM.org

Editor:	Section:	Designation:
Perlman	Virus-Cell Interactions	T

Mutations across Murine Hepatitis Virus nsp4 Alter Virus Fitness and Membrane Modifications

Dia C. Beachboard,[a,c] Jordan M. Anderson-Daniels,[a] Mark R. Denison[a,b,c]

Departments of Pathology, Microbiology, and Immunology[a] and Pediatrics,[b] and The Elizabeth B. Lamb Center for Pediatric Research,[c] Vanderbilt University Medical Center, Nashville, Tennessee, USA

ABSTRACT

A common feature of infection by positive-sense RNA virus is the modification of host cell cytoplasmic membranes that serve as sites of viral RNA synthesis. Coronaviruses induce double-membrane vesicles (DMVs), but the role of DMVs in replication and virus fitness remains unclear. Coronaviruses encode 16 nonstructural proteins (nsps), three of which, nsp3, nsp4, and nsp6, are necessary and sufficient for DMV formation. It has been shown previously that mutations in murine hepatitis virus (MHV) nsp4 loop 1 that alter nsp4 glycosylation are associated with disrupted DMV formation and result in changes in virus replication and RNA synthesis. However, it is not known whether DMV morphology or another function of nsp4 glycosylation is responsible for effects on virus replication. In this study, we tested whether mutations across nsp4, both alone and in combination with mutations that abolish nsp4 glycosylation, affected DMV formation, replication, and fitness. Residues in nsp4 distinct from glycosylation sites, particularly in the endoplasmic reticulum (ER) luminal loop 1, independently disrupted both the number and morphology of DMVs and exacerbated DMV changes associated with loss of glycosylation. Mutations that altered DMV morphology but not glycosylation did not affect virus fitness while viruses lacking nsp4 glycosylation exhibited a loss in fitness. The results support the hypothesis that DMV morphology and numbers are not key determinants of virus fitness. The results also suggest that nsp4 glycosylation serves roles in replication in addition to the organization and stability of MHV-induced double-membrane vesicles.

IMPORTANCE

All positive-sense RNA viruses modify host cytoplasmic membranes for viral replication complex formation. Thus, defining the mechanisms of virus-induced membrane modifications is essential for both understanding virus replication and development of novel approaches to virus inhibition. Coronavirus-induced membrane changes include double-membrane vesicles (DMVs) and convoluted membranes. Three viral nonstructural proteins (nsps), nsp3, nsp4, and nsp6, are known to be required for DMV formation. It is unknown how these proteins induce membrane modification or which regions of the proteins are involved in DMV formation and stability. In this study, we show that mutations across nsp4 delay virus replication and disrupt DMV formation and that loss of nsp4 glycosylation is associated with a substantial fitness cost. These results support a critical role for nsp4 in DMV formation and virus fitness.

RNA viruses modify host cytoplasmic membranes for the formation of viral replication complexes (1–3). Coronaviruses (CoVs) induce substantial membrane rearrangements, including a reticulovesicular network composed of two types of membrane modifications, double-membrane vesicles (DMVs) and convoluted membranes (CM). The reticulovesicular network is contiguous with the endoplasmic reticulum (ER) membranes and is the site of viral RNA synthesis (4). CoV genomes, which are 27 to 32 kb, encode two replicase/transcriptase open reading frames (ORFS), orf1a and orf1b, which are translated into the polyproteins 1a and 1ab incorporating nonstructural proteins 1 to 16 (nsps 1 to 16). The replicase polyproteins are cleaved by virus-encoded proteases within nsp3 (PLP1/2) and nsp5 (3CLpro). All nsps tested to date have been shown to colocalize by immunoelectron microscopy to DMVs and/or CM and by immunofluorescence at probable sites of viral RNA synthesis (4–11).

Nonstructural proteins 3, 4, and 6 are integral membrane proteins, and the topology of these proteins has been determined *in vitro* for both severe acute respiratory syndrome-CoV (SARS-CoV) and murine hepatitis virus (MHV) (11–13). nsp3 contains two transmembrane domains, nsp4 contains four transmembrane domains, and nsp6 contains six transmembrane domains (14–17). SARS-CoV nsp3, nsp4, and nsp6 are necessary and sufficient for double-membrane vesicle formation. When expressed alone, nsp3 causes membrane proliferation, and nsp6 induces single-membrane vesicles. When coexpressed, nsp3 and nsp4 together have the capacity to pair membranes; however, all three proteins are required for formation of DMVs (3). Likely, interactions among these proteins mediate membrane modifications. Hagemeijer et al. demonstrated by using immunoprecipitation and protein complementation assays that MHV nsp4 forms homotypic and heterotypic interactions with the transmembrane domains of nsp3 and nsp6 (18). The region of nsp4 that

Received 25 September 2014 **Accepted** 24 November 2014

Accepted manuscript posted online 3 December 2014

Citation Beachboard DC, Anderson-Daniels JM, Denison MR. 2015. Mutations across murine hepatitis virus nsp4 alter virus fitness and membrane modifications. J Virol 89:000 –000. doi:10.1128/JVI.02776-14.

Editor: S. Perlman

Address correspondence to Mark R. Denison, mark.denison@vanderbilt.edu.

doi:10.1128/JVI.02776-14

TABLE 1 Primers used for alternate NXS/T mutagenesis

Primer name	Sequence[a]	Purpose
K85S sense	5′-CCGCAACTCT**TTC**GCTTGTCCTG-3′	Mutagenesis for K85S
K85S antisense	5′-CAGGACAAGC**GGA**AGAGTTGCGG-3′	Mutagenesis for K85S
P106N sense	5′-CTTATTTAATGTT**AAC**ACCACAGTTTTAAG-3′	Mutagenesis for P106N
P106N antisense	5′-CTTAAAACTGTGGT**GTT**AACATTAAATAAG-3′	Mutagenesis for P106N
V129N sense	5′-CTACTGATAGC**AAC**CAGTGTTACACGC-3′	Mutagenesis for V129N
V129N antisense	5′-GCGTGTAACACTG**GTT**GCTATCAGTAG-3′	Mutagenesis for V129N
Q130I sense	5′-CTACTGATAGCAAC**ATA**TGTTACACGC-3′	Mutagenesis for Q130I
Q130I antisense	5′-GCGTGTAACA**TAT**GTTGCTATCAGTAG-3′	Mutagenesis for Q130I
C133N sense	5′-GATAGCGTGCAG**AAC**TACACGCCAC-3′	Mutagenesis for C133N
C133N antisense	5′-GTGGCGTGTA**GTT**CTGCACGCTAG-3′	Mutagenesis for C133N
V214N sense	5′-GTGCGTGTT**AAC**CGCACTCGC-3′	Mutagenesis for V214N
V214N antisense	5′-GCGAGTGCG**GTT**AACACGCAC-3′	Mutagenesis for V214N
E355N sense	5′-CAACACTTAT**ATT**CGAAGGG-3′	Mutagenesis for E355N
E355N antisense	5′-CCCTTCG**AAT**ATAAGTGTTG-3′	Mutagenesis for E355N
N479S sense	5′-CATAATAATGGT**TCC**GATGTTCTC-3′	Mutagenesis for N479S
N479S antisense	5′-GAGAACATC**GGA**ACCATTATTATG-3′	Mutagenesis for N479S

[a] Bold letters denote nucleotides used to introduce mutations.

interacts with nsp3 and nsp6, as well as the regions of these proteins required for membrane modifications, remains unknown.

nsp4 contains four transmembrane domains and three loop regions. Loops 1 and 3 are ER luminal, whereas loop 2 and the N and C termini are cytosolic (13, 14). nsp4 is likely required for replication, as demonstrated by the inability to recover a virus with an nsp4 deletion (5). Deletion of transmembrane 4 (TM4) and truncation of the C terminus of nsp4 allow recovery of viable mutants; however, these viruses have altered viral replication and RNA synthesis (5). Additionally, charge-to-alanine mutagenesis of nsp4 identified viral mutants having a range of replicative capacities, ranging from wild-type (WT)-like replication to delayed exponential replication with a 3-$\log_{10}$ reduction in peak viral titers (5).

MHV nsp4 is N-linked glycosylated at two asparagine residues (N176 and N237) within loop 1, as demonstrated by endo-β-*N*-acetylglucosaminidase H (endo-H) sensitivity (1, 12, 13). Glycosylation has many functions, including protein folding, sorting, and trafficking (19). SARS-CoV nsp4 also has been demonstrated to be glycosylated *in vitro* at an atypical glycosylation site, N_{131}IC (13). All coronavirus nsp4 proteins tested to date contain at least one predicted glycosylation site; however, the location and number of the glycosylation sites vary (data not shown). Our lab previously generated an MHV nsp4 mutant lacking both glycosylation sites (N176A/N237A), referred to as the DGM (double-glycosylation mutant). The DGM virus exhibited delayed exponential replication and a reduction in RNA synthesis and formed DMVs with aberrant morphologies (1). These observations suggested a direct link between the capacity of the virus to induce stable DMVs and virus fitness. However, recently, the relationship of DMV size and number to virus fitness has been questioned (20). Since nsp4 is directly involved in DMV formation, we sought to test the role of the DGM and other mutations across nsp4 on the stability and number of DMVs. Additionally, we determined the fitness of these viruses over multiple passages compared to wild-type and the DGM viruses. Our data demonstrate that mutations across nsp4 domains, in addition to glycosylation mutants, result in alterations of DMV morphology and number and that loss of nsp4 glycosylation is clearly associated with fitness cost when directly competed.

MATERIALS AND METHODS

WT virus, previously reported mutant viruses, cells, and antibodies. Recombinant MHV A59 (GenBank accession number AY910861) virus was used as a WT control virus for all experiments. The double-glycosylation mutant (DGM; N176A/N237A), VUJS11 (K44A/D47A), VUJS17 (E226A/E227A), and N258T viruses were previously described (1, 5, 21). Delayed brain tumor (DBT) cells and baby hamster kidney (BHK) cells were grown in Dulbecco's modified Eagle medium (DMEM; Gibco) supplemented with 10% fetal bovine serum, 1% HEPES, 1% penicillin-streptomycin, and 0.1% amphotericin B (complete DMEM). Medium for the BHK-MHV receptor (MHVR) cells was supplemented with G418 (Mediatech) at 0.8 mg/ml to maintain selection of MHVR. Rabbit polyclonal antibodies were used for biochemical studies and immunofluorescence directed at the viral protein, nsp4 (VU158) (5).

Mutagenesis. In order to introduce substitutions into nsp4, an MHV reverse genetics system was used. Briefly, the MHV genome was divided into seven plasmids, with nsp4 spanning two of these plasmids (pCR-XL-pSMART B and pCR-XL-pSMART C). Nucleotides 8721 to 9555 of the MHV A59 clone were located in fragment B, and nucleotides 9556 to 10208 were in fragment C. Substitutions were introduced into the B or C fragment by PCR mutagenesis using the QuickChange method (Stratagene) and the primers listed in Table 1. Changes to the manufacturer's protocol include the use of *Pfu* Turbo and the following PCR conditions: initial denaturation at 95°C for 2 min, followed by 16 cycles of denaturation at 95°C for 30 s, annealing at temperatures dependent on the primers for 1 min, and extension for 10 min at 72°C. All B and C fragment plasmids containing mutations in nsp4 were sequenced to ensure that PCR amplification did not introduce additional changes in the coding region.

Virus recovery. Viruses containing the nsp4 mutations were generated using a reverse genetics system for MHV A59 as described by Yount et al. (22) and modified by Denison et al. (23) and Sparks et al. (5). Briefly, the MHV A59 genome was divided into seven cDNA fragments, which were digested using the appropriate restriction enzymes. These digested fragments were then ligated at 16°C overnight before the DNA was purified, *in vitro* transcribed, and electroporated into BHK-MHVR cells along with N gene transcripts. Electroporated cells were cocultured with DBT cells and incubated at 37°C until cytopathic effects (CPE) were seen. The cytopathic effect see in MHV-infected cells is the formation of multinucleated giant cells (syncytium formation). The virus produced from electroporated cells (passage 0 [P0]) was passaged onto uninfected DBT cells to generate a P1 stock virus that was used for all experiments. The P1 virus was sequenced across the region of the nsp3 to nsp6 genes to ensure that

no additional mutations were present in the membrane proteins. If the *in vitro*-transcribed genome did not produce virus on the first attempt, virus assembly was attempted at least two additional times.

Reverse transcription-PCR (RT-PCR) and sequencing. Total intracellular RNA was isolated using TRIzol (Invitrogen) and the manufacturer's protocol. Viral RNA was then reverse transcribed using Superscript III (Invitrogen) and random hexamers (Roche). The coding sequences of nsp3 through nsp6 were amplified by PCR to generate four amplicons covering nucleotides 2389 to 13219. The amplicons generated were directly Sanger sequenced to analyze retention of the engineered mutations and absence of additional mutations.

Viral replication assay. DBT cells were infected with either WT or nsp4 mutant viruses at a multiplicity of infection (MOI) of 1 PFU/cell and absorbed for 30 min. Cells were then washed twice with phosphate-buffered saline (PBS), medium was replaced, and cells were incubated at 37°C. Supernatants were sampled from 30 min to 24 h postinfection (p.i.), and viral titers were determined by plaque assay, as previously described (24).

Radiolabeling of viral proteins and protein immunoprecipitation. DBT cells were infected at an MOI of 10 PFU/cell or mock infected. At 4 h p.i., the medium was replaced with DMEM lacking cysteine and methionine and supplemented with 20 μg/ml actinomycin D (ActD; Sigma). At 5 h p.i., [^{35}S]methionine/cysteine ([^{35}S]Met-Cys) was added to the cells and monitored for CPE. When cells were 90 to 100% involved in CPE, lysates were harvested in lysis buffer (1% NP-40, 0.5% sodium deoxycholate, 150 mM NaCl, and 50 mM Tris, pH 8.0). Lysates were immunoprecipitated as previously described (1).

Immunofluorescence assay. DBT cells on glass coverslips were mock infected or infected with WT or nsp4 mutant viruses. At 7 h p.i., medium was aspirated, and cells were fixed in 100% methanol at −20°C. Cells were then rehydrated in PBS for 10 min and blocked in PBS containing 5% bovine serum albumin. For indirect immunofluorescence, cell were incubated with nsp4 in wash solution (1% bovine serum albumin and 0.05% NP-40 in PBS) containing 2% normal goat serum for 45 min. Cells were then washed three times for 5 min each time in wash solution. Cells were then incubated with goat anti-rabbit Alexa-488 at 1:1,000 for 30 min at room temperature. Anti-nsp8 directly conjugated to Alexa-546 was used for direct immunofluorescence, as previously described (1). Cells were incubated with anti-nsp8 at a 1:200 dilution for 30 min at room temperature. Cells were then washed three times in wash solution for 5 min each before a final wash in PBS for 30 min. PBS was then aspirated and replaced with distilled water. Coverslips were mounted to glass slides using Aqua-Poly/Mount (Polysciences) and visualized using a Zeiss LSM 510 Meta inverted confocal microscope with a 40× oil immersion lens. Images were merged and processed using Adobe Photoshop CS5.

qRT-PCR. Total intracellular RNA was extracted in TRIzol (Invitrogen) using the manufacturer's protocol. Viral RNA (1 μg) was then reverse transcribed using Superscript III (Invitrogen) and random hexamers (Roche). Quantitative RT-PCR (qRT-PCR) was performed as previously described (25). Briefly, quantitative PCR (qPCR) was performed on the RT product using an Applied Biosciences 7500 real-time PCR system with Power SYBR green PCR master mix (Life Technologies). Values were normalized to glyceraldehyde-3-phosphate dehydrogenase (GAPDH). A Kruskal-Wallis test was used to determine statistical differences between WT and mutant levels of RNA synthesis.

TEM. DBT cells were mock infected or infected with WT or nsp4 glycosylation mutant viruses at an MOI of 5 PFU/cell in three 60-mm dishes per sample and incubated at 37°C. At 8 h p.i., medium was aspirated, and cells were washed once with PBS. The cells were then fixed in 2% glutaraldehyde for 10 min, scraped off the dishes, and pelleted. The initial 2% glutaraldehyde was aspirated, fresh 2% glutaraldehyde was added to the fixed cells for 1 h and aspirated, and then fresh glutaraldehyde was added to the fixed cells for overnight incubation at 4°C. Cells were washed three times in PBS, transferred to 1% osmium tetroxide in distilled H_2O (diH_2O) for 1 h, and washed three times in diH_2O. Cells were stained *en bloc* in 1% aqueous uranyl acetate for 1 h and washed three times in diH_2O. Dehydration of cells was carried out gradually using a graded series of ethanol and increasing the times each sample remained in solution, starting with 30%, followed by 50%, 70%, 95%, and finally absolute ethanol. Propylene oxide was used as a transitional solvent to replace the dehydration solution. Cells were transferred to a 1:1 PolyEmbed 812-propylene oxide mixture for 1 h and then placed in pure PolyEmbed 812 for four exchanges over 36 h. Pure resin specimens were then transferred into capsules containing fresh resin and finally placed into an oven overnight to polymerize. Ultrathin serial sections (50 to 60 nm) from polymerized blocks were obtained using a Leica UCT ultracut microtome (Leica Microsystems, Vienna, Austria), transferred to Formvar-coated slot grids, and examined using a Phillips/FEI T-12 transmission electron microscope (TEM; FEI Company, Hillsboro, OR) equipped with an ATM XR41-S side-mounted charge-coupled-device (CCD) camera (2,000 by 2,000 pixels; Advanced Microscopy Techniques Corp., Woburn, MA). For mock-infected cells, fields were chosen randomly. For virus-infected cells, cells were imaged if there were signs of infection, which included DMVs, convoluted membranes, and virions. DMVs were categorized as either normal or aberrant (inner membrane appears collapsed). For statistical analysis, the area of cytoplasm was calculated using ImageJ software (26), and the number of DMVs per area of cytoplasm was determined. A Kruskal-Wallis test was used to determine statistical significance of DMVs per area among the viruses.

Competition assay. DBT cells were infected at a final MOI of 0.1 PFU/cell with the WT and DGM, with the DGM and DGM-K85S, and with the DGM and N258T viruses at ratios of 1:1. Supernatants were collected for passage, and total RNA was harvested in TRIzol. Supernatants were passaged three times. RNA extraction and RT-PCR were performed as described above. The nsp4 amplicon electropherograms were then analyzed using MacVector, version 13, to measure the area under the curve for each mutation. Then for each virus pair, the percentage of virus A nucleotides compared to virus B nucleotides was calculated. At least three nucleotide positions per pair of viruses was analyzed and averaged to calculate the final percentages. There were at least two biological replicates for each competition.

RESULTS

Mutations across nsp4 impair DMV morphology and numbers. In order to test whether nsp4 glycosylation regulates proper DMV formation independent of its position in the protein, we engineered mutations to introduce a glycosylation sequon, NX(S/T) at different locations in the nsp4 DGM (double-glycosylation mutant, N176A/N237A) background (Fig. 1). Two viruses were engineered to insert predicted glycosylation sites from other coronaviruses; V129N/Q130I is the glycosylation sequon of SARS-CoV, and N479S introduced the sequon present in both human CoV (HCoV) OC43 and bovine CoV (BCoV). All other mutations were inserted near highly conserved asparagine, serine, or threonine residues to introduce new potential NX(S/T) sequons (Fig. 1). Both strategies have successfully been used to introduce glycosylation sites into proteins (27–30). We recovered three mutants in the DGM background and one in the WT background; two DGM viruses contained NX(S/T) mutations from other coronaviruses (DGM-V129N/Q130I and DGM-N479S) one DGM virus had a mutation that was introduced after a conserved asparagine (DGM-K85S). Additionally, N479S was recovered in the WT nsp4 background. Recovered viruses were sequenced across the region of nsp3 through nsp6 and contained no additional mutations. Recovery of all other engineered genomes was attempted at least three times with no signs of virus-induced CPE.

To determine whether the mutations that introduce potential alternate glycosylation sequons restored proper DMV morphology, murine delayed brain tumor (DBT) cells were infected with

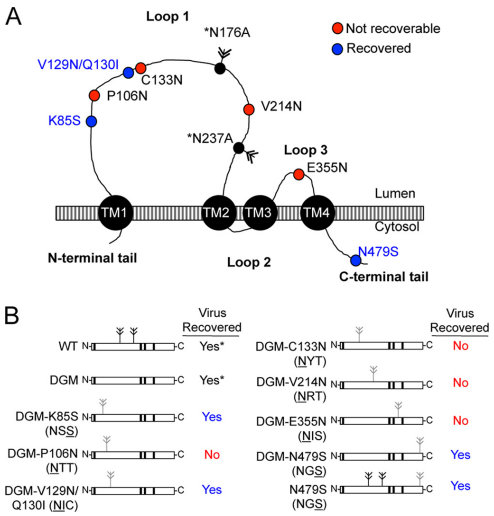

FIG 1 Engineering nsp4 mutants. (A) Proposed topology of nsp4: nsp4 has four transmembrane regions (TM1 to TM4) and three loops (loop 1 to 3). Mutations in nsp4 tested in this study are shown on the diagram. Red circles represent nonviable mutations; green circles represent viable viruses that were recovered in this study. The double-headed arrows represent native glycosylation sites within MHV nsp4. (B) nsp4 mutants were engineered with alternate NX(S/T) sites (gray double-headed arrows) in the DGM background. The locations of the introduced NX(S/T) sequons (gray double-headed arrows) are shown. Viruses are identified with the introduced NX(S/T) site shown below the designation. *, previously recovered viruses (1).

WT or nsp4 mutant viruses and analyzed for membrane changes by TEM (Fig. 2). Mock-infected cells exhibited regular cellular architecture and normal organelles. WT-infected cells displayed swollen ER and Golgi compartments, as well as the presence of several virus-induced structures, including DMVs, convoluted membranes (CM), and vesicles containing newly formed virions (Fig. 2). The DMVs in WT-infected cells had membranes containing two lipid bilayers in close proximity to one another. Similarly, DGM-infected cells had swollen ER and Golgi compartments; however, the DMVs were aberrant. Aberrant DMVs in this study are defined as vesicles having inner membranes that are separated or collapsed away from the outer membrane. The degree of inner membrane collapse varied; however, the majority of aberrant DMV inner membranes were completely collapsed and appeared as electron-dense structures at one side of the vesicles. This is in contrast to the DMV artifacts with spiderweb-like content seen with standard electron microscopy (EM) of SARS-CoV-infected cells (7). All DMVs considered normal in this study had both lipid bilayers intact and contained no spiderweb-like contents. Each of the viruses that contained engineered NX(S/T) sequons exhibited aberrant DMVs similar to the DGM virus. The numbers of normal and aberrant DMVs were calculated for each virus. DGM-K85S- and DGM-V129N/Q130I-infected cells produced increased numbers of aberrant DMVs (88% and 78%, respectively) compared to DGM (67%) (Fig. 2 and Table 2). Cells infected with DGM-N479S and N479S viruses produced fewer aberrant DMVs (54% and 53%, respectively) than DGM but more aberrant DMVs than the WT (37%). Next, the number of DMVs per area of cytoplasm was calculated to determine whether the differences in total numbers of DMVs counted per sample corresponded to differences in total numbers of DMVs (Fig. 2). DGM, DGM-K85S, and N479S had significantly decreased numbers of DMVs compared to the WT (Fig. 2I). The differences in total numbers of DMVs may be due to direct effects of mutations in nsp4 or may reflect differences in the degree of viral replication occurring. These data demonstrate that inserting additional mutations within loop 1 of nsp4 exacerbates the aberrant DMV formation associated with the DGM phenotype. Additionally, these data demonstrate that mutations within the C terminus of nsp4 cause aberrant DMVs independent of mutations within loop 1.

nsp4 NX(S/T) sequons do not complement defects in replication or nsp4 glycosylation. Next, we sought to determine whether the viruses with aberrant DMVs were associated with altered replication kinetics. DBT cells were mock infected or infected with indicated viruses at an MOI of 1 PFU/cell. At indicated times, supernatants were sampled, and titers were determined by plaque assay (Fig. 3). WT virus began exponential replication between 4 and 6 h p.i. and achieved a peak titer at 10 h p.i. The DGM virus replicated with delayed kinetics, began exponential replication between 6 to 8 h p.i., and achieved a WT-like peak titer at 12 h p.i. N479S replicated indistinguishably from the WT, and the DGM-K85S and DGM-N479S viruses replicated indistinguishably from the parental DGM virus. The DGM-V129N/Q130I mutant displayed delayed exponential replication and peak titer compared with both the WT and the parental DGM viruses.

These data suggested that either glycosylation at alternate residues did not complement the replication delay of DGM or that these nsp4 proteins were not glycosylated. To determine the glycosylation status of the mutant nsp4 proteins, virus-infected cells were radiolabeled, and cell lysates were immunoprecipitated with antibodies specific for nsp4, followed by treatment with endo-H to remove N-linked glycans (Fig. 3). WT nsp4 migrated at 44 kDa in the absence of endo-H and displayed a mobility shift to 39 kDa following endo-H treatment, indicative of the removal of two glycans, each with an expected mobility shift of 2.5 kDa. The N176A virus was glycosylated at one site (42 kDa), and DGM lacked glycosylation and migrated at 39 kDa. In contrast, all of the alternate NX(S/T) mutant viruses in the DGM background migrated at 39 kDa regardless of endo-H treatment, indicating that the mutant nsp4 proteins were not glycosylated. The N479S nsp4 protein migrated at 44 kDa in the absence of endo-H and shifted to 39 kDa in the presence of endo-H, demonstrating that this nsp4 protein is glycosylated at the native glycosylation sites only. While we can draw no conclusions from an inability to recover virus mutants, we did observe that all recovered viruses failed to confer glycosylation at the introduced sequon, whereas compared with a large number of mutations that are tolerated in nsp4, several new NX(S/T) sequons in loop 1 could not be recovered after multiple attempts. The results led us to consider the possibility that sequons capable of glycosylation may not be tolerated in loop 1.

nsp4 NX(S/T) mutants have WT-like RNA synthesis. Since the differences in total DMV numbers demonstrated by EM may reflect overall differences in viral replication, next we assessed the RNA synthesis capacities of these viruses. DBT cells were infected at an MOI of 1 PFU/cell for 10 h. Total cellular RNA was harvested in TRIzol, and qRT-PCR was performed to amplify nsp10 and

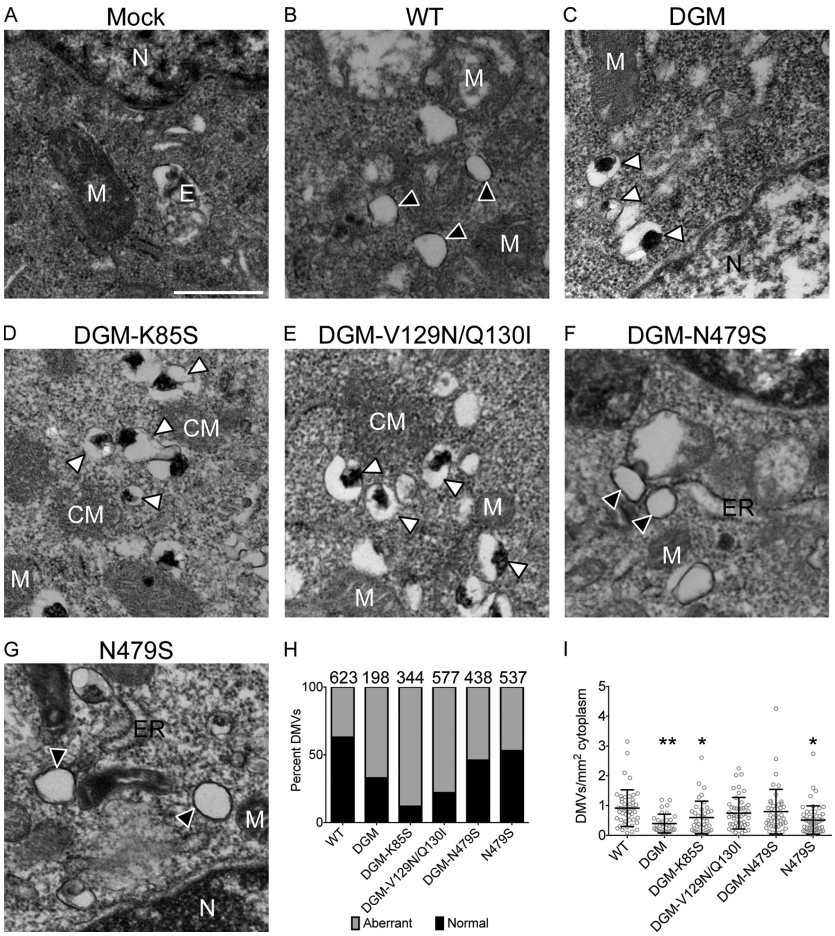

FIG 2 Electron microscopic analysis of alternate NX(S/T) sequon mutants. (A to F) DBT cells were mock infected (A) or infected with the WT (B), DGM (C), DGM-K85S (D), DGM-V129N/Q130I (E), DGM-N479S (F), or N479S (G) virus at an MOI of 5 PFU/cell for 8 h before being fixed in 2% glutaraldehyde and processed for TEM. Black arrowheads indicate normal DMVs; the white arrowheads indicate aberrant DMVs. CM, convoluted membranes; N, nucleus; M, mitochondrion; E, endosome; VV, virions in vesicles; ER, endoplasmic reticulum. Scale bar, 500 nm. (H) Normal and aberrant DMVs were quantified for each virus. Percentages are shown as indicated on the figure. The total number of DMVs analyzed is shown above each bar. (I) The numbers of DMVs per area of cytoplasm were calculated and are shown on the graph. Each circle represents an individual field, and the bars show the means ± standard deviations. Fields were chosen based on the presence of signs of virus infection that included DMVs, convoluted membranes, and virions. A Kruskal-Wallis test was used to analyze for significant differences in numbers of DMVs per area of cytoplasm. *, $P = 0.008$; **, $P < 0.0001$ (compared to the WT).

GAPDH. All viruses had RNA synthesis levels indistinguishable from the WT level (Fig. 4). It is likely that, similar to the replication kinetics, if time points were taken, there would have been a delay in RNA synthesis. These data suggest that the viruses have no significant decrease in viral replication at 10 h p.i. and that aberrant DMVs are capable of supporting RNA synthesis.

nsp4 NX(S/T) mutants localize to the replication complex. In order to determine whether differences in total numbers of DMVs correspond to differences in replication complex formation and overall protein levels, DBT cells on coverslips were infected with the WT or the nsp4 NX(S/T) viruses at an MOI of 5 PFU/cell for 6.5 h (Fig. 5). Cells were then fixed in methanol and stained with antibodies specific to nsp4 and nsp8, a marker for the replication complex. In WT-infected cells, nsp4 and nsp8 colocalized at punctate perinuclear foci. All mutant nsp4 proteins extensively colocalized with nsp8 at perinuclear foci. These data demonstrate that

TABLE 2 Quantification of normal and aberrant DMVs

Virus	No. of DMVs		
	Total	Normal	Aberrant (% of total)
WT	623	393	230 (37)
DGM	198	65	133 (67)
DGM-K85S	344	40	304 (88)
DGM-V129I/Q130I	577	126	451 (78)
DGM- N479S	438	202	236 (54)
K44A/D47A	308	101	207 (67)
E226A/E227A	326	96	230 (71)
N258T	412	128	284 (69)
N479S	587	310	277 (53)

the NX(S/T) mutant nsp4 proteins localize to the replication complex. Additionally, there is no apparent correlation between aberrant DMV formation and the level of replication complex formation or protein expression. Collectively, the RNA synthesis and immunofluorescence data indicate that the difference in total numbers of DMVs does not reflect overall replication or protein expression within these infected cells.

Substitutions in nsp4 loop 1 alter replication kinetics and DMV morphology independent from glycosylation status. Having demonstrated that mutations in nsp4 loop 1 exacerbate the aberrant DMV morphology associated with the DGM phenotype, we tested whether any mutation in nsp4 loop 1, independent of glycosylation potential, impacted replication and DMV morphology/numbers. nsp4 loop 1 mutants previously reported from our lab were tested (Fig. 6); these consist of mutants K44A/D47A (VUJS11), E226A/E227A (VUJS17), and N258T (5, 21). In contrast to WT MHV A59, all three mutant viruses exhibited a range of replication defects. The N258T mutant was minimally delayed but achieved WT-like titers, the K44A/D47A mutant was more delayed in both exponential replication and peak titer, and the E226A/E227A mutant showed a significant delay but achieved WT-like peak titer (Fig. 6C). We then tested for the glycosylation status of the mutant nsp4 proteins by radiolabeling and immunoprecipitation. All nsp4 loop 1 mutant nsp4 proteins migrated at 44 kDa in the absence of endo-H and at 39 kDa in the presence of endo-H. These results show that all tested nsp4 loop 1 mutants are glycosylated at both native asparagine residues. Thus, the observed replication defects were not due to changes in the glycosylation status of the protein. Finally, we examined the DMV morphology and numbers in mutant virus-infected cells (Fig. 7 and Table 2). Similar to the N479S mutation alone, each of the nsp4 mutant virus-infected cells produced aberrant DMVs. The percentage of aberrant DMVs was calculated for each virus and showed an increase compared to the WT level. All of the loop 1 mutant viruses produced numbers of aberrant DMVs similar to level in the DGM mutant. Infection with K44A/D47A and E226A/E227A also resulted in significantly fewer DMVs than infection with WT virus. In contrast, N258T produced a similar number of DMVs as the WT. Thus, our results indicate that in addition to mutations that affect glycosylation of nsp4, substitutions at other locations in nsp4 loop 1 result in altered DMV morphology.

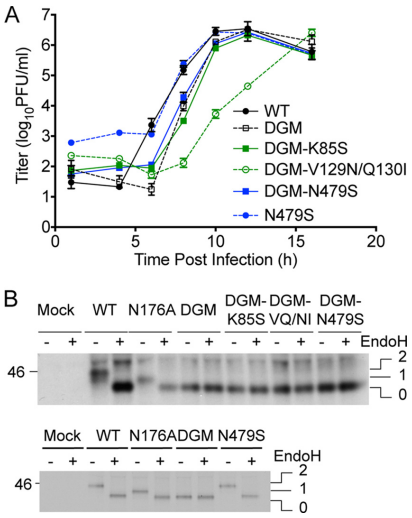

FIG 3 Replication kinetics and glycosylation of alternate NX(S/T) sequon viruses. (A) DBT cells were infected with the indicated viruses at an MOI of 1 PFU/cell. Supernatants were sampled from 0 to 16 h p.i., and titers were determined by plaque assay. Error bars represent the standard errors of the means of three replicates plated in duplicate. (B) DBT cells were infected with the indicated viruses at an MOI of 10 PFU/cell. At 4 h p.i., cells were starved in DMEM lacking Met and Cys and treated with ActD for 1 h before being radiolabeled with [^{35}S]Met-Cys. At 7 h p.i., lysates were harvested and immunoprecipitated with antibodies specific for nsp4 and treated in the presence or absence of endo-H. Proteins were resolved by SDS-PAGE ($n \geq 2$). DGM-VQ/NI, DGM-V129N/Q130I.

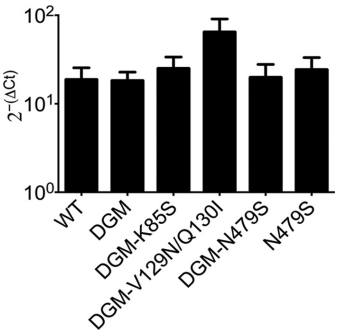

FIG 4 RNA synthesis of nsp4 NX(S/T) mutants. DBT cells were infected with the indicated viruses at an MOI of 1 PFU/cell for 10 h. Cells were then harvested in TRIzol, and genomic RNA was extracted. Genomic RNA levels were determined by qRT-PCR using primers specific to Orf1a. RNA levels were normalized using the $2^{-\Delta CT}$ (where C_T is threshold cycle) method to endogenous GAPDH expression. Mean values ± standard errors of the means are shown ($n \geq 3$). RNA synthesis levels were not significantly different from the WT level according to a Kruskal-Wallis test.

Loss of nsp4 glycosylation results in decreased virus fitness. We next tested the effect of nsp4 mutations on virus competitive fitness. In order to test the fitness of nsp4 mutant viruses compared to the WT or the DGM, DBT cells were coinfected at a ratio

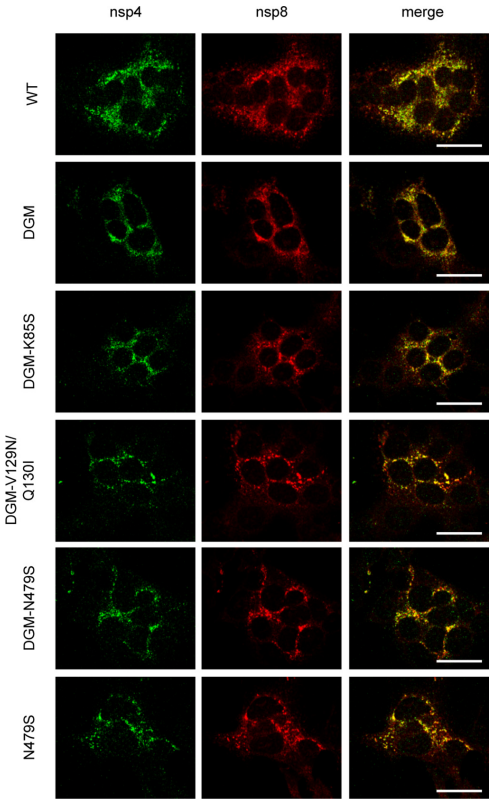

FIG 5 nsp4 localization in NX(S/T) mutant-infected cells. DBT cells were infected with the indicated viruses at an MOI of 5 PFU/cell for 6.5 h. Cells were then fixed in 100% methanol and stained with antibodies specific for nsp4 (green) and nsp8 (red). Yellow pixels represent colocalization of red and green pixels. Scale bar, 20 μm.

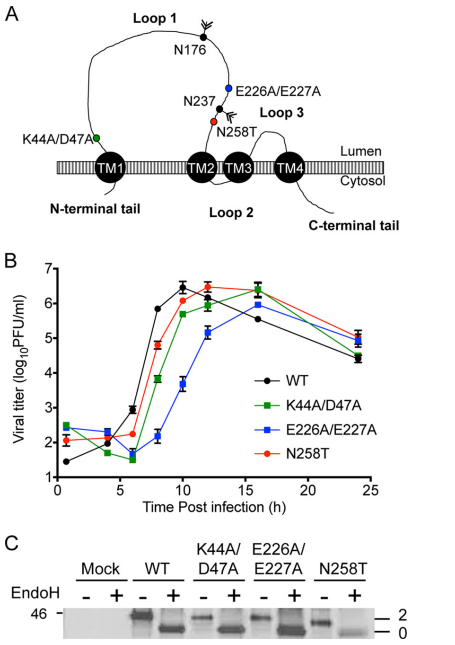

FIG 6 Replication and glycosylation of nsp4 mutants. (A) Schematic of nsp4 showing the location of the nsp4 mutations. (B) DBT cells were infected with the indicated viruses at an MOI of 1 PFU/cell for 24 h. At the indicated time points, supernatants were sampled, and titers were determined by plaque assay. Error bars represent the standard errors of the means of three replicates plated in duplicate. (C) DBT cells were infected with the indicated viruses at an MOI of 10 PFU/cell. Cells were starved with DMEM lacking Cys and Met in the presence of ActD for 1 h prior to being radiolabeled with [^{35}S]Cys-Met for 2 h before lysates were harvested. Lysates were immunoprecipitated with antibodies specific to nsp4 in the presence or absence of endo-H, and proteins were resolved by SDS-PAGE ($n = 2$).

of 1:1 and passaged three times at 37°C (Fig. 8A). The N258T and N479S viruses competed equally with the WT and were maintained at about 50% of the population. In contrast, viruses lacking glycosylation of nsp4 exhibited profoundly decreased fitness compared to the WT. We next competed DGM-K85S and DGM-N479S with the DGM to test the effects of additional mutations within the DGM virus on fitness (Fig. 8B). When K85S was introduced into DGM nsp4 loop 1 (DGM-K85S), virus fitness was further deceased relative to that of the DGM. However, DGM-N479S competed equally with DGM, and each remained at approximately 50% of the population. The results suggest that the decrease in fitness of DGM-N479S compared to the WT is likely due to the DGM phenotype and that the N479S mutation does not alter virus fitness. Collectively, these data demonstrate that loss of nsp4 glycosylation is associated with a substantial decrease in virus fitness that can then be further decreased by introduction of additional mutations into DGM nsp4 loop 1.

DISCUSSION

The role of host cytoplasmic membrane modifications in coronavirus replication and fitness is a subject of increasing investigation and interest for understanding replication, pathogenesis, and possible pathways for broad-spectrum inhibition of coronavirus infection. Recently, nsp3, nsp4, and nsp6 have been shown to mediate membrane modifications during individual expression and coexpression in cells (3). Further, recent studies with a novel inhibitor have shown that drugs targeting coronavirus membrane modifications are associated with profoundly impaired replication (31). Studies have shown that nsp4 is necessary for DMV formation and that mutations at nsp4 glycosylation sites result in aberrant DMVs (1, 3). In the current study, we show that mutations across nsp4, independently or in combination with mutations that abolish glycosylation, cause or exacerbate defects in DMV formation. Further, we show that loss of nsp4 glycosylation is associated with a substantial fitness cost.

Intact nsp4 is required for proper DMV morphology. We previously reported that mutations in nsp4 loop 1 were important

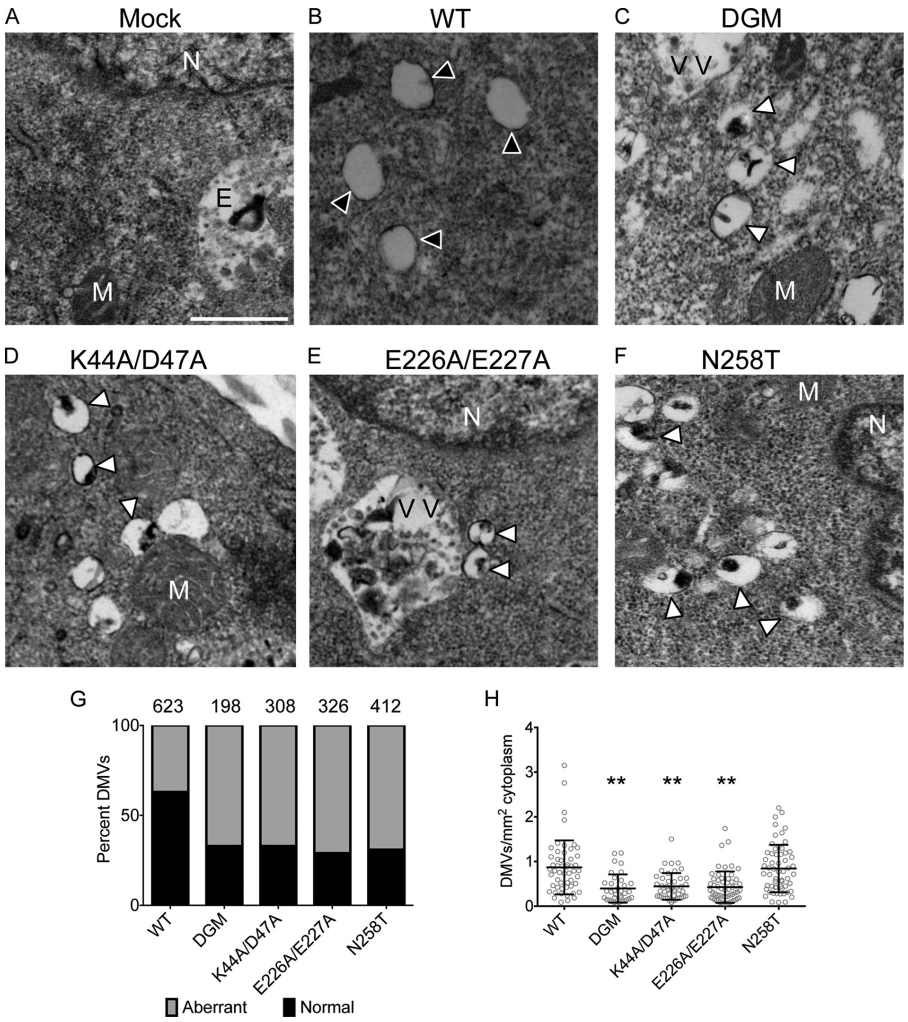

FIG 7 EM of nsp4 mutant-infected cells. (A to F) DBT cells were mock infected (A) or infected with the WT (B), DGM (C), K44A/D47A (D), E226A/E227A (E), or N258T (F) virus for 8 h before fixation in 2% glutaraldehyde and processed for TEM. Black arrowheads indicate normal DMVs, and white arrowheads indicate aberrant DMVs. N, nucleus; M, mitochondrion; VV, virion in vesicles; E, endosome. (G) Normal and aberrant DMVs were quantified, and results are shown as percentages of total DMVs, as indicated on the figure. The total number of DMVs analyzed is shown above each bar. (H) The total number of DMVs per area of cytoplasm was calculated. Circles represent the number of DMVs per area of cytoplasm for a single field. Bars represent the means ± standard deviations. A Kruskal-Wallis test was used to analyze for significant differences in numbers of DMVs per area of cytoplasm. *, $P = 0.008$; **, $P < 0.0001$ (compared to the WT).

for efficient RNA synthesis (5). We also described glycosylation of nsp4 at N-linked glycosylation sites in loop 1 and the negative effect on DMV formation by elimination of these sites (1). Our current results indicate that multiple residues and domains within nsp4, even in the C-terminal non-TM domain, impact DMV morphology rather than glycosylation alone. In addition, mutations in other regions of nsp4 loop 1 exacerbated changes in membrane structures of the DGM virus. Angelini et al. demonstrated that when coexpressed, nsp3 and nsp4 have the capacity to pair membranes (3). It is likely that nsp3 and nsp4 interact across the DMV lipid bilayer to hold both membranes in close proximity. In this model, any perturbation of the nsp3-nsp4 interaction could result

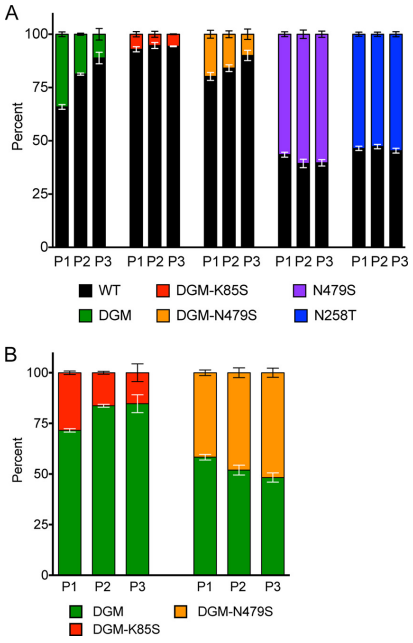

FIG 8 Competition assay of nsp4 mutants. DBT cells were infected with the indicated pairs of viruses at a total MOI of 0.1 PFU/cell at a ratio of 1:1. When cells were at least 50% involved in cytopathic effect, supernatants were collected, and cell monolayers were harvested in TRIzol. Supernatants were used for subsequent passages, for a total of three passages. Total RNA was extracted, and nsp4 amplicons were generated by RT-PCR and sequenced. For residues of interest, the area under the peak was calculated using MacVector, version 13. Then, the percentage of nucleotides of virus A to virus B was calculated and plotted on the graph. Error bars represent standard errors of the means ($n \geq 2$).

in separations of the inner and outer membranes. Our present results in fact support that idea that it is possible to dysregulate nsp4 functions in DMV formation by mutations at several locations in nsp4 loop 1, as well as other locations, including the C-terminal 10-kDa region, not predicted to be luminal or transmembrane. Since the mutation in the C terminus induced aberrant DMV formation, this would suggest that the nsp4 C terminus is also involved in DMV formation or stability after formation. We previously have demonstrated that the nsp4 C-terminal 10-kDa portion of the protein is dispensable for viral replication in culture (5). The crystal structures of the C termini of the nsp4s for MHV A59 and feline CoV have been determined and are structurally conserved (32, 33). The N479S residue maps to a surface-exposed loop in the MHV A59 C terminus crystal structure. The DMV morphology phenotypes were the same between N479S and DGM-N479S even though the viruses exhibited differences in replication kinetics (Fig. 2 and 3). This suggests that even mutations that do not affect viral replication can alter DMV morphology and numbers. Our data, in combination with other studies, suggest that DMV presence and not morphology is critical for efficient viral replication (31, 34).

Membrane modifications and virus fitness. All published studies to date are similar in demonstrating that disruption of "normal" DMV formation is not necessarily lethal to virus replication and likely represents an evolutionarily optimized process for maximum organization of replication components (1, 20, 31, 34). However, the direct role attributed to DMVs in virus replication and fitness has recently been called into question by a study by Al-Mulla et al. which used temperature-sensitive (ts) mutants in multiple replicase proteins to study the relationship of DMV size and number to virus fitness (20). In our study, we tested whether mutations within nsp4, one of the proteins directly involved in DMV formation and stability, affect DMV morphology and viral fitness. Our results support the conclusions of Al-Mulla et al. by demonstrating that alterations in DMV morphology and total numbers are not associated with a fitness cost compared to WT virus (WT versus N258T or N479S) (Fig. 8). Previously we observed that mutation of the nsp4 glycosylation sites alters DMV morphology, and the current study extends the result by demonstrating that loss of nsp4 glycosylation is associated with a substantial fitness cost. We cannot conclude that the decreased fitness is due to changes in DMV morphology or numbers because mutations across nsp4 that do not alter virus fitness cause aberrant DMVs and decreased numbers, regardless of location.

The relationship of DMVs to viral replication remains complex. Multiple mutations in nsp4, particularly loop 1, have significant effects on viral replication. Additionally, a small-molecule inhibitor was identified that prevents coronavirus DMV formation, likely by targeting nsp6 (31). The inhibitor profoundly knocked down virus replication, demonstrating that DMVs are linked to virus replication. The mechanisms of DMV formation and how the small molecule inhibits DMV formation remain unknown. Therefore, understanding how viruses induce membrane modifications and form replication complexes will help in the designing of antivirals to target this process. This work emphasizes the role of nsp4 loop 1 in the proper formation of DMVs and identifies nsp4 glycosylation as a putative target for antiviral therapy.

ACKNOWLEDGMENTS

We thank Janice Williams for TEM assistance and image analysis. We thank Megan Culler Freeman and Clint Smith for critical review of the manuscript.

This work was supported by the NIH grant RO1 AI50083 (M.R.D. and D.C.B.) from the National Institute of Allergy and Infectious Disease. D.C.B. was supported by a Training Grant in Immunobiology of Blood and Vascular Systems through the Vanderbilt University School of Medicine (T32HL697659). Experiments were performed in part through the use of the VUMC Cell Imaging Shared Resource (supported by NIH grants CA68485, DK20593, DK58404, DK59637, and EY08126).

REFERENCES

1. **Gadlage MJ, Sparks JS, Beachboard DC, Cox RG, Doyle JD, Stobart CC, Denison MR.** 2010. Murine hepatitis virus nonstructural protein 4 regulates virus-induced membrane modifications and replication complex function. J Virol **84:**280–290. http://dx.doi.org/10.1128/JVI.01772-09.
2. **Miller S, Krijnse-Locker J.** 2008. Modification of intracellular membrane structures for virus replication. Nat Rev Microbiol **6:**363–374. http://dx.doi.org/10.1038/nrmicro1890.
3. **Angelini MM, Akhlaghpour M, Neuman BW, Buchmeier MJ.** 2013. Severe acute respiratory syndrome coronavirus nonstructural proteins 3, 4, and 6 induce double-membrane vesicles. mBio **4**(4):e00524-13. http://dx.doi.org/10.1128/mBio.00524-13.
4. **Knoops K, Kikkert M, van den Worm SHE, Zevenhoven-Dobbe JC, van**

der Meer Y, Koster AJ, Mommaas AM, Snijder EJ. 2008. SARS-coronavirus replication is supported by a reticulovesicular network of modified endoplasmic reticulum. PLoS Biol **6:**e226. http://dx.doi.org/10.1371/journal.pbio.0060226.
5. **Sparks JS, Lu X, Denison MR.** 2007. Genetic analysis of murine hepatitis virus nsp4 in virus replication. J Virol **81:**12554–12563. http://dx.doi.org/10.1128/JVI.01257-07.
6. **Ulasli M, Verheije MH, de Haan CAM, Reggiori F.** 2010. Qualitative and quantitative ultrastructural analysis of the membrane rearrangements induced by coronavirus. Cell Microbiol **12:**844–861. http://dx.doi.org/10.1111/j.1462-5822.2010.01437.x.
7. **Snijder EJ, van der Meer Y, Zevenhoven-Dobbe J, Onderwater JJM, van der Meulen J, Koerten HK, Mommaas AM.** 2006. Ultrastructure and origin of membrane vesicles associated with the severe acute respiratory syndrome coronavirus replication complex. J Virol **80:**5927–5940. http://dx.doi.org/10.1128/JVI.02501-05.
8. **Bost AG, Carnahan RH, Lu XT, Denison MR.** 2000. Four proteins processed from the replicase gene polyprotein of mouse hepatitis virus colocalize in the cell periphery and adjacent to sites of virion assembly. J Virol **74:**3379–3387. http://dx.doi.org/10.1128/JVI.74.7.3379-3387.2000.
9. **Brockway SM, Clay CT, Lu XT, Denison MR.** 2003. Characterization of the expression, intracellular localization, and replication complex association of the putative mouse hepatitis virus RNA-dependent RNA polymerase. J Virol **77:**10515–10527. http://dx.doi.org/10.1128/JVI.77.19.10515-10527.2003.
10. **van der Meer Y, Snijder EJ, Dobbe JC, Schleich S, Denison MR, Spaan WJ, Locker JK.** 1999. Localization of mouse hepatitis virus nonstructural proteins and RNA synthesis indicates a role for late endosomes in viral replication. J Virol **73:**7641–7657.
11. **Gosert R, Kanjanahaluethai A, Egger D, Bienz K, Baker SC.** 2002. RNA replication of mouse hepatitis virus takes place at double-membrane vesicles. J Virol **76:**3697–3708. http://dx.doi.org/10.1128/JVI.76.8.3697-3708.2002.
12. **Clementz MA, Kanjanahaluethai A, O'Brien TE, Baker SC.** 2008. Mutation in murine coronavirus replication protein nsp4 alters assembly of double membrane vesicles. Virology **375:**118–129. http://dx.doi.org/10.1016/j.virol.2008.01.018.
13. **Oostra M, Hagemeijer MC, van Gent M, Bekker CPJ, Lintelo te EG, Rottier PJM, de Haan CAM.** 2008. Topology and membrane anchoring of the coronavirus replication complex: not all hydrophobic domains of nsp3 and nsp6 are membrane spanning. J Virol **82:**12392–12405. http://dx.doi.org/10.1128/JVI.01219-08.
14. **Oostra M, Lintelo te EG, Deijs M, Verheije MH, Rottier PJM, de Haan CAM.** 2007. Localization and membrane topology of coronavirus nonstructural protein 4: involvement of the early secretory pathway in replication. J Virol **81:**12323–12336. http://dx.doi.org/10.1128/JVI.01506-07.
15. **Oostra M, de Haan CAM, de Groot RJ, Rottier PJM.** 2006. Glycosylation of the severe acute respiratory syndrome coronavirus triple-spanning membrane proteins 3a and M. J Virol **80:**2326–2336. http://dx.doi.org/10.1128/JVI.80.5.2326-2336.2006.
16. **Baliji S, Cammer SA, Sobral B, Baker SC.** 2009. Detection of nonstructural protein 6 in murine coronavirus-infected cells and analysis of the transmembrane topology by using bioinformatics and molecular approaches. J Virol **83:**6957–6962. http://dx.doi.org/10.1128/JVI.00254-09.
17. **Kanjanahaluethai A, Chen Z, Jukneliene D, Baker SC.** 2007. Membrane topology of murine coronavirus replicase nonstructural protein 3. Virology **361:**391–401. http://dx.doi.org/10.1016/j.virol.2006.12.009.
18. **Hagemeijer MC, Ulasli M, Vonk AM, Reggiori F, Rottier PJM, de Haan CAM.** 2011. Mobility and interactions of coronavirus nonstructural protein 4. J Virol **85:**4572–4577. http://dx.doi.org/10.1128/JVI.00042-11.
19. **Helenius A, Aebi M.** 2004. Roles of N-linked glycans in the endoplasmic reticulum. Annu Rev Biochem **73:**1019–1049. http://dx.doi.org/10.1146/annurev.biochem.73.011303.073752.
20. **Al-Mulla HMN, Turrell L, Smith NM, Payne L, Baliji S, Zust R, Thiel V, Baker SC, Siddell SG, Neuman BW.** 2014. Competitive fitness in coronaviruses is not correlated with size or number of double-membrane vesicles under reduced-temperature growth conditions. mBio **5**(2): e01107-13. http://dx.doi.org/10.1128/mBio.01107-13.
21. **Beachboard DC, Lu X, Baker SC, Denison MR.** 2013. Murine hepatitis virus nsp4 N258T mutants are not temperature-sensitive. Virology **435:**210–213. http://dx.doi.org/10.1016/j.virol.2012.10.001.
22. **Yount B, Denison MR, Weiss SR, Baric RS.** 2002. Systematic assembly of a full-length infectious cDNA of mouse hepatitis virus strain A59. J Virol **76:**11065–11078. http://dx.doi.org/10.1128/JVI.76.21.11065-11078.2002.
23. **Denison MR, Yount B, Brockway SM, Graham RL, Sims AC, Lu X, Baric RS.** 2004. Cleavage between replicase proteins p28 and p65 of mouse hepatitis virus is not required for virus replication. J Virol **78:**5957–5965. http://dx.doi.org/10.1128/JVI.78.11.5957-5965.2004.
24. **Kim JC, Spence RA, Currier PF, Lu X, Denison MR.** 1995. Coronavirus protein processing and RNA synthesis is inhibited by the cysteine proteinase inhibitor E64d. Virology **208:**1–8. http://dx.doi.org/10.1006/viro.1995.1123.
25. **Smith EC, Blanc H, Vignuzzi M, Denison MR.** 2013. Coronaviruses lacking exoribonuclease activity are susceptible to lethal mutagenesis: evidence for proofreading and potential therapeutics. PLoS Pathog **9:**e1003565. http://dx.doi.org/10.1371/journal.ppat.1003565.
26. **Schneider CA, Rasband WS, Eliceiri KW.** 2012. NIH Image to ImageJ: 25 years of image analysis. Nat Methods **9:**671–675. http://dx.doi.org/10.1038/nmeth.2089.
27. **Hresko RC, Kruse M, Strube M, Mueckler M.** 1994. Topology of the Glut 1 glucose transporter deduced from glycosylation scanning mutagenesis. J Biol Chem **269:**20482–20488.
28. **Chang XB, Hou YX, Jensen TJ, Riordan JR.** 1994. Mapping of cystic fibrosis transmembrane conductance regulator membrane topology by glycosylation site insertion. J Biol Chem **269:**18572–18575.
29. **Popov M, Tam LY, Li J, Reithmeier RA.** 1997. Mapping the ends of transmembrane segments in a polytopic membrane protein. Scanning N-glycosylation mutagenesis of extracytosolic loops in the anion exchanger, band 3. J Biol Chem **272:**18325–18332.
30. **Vagin O, Turdikulova S, Sachs G.** 2005. Recombinant addition of N-glycosylation sites to the basolateral Na,K-ATPase β1 subunit results in its clustering in caveolae and apical sorting in HGT-1 cells. J Biol Chem **280:**43159–43167. http://dx.doi.org/10.1074/jbc.M508262200.
31. **Lundin A, Dijkman R, Bergström T, Kann N, Adamiak B, Hannoun C, Kindler E, Jónsdóttir HR, Muth D, Kint J, Forlenza M, Müller MA, Drosten C, Thiel V, Trybala E.** 2014. Targeting membrane-bound viral RNA synthesis reveals potent inhibition of diverse coronaviruses including the Middle East respiratory syndrome virus. PLoS Pathog **10:**e1004166. http://dx.doi.org/10.1371/journal.ppat.1004166.
32. **Xu X, Lou Z, Ma Y, Chen X, Yang Z, Tong X, Zhao Q, Xu Y, Deng H, Bartlam M, Rao Z.** 2009. Crystal structure of the C-terminal cytoplasmic domain of non-structural protein 4 from mouse hepatitis virus A59. PLoS One **4:**e6217. http://dx.doi.org/10.1371/journal.pone.0006217.
33. **Manolaridis I, Wojdyla JA, Panjikar S, Snijder EJ, Gorbalenya AE, Berglind H, Nordlund P, Coutard B, Tucker PA.** 2009. Structure of the C-terminal domain of nsp4 from feline coronavirus. Acta Crystallogr D Biol Crystallogr **65:**839–846. http://dx.doi.org/10.1107/S0907444909018253.
34. **Prentice E.** 2004. Coronavirus replication complex formation utilizes components of cellular autophagy. J Biol Chem **279:**10136–10141. http://dx.doi.org/10.1074/jbc.M306124200.

APPENDIX C: MURINE HEPATITIS VIRUS NONSTRUCTURAL PROTEIN 4 REGULATES VIRUS-INDUCED MEMBRANE MODIFICATIONS AND REPLICATION COMPLEX FUNCTION

JOURNAL OF VIROLOGY, Jan. 2010, p. 280–290 Vol. 84, No. 1
0022-538X/10/$12.00 doi:10.1128/JVI.01772-09

Murine Hepatitis Virus Nonstructural Protein 4 Regulates Virus-Induced Membrane Modifications and Replication Complex Function▽

Mark J. Gadlage,[2,3] Jennifer S. Sparks,[2,3] Dia C. Beachboard,[2] Reagan G. Cox,[2] Joshua D. Doyle,[2,3] Christopher C. Stobart,[2,3] and Mark R. Denison[1,2,3,4]*

Departments of Pediatrics,[1] Microbiology and Immunology,[2] The Elizabeth Lamb Center for Pediatric Research,[3] and the Monroe Carroll, Jr., Children's Hospital,[4] Vanderbilt University Medical Center, Nashville, Tennessee

Received 21 August 2009/Accepted 13 October 2009

Positive-strand RNA viruses induce modifications of cytoplasmic membranes to form replication complexes. For coronaviruses, replicase nonstructural protein 4 (nsp4) has been proposed to function in the formation and organization of replication complexes. Murine hepatitis virus (MHV) nsp4 is glycosylated at residues Asn176 (N176) and N237 during plasmid expression of nsp4 in cells. To test if MHV nsp4 residues N176 and N237 are glycosylated during virus replication and to determine the effects of N176 and N237 on nsp4 function and MHV replication, alanine substitutions of nsp4 N176, N237, or both were engineered into the MHV-A59 genome. The N176A, N237A, and N176A/N237A mutant viruses were viable, and N176 and N237 were glycosylated during infection of wild-type (wt) and mutant viruses. The nsp4 glycosylation mutants exhibited impaired virus growth and RNA synthesis, with the N237A and N176A/N237A mutant viruses demonstrating more profound defects in virus growth and RNA synthesis. Electron microscopic analysis of ultrastructure from infected cells demonstrated that the nsp4 mutants had aberrant morphology of virus-induced double-membrane vesicles (DMVs) compared to those infected with wt virus. The degree of altered DMV morphology directly correlated with the extent of impairment in viral RNA synthesis and virus growth of the nsp4 mutant viruses. The results indicate that nsp4 plays a critical role in the organization and stability of DMVs. The results also support the conclusion that the structure of DMVs is essential for efficient RNA synthesis and optimal replication of coronaviruses.

Positive-strand RNA viruses rely on host intracellular membranes to form replication complexes, defined as sites of viral RNA synthesis (11, 34, 40–42). These virus-induced membrane modifications are crucial for creating an environment that supports viral RNA synthesis, as well as protecting newly synthesized viral RNA. For many positive-strand RNA viruses, specific replicase proteins, often containing multiple hydrophobic domains, have been implicated in targeting to and modifying host membranes, ultimately leading to the formation of replication complexes.

The coronavirus murine hepatitis virus (MHV) is an enveloped, positive-strand RNA virus that contains a 31.4-kb genome, consisting of seven open reading frames (ORFs). ORF1 encodes the replicase/transcriptase polyprotein, while ORFs 2 to 7 encode structural and accessory proteins. ORF1 comprises approximately two-thirds of the genome and is translated as either polyprotein 1a (pp1a) or, due to a −1 ribosomal frameshift, pp1ab (3, 5, 6, 28, 34). pp1a and pp1ab are processed by three virus-encoded proteases to yield 16 nonstructural proteins (nsp1 to 16) (Fig. 1A) (1, 3, 13, 21, 32, 48). Analysis of nsp3, nsp4, and nsp6 amino acid sequences and *in vitro* biochemical studies have shown that these three nsp's all have transmembrane domains that are likely important for virus-induced membrane modifications (2, 23, 28). MHV nsp4 is processed by papain-like protease 2 (PLP2) at its amino terminus, resulting in an nsp4-to-10 precursor, and after this initial processing event, nsp5 (3Clpro) mediates processing at the carboxy terminus of nsp4 (15, 17, 21, 22, 24). The predicted molecular mass of nsp4 is 56 kDa, but it is detected as a 44-kDa protein by sodium dodecyl sulfate-polyacrylamide gel electrophoresis (SDS-PAGE) (22, 31).

All tested coronavirus nsp's localize to replication complexes that are located on virus-induced double-membrane vesicles (DMVs), and nsp4 has been proposed to play roles in the formation, organization, and function of these virus replication complexes (15, 38). nsp4 has been shown to associate with membrane fractions of infected cells and is resistant to membrane extraction following Triton X-114 treatment, indicating that nsp4 is an integral membrane protein (15). Bioinformatics of the MHV nsp4 amino acid sequence predicted that nsp4 has four transmembrane domains (TM1 to 4). MHV nsp4 has also been shown to be required for rescue of infectious virus (45), as have TM1 to 3, but TM4 is dispensable for recovery of infectious virus in culture. Charge-to-alanine substitutions between TM1 and TM2 of nsp4 result in viruses with phenotypes ranging from nonrecoverable to viruses that exhibit reduced virus growth, RNA synthesis, and protein processing (45).

Analysis of nsp4 from multiple coronaviruses across all coronavirus groups predicts N-linked glycosylation sites for all tested nsp4 sequences. The glycosylation sites, or sequons, Asn-X-Ser, Asn-X-Thr, and rarely Asn-X-Cys, are amino acid sequences

* Corresponding author. Mailing address: Department of Pediatrics, Vanderbilt University Medical Center, D6217 MCN, 1161 21st Ave. S., Nashville, TN 37232-2581. Phone: (615) 343-9881. Fax: (615) 343-9723. E-mail: mark.denison@vanderbilt.edu.

▽ Published ahead of print on 21 October 2009.

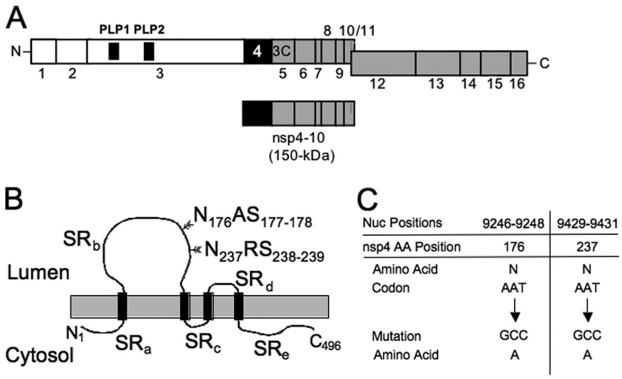

FIG. 1. Processing, glycosylation, and mutagenesis of nsp4. (A) Schematic of MHV nsp4 processing. Three virus-encoded proteases process pp1ab into intermediate precursors and 16 mature nsp's. PLP1 and PLP2 are shown as black boxes within nsp3, while the nsp5 protease (3CLpro) is shown in gray. PLP-mediated processing of nsp's is linked by white boxes, and 3CLpro processing is linked by gray boxes. Nsp4 is shown in black. Nsp's are indicated by number. The nsp4-to-10 precursor is also shown. (B) Proposed topology and N-linked glycosylation sites of nsp4. MHV nsp4 is a 496-amino acid protein that has four predicted transmembrane domains (TM1 to 4, black rectangles) and five soluble regions ($SR_{a\ to\ e}$). Locations of N-linked glycosylation residues Asn176 and Asn237 (N176 and N237) are indicated in SR_b, and predicted luminal and cytoplasmic domains are indicated (35). (C) Engineered nsp4 glycosylation mutants. Nsp4 glycosylation mutants were engineered by replacing the AAT asparagine codons at both N176 and N237 with a GCC alanine codon. Nucleotide numbers correspond to genomic position, and amino acid numbers correspond to nsp4 position.

that are recognized for glycosylation of the Asn (N) residue. Even though coronaviruses contain putative glycosylation sites within nsp4, there is little conservation of these sites between groups. Group 2a coronaviruses, such as MHV and human coronavirus HCoV-OC43, have two conserved putative N-linked glycosylation sites, N176 and N237 (Fig. 1B), while the group 2b severe acute respiratory syndrome coronavirus (SARS-CoV) and group 3 avian infectious bronchitis virus (IBV), have different putative glycosylation sites, N131 and N48, respectively (29, 35). Although the glycosylation of nsp4 from group 1 coronaviruses has not been investigated, residues N176 and N237 of MHV nsp4, N131 of SARS-CoV, and N48 of IBV nsp4 have been shown to be glycosylated when nsp4 is plasmid expressed in cells or when nsp4 is expressed from nonnative locations in the coronavirus genome (10, 29, 35). Clementz et al. reported that N176 of MHV nsp4 is not required for virus replication and that an N176A mutant virus grows identically to wild-type (wt) virus (10). In that study, the N176A mutant virus-expressed nsp4 migrated faster than wt nsp4 as determined by SDS-PAGE, consistent with altered protein modification, such as loss of glycosylation. However, this was not further investigated in the study. In contrast, N237A and N176A/N237A mutant viruses could not be recovered.

Although these studies have led to an increased understanding of various aspects of nsp4, it remains unknown if N176 and/or N237 is glycosylated during infection and if the putative nsp4 glycosylation sites of MHV or other coronaviruses serve roles in membrane modifications or replication complex formation and function. In this study, we tested the glycosylation status of MHV nsp4, expressed from its native genomic location, and the role of nsp4 glycosylation sites on virus growth, viral RNA synthesis, nsp4 localization, and replication complex morphology by engineering and recovering nsp4 mutants with alanine substitutions at N176 (N176A), N237 (N237A), or both (N176A/N237A). We show that virus-expressed nsp4 is glycosylated at both N176 and N237 during infection, that glycosylation at either or both sites is dispensable for virus growth in cell culture, and that alanine substitution of N176, N237, or both results in defects in virus growth and RNA synthesis. Further, we show that loss of nsp4 glycosylation is associated with the presence of aberrant or disrupted DMVs (hereafter referred to as irregular DMVs) and increased prevalence of virus-induced convoluted membranes (CMs). The degree of irregular DMVs and increased CMs from the nsp4 mutant viruses directly correlated with an impairment in viral RNA synthesis and growth. These results demonstrate that nsp4 plays a critical role in the formation, stability, and structure of virus-induced membrane modifications. Finally, the results also support the conclusion that the physical structure and stability of DMVs are essential for efficient RNA synthesis and/or protection of viral RNAs and optimal replication of coronaviruses.

MATERIALS AND METHODS

wt virus, cells, and antibodies. Recombinant wt MHV strain A59 (GenBank accession number AY910861) was used as the wt control for all experiments. Delayed brain tumor (DBT) cells expressing the MHV receptor carcinoembryonic antigen cell adhesion molecule-1 (9, 20, 47) and baby hamster kidney cells expressing the MHV receptor (BHK-MHVR) (8, 9, 47) were grown in Dulbecco's modified Eagle medium (Gibco) supplemented with 10% fetal calf serum for all experiments. Medium for BHK-MHVR cells was supplemented with G418 (Mediatech) at 0.8 mg/ml to maintain selection for cells expressing the MHVR. Rabbit polyclonal antibodies were used in biochemical experiments and have been described previously. Antibodies include anti-nsp4 (VU158) (45), anti-nsp8 (VU123) (4), and anti-M (J.1.3) (7).

Asparagine-to-alanine mutagenesis of nsp4. For introduction of asparagine-to-alanine substitutions in the nsp4 coding sequence (ORF1a nucleotides 8721 to 10208), PCR was performed using the MHV-A59 infectious clone fragment B

TABLE 1. Asparagine-to-alanine mutagenesis of MHV nsp4

Primer name	Sequence[a]	Purpose
N176A Sense	5′-GCC GCC TCT CTG TAT AGT TCT TTG GCT-3′	Mutagenesis for N176A
N176A Antisense	5′P-GTG CAT AAC ACC CCC TGT ATA ACA ATA AGG-3′	Mutagenesis for N176A
N237A Sense	5′-GCC CGT TCA TGG GTA TTG AAC AAC CCG TAT-3′	Mutagenesis for N237A
N237A Antisense	5′P-AAA ATT AAA GCA GAT ACC CTC CTC GGC-3′	Mutagenesis for N237A

[a] Underlined letters denote nucleotides used to introduce alanine substitutions.

(pCR-XL-pSMART B) as a template. Fragment B of the MHV-A59 clone contains MHV ORF1a nsp4 nucleotides 8721 to 9555 (47). Asparagine-to-alanine codon changes were introduced using the ExSite/QuikChange mutagenesis kit (Stratagene) with the primers listed in Table 1. Changes to the manufacturer's protocol included the use of *Pfu* Turbo and *Pfu* Ultra instead of the ExSite DNA polymerase blend. PCR was performed using the following parameters: initial denaturation at 95°C once for 2 min, denaturation at 95°C for 1 min, annealing at various temperatures depending on the primers for 1 min, extension at 72°C for 7 min, and repeating of the denaturing, annealing, and extension steps for a total of 40 cycles. Products were ligated and sequenced across the MHV genome-containing region of fragment B to ensure that PCR amplification did not introduce any unintended mutations. For introduction of both N176A and N237A, restriction endonuclease EcoN I was used to digest both single nsp4 glycosylation mutant plasmids, and ligation was used to introduce both mutations into the same plasmid.

Generation of MHV nsp4 glycosylation mutant viruses. Viruses containing the engineered mutations within nsp4 were produced using the infectious cDNA assembly strategy for MHV-A59 that has previously been described by Yount et al. (47) and modified by Denison et al. (12) and Sparks et al. (45). Briefly, plasmids containing the seven cDNA cassettes that make up the MHV genome were digested using the appropriate restriction enzymes. The correct restriction fragments were gel purified and ligated together overnight at 16°C. The ligated DNA was purified, in vitro transcribed, and electroporated with N gene transcripts into BHK-MHVR cells. The electroporated cells were then laid over a layer of 2.5×10^6 uninfected DBT cells in a 75-cm^2 flask and incubated at 37°C. Virus viability was determined by cytopathic effect, in this case syncytium formation, in the electroporated cell culture. Progeny virus in the cell culture medium of electroporated cells (passage 0 [P0]) was passaged onto uninfected DBT cells (P1), and the virus released from cells in the culture medium was designated P1 stock, the titer was determined, and it was used for all experiments.

RT-PCR and sequencing of recovered viruses. Total intracellular RNA was harvested from P1-infected cells using TRIzol (Invitrogen) according to the manufacturer's protocol. Extracted RNA was used as a template for reverse transcription (RT)-PCR. RT was performed using Superscript III reverse transcriptase (Invitrogen) and random hexamers (Roche). Primers complementary to genome nucleotides 8486 to 8502 (sense) and 10361 to 10345 (antisense) were then used to amplify the nsp4 coding region by PCR. These PCR products were sequenced to confirm the retention of the engineered mutations and the absence of additional mutations in the nsp4 coding sequence.

Protein immunoprecipitations. For radiolabeling of proteins and immunoprecipitations, cells were grown on 60-mm dishes and infected at a multiplicity of infection (MOI) of 10 PFU/cell with wt or nsp4 glycosylation mutant viruses and incubated at 37°C. At 4 h postinfection (p.i.), medium was aspirated and replaced with medium lacking methionine and cysteine and supplemented with actinomycin D (Act D; Sigma) at a final concentration of 20 μg/ml. At 5 h p.i., cells were radiolabeled with [^{35}S]methionine-cysteine ([^{35}S]Met-Cys) at a concentration of 0.08 mCi/ml. When cells reached ~90% involvement in syncytia, radiolabeled cells were washed once in phosphate-buffered saline (PBS), and then lysed in 1 ml of lysis buffer lacking SDS (1% NP-40, 0.5% sodium deoxycholate, 150 mM NaCl, and 50 mM Tris, pH 8.0). Lysates were then centrifuged at $6,000 \times g$ for 3 min to remove cellular debris and nuclei, and the supernatant was collected. Immunoprecipitations were performed in a final volume of 1 ml, using protein A-Sepharose beads (Sigma), 50 μl of radiolabeled lysate, 1:200 (anti-nsp4) or 1:500 (anti-nsp8) dilutions of polyclonal antisera, and proteinase inhibitor (Roche) in lysis buffer. Immunoprecipitations were then performed as previously described (45). For endoglycosidase H (Endo H) treatment, supernatant was transferred to a new tube after heating at 70°C for 10 min. Endo H (Sigma) was added to the supernatant according to the manufacturer's protocol, and the mixture was incubated at 37°C for 3 h. Proteins were resolved by SDS-PAGE in 4 to 12% polyacrylamide gradient Bis-Tris gels (NuPage; Invitrogen) and analyzed by fluorography. ^{14}C-labeled high-molecular-weight markers (NEB) and a full-range rainbow marker were used as molecular weight standards.

Viral growth assays. For viral growth determination (12), DBT cells were infected with wt or nsp4 glycosylation mutant viruses at the MOIs indicated. Following a 45-min absorption period at 37°C with periodic swirling, medium was aspirated, and the cells were washed three times in PBS. Prewarmed 37°C medium was then added back to the cells, and the cells were incubated at 37°C. Aliquots of medium were taken from 1 to 30 h p.i., and virus titers were determined by plaque assay as previously described (25).

Metabolic labeling of viral RNA. DBT cells were either mock infected or infected at an MOI of 5 PFU/cell with wt or nsp4 glycosylation mutant viruses in six-well plates. Following a 45-min absorption at 37°C, medium containing virus was removed, and cells were washed twice in PBS. Cells were then incubated in growth medium at 37°C until 30 min prior to labeling, when medium was replaced with fresh medium containing 20 μg/ml Act D. After this 30-min treatment, [^{3}H]uridine was added to a final concentration of 40 μCi/ml, and cells were incubated at 37°C for 2-h intervals from 3 to 15 h p.i. At the end of each labeling period, cells were lysed in lysis buffer (described above), and nuclei were removed by centrifugation at $14,000 \times g$ for 3 min. RNA in 10% of each lysate was precipitated with chilled 5% trichloroacetic acid (TCA) onto glass microfiber filters (Whatman), washed twice in fresh 5% TCA and twice in 95% ethanol, and dried using vacuum filtration. Radiolabel incorporation was quantitated by liquid scintillation counting.

Immunofluorescence assays. DBT cells grown on glass coverslips were infected with wt or nsp4 glycosylation mutant viruses at an MOI of 10 PFU/cell. At 6 h p.i., medium was aspirated from cells, and cells were fixed in 100% methanol at −20°C. Cells were rehydrated in PBS for 10 min, blocked in PBS containing 5% bovine serum albumin, and then aspirated. For indirect immunofluorescence, cells were incubated with primary antibody (anti-nsp4, 1:200; anti-M, 1:1,000) in wash solution (PBS containing 1% bovine serum albumin and 0.05% NP-40) for 1 h at room temperature. Cells were washed in wash solution three times for 5 min/wash. Cells were then incubated with secondary antibody (goat anti-rabbit Alexa 488, 1:1,000; goat anti-mouse Alexa 546, 1:1,000; Molecular Probes) for 30 min at room temperature. Cells were washed again three times for 5 min/wash, subjected to a final wash in PBS, and rinsed with distilled water. For direct immunofluorescence, anti-nsp8 was purified using HiTrap rProtein A FF columns (GE Life Sciences) for fast protein liquid chromatography. Anti-nsp8 was directly conjugated using the Alexa Fluor 546 protein labeling kit (Invitrogen) according to the manufacturer's protocol. Cells were incubated with anti-nsp8 at a concentration of 1:500, following the same procedure as above. Coverslips were mounted with Aquapolymount (Polysciences) and visualized using a Zeiss Axiovert 200 microscope with a 40× oil immersion lens. Images were processed and merged using Adobe Photoshop CS3.

TEM analysis. DBT cells were mock infected or infected with wt or nsp4 glycosylation mutant viruses at an MOI of 5 PFU/cell in a 60-mm dish and incubated at 37°C. At 6 h p.i., medium was aspirated, and cells were washed once with PBS. The cells were then fixed in 2% glutaraldehyde for 10 min, scraped off the dishes, and centrifuged at $0.5 \times g$ for 3 min. The initial 2% glutaraldehyde was aspirated, fresh 2% glutaraldehyde was added to the fixed cells for 1 h and aspirated, and fresh glutaraldehyde was added to the fixed cells for overnight incubation at 4°C. Cells were washed three times in PBS, transferred to 1% osmium tetroxide in distilled water (diH_2O) for 1 h, and washed three times in diH_2O. Cells were stained en bloc in 1% aqueous uranyl acetate for 1 h and washed three times in diH_2O. Dehydration of cells was carried out gradually using a graded series of ethanol and increasing the times each remained in solution, starting with 30%, followed by 50%, 70%, 95%, and finally absolute ethanol. Propylene oxide was used as a transitional solvent to replace the dehydration solution. Cells were transferred to a 1:1 araldite-propylene oxide mixture for 1 h and then placed in pure araldite in a vacuum oven for another hour to help pull resin through the tissue. Pure resin specimens were then transferred into capsules containing fresh resin and finally placed into an oven overnight to polymerize. Ultra-thin serial sections (50 to 60 nm) from polymerized blocks were obtained using a Leica UCT Ultracut microtome (Leica Microsystems,

Vienna, Austria), transferred to formvar-coated slot grids, and examined using a Phillips CM10 TEM (FEI Company, Hillsboro, OR) equipped with an Advantage Plus 2-megapixel digital charge-coupled-device system for CM10 transmission electron microscopy (TEM) (Advanced Microscopy Techniques, Danvers, MA).

Statistical analyses. For statistical analyses, DMVs were characterized into two groups, either regular (defined by inner membranes in close approximation with the outer membrane) or irregular DMVs (defined by moderate to severe disruption or separation of the inner membrane with the outer membrane). Chi-square analysis using contingency tables was performed by comparing the number of regularly formed DMVs to irregularly formed DMVs of wt and nsp4 glycosylation mutant viruses. Chi-square analysis was also performed to compare the presence of both CMs and DMVs to the presence of DMVs only. Because CMs were found only in the presence of DMVs, the presence of CMs and DMVs was compared to the presence of DMVs alone in a given TEM section. Diameters of DMVs were measured using ImageJ 1.40g (http://rsb.info.nih.gov/ij). Diameters were defined by measuring the widest diameter from the outside membrane of one side to the outside membrane of the opposite side of a single DMV. To determine whether there was a statistical difference between the diameters of DMVs, analysis of variance (ANOVA) was used to compare wt and nsp4 glycosylation mutant viruses. Because a statistical difference was indicated through ANOVA, Tukey tests were used to perform pair-wise comparisons of all viruses. *P* values were determined to indicate significance.

RESULTS

Recovery of nsp4 glycosylation mutant viruses. Group 2a coronaviruses contain conservation of putative glycosylation sites in nsp4 at N176 and N237 (Fig. 1B). To determine if nsp4 is glycosylated at residues N176 and N237 in the context of MHV infection and what roles nsp4 glycosylation may play in the virus life cycle, viruses were engineered to contain asparagine-to-alanine substitutions at either N176, N237, or both residues N176 and N237 of nsp4 (Fig. 1C). Cells were electroporated with genomic RNA for N176A, N237A, or N176A/N237A mutant viruses. All three mutant viruses induced cytopathic effect by 36 h postelectroporation, and 90 to 100% of cells were involved in syncytia by 46 to 50 h postelectroporation, similar to wt virus. Viruses were passaged and sequenced across the nsp4 coding sequence, confirming both the presence of engineered mutations and lack of any other mutations in nsp4. In contrast to previous reports, our results demonstrate that mutants with alanine substitution at N176, N237, or both are viable, demonstrating that the N176 and N237 residues are not required for replication in cell culture. To determine if compensating mutations occurred outside of the nsp4 sequence during recovery of the N237A and N176A/N237A mutant viruses, the complete genome of the N176A/N237A mutant virus was sequenced, and there were no additional mutations present in the genome. These results demonstrate that the recovery of the N237A and N176A/N237A mutant viruses was not due to second-site compensating mutations and that the Asn residues are not required for virus viability.

nsp4 is glycosylated at both N176 and N237 during MHV infection. Previous studies have demonstrated that treatment of lysates with Endo H results in a mobility shift of nsp4 expressed from plasmid in HeLa cells (10, 35) or from nsp4-enhanced green fluorescent protein expressed in recombinant virus from an alternate location (in place of ORF2) (10, 35), consistent with glycosylation of nsp4 with mannose-rich oligosaccharides in the endoplasmic reticulum (ER) and the lack of nsp4 trafficking through Golgi. However, there has been no demonstration of N-linked glycosylation of native nsp4 in wt virus or identification of specific Asn residues subject to N-linked glycosylation. To test whether natively expressed MHV nsp4 is glycosylated during infection, immunoprecipitated nsp4 from wt MHV infection was mock treated or treated with Endo H (Fig. 2A). Mock-treated nsp4 was detected as a 44-kDa protein by SDS-PAGE, while Endo H treatment resulted in a faster-migrating, 39-kDa protein. The nsp4-to-10 precursor was detected in both cases by anti-nsp4. The replicase protein nsp8 is not modified by N-linked glycosylation and was not affected by Endo H treatment (Fig. 2A). The nsp4-to-10 precursor that was treated with Endo H and detected using anti-nsp8 exhibited a sharper band than that of the untreated nsp4-to-10 precursor. A possible explanation for this is that removal of N-linked glycans may alter which nsp4-to-10 precursors can be detected by anti-nsp8, e.g., nsp4-to-10 with certain post-translational modifications.

To test whether N176 and/or N237 was targeted for glycosylation, nsp4 immunoprecipitated following infection of DBT cells with N176A, N237A, and N176A/N237A mutant viruses was treated with Endo H (Fig. 2B). Untreated nsp4 from N176A

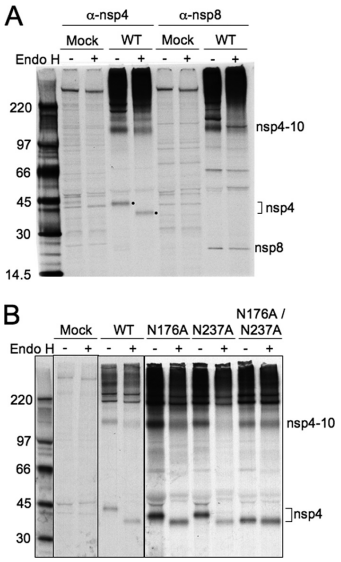

FIG. 2. Protein expression and glycosylation of nsp4. Cytoplasmic lysates were generated from radiolabeled DBT cells that were either mock infected or infected with wt, N176A, N237A, or N176A/N237A viruses. Labeled proteins were immunoprecipitated using antiserum against nsp4 or nsp8. (A) Endo H treatment of wt nsp4 and nsp8. Immunoprecipitated nsp4 and nsp8 were either mock treated or treated with Endo H to analyze N-linked glycosylation. After Endo H treatment for 3 h, proteins were resolved on SDS-PAGE and visualized by fluorography. Black dots indicate either glycosylated or unglycosylated forms of nsp4. α-nsp4, anti-nsp4; α-nsp8, anti-nsp8. (B) Endo H treatment of nsp4 glycosylation mutants. Immunoprecipitated nsp4 from the wt or nsp4 glycosylation mutants was mock treated or treated with Endo H. All samples in each panel were resolved on the same gel and had the same exposure time, but the images shown in panel B were cropped to remove nonrelevant lanes. Molecular weight markers (in thousands) are shown to the left of each gel.

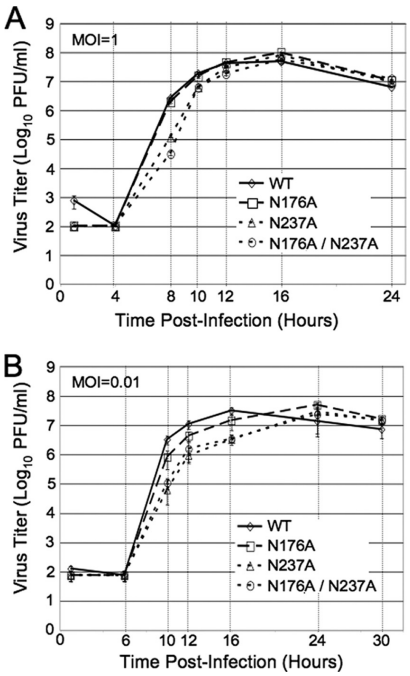

FIG. 3. Growth analysis of nsp4 glycosylation mutant viruses. DBT cells were infected with the indicated viruses for single cycle growth at an MOI of 1 PFU/cell for 24 h (A) or for multiple cycle growth at an MOI of 0.01 PFU/cell for 30 h (B). Samples of virus supernatants were collected at the times indicated beneath the graphs. Virus titers were determined by plaque assay with DBT cells. Error bars represent standard deviations from the mean based on samples from multiple replicates.

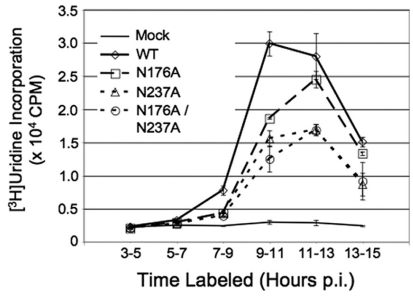

FIG. 4. RNA synthesis of nsp4 glycosylation mutant viruses. DBT cells in six-well plates were mock infected or infected with wt, N176A, N237A, or N176A/N237A viruses at an MOI of 5 PFU/cell. Cells were treated with Act D for 30 min prior to addition of radiolabel. Cells were metabolically labeled with [^{3}H]uridine for the intervals indicated, cells were lysed, and [^{3}H]uridine incorporation was quantified by liquid scintillation counting of TCA-precipitable RNA. Data points represent the mean counts/minute (CPM) of two individual experiments, and error bars represent the standard deviations between two experiments.

and N237A mutants migrated identically and more rapidly than untreated wt nsp4 (42 kDa) but more slowly than wt nsp4 treated with Endo H (39 kDa). When nsp4 from N176A and N237A mutant viruses was treated with Endo H, both proteins were detected at 39 kDa, identical to Endo H-treated wt nsp4. nsp4 from the N176A/N237A mutant virus migrated to 39 kDa, whether untreated or treated with Endo H. The results indicate that nsp4 expressed from its native genomic location is specifically glycosylated at residues N176 and N237 and also demonstrate that no other N-linked glycosylation occurs in nsp4.

nsp4 glycosylation mutant viruses exhibit defects in virus replication. To determine whether nsp4 glycosylation mutant viruses display replication defects, DBT cells were infected with wt, N176A, N237A, and N176A/N237A viruses at an MOI of 1 PFU/cell (Fig. 3A). Samples of infected cell culture medium were taken at predetermined time points from 1 to 24 h p.i., and virus titers of each sample were determined by plaque assay. The N176A mutant virus exhibited growth kinetics and peak titers indistinguishable from those of wt virus, consistent with the study by Clementz et al. (10). The N237A and N176A/N237A mutant viruses grew indistinguishably from each other and reached peak titers similar to those of wt virus; however, compared to wt and N176A, the N237A and N176A/N237A viruses exhibited a delay and decrease in growth between 4 and 12 h p.i. The N176A/N237A mutant did not appear more impaired in growth than the N237A mutant alone. Since the N237A and N176A/N237A mutant viruses exhibited growth defects, we next tested whether N176A had subtle growth defects by repeating the growth assays at an MOI of 0.01 PFU/cell (Fig. 3B). Under these conditions, the N237A and N176A/N237A mutants demonstrated the same delay compared to mutants infected at a higher MOI. In contrast, for the N176A mutant virus, the lower MOI infection revealed a subtle defect in growth, displaying a delay in peak titer similar to that of N237A and N176A/N237A mutants. The experiments demonstrate that N176 and N237 both are important for exponential growth, but loss of either or both glycosylation sites still allows for wt peak titers. The contributions of N176 and N237 are independent and nonredundant, as indicated by growth defects of either N176A or N237A but are not additive or synergistic. Finally, the results suggest that glycosylation of nsp4 is important for nsp4 function during virus replication.

nsp4 glycosylation mutants have reduced viral RNA synthesis. Since previous studies have shown that mutations in nsp4 affect viral RNA synthesis (45), we conducted experiments to determine if the growth defects of nsp4 glycosylation mutants were associated with changes in viral RNA synthesis (Fig. 4). DBT cells were mock infected or infected with wt, N176A, N237A, or N176A/N237A mutant viruses at an MOI of 5 PFU/cell to maximize single-round infection, and infected cells were metabolically labeled with [^{3}H]uridine in the presence of Act D for 2-h intervals from 3 to 15 h p.i. Total RNA was extracted from harvested cells and measured for incorporation of [^{3}H]uridine. Peak incorporation of [^{3}H]uridine for wt MHV occurred from 9 to 11 h p.i., similar to the results from a

previously published report (16). For all three nsp4 mutant viruses, peak incorporation was delayed compared to wt, occurring between 11 and 13 h p.i. Delays in the timing of peak viral RNA synthesis displayed by the nsp4 glycosylation mutant viruses were also associated with decreases in the amount of RNA synthesized over the course of the infection. The N176A mutant virus synthesized approximately 80% of the maximum amount of incorporation seen for wt over a 2-h labeling period. Both the N237A and the N176A/N237A mutant viruses exhibited a 50% reduction in peak viral RNA synthesis. These data demonstrate that there is an overall decrease in viral RNA synthesis in the nsp4 mutant viruses compared to wt virus. In addition, the delay and decrease in RNA synthesis correlated with the kinetics and peak titer of infectious viruses, suggesting that alteration of viral RNA synthesis was responsible for the growth defects from the N176A and N237A substitutions.

Removal of nsp4 glycosylation sites does not alter nsp4 localization. nsp4 colocalizes with other replicase nsp's in cytoplasmic replication complexes that are sites of viral RNA synthesis, and nsp4 has been predicted to be critical for formation of these complexes. To test if altered RNA synthesis resulting from the N176A and N237A substitutions was associated with altered nsp4 interactions with other replicase proteins, the localization of nsp4 was compared by immunofluorescence with nsp8, a well-described marker for replication complexes, and with the viral membrane protein (M), a marker for sites of virus assembly in the ER-Golgi intermediate compartment and Golgi and distinct from replication complexes. DBT cells on glass coverslips were infected with wt, N176A, N237A, or N176A/N237A viruses for 6 h, fixed, and probed for nsp4, nsp8, and M. For wt and all nsp4 mutant viruses, nsp4 colocalized extensively with nsp8 in punctate perinuclear and cytoplasmic foci (Fig. 5A). However, there was a visual trend for fewer and less-intense fluorescent foci in the cells infected with the nsp4 mutants compared to wt virus, suggesting that there may be fewer-forming or altered replication complexes in the nsp4 mutant virus infections (Fig. 5A and data not shown). When nsp4 was compared with M (Fig. 5B), wt and mutant viruses had identical patterns of noncolocalization of nsp4 with M, consistent with previous studies of MHV replicase proteins and indicating that nsp4 is not altered in its relationship to sites of assembly and not localized to the ER-Golgi intermediate compartment or Golgi. The results demonstrate that nsp4 mutant viruses are able to form cytoplasmic replication complexes and retain interactions with other replicase nsp's and that glycosylation of nsp4 is not required for this process.

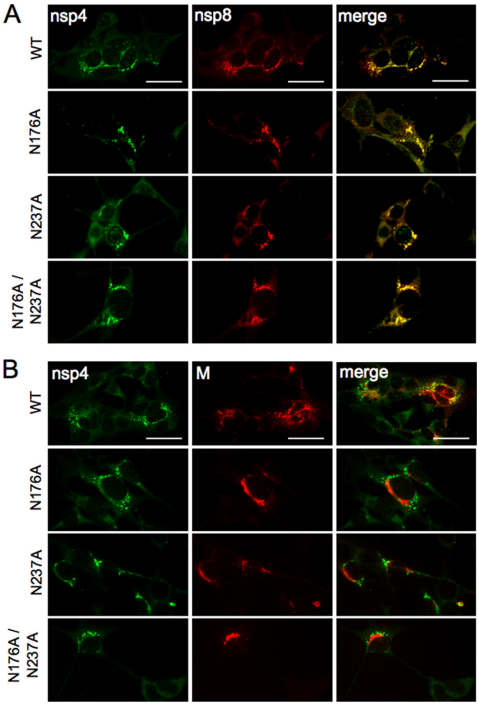

FIG. 5. Immunofluorescence of nsp4 localization. DBT cells on glass coverslips were infected with the indicated viruses at an MOI of 10 PFU/cell. At 6 h p.i., cells were fixed, probed with antibodies to nsp4, nsp8, and membrane (M) protein, and analyzed by immunofluorescence using a Zeiss Axiovert 200 microscope at ×40 magnification. (A) nsp4 colocalizes with nsp8. Infected cells were analyzed by indirect immunofluorescence using anti-nsp4 (Alexa 488, green) and direct immunofluorescence by Alexa 546 conjugated to anti-nsp8 (red). Yellow pixels represent colocalization of overlapping green and red pixels. (B) nsp4 does not colocalize with M protein. Infected cells were probed by indirect immunofluorescence using rabbit anti-nsp4 (green) and mouse anti-M (red). The scale bar in the upper images in panels A and B equals 20 μM and is representative of all other images.

nsp4 glycosylation mutant viruses induce altered membrane rearrangements and irregular DMVs. Based on the replication defects and subtle visual variability observed during immunofluorescence analysis of nsp4 mutants, we next investigated whether nsp4 glycosylation mutants have altered membrane rearrangements. TEM was used to visualize the ultrastructure of membrane modifications in infected cells. DBT cells were mock infected or infected with wt or the nsp4 glycosylation mutant viruses at an MOI of 5 PFU/cell. At 6 h p.i., cells were fixed in 2% glutaraldehyde and processed for TEM analysis. For mock-infected cells, the cellular architecture and organelle morphology were intact (Fig. 6A). Cells infected with wt virus exhibited clearing of cytoplasmic contents and swollen ER and Golgi (Fig. 6B). Cells infected with the three nsp4 glycosylation mutant viruses also demonstrated swelling of ER and Golgi and cytoplasmic clearing, albeit less so than during wt infection (Fig. 6C to E).

In contrast, there was a striking difference between cells infected with wt and nsp4 mutants in the relationship and ultrastructure of virus-induced DMVs and CMs. wt- and nsp4 mutant-infected cells exhibited virus-induced CMs and DMVs, structures that have been identified with replication complexes and associated with viral RNA synthesis (15, 27), while no DMVs or CMs were observed with mock-infected cells. CMs were detected with wt and mutant virus-infected cells and always in close proximity to DMVs. However, DMVs were observed in the presence or absence of CMs for all viruses. The CMs were observed more frequently with electron microscopy (EM)

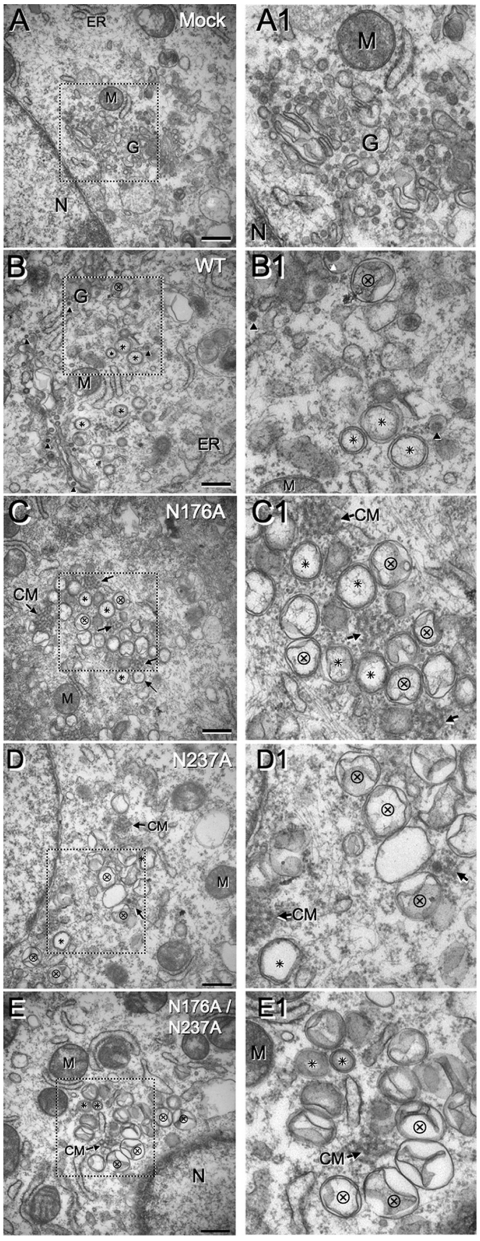

FIG. 6. TEM analysis of replication complexes and DMVs from the wt and nsp4 mutants. DBT cells were mock infected or infected with wt, N176A, N237A, or N176A/N237A viruses. Cells were harvested in 2% glutaraldehyde and processed for TEM analysis. (A and A1) Mock-infected cells. (B and B1) wt MHV infection. (C and C1) N176A mutant virus infection. (D and D1) N237A mutant virus infection. (E and E1) N176A/N237A mutant virus infection. Dotted boxes in the left images indicate area of magnification in right image. The scale bar in the left images represents 500 nm. Arrowheads indicate dark-stained, individual virions, which are located above the arrowheads. Black arrows point to CMs. ⁎ indicates examples of regular DMV structure. ⊗ shows examples of irregular DMV structure. N, nucleus; G, Golgi apparatus; M, mitochondria.

sections of cells infected with N176A, N237A, and N176A/N237A mutant viruses compared to wt (Fig. 6C to E). The vast majority of DMVs in wt-infected cells exhibited the characteristic DMV morphology of a circular shape, regular diameter, and ultrastructure of closely approximated inner and outer membranes. A small subset of DMVs manifested a partial separation of the inner and outer membranes and exhibited a slightly larger diameter, but these were rare. In contrast, cells infected with the nsp4 glycosylation mutants demonstrated DMVs with altered shape and diameter and with increasingly aberrant (irregular) ultrastructure, consisting of severely detached and collapsed inner membranes that were not observed with any wt-infected cells. The number of irregular DMVs and the extent of DMV derangement were most profound in N237A and N176A/N237A mutant-infected cells and visibly greater than those detected with cells infected with N176A alone.

Because the EM images were originally selected based on the detection of DMVs, we used EM images to quantitatively compare (i) the prevalences of CMs, (ii) the ratios of regular (wt-like) and irregular DMVs, and (iii) the diameters of regular and irregular DMVs (Table 2 and Fig. 7). Since the images were selected only for the presence of DMVs, we proposed that quantitative analysis was unbiased for these parameters. The prevalence of CMs was determined by comparing images in which CMs were observed or not observed in EM sections selected based on the presence of DMVs, since CMs were found only in the presence of DMVs. While there was no statistical difference between wt and N176A in the ratios of sections with both CMs and DMVs versus DMVs alone, the N237A and N176A/N237A mutants had significantly increased ratios of detection of both CMs and DMVs compared to DMVs alone ($P < 0.01$ for N237A and $P < 0.001$ for N176A/N237A) (Fig. 7A). Analysis of the ratio of regular DMVs to total DMVs (regular plus irregular) demonstrated a significant increase in irregular DMVs in cells infected with N237A and N176A/N237A mutant viruses ($P < 0.001$) compared to cells infected with wt or N176A viruses (Fig. 7B). We did observe more irregular DMVs with N176A than with wt, but the regular DMV/total DMV ratios were not significantly different. Finally, the measurements of the regular DMVs of both wt and all nsp4 glycosylation mutant viruses reveal no difference in their diameters (widest diameter of outer membrane) (Fig. 7C). In contrast, the mean diameter of irregular DMVs in the N237A and N176A/N237A mutant viruses was significantly larger than that of either wt virus or the N176A mutant virus (Fig. 7C). This analysis indicates that nsp4 is likely critical for the organization and stability of DMVs and for the relation-

TABLE 2. Analysis of virus-induced membrane structures

Virus	Total no. of:						Avg regular DMV diam (nm)	Avg irregular DMV diam (nm)
	Cell sections with evidence of infection	Sections with CMs and DMVs	Sections with DMVs only	DMVs counted	Regular DMVs	Irregular DMVs		
WT	24	8	16	102	86	16	255.2 ± 31.4	323.2 ± 35.6
N176A	21	11	10	127	96	31	257.0 ± 52.3	324.2 ± 31.8
N237A	11	9	2	72	36	36	264.6 ± 53.6	372.5 ± 41.6
N176A/N237A	21	18	3	117	60	57	270.4 ± 56.1	371.3 ± 41.6

ship and evolution of membrane modifications (CMs and DMVs) over the course of infection.

DISCUSSION

Although multiple studies have investigated the roles of nsp's in inducing membrane rearrangements, understanding the role of glycosylation of nsp's from positive-strand RNA viruses remains limited. A study of the flavivirus yellow fever virus demonstrated that NS1 glycosylation was important for several functions in the virus life cycle (30, 33). NS1 interacts with membranes and is involved in replicase function (30), and removal of NS1 glycosylation by asparagine-to-alanine substitution results in impaired virus growth, RNA synthesis, and pathogenesis (33).

Coronaviruses, like other positive-strand RNA viruses, induce the formation of DMVs that serve as scaffolds for replication/transcription complexes. Exogenous expression of the poliovirus transmembrane proteins 2BC and 3A results in DMVs that are indistinguishable from those formed during wt infection (43, 46). Equine arteritis virus (EAV), which is classified with coronaviruses in the order *Nidovirales*, induces DMVs similar to coronaviruses (37). Exogenous plasmid expression of EAV nsp2 and nsp3 is sufficient to induce membrane modifications resulting in membrane structures similar to those seen during EAV infection, and mutations within EAV nsp3 also result in altered virus-induced membrane rearrangements (39, 44). EAV nsp3 is a tetra-spanning integral membrane protein implicated in DMV formation and organization. Of interest, an introduced Asn substitution (T873N) in an EAV nsp3 luminal domain resulted in nsp3 glycosylation *in vitro* but was highly detrimental when introduced into the genome and recovered only as a pseudoreversion (N873H) that abolished the glycosylation site. Thus, for another nidovirus, the glycosylation status of a membrane-modifying replicase protein is also important for DMV formation and RNA synthesis during virus replication.

Our report confirms multiple roles of MHV nsp4 in the virus life cycle, including optimal virus replication and RNA synthesis, as well as its importance in the modification and morphology of virus-induced membrane structures. In this study, we show that MHV nsp4 is glycosylated and functions as a membrane modification protein that regulates virus-induced membrane rearrangements. nsp4 glycosylation mutant viruses display highly irregular DMVs and an increased prevalence of CMs relative to DMVs alone. The extent of disrupted DMVs in the nsp4 glycosylation mutant viruses correlated directly with decreases in RNA synthesis and virus replication. These data suggest that altered membranous structures from the nsp4 glycosylation mutants result in a reduced capacity to synthesize viral RNA and/or protect viral RNA from degradation, ultimately leading to impaired virus fitness.

Previous studies have concluded that nsp4 is required for MHV replication and have identified determinants of membrane topology, subcellular localization, and function (10, 35, 45). This study is the first to recover and characterize the importance of multiple nsp4 glycosylation events to virus replication, viral RNA synthesis, and virus-induced membrane modifications during coronavirus infection. Clementz et al. recovered an nsp4 N176A mutant but were unable to recover an N237A or N176A/N237A mutant (10). Their N176A mutant grew with kinetics similar to those of wt at an MOI of 0.1 PFU/cell at 33°C and 39°C but was not further characterized in that report. In contrast to the results in the previously published report, we were able to recover and characterize the N237A and N176A/N237A mutant viruses. The reasons for the differences in recovery can only be speculated. The backgrounds of cloned MHV genome fragments should be identical since the MHV genome fragments were jointly developed by our lab and the lab of Baric and coworkers (47). In addition, we performed RT-PCR sequencing of the complete genome from the recovered N176A/N237A mutant virus, which verified the engineered mutations and also confirmed that the rest of the genome was identical, with no additional mutations of any kind, to the published recombinant MHV-A59 sequence. Thus, there were no other compensating mutations to account for or consider for the recovery of the mutant virus. We have experienced occasional mutations in the genome fragments during preparation for genome assembly that have prevented recovery of even known viable mutants and would therefore speculate that this could account for the nonrecovery of N237A and N176A/N237A mutant viruses by Clementz et al. Our results clearly demonstrate that the N176 and N137 residues and the associated glycosylation events are not required for MHV replication in cell culture. Since no other mutations in the genome RNA from the recovered N176A/N237A mutant virus were identified, we can conclude that the profound and distinct phenotypes in virus replication, RNA synthesis, and virus-induced cellular membrane modifications are due to the introduced mutations alone.

Potential functions of nsp4 glycosylation. Modification of proteins by addition of N-linked glycans may result in numerous effects on protein functions (14, 19). Therefore, glycosylation of nsp4 may be important for a variety of reasons. One potential mechanism of nsp4 glycosylation is proper protein folding (18, 36). By removing N-linked glycans, the overall

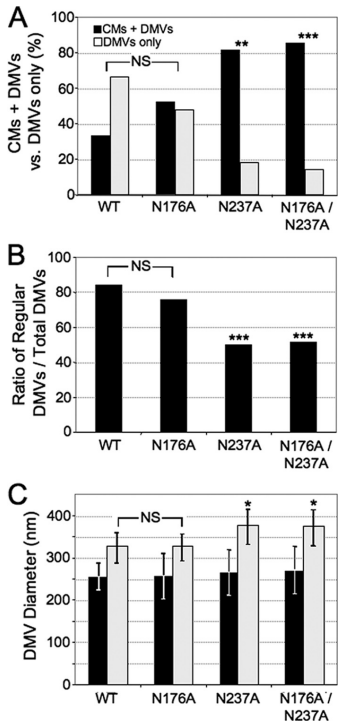

FIG. 7. Quantitative analysis of CMs and DMVs. (A) CMs and DMVs. All EM images were analyzed for the presence of CMs and DMVs based on characteristic EM morphology. Because CMs were found only in the presence of DMVs in all TEM sections observed, the ratio of total cell sections with CMs plus DMVs to the total of cell sections with DMVs alone could be examined. Black bars indicate presence of both CMs and DMVs, while white bars represent the presence of DMVs alone. Chi-square analysis was used to compare the presence of CMs plus DMVs to DMVs alone. (B) Ratios of DMVs with regular morphology to total DMVs (regular plus irregular). Total DMVs and DMVs with regular morphology were counted with TEM images for all viruses, and the ratio of regular DMVs to total DMVs was determined. (C) Diameter of regular and irregular DMVs of the wt and nsp4 mutants. DMVs were measured in Image J by the widest diameter in nm of outer membranes. Black bars indicate regular DMVs, while white bars indicate irregular DMVs. Error bars indicate standard deviation. There was no significant difference (not labeled in the figure) in the diameters of regular DMVs between wt and nsp4 mutant viruses. ANOVA followed by Tukey tests indicated a significant difference in the diameters of irregular DMVs of the N237A and N176A/N237A viruses compared to those of both wt and N176A viruses. * ($P < 0.05$), ** ($P < 0.01$), and *** ($p < 0.001$) indicate levels of statistical significance compared to wt virus. NS, no significance.

structure of nsp4 may be altered during protein folding. This mechanism is supported by the findings in this report, in that the nsp4 glycosylation mutant viruses displayed impairments in virus replication, viral RNA synthesis, and virus-induced membrane modifications. Other explanations are possible for the role of nsp4 glycosylation in replication complex formation and membrane modifications. For instance, glycosylation of nsp4 may be important for protein stability and prevention of nsp4 degradation (26). Lastly, it is possible that the N-linked glycans, either directly or through modification of nsp4 structure, recruit cellular factors that are involved in membrane rearrangements. Future studies are needed to distinguish between these possibilities.

Models of nsp4 function in replication complex formation, morphology, and organization. Evidence from this study has led to potential models addressing the effect nsp4 has on replication complex formation, morphology, and organization. One possible model is that nsp4 may regulate the transition or formation of different membrane modifications (i.e., CMs and DMVs). The evidence from this report that there was an increased prevalence of CMs in relation to DMVs in the N237A and N176A/N237A mutant viruses suggests that MHV nsp4 may be a major player in the transition of these virus-induced membrane rearrangements from one membrane structure to another. Other findings from this report that there was an increased presence of aberrant or deranged DMVs in the N237A and N176A/N237A mutant viruses suggest another possibility that the formation of intact, functional DMVs is regulated by nsp4.

A second potential model of nsp4 function is that the curvature and size of DMVs are regulated by nsp4 (38). In N237A and N176A/N237A mutant virus-infected cells, irregular DMVs were much larger and had highly disrupted inner membranes. The N237A and N176A/N237A mutant viruses also exhibited decreases in RNA synthesis, indicating that these irregular DMVs may not be functioning properly and that curvature and size may be important for proper function. This model is supported by the fact that all virus-infected cells produced regular DMVs, although at different proportions, and that all regular DMVs were similar in size. Cells infected with wt or N176A viruses, those that had levels of RNA synthesis higher than those of the N237A and N176A/N237A mutant viruses, also had a higher percentage of regular DMVs. These data suggest that curvature and size are important for DMV function.

A third model is that nsp4 functions in tethering or "pushing" the inner membrane to the outer membrane of the DMVs. The proximity of the inner membrane to the outer membrane may be important for creating an environment optimal for RNA synthesis and/or protection of newly synthesized viral RNAs. This model is supported by the fact that the prevalence of aberrant DMVs in the nsp4 glycosylation mutants was directly related to the extent of impairment of RNA synthesis and virus growth. These results suggest that irregular DMVs have a reduced capacity to synthesize and/or protect viral RNAs and are also the first to provide direct evidence suggesting that the physical size, morphology, and stability of virus-induced DMVs are important for efficient viral RNA synthesis and optimal virus production. On the other hand, the results also show clearly that glycosylation of nsp4 is not absolutely required for formation of "regular" DMVs and that replication complex function can still ultimately allow virus replication to wt titers, albeit with delayed kinetics.

To date, all coronavirus nsp4's that were subjected to Endo H treatment have been shown to be glycosylated in the lumen

of the ER between the first and second predicted transmembrane domains of nsp4 in exogenous expression experiments, including group 2a MHV nsp4, group 2b SARS-CoV nsp4, and group 3 IBV nsp4 (10, 29, 35). It will be interesting to see whether glycosylation of nsp4 is conserved among other coronaviruses, specifically group 1 coronaviruses, and what effect the loss of glycosylation sites has on virus replication, RNA synthesis, and replication complex morphology.

This study has demonstrated the importance of MHV nsp4 glycosylation sites in virus replication, replication complex morphology and organization, and viral RNA synthesis. Because nsp4 has been shown to have integral membrane characteristics and no predicted enzymatic activities, it is rational to propose that nsp4 involvement in viral RNA synthesis is due to replication complex formation, other possible membrane modifications, and/or protein interactions. The nsp4 glycosylation mutant viruses generated in this study will provide powerful tools to further dissect the definitive mechanisms of nsp4 function on replication complex formation and its roles in the virus life cycle.

ACKNOWLEDGMENTS

We thank Elvin Woodruff for TEM assistance and image analysis. We also thank Megan Culler and Xiaotao Lu for technical assistance. We thank Michelle Becker and Lance Eckerle for advice and critical reviews of the manuscript.

Support for this work was provided by National Institutes of Health grant R01 AI50083 (M.R.D.) from the National Institute of Allergy and Infectious Diseases. M.J.G. was supported by the Training Grant in Mechanisms of Vascular Disease through the Vanderbilt University School of Medicine (T32 HL007751). J.S.S. was supported by Public Health Service award T32 CA009385. This work was also supported by the Elizabeth B. Lamb Center for Pediatric Research.

REFERENCES

1. **Baker, S. C., K. Yokomori, S. Dong, R. Carlisle, A. E. Gorbalenya, E. V. Koonin, and M. M. Lai.** 1993. Identification of the catalytic sites of a papain-like cysteine proteinase of murine coronavirus. J. Virol. **67:**6056–6063.
2. **Baliji, S., S. A. Cammer, B. Sobral, and S. C. Baker.** 2009. Detection of nonstructural protein 6 (nsp6) in murine coronavirus-infected cells and analysis of the transmembrane topology using bioinformatics and molecular approaches. J. Virol. **83:**6957–6962.
3. **Bonilla, P. J., A. E. Gorbalenya, and S. R. Weiss.** 1994. Mouse hepatitis virus strain A59 RNA polymerase gene ORF 1a: heterogeneity among MHV strains. Virology **198:**736–740.
4. **Bost, A. G., E. Prentice, and M. R. Denison.** 2001. Mouse hepatitis virus replicase protein complexes are translocated to sites of M protein accumulation in the ERGIC at late times of infection. Virology **285:**21–29.
5. **Bredenbeek, P. J., C. J. Pachuk, A. F. H. Noten, J. Charite, W. Luytjes, S. R. Weiss, and W. J. M. Spaan.** 1990. The primary structure and expression of the second open reading frame of the polymerase gene of the coronavirus MHV-A59; a highly conserved polymerase is expressed by an efficient ribosomal frameshifting mechanism. Nucleic Acids Res. **18:**1825–1832.
6. **Brierley, I., P. Digard, and S. C. Inglis.** 1989. Characterization of an efficient coronavirus ribosomal frameshift signal: requirement for an RNA pseudoknot. Cell **57:**537–547.
7. **Brockway, S. M., C. T. Clay, X. T. Lu, and M. R. Denison.** 2003. Characterization of the expression, intracellular localization, and replication complex association of the putative mouse hepatitis virus RNA-dependent RNA polymerase. J. Virol. **77:**10515–10527.
8. **Chen, W., and R. S. Baric.** 1996. Molecular anatomy of mouse hepatitis virus persistence: coevolution of increased host cell resistance and virus virulence. J. Virol. **70:**3947–3960.
9. **Chen, W., V. J. Madden, C. J. Bagnell, and R. S. Baric.** 1997. Host-derived intracellular immunization against mouse hepatitis virus infection. Virology **228:**318–332.
10. **Clementz, M. A., A. Kanjanahaluethai, T. E. O'Brien, and S. C. Baker.** 2008. Mutation in murine coronavirus replication protein nsp4 alters assembly of double membrane vesicles. Virology **375:**118–129.
11. **Denison, M. R.** 2008. Seeking membranes: positive-strand RNA virus replication complexes. PLoS Biol. **6:**e270.
12. **Denison, M. R., B. Yount, S. M. Brockway, R. L. Graham, A. C. Sims, X. Lu, and R. S. Baric.** 2004. Cleavage between replicase proteins p28 and p65 of mouse hepatitis virus is not required for virus replication. J. Virol. **78:**5957–5965.
13. **Denison, M. R., P. W. Zoltick, S. A. Hughes, B. Giangreco, A. L. Olson, S. Perlman, J. L. Leibowitz, and S. R. Weiss.** 1992. Intracellular processing of the N-terminal ORF 1a proteins of the coronavirus MHV-A59 requires multiple proteolytic events. Virology **189:**274–284.
14. **Fiedler, K., and K. Simons.** 1995. The role of N-glycans in the secretory pathway. Cell **81:**309–312.
15. **Gosert, R., A. Kanjanahaluethai, D. Egger, K. Bienz, and S. C. Baker.** 2002. RNA replication of mouse hepatitis virus takes place at double-membrane vesicles. J. Virol. **76:**3697–3708.
16. **Graham, R. L., and M. R. Denison.** 2006. Replication of murine hepatitis virus is regulated by papain-like proteinase 1 processing of nonstructural proteins 1, 2, and 3. J. Virol. **80:**11610–11620.
17. **Harcourt, B. H., D. Jukneliene, A. Kanjanahaluethai, J. Bechill, K. M. Severson, C. M. Smith, P. A. Rota, and S. C. Baker.** 2004. Identification of severe acute respiratory syndrome coronavirus replicase products and characterization of papain-like protease activity. J. Virol. **78:**13600–13612.
18. **Helenius, A.** 1994. How N-linked oligosaccharides affect glycoprotein folding in the endoplasmic reticulum. Mol. Biol. Cell **5:**253–265.
19. **Helenius, A., and M. Aebi.** 2001. Intracellular functions of N-linked glycans. Science **291:**2364–2369.
20. **Hirano, N., K. Fujiwara, and M. Matumoto.** 1976. Mouse hepatitis virus (MHV-2). Plaque assay and propagation in mouse cell line DBT cells. Jpn. J. Microbiol. **20:**219–225.
21. **Kanjanahaluethai, A., and S. C. Baker.** 2000. Identification of mouse hepatitis virus papain-like proteinase 2 activity. J. Virol. **74:**7911–7921.
22. **Kanjanahaluethai, A., and S. C. Baker.** 2001. Processing of the replicase of murine coronavirus: papain-like proteinase 2 (PLP2) acts to generate p150 and p44. Adv. Exp. Med. Biol. **494:**267–273.
23. **Kanjanahaluethai, A., Z. Chen, D. Jukneliene, and S. C. Baker.** 2007. Membrane topology of murine coronavirus replicase nonstructural protein 3. Virology **361:**391–401.
24. **Kanjanahaluethai, A., D. Jukneliene, and S. C. Baker.** 2003. Identification of the murine coronavirus MP1 cleavage site recognized by papain-like proteinase 2. J. Virol. **77:**7376–7382.
25. **Kim, J. C., R. A. Spence, P. F. Currier, X. T. Lu, and M. R. Denison.** 1995. Coronavirus protein processing and RNA synthesis is inhibited by the cysteine proteinase inhibitor e64dd. Virology **208:**1–8.
26. **Klausner, R. D., and R. Sitia.** 1990. Protein degradation in the endoplasmic reticulum. Cell **62:**611–614.
27. **Knoops, K., M. Kikkert, S. H. Worm, J. C. Zevenhoven-Dobbe, Y. van der Meer, A. J. Koster, A. M. Mommaas, and E. J. Snijder.** 2008. SARS-coronavirus replication is supported by a reticulovesicular network of modified endoplasmic reticulum. PLoS Biol. **6:**e226.
28. **Lee, H.-J., C.-K. Shieh, A. E. Gorbalenya, E. V. Koonin, N. LaMonica, J. Tuler, A. Bagdzhadhzyan, and M. M. C. Lai.** 1991. The complete sequence (22 kilobases) of murine coronavirus gene 1 encoding the putative proteases and RNA polymerase. Virology **180:**567–582.
29. **Lim, K. P., L. F. Ng, and D. X. Liu.** 2000. Identification of a novel cleavage activity of the first papain-like proteinase domain encoded by open reading frame 1a of the coronavirus Avian infectious bronchitis virus and characterization of the cleavage products. J. Virol. **74:**1674–1685.
30. **Lindenbach, B. D., and C. M. Rice.** 1999. Genetic interaction of flavivirus nonstructural proteins NS1 and NS4A as a determinant of replicase function. J. Virol. **73:**4611–4621.
31. **Lu, X. T., Y. Q. Lu, and M. R. Denison.** 1996. Intracellular and in vitro translated 27-kDa proteins contain the 3C-like proteinase activity of the coronavirus MHV-A59. Virology **222:**375–382.
32. **Lu, Y., X. Lu, and M. R. Denison.** 1995. Identification and characterization of a serine-like proteinase of the murine coronavirus MHV-A59. J. Virol. **69:**3554–3559.
33. **Muylaert, I. R., T. J. Chambers, R. Galler, and C. M. Rice.** 1996. Mutagenesis of the N-linked glycosylation sites of the yellow fever virus NS1 protein: effects on virus replication and mouse neurovirulence. Virology **222:**159–168.
34. **Novoa, R. R., G. Calderita, R. Arranz, J. Fontana, H. Granzow, and C. Risco.** 2005. Virus factories: associations of cell organelles for viral replication and morphogenesis. Biol. Cell **97:**147–172.
35. **Oostra, M., E. G. te Lintelo, M. Deijs, M. H. Verheije, P. J. M. Rottier, and C. A. M. de Haan.** 2007. Localization and membrane topology of coronavirus nonstructural protein 4: involvement of the early secretory pathway in replication. J. Virol. **81:**12323–12336.
36. **Paulson, J. C.** 1989. Glycoproteins: what are the sugar chains for? Trends Biochem. Sci. **14:**272–276.
37. **Pedersen, K. W., Y. van der Meer, N. Roos, and E. J. Snijder.** 1999. Open reading frame 1a-encoded subunits of the arterivirus replicase induce endoplasmic reticulum-derived double-membrane vesicles which carry the viral replication complex. J. Virol. **73:**2016–2026.
38. **Perlman, S., and J. Netland.** 2009. Coronaviruses post-SARS: update on replication and pathogenesis. Nat. Rev. Microbiol. **7:**439–450.

39. **Posthuma, C. C., K. W. Pedersen, Z. Lu, R. G. Joosten, N. Roos, J. C. Zevenhoven-Dobbe, and E. J. Snijder.** 2008. Formation of the arterivirus replication/transcription complex: a key role for nonstructural protein 3 in the remodeling of intracellular membranes. J. Virol. **82:**4480–4491.
40. **Restrepo-Hartwig, M. A., and P. Ahlquist.** 1996. Brome mosaic virus helicase- and polymerase-like proteins colocalize on the endoplasmic reticulum at sites of viral RNA synthesis. J. Virol. **70:**8908–8916.
41. **Salonen, A., T. Ahola, and L. Kaariainen.** 2005. Viral RNA replication in association with cellular membranes. Curr. Top. Microbiol. Immunol. **285:**139–173.
42. **Schaad, M. C., P. E. Jensen, and J. C. Carrington.** 1997. Formation of plant RNA virus replication complexes on membranes: role of an endoplasmic reticulum-targeted viral protein. EMBO J. **16:**4049–4059.
43. **Schlegel, A., T. J. Giddings, M. S. Ladinsky, and K. Kirkegaard.** 1996. Cellular origin and ultrastructure of membranes induced during poliovirus infection. J. Virol. **70:**6576–6588.
44. **Snijder, E. J., H. van Tol, N. Roos, and K. W. Pedersen.** 2001. Non-structural proteins 2 and 3 interact to modify host cell membranes during the formation of the arterivirus replication complex. J. Gen. Virol. **82:**985–994.
45. **Sparks, J. S., X. Lu, and M. R. Denison.** 2007. Genetic analysis of murine hepatitis virus nsp4 in virus replication. J. Virol. **81:**12554–12563.
46. **Suhy, D. A., T. H. Giddings, and K. Kirkegaard.** 2000. Remodeling the ER by poliovirus infection and by individual viral proteins: an autophagy-like origin for virus-induced vesicles. J. Virol. **74:**8953–8965.
47. **Yount, B., M. R. Denison, S. R. Weiss, and R. S. Baric.** 2002. Systematic assembly of a full-length infectious cDNA of mouse hepatitis virus strain A59. J. Virol. **76:**11065–11078.
48. **Ziebuhr, J., E. J. Snijder, and A. E. Gorbalenya.** 2000. Virus-encoded proteinases and proteolytic processing in the Nidovirales. J. Gen. Virol. **81**(4)**:** 853–879.

REFERENCES

Agnihothram, S., Yount, B.L., Donaldson, E.F., Huynh, J., Menachery, V.D., Gralinski, L.E., Graham, R.L., Becker, M.M., Tomar, S., Scobey, T.D., Osswald, H.L., Whitmore, A., Gopal, R., Ghosh, A.K., Mesecar, A., Zambon, M., Heise, M., Denison, M.R., Baric, R.S., 2014. A Mouse Model for Betacoronavirus Subgroup 2c Using a Bat Coronavirus Strain HKU5 Variant. mBio 5, e00047–14–e00047–14. doi:10.1128/mBio.00047-14

Al-Mulla, H.M.N., Turrell, L., Smith, N.M., Payne, L., Baliji, S., Zust, R., Thiel, V., Baker, S.C., Siddell, S.G., Neuman, B.W., 2014. Competitive Fitness in Coronaviruses Is Not Correlated with Size or Number of Double-Membrane Vesicles under Reduced-Temperature Growth Conditions. mBio 5, e01107–13–e01107–13. doi:10.1128/mBio.01107-13

Alagaili, A.N., Briese, T., Mishra, N., Kapoor, V., Sameroff, S.C., de Wit, E., Munster, V.J., Hensley, L.E., Zalmout, I.S., Kapoor, A., Epstein, J.H., Karesh, W.B., Daszak, P., Mohammed, O.B., Lipkin, W.I., 2014. Middle East Respiratory Syndrome Coronavirus Infection in Dromedary Camels in Saudi Arabia. mBio 5, e00884–14–e00884–14. doi:10.1128/mBio.00884-14

Angelini, M.M., Akhlaghpour, M., Neuman, B.W., Buchmeier, M.J., 2013. Severe Acute Respiratory Syndrome Coronavirus Nonstructural Proteins 3, 4, and 6 Induce Double-Membrane Vesicles. mBio 4, e00524–13–e00524–13. doi:10.1128/mBio.00524-13

Annan, A., Baldwin, H.J., Corman, V.M., Klose, S.M., Owusu, M., Nkrumah, E.E., Badu, E.K., Anti, P., Agbenyega, O., Meyer, B., Oppong, S., Sarkodie, Y.A., Kalko, E.K.V., Lina, P.H.C., Godlevska, E.V., Reusken, C., Seebens, A., Gloza-Rausch, F., Vallo, P., Tschapka, M., Drosten, C., Drexler, J.F., 2013. Human Betacoronavirus 2c EMC/2012–related Viruses in Bats, Ghana and Europe. Emerg. Infect. Dis. 19, 456–459. doi:10.3201/eid1903.121503

Azhar, E.I., El-Kafrawy, S.A., Farraj, S.A., Hassan, A.M., Al-Saeed, M.S., Hashem, A.M., Madani, T.A., 2014. Evidence for Camel-to-Human Transmission of MERS Coronavirus. N Engl J Med 140609133235000. doi:10.1056/NEJMoa1401505

Baker, S.C., Yokomori, K., Dong, S., Carlisle, R., Gorbalenya, A.E., Koonin, E.V., Lai, M.M., 1993. Identification of the catalytic sites of a papain-like cysteine proteinase of murine coronavirus. J. Virol. 67, 6056–6063.

Baliji, S., Cammer, S.A., Sobral, B., Baker, S.C., 2009. Detection of Nonstructural Protein 6 in Murine Coronavirus-Infected Cells and Analysis of the Transmembrane Topology by Using Bioinformatics and Molecular Approaches. J. Virol. 83, 6957–6962. doi:10.1128/JVI.00254-09

Barajas, D., Jiang, Y., Nagy, P.D., 2009. A Unique Role for the Host ESCRT Proteins in Replication of Tomato bushy stunt virus. PLoS Pathog 5, e1000705. doi:10.1371/journal.ppat.1000705.s005

Barretto, N., Jukneliene, D., Ratia, K., Chen, Z., Mesecar, A.D., Baker, S.C., 2005. The Papain-Like Protease of Severe Acute Respiratory Syndrome Coronavirus Has Deubiquitinating Activity. J. Virol. 79, 15189–15198. doi:10.1128/JVI.79.24.15189-15198.2005

Beachboard, D.C., Anderson-Daniels, J.M., Denison, M.R., 2014. Mutations across murine hepatitis virus nsp4 alter virus fitness and membrane modifications. J. Virol. doi:10.1128/JVI.02776-14

Beachboard, D.C., Lu, X., Baker, S.C., Denison, M.R., 2013. Murine hepatitis virus nsp4 N258T mutants are not temperature-sensitive. Virology 435, 210–213. doi:10.1016/j.virol.2012.10.001

Belov, G.A., Altan-Bonnet, N., Kovtunovych, G., Jackson, C.L., Lippincott-Schwartz, J., Ehrenfeld, E., 2006. Hijacking Components of the Cellular Secretory Pathway for Replication of Poliovirus RNA. J. Virol. 81, 558–567. doi:10.1128/JVI.01820-06

Belov, G.A., Nair, V., Hansen, B.T., Hoyt, F.H., Fischer, E.R., Ehrenfeld, E., 2011. Complex Dynamic Development of Poliovirus Membranous Replication Complexes. J. Virol. 86, 302–312. doi:10.1128/JVI.05937-11

Bernasconi, R., Noack, J., Molinari, M., 2012. Unconventional roles of nonlipidated LC3 in ERAD tuning and coronavirus infection. autophagy 8, 16–18. doi:10.4161/auto.21229

Bolte, S., Cordelières, F.P., 2006. A guided tour into subcellular colocalization analysis in light microscopy. J Microsc 224, 213–232. doi:10.1111/j.1365-2818.2006.01706.x

Bonilla, P.J., Gorbalenya, A.E., Weiss, S.R., 1994. Mouse hepatitis virus strain A59 RNA polymerase gene ORF 1a: heterogeneity among MHV strains. Virology 198, 736–740. doi:10.1006/viro.1994.1088

Borschensky, C.M., Reinacher, M., 2014. Research in Veterinary Science. Research in Veterinary Science 97, 333–340. doi:10.1016/j.rvsc.2014.07.016

Bost, A.G., Carnahan, R.H., Lu, X.T., Denison, M.R., 2000. Four proteins processed from the replicase gene polyprotein of mouse hepatitis virus colocalize in the cell periphery and adjacent to sites of virion assembly. J. Virol. 74, 3379–3387.

Bost, A.G., Prentice, E., Denison, M.R., 2001. Mouse Hepatitis Virus Replicase Protein Complexes Are Translocated to Sites of M Protein Accumulation in the ERGIC at Late Times of Infection. Virology 285, 21–29. doi:10.1006/viro.2001.0932

Brayton, P.R., Lai, M.M., Patton, C.D., Stohlman, S.A., 1982. Characterization of two

RNA polymerase activities induced by mouse hepatitis virus. J. Virol. 42, 847–853.

Brockway, S.M., Clay, C.T., Lu, X.T., Denison, M.R., 2003. Characterization of the Expression, Intracellular Localization, and Replication Complex Association of the Putative Mouse Hepatitis Virus RNA-Dependent RNA Polymerase. J. Virol. 77, 10515–10527. doi:10.1128/JVI.77.19.10515-10527.2003

Brunn, von, A., Teepe, C., Simpson, J.C., Pepperkok, R., Friedel, C.C., Zimmer, R., Roberts, R., Baric, R., Haas, J., 2007. Analysis of Intraviral Protein-Protein Interactions of the SARS Coronavirus ORFeome. PLoS ONE 2, e459. doi:10.1371/journal.pone.0000459.s004

Chang, X.B., Hou, Y.X., Jensen, T.J., Riordan, J.R., 1994. Mapping of cystic fibrosis transmembrane conductance regulator membrane topology by glycosylation site insertion. J. Biol. Chem. 269, 18572–18575.

Chen, S., Hu, T., Zhang, J., Chen, J., Chen, K., Ding, J., Jiang, H., Shen, X., 2007. Mutation of Gly-11 on the Dimer Interface Results in the Complete Crystallographic Dimer Dissociation of Severe Acute Respiratory Syndrome Coronavirus 3C-like Protease: CRYSTAL STRUCTURE WITH MOLECULAR DYNAMICS SIMULATIONS. Journal of Biological Chemistry 283, 554–564. doi:10.1074/jbc.M705240200

Chen, S., Jonas, F., Shen, C., Higenfeld, R., 2010. Liberation of SARS-CoV main protease from the viral polyprotein: N-terminal autocleavage does not depend on the mature dimerization mode. Protein Cell 1, 59–74. doi:10.1007/s13238-010-0011-4

Chen, Y., Cai, H., Pan, J., Xiang, N., Tien, P., Ahola, T., Guo, D., 2009. Functional screen reveals SARS coronavirus nonstructural protein nsp14 as a novel cap N7 methyltransferase. Proc. Natl. Acad. Sci. U.S.A. 106, 3484–3489.

Cho, M.W., Teterina, N., Egger, D., Bienz, K., Ehrenfeld, E., 1994. Membrane rearrangement and vesicle induction by recombinant poliovirus 2C and 2BC in human cells. Virology 202, 129–145. doi:10.1006/viro.1994.1329

Clementz, M.A., Kanjanahaluethai, A., O'Brien, T.E., Baker, S.C., 2008. Mutation in murine coronavirus replication protein nsp4 alters assembly of double membrane vesicles. Virology 375, 118–129. doi:10.1016/j.virol.2008.01.018

Cleri, D.J., Ricketti, A.J., Vernaleo, J.R., 2010. Sevevere Acute Respiratory Syndrome (SARS). Infectious Disease Clinics of NA 24, 175–202. doi:10.1016/j.idc.2009.10.005

Cottam, E.M., Maier, H.J., Manifava, M., Vaux, L.C., Chandra-Schoenfelder, P., Gerner, W., Britton, P., Ktistakis, N.T., Wileman, T., 2011. Coronavirus nsp6 proteins generate autophagosomes from the endoplasmic reticulum via an omegasome intermediate. autophagy 7, 1335–1347. doi:10.4161/auto.7.11.16642

Day, C.W., Baric, R., Cai, S.X., Frieman, M., Kumaki, Y., Morrey, J.D., Smee, D.F., Barnard, D.L., 2009. A new mouse-adapted strain of SARS-CoV as a lethal model for evaluating antiviral agents in vitro and in vivo. Virology 395, 210–222. doi:10.1016/j.virol.2009.09.023

Decroly, E., Imbert, I., Coutard, B., Bouvet, M., Selisko, B., Alvarez, K., Gorbalenya, A.E., Snijder, E.J., Canard, B., 2008. Coronavirus Nonstructural Protein 16 Is a Cap-0 Binding Enzyme Possessing (Nucleoside-2'O)-Methyltransferase Activity. J. Virol. 82, 8071–8084. doi:10.1128/JVI.00407-08

Deming, D.J., Graham, R.L., Denison, M.R., Baric, R.S., 2007. Processing of Open Reading Frame 1a Replicase Proteins nsp7 to nsp10 in Murine Hepatitis Virus Strain A59 Replication. J. Virol. 81, 10280–10291. doi:10.1128/JVI.00017-07

Deng, X., St John, S.E., Osswald, H.L., O'Brien, A., Banach, B.S., Sleeman, K., Ghosh, A.K., Mesecar, A.D., Baker, S.C., 2014. Coronaviruses Resistant to a 3C-like Protease Inhibitor Are Attenuated for Replication and Pathogenesis Revealing a Low Genetic Barrier but High Fitness Cost of Resistance. J. Virol. doi:10.1128/JVI.01528-14

Denison, M.R., Yount, B., Brockway, S.M., Graham, R.L., Sims, A.C., Lu, X., Baric, R.S., 2004. Cleavage between Replicase Proteins p28 and p65 of Mouse Hepatitis Virus Is Not Required for Virus Replication. J. Virol. 78, 5957–5965. doi:10.1128/JVI.78.11.5957-5965.2004

Dennis, D.E., Brian, D.A., 1982. RNA-dependent RNA polymerase activity in coronavirus- infected cells. J. Virol. 42, 153–164.

Eckerle, L.D., Lu, X., Sperry, S.M., Choi, L., Denison, M.R., 2007. High Fidelity of Murine Hepatitis Virus Replication Is Decreased in nsp14 Exoribonuclease Mutants. J. Virol. 81, 12135–12144. doi:10.1128/JVI.01296-07

Egger, D., Wolk, B., Gosert, R., Bianchi, L., Blum, H.E., Moradpour, D., Bienz, K., 2002. Expression of Hepatitis C Virus Proteins Induces Distinct Membrane Alterations Including a Candidate Viral Replication Complex. J. Virol. 76, 5974–5984. doi:10.1128/JVI.76.12.5974-5984.2002

Freeman, M.C., Graham, R.L., Lu, X., Peek, C.T., Denison, M.R., 2014a. Coronavirus Replicase-Reporter Fusions Provide Quantitative Analysis of Replication and Replication Complex Formation. J. Virol. doi:10.1128/JVI.00021-14

Freeman, M.C., Peek, C.T., Becker, M.M., Smith, E.C., Denison, M.R., 2014b. Coronaviruses Induce Entry-Independent, Continuous Macropinocytosis. mBio 5, e01340–14–e01340–14. doi:10.1128/mBio.01340-14

Gadlage, M.J., Sparks, J.S., Beachboard, D.C., Cox, R.G., Doyle, J.D., Stobart, C.C., Denison, M.R., 2009. Murine hepatitis virus nonstructural protein 4 regulates virus-induced membrane modifications and replication complex function. J. Virol. 84,

280–290. doi:10.1128/JVI.01772-09

Ge, X.-Y., Li, J.-L., Yang, X.-L., Chmura, A.A., Zhu, G., Epstein, J.H., Mazet, J.K., Ben Hu, Zhang, W., Peng, C., Zhang, Y.-J., Luo, C.-M., Tan, B., Wang, N., Zhu, Y., Crameri, G., Zhang, S.-Y., Wang, L.-F., Daszak, P., Shi, Z.-L., 2014. Isolation and characterization of a bat SARS-like coronavirus that uses the ACE2 receptor. Nature 503, 535–538. doi:10.1038/nature12711

Ghosh, A.K., Gong, G., Grum-Tokars, V., Mulhearn, D.C., Baker, S.C., Coughlin, M., Prabhakar, B.S., Sleeman, K., Johnson, M.E., Mesecar, A.D., 2008. Bioorganic & Medicinal Chemistry Letters. Bioorganic & Medicinal Chemistry Letters 18, 5684–5688. doi:10.1016/j.bmcl.2008.08.082

Gillespie, L.K., Hoenen, A., Morgan, G., Mackenzie, J.M., 2010. The Endoplasmic Reticulum Provides the Membrane Platform for Biogenesis of the Flavivirus Replication Complex. J. Virol. 84, 10438–10447. doi:10.1128/JVI.00986-10

Gorbalenya, A.E., Koonin, E.V., DONCHENKO, A.P., BLINOV, V.M., 1989. Coronavirus Genome - Prediction of Putative Functional Domains in the Non-Structural Polyprotein by Comparative Amino-Acid Sequence-Analysis. Nucleic Acids Research 17, 4847–4861.

Gosert, R., Kanjanahaluethai, A., Egger, D., Bienz, K., Baker, S.C., 2002. RNA Replication of Mouse Hepatitis Virus Takes Place at Double-Membrane Vesicles. J. Virol. 76, 3697–3708. doi:10.1128/JVI.76.8.3697-3708.2002

Graham, R.L., Sims, A.C., Brockway, S.M., Baric, R.S., Denison, M.R., 2005. The nsp2 Replicase Proteins of Murine Hepatitis Virus and Severe Acute Respiratory Syndrome Coronavirus Are Dispensable for Viral Replication. J. Virol. 79, 13399–13411. doi:10.1128/JVI.79.21.13399-13411.2005

Guedj, J., Dahari, H., Rong, L., Sansone, N.D., Nettles, R.E., Cotler, S.J., Layden, T.J., Uprichard, S.L., Perelson, A.S., 2013. Modeling shows that the NS5A inhibitor daclatasvir has two modes of action and yields a shorter estimate of the hepatitis C virus half-life. Proceedings of the National Academy of Sciences 110, 3991–3996. doi:10.1073/pnas.1203110110

Hagemeijer, M.C., Monastyrska, I., Griffith, J., van der Sluijs, P., Voortman, J., van Bergen en Henegouwen, P.M., Vonk, A.M., Rottier, P.J.M., Reggiori, F., de Haan, C.A.M., 2014. Membrane rearrangements mediated by coronavirus nonstructural proteins 3 and 4. Virology 458-459, 125–135. doi:10.1016/j.virol.2014.04.027

Hagemeijer, M.C., Ulasli, M., Vonk, A.M., Reggiori, F., Rottier, P.J.M., de Haan, C.A.M., 2011. Mobility and Interactions of Coronavirus Nonstructural Protein 4. J. Virol. 85, 4572–4577. doi:10.1128/JVI.00042-11

Hagemeijer, M.C., Verheije, M.H., Ulasli, M., Shaltiel, I.A., de Vries, L.A., Reggiori, F., Rottier, P.J.M., de Haan, C.A.M., 2010. Dynamics of Coronavirus Replication-

Transcription Complexes. J. Virol. 84, 2134–2149. doi:10.1128/JVI.01716-09

Hansen, G.H., Delmas, B., Besnardeau, L., Vogel, L.K., Laude, H., Sjöström, H., Norén, O., 1998. The coronavirus transmissible gastroenteritis virus causes infection after receptor-mediated endocytosis and acid-dependent fusion with an intracellular compartment. J. Virol. 72, 527–534.

Helenius, A., Aebi, M., 2004. Roles of N-linked glycans in the endoplasmic reticulum. Biochemistry 73, 1019–1049. doi:10.1146/annurev.biochem.73.011303.073752

Hemmila, E., Turbide, C., Olson, M., Jothy, S., Holmes, K.V., Beauchemin, N., 2004. Ceacam1a-/- Mice Are Completely Resistant to Infection by Murine Coronavirus Mouse Hepatitis Virus A59. J. Virol. 78, 10156–10165. doi:10.1128/JVI.78.18.10156-10165.2004

Hofmann, H., Hattermann, K., Marzi, A., Gramberg, T., Geier, M., Krumbiegel, M., Kuate, S., Uberla, K., Niedrig, M., Pohlmann, S., 2004. S Protein of Severe Acute Respiratory Syndrome-Associated Coronavirus Mediates Entry into Hepatoma Cell Lines and Is Targeted by Neutralizing Antibodies in Infected Patients. J. Virol. 78, 6134–6142. doi:10.1128/JVI.78.12.6134-6142.2004

Hresko, R.C., Kruse, M., Strube, M., Mueckler, M., 1994. Topology of the Glut 1 glucose transporter deduced from glycosylation scanning mutagenesis. J. Biol. Chem. 269, 20482–20488.

Hsu, N.-Y., Ilnytska, O., Belov, G., Santiana, M., Chen, Y.-H., Takvorian, P.M., Pau, C., van der Schaar, H., Kaushik-Basu, N., Balla, T., Cameron, C.E., Ehrenfeld, E., van Kuppeveld, F.J.M., Altan-Bonnet, N., 2010. Viral Reorganization of the Secretory Pathway Generates Distinct Organelles for RNA Replication. Cell 141, 799–811. doi:10.1016/j.cell.2010.03.050

Hurst, K.R., Ye, R., Goebel, S.J., Jayaraman, P., Masters, P.S., 2010. An Interaction between the Nucleocapsid Protein and a Component of the Replicase-Transcriptase Complex Is Crucial for the Infectivity of Coronavirus Genomic RNA. J. Virol. 84, 10276–10288. doi:10.1128/JVI.01287-10

ICTV, 2013. ICTV Virus Taxonomy 2013 [WWW Document]. ictvonline.org. URL http://ictvonline.org (accessed 1.19.15).

Imbert, I., Guillemot, J.-C., Bourhis, J.-M., Bussetta, C., Coutard, B., Egloff, M.-P., Ferron, F., Gorbalenya, A.E., Canard, B., 2006. A second, non-canonical RNA-dependent RNA polymerase in SARS coronavirus. EMBO J. 25, 4933–4942. doi:10.1038/sj.emboj.7601368

Imbert, I., Snijder, E.J., Dimitrova, M., Guillemot, J.-C., Lécine, P., Canard, B., 2008. The SARS-Coronavirus PLnc domain of nsp3 as a replication/transcription scaffolding protein. Virus Research 133, 136–148. doi:10.1016/j.virusres.2007.11.017

Ivanov, K.A., Hertzig, T., Rozanov, M., Bayer, S., Thiel, V., Gorbalenya, A.E., Ziebuhr, J., 2004a. Major genetic marker of nidoviruses encodes a replicative endoribonuclease. Proc. Natl. Acad. Sci. U.S.A. 101, 12694–12699. doi:10.1073/pnas.0403127101

Ivanov, K.A., Thiel, V., Dobbe, J.C., van der Meer, Y., Snijder, E.J., Ziebuhr, J., 2004b. Multiple Enzymatic Activities Associated with Severe Acute Respiratory Syndrome Coronavirus Helicase. J. Virol. 78, 5619–5632. doi:10.1128/JVI.78.11.5619-5632.2004

Ivanov, K.A., Ziebuhr, J., 2004. Human Coronavirus 229E Nonstructural Protein 13: Characterization of Duplex-Unwinding, Nucleoside Triphosphatase, and RNA 5'-Triphosphatase Activities. J. Virol. 78, 7833–7838. doi:10.1128/JVI.78.14.7833-7838.2004

Kamitani, W., Narayanan, K., Huang, C., Lokugamage, K., Ikegami, T., Ito, N., Kubo, H., Makino, S., 2006. Severe acute respiratory syndrome coronavirus nsp1 protein suppresses host gene expression by promoting host mRNA degradation. Proc. Natl. Acad. Sci. U.S.A. 103, 12885–12890.

Kanjanahaluethai, A., Baker, S.C., 2001. Processing of the replicase of murine coronavirus: papain-like proteinase 2 (PLP2) acts to generate p150 and p44. Adv. Exp. Med. Biol. 494, 267–273.

Kanjanahaluethai, A., Chen, Z., Jukneliene, D., Baker, S.C., 2007. Membrane topology of murine coronavirus replicase nonstructural protein 3. Virology 361, 391–401. doi:10.1016/j.virol.2006.12.009

Kilianski, A., Mielech, A.M., Deng, X., Baker, S.C., 2013. Assessing Activity and Inhibition of Middle East Respiratory Syndrome Coronavirus Papain-Like and 3C-Like Proteases Using Luciferase-Based Biosensors. J. Virol. 87, 11955–11962. doi:10.1128/JVI.02105-13

Kim, J.C., Spence, R.A., Currier, P.F., Lu, X., Denison, M.R., 1995. Coronavirus protein processing and RNA synthesis is inhibited by the cysteine proteinase inhibitor E64d. Virology 208, 1–8. doi:10.1006/viro.1995.1123

Klumperman, J., Locker, J.K., Meijer, A., Horzinek, M.C., Geuze, H.J., Rottier, P.J., 1994. Coronavirus M proteins accumulate in the Golgi complex beyond the site of virion budding. J. Virol. 68, 6523–6534.

Knoops, K., Kikkert, M., van den Worm, S.H.E., Zevenhoven-Dobbe, J.C., van der Meer, Y., Koster, A.J., Mommaas, A.M., Snijder, E.J., 2008a. SARS-Coronavirus Replication Is Supported by a Reticulovesicular Network of Modified Endoplasmic Reticulum 6, e226. doi:10.1371/journal.pbio.0060226

Knoops, K., Kikkert, M., Worm, S.H.E.V.D., Zevenhoven-Dobbe, J.C., van der Meer, Y., Koster, A.J., Mommaas, A.M., Snijder, E.J., 2008b. SARS-Coronavirus Replication

Is Supported by a Reticulovesicular Network of Modified Endoplasmic Reticulum. Plos Biol 6, e226. doi:10.1371/journal.pbio.0060226.sv004

Knoops, K., Swett-Tapia, C., van den Worm, S.H.E., Velthuis, te, A.J.W., Koster, A.J., Mommaas, A.M., Snijder, E.J., Kikkert, M., 2009. Integrity of the Early Secretory Pathway Promotes, but Is Not Required for, Severe Acute Respiratory Syndrome Coronavirus RNA Synthesis and Virus-Induced Remodeling of Endoplasmic Reticulum Membranes. J. Virol. 84, 833–846. doi:10.1128/JVI.01826-09

Kopek, B.G., Perkins, G., Miller, D.J., Ellisman, M.H., Ahlquist, P., 2007. Three-dimensional analysis of a viral RNA replication complex reveals a virus-induced mini-organelle. Plos Biol 5, e220. doi:10.1371/journal.pbio.0050220

Kopek, B.G., Shtengel, G., Xu, C.S., Clayton, D.A., Hess, H.F., 2012. Correlative 3D superresolution fluorescence and electron microscopy reveal the relationship of mitochondrial nucleoids to membranes. Proceedings of the National Academy of Sciences 109, 6136–6141. doi:10.1073/pnas.1121558109

Kujala, P., Ikaheimonen, A., Ehsani, N., Vihinen, H., Auvinen, P., Kaariainen, L., 2001. Biogenesis of the Semliki Forest Virus RNA Replication Complex. J. Virol. 75, 3873–3884. doi:10.1128/JVI.75.8.3873-3884.2001

Lee, C., Ma, H., Hang, J.Q., Leveque, V., Sklan, E.H., Elazar, M., Klumpp, K., Glenn, J.S., 2011. The hepatitis C virus NS5A inhibitor (BMS-790052) alters the subcellular localization of the NS5A non-structural viral protein. Virology 414, 10–18. doi:10.1016/j.virol.2011.03.026

Lee, C., Sheih, C.K., Gorbalenya, A.E., Koonin, E.V., La Monica, N., Tuler, J., Bagdzhadzhyan, A., Lai, M.M., 1991. The complete sequence (22 kilobases) of murine coronavirus gene 1 encoding the putative proteases and RNA polymerase. Virology 180, 567–582.

Li, W., Moore, M.J., Vasilieva, N., Sui, J., Wong, S.K., Berne, M.A., Somasundaran, M., Sullivan, J.L., Luzuriaga, K., Greenough, T.C., Farzan, H.C.M., 2003. Angiotensin-converting enzyme 2 is a functional receptor forthe SARS coronavirus 1–5.

Lindner, H.A., Fotouhi-Ardakani, N., Lytvyn, V., Lachance, P., Sulea, T., Menard, R., 2005. The Papain-Like Protease from the Severe Acute Respiratory Syndrome Coronavirus Is a Deubiquitinating Enzyme. J. Virol. 79, 15199–15208. doi:10.1128/JVI.79.24.15199-15208.2005

Lu, X., Lu, Y., Denison, M.R., 1996. Intracellular and in vitro-translated 27-kDa proteins contain the 3C-like proteinase activity of the coronavirus MHV-A59. Virology 222, 375–382. doi:10.1006/viro.1996.0434

Lu, Y., Lu, X., Denison, M.R., 1995. Identification and characterization of a serine-like proteinase of the murine coronavirus MHV-A59. J. Virol. 69, 3554–3559.

Lundin, A., Dijkman, R., Bergström, T., Kann, N., Adamiak, B., Hannoun, C., Kindler, E., Jónsdóttir, H.R., Muth, D., Kint, J., Forlenza, M., Müller, M.A., Drosten, C., Thiel, V., Trybala, E., 2014. Targeting Membrane-Bound Viral RNA Synthesis Reveals Potent Inhibition of Diverse Coronaviruses Including the Middle East Respiratory Syndrome Virus. PLoS Pathog 10, e1004166. doi:10.1371/journal.ppat.1004166.s007

Magliano, D.D., Marshall, J.A.J., Bowden, D.S.D., Vardaxis, N.N., Meanger, J.J., Lee, J.Y.J., 1998. Rubella Virus Replication Complexes Are Virus-Modified Lysosomes. Virology 240, 7–7. doi:10.1006/viro.1997.8906

Maier, H., Britton, P., 2012. Involvement of Autophagy in Coronavirus Replication. Viruses 4, 3440–3451. doi:10.3390/v4123440

Maier, H.J., Hawes, P.C., Cottam, E.M., Mantell, J., Verkade, P., Monaghan, P., Wileman, T., Britton, P., 2013. Infectious Bronchitis Virus Generates Spherules from Zippered Endoplasmic Reticulum Membranes. mBio 4, e00801–13–e00801–13. doi:10.1128/mBio.00801-13

Manolaridis, I., Wojdyla, J.A., Panjikar, S., Snijder, E.J., Gorbalenya, A.E., Berglind, H., Nordlund, P., Coutard, B., Tucker, P.A., 2009. Structure of the C-terminal domain of nsp4 from feline coronavirus. Acta Cryst (2009). D65, 839-846 [doi:10.1107/S0907444909018253] 1–8. doi:10.1107/S0907444909018253

Masters, P.S., 2006. The Molecular Biology of Coronaviruses, in: Advances in Virus Research, Advances in Virus Research. Elsevier, pp. 193–292. doi:10.1016/S0065-3527(06)66005-3

Memish, Z.A., Mishra, N., Olival, K.J., Fagbo, S.F., Kapoor, V., Epstein, J.H., AlHakeem, R., Durosinloun, A., Asmari, Al, M., Islam, A., Kapoor, A., Briese, T., Daszak, P., Rabeeah, Al, A.A., Lipkin, W.I., 2013. Middle East Respiratory Syndrome Coronavirus in Bats, Saudi Arabia. Emerg. Infect. Dis. 19. doi:10.3201/eid1911.131172

Meyer, B., Müller, M.A., Corman, V.M., Reusken, C.B.E.M., Ritz, D., Godeke, G.-J., Lattwein, E., Kallies, S., Siemens, A., van Beek, J., Drexler, J.F., Muth, D., Bosch, B.J., Wernery, U., Koopmans, M.P.G., Wernery, R., Drosten, C., 2014. Antibodies against MERS Coronavirus in Dromedary Camels, United Arab Emirates, 2003 and 2013. Emerg. Infect. Dis. 20, 552–559. doi:10.3201/eid2004.131746

Miller, S., Krijnse-Locker, J., 2008. Modification of intracellular membrane structures for virus replication 6, 363–374. doi:10.1038/nrmicro1890

Mole, B., 2013. Deadly pig virus slips through US borders. Nature 499, 388. doi:10.1038/499388a

Narayanan, K., Huang, C., Lokugamage, K., Kamitani, W., Ikegami, T., Tseng, C.T.K., Makino, S., 2008. Severe Acute Respiratory Syndrome Coronavirus nsp1 Suppresses

Host Gene Expression, Including That of Type I Interferon, in Infected Cells. J. Virol. 82, 4471–4479. doi:10.1128/JVI.02472-07

Nomura, R., Kiyota, A., Suzaki, E., Kataoka, K., Ohe, Y., Miyamoto, K., Senda, T., Fujimoto, T., 2004. Human Coronavirus 229E Binds to CD13 in Rafts and Enters the Cell through Caveolae. J. Virol. 78, 8701–8708. doi:10.1128/JVI.78.16.8701-8708.2004

Oostra, M., de Haan, C.A.M., de Groot, R.J., Rottier, P.J.M., 2006. Glycosylation of the Severe Acute Respiratory Syndrome Coronavirus Triple-Spanning Membrane Proteins 3a and M. J. Virol. 80, 2326–2336. doi:10.1128/JVI.80.5.2326-2336.2006

Oostra, M., Hagemeijer, M.C., van Gent, M., Bekker, C.P.J., Lintelo, te, E.G., Rottier, P.J.M., de Haan, C.A.M., 2008. Topology and Membrane Anchoring of the Coronavirus Replication Complex: Not All Hydrophobic Domains of nsp3 and nsp6 Are Membrane Spanning. J. Virol. 82, 12392–12405. doi:10.1128/JVI.01219-08

Oostra, M., Lintelo, te, E.G., Deijs, M., Verheije, M.H., Rottier, P.J.M., de Haan, C.A.M., 2007. Localization and Membrane Topology of Coronavirus Nonstructural Protein 4: Involvement of the Early Secretory Pathway in Replication. J. Virol. 81, 12323–12336. doi:10.1128/JVI.01506-07

Pan, J., Peng, X., Gao, Y., Li, Z., Lu, X., Chen, Y., Ishaq, M., Liu, D., DeDiego, M.L., Enjuanes, L., Guo, D., 2008. Genome-Wide Analysis of Protein-Protein Interactions and Involvement of Viral Proteins in SARS-CoV Replication. PLoS ONE 3, e3299. doi:10.1371/journal.pone.0003299.t001

Perlman, S., Netland, J., 2009. Coronaviruses post-SARS: update on replication and pathogenesis 7, 439–450. doi:10.1038/nrmicro2147

Popov, M., Tam, L.Y., Li, J., Reithmeier, R.A., 1997. Mapping the ends of transmembrane segments in a polytopic membrane protein. Scanning N-glycosylation mutagenesis of extracytosolic loops in the anion exchanger, band 3. J. Biol. Chem. 272, 18325–18332.

Prentice, E., 2003. Coronavirus Replication Complex Formation Utilizes Components of Cellular Autophagy. Journal of Biological Chemistry 279, 10136–10141. doi:10.1074/jbc.M306124200

Prentice, E., McAuliffe, J., Lu, X., Subbarao, K., Denison, M.R., 2004. Identification and Characterization of Severe Acute Respiratory Syndrome Coronavirus Replicase Proteins. J. Virol. 78, 9977–9986. doi:10.1128/JVI.78.18.9977-9986.2004

Raj, V.S., Mou, H., Smits, S.L., Dekkers, D.H.W., Müller, M.A., Dijkman, R., Muth, D., Demmers, J.A.A., Zaki, A., Fouchier, R.A.M., Thiel, V., Drosten, C., Rottier, P.J.M., Osterhaus, A.D.M.E., Bosch, B.J., Haagmans, B.L., 2013. Dipeptidyl peptidase 4 is a functional receptor for the emerging human coronavirus-EMC. Nature 495, 251–254. doi:10.1038/nature12005

Ratia, K., Saikatendu, K.S., Santarsiero, B.D., Barretto, N., Baker, S.C., Stevens, R.C., Mesecar, A.D., 2006. Severe acute respiratory syndrome coronavirus papain-like protease: structure of a viral deubiquitinating enzyme. Proc. Natl. Acad. Sci. U.S.A. 103, 5717–5722. doi:10.1073/pnas.0510851103

Reggiori, F., de Haan, C.A.M., Molinari, M., 2011. Unconventional Use of LC3 by Coronaviruses through the Alleged Subversion of the ERAD Tuning Pathway. Viruses 3, 1610–1623. doi:10.3390/v3091610

Reggiori, F., Monastyrska, I., Verheije, M.H., Calì, T., Ulasli, M., Bianchi, S., Bernasconi, R., de Haan, C.A.M., Molinari, M., 2010. Coronaviruses Hijack the LC3-I-Positive EDEMosomes, ER-Derived Vesicles Exporting Short-Lived ERAD Regulators, for Replication. Cell Host and Microbe 7, 500–508. doi:10.1016/j.chom.2010.05.013

Reghellin, V., Donnici, L., Fenu, S., Berno, V., Calabrese, V., Pagani, M., Abrignani, S., Peri, F., De Francesco, R., Neddermann, P., 2014. NS5A inhibitors impair NS5A-PI4KIII complex formation and cause a decrease of PI4P and cholesterol levels in HCV-associated membranes. Antimicrobial Agents and Chemotherapy. doi:10.1128/AAC.03293-14

Reusken, C.B.E.M., Haagmans, B.L., Müller, M.A., Gutierrez, C., Godeke, G.-J., Meyer, B., Muth, D., Raj, V.S., Smits-De Vries, L., Corman, V.M., Drexler, J.F., Smits, S.L., Tahir, El, Y.E., De Sousa, R., van Beek, J., Nowotny, N., van Maanen, K., Hidalgo-Hermoso, E., Bosch, B.J., Rottier, P., Osterhaus, A., Gortázar-Schmidt, C., Drosten, C., Koopmans, M.P.G., 2013. Middle East respiratory syndrome coronavirus neutralising serum antibodies in dromedary camels: a comparative serological study. Lancet Infect Dis 13, 859–866. doi:10.1016/S1473-3099(13)70164-6

Romero-Brey, I., Merz, A., Chiramel, A., Lee, J.-Y., Chlanda, P., Haselman, U., Santarella-Mellwig, R., Habermann, A., Hoppe, S., Kallis, S., Walther, P., Antony, C., Krijnse-Locker, J., Bartenschlager, R., 2012. Three-Dimensional Architecture and Biogenesis of Membrane Structures Associated with Hepatitis C Virus Replication. PLoS Pathog 8, e1003056. doi:10.1371/journal.ppat.1003056.s008

Rottier, P.J., Horzinek, M.C., van der Zeijst, B.A., 1981. Viral protein synthesis in mouse hepatitis virus strain A59-infected cells: effect of tunicamycin. J. Virol. 40, 350–357.

Saikatendu, K.S., Joseph, J.S., Subramanian, V., Clayton, T., Griffith, M., Moy, K., Velasquez, J., Neuman, B.W., Buchmeier, M.J., Stevens, R.C., Kuhn, P., 2005. Structural Basis of Severe Acute Respiratory Syndrome Coronavirus ADP-Ribose-1″-Phosphate Dephosphorylation by a Conserved Domain of nsP3. Structure 13, 1665–1675. doi:10.1016/j.str.2005.07.022

Sawicki, S.G., Sawicki, D.L., Younker, D., Meyer, Y., Thiel, V., Stokes, H., Siddell, S.G., 2005. Functional and Genetic Analysis of Coronavirus Replicase-Transcriptase Proteins. PLoS Pathog 1, e39. doi:10.1371/journal.ppat.0010039.st001

Schneider, C.A., Rasband, W.S., Eliceiri, K.W., 2014. NIH Image to ImageJ: 25 years of image analysis. Nat Meth 9, 671–675. doi:10.1038/nmeth.2089

Scobey, T., Yount, B.L., Sims, A.C., Donaldson, E.F., Agnihothram, S.S., Menachery, V.D., Graham, R.L., Swanstrom, J., Bove, P.F., Kim, J.D., Grego, S., Randell, S.H., Baric, R.S., 2013. Reverse genetics with a full-length infectious cDNA of the Middle East respiratory syndrome coronavirus. Proceedings of the National Academy of Sciences 110, 16157–16162. doi:10.1073/pnas.1311542110

Seybert, A., Hegyi, A., Siddell, S.G., Ziebuhr, J., 2000. The human coronavirus 229E superfamily 1 helicase has RNA and DNA duplex-unwinding activities with 5“-to-3” polarity. RNA 6, 1056–1068.

Shi, J., Sivaraman, J., Song, J., 2008. Mechanism for Controlling the Dimer-Monomer Switch and Coupling Dimerization to Catalysis of the Severe Acute Respiratory Syndrome Coronavirus 3C-Like Protease. J. Virol. 82, 4620–4629. doi:10.1128/JVI.02680-07

Simmons, G., Reeves, J.D., Rennekamp, A.J., Amberg, S.M., Piefer, A.J., Bates, P., 2004. Characterization of severe acute respiratory syndrome-associated coronavirus (SARS-CoV) spike glycoprotein-mediated viral entry. Proc. Natl. Acad. Sci. U.S.A. 101, 4240–4245. doi:10.1073/pnas.0306446101

Sims, A.C., Ostermann, J., Denison, M.R., 2000. Mouse hepatitis virus replicase proteins associate with two distinct populations of intracellular membranes. J. Virol. 74, 5647–5654. doi:10.1128/JVI.74.12.5647-5654.2000

Smith, E.C., Blanc, H., Vignuzzi, M., Denison, M.R., 2013. Coronaviruses Lacking Exoribonuclease Activity Are Susceptible to Lethal Mutagenesis: Evidence for Proofreading and Potential Therapeutics. PLoS Pathog 9, e1003565. doi:10.1371/journal.ppat.1003565.t001

Smith, E.C., Denison, M.R., 2013. Coronaviruses as DNA Wannabes: A New Model for the Regulation of RNA Virus Replication Fidelity. PLoS Pathog 9, e1003760. doi:10.1371/journal.ppat.1003760.g002

Snijder, E.J., van der Meer, Y., Zevenhoven-Dobbe, J., Onderwater, J.J.M., van der Meulen, J., Koerten, H.K., Mommaas, A.M., 2006. Ultrastructure and Origin of Membrane Vesicles Associated with the Severe Acute Respiratory Syndrome Coronavirus Replication Complex. J. Virol. 80, 5927–5940. doi:10.1128/JVI.02501-05

Snijder, E.J., van Tol, H., Roos, N., Pedersen, K.W., 2001. Non-structural proteins 2 and 3 interact to modify host cell membranes during the formation of the arterivirus replication complex. Journal of General Virology 82, 985–994.

Sparks, J.S., Donaldson, E.F., Lu, X., Baric, R.S., Denison, M.R., 2008. A Novel Mutation in Murine Hepatitis Virus nsp5, the Viral 3C-Like Proteinase, Causes

Temperature-Sensitive Defects in Viral Growth and Protein Processing. J. Virol. 82, 5999–6008. doi:10.1128/JVI.00203-08

Sparks, J.S., Lu, X., Denison, M.R., 2007. Genetic Analysis of Murine Hepatitis Virus nsp4 in Virus Replication. J. Virol. 81, 12554–12563. doi:10.1128/JVI.01257-07

Sperry, S.M., Kazi, L., Graham, R.L., Baric, R.S., Weiss, S.R., Denison, M.R., 2005. Single-Amino-Acid Substitutions in Open Reading Frame (ORF) 1b-nsp14 and ORF 2a Proteins of the Coronavirus Mouse Hepatitis Virus Are Attenuating in Mice. J. Virol. 79, 3391–3400. doi:10.1128/JVI.79.6.3391-3400.2005

Spuul, P., Balistreri, G., Kaariainen, L., Ahola, T., 2010. Phosphatidylinositol 3-Kinase-, Actin-, and Microtubule-Dependent Transport of Semliki Forest Virus Replication Complexes from the Plasma Membrane to Modified Lysosomes. J. Virol. 84, 7543–7557. doi:10.1128/JVI.00477-10

Stobart, C.C., Lee, A.S., Lu, X., Denison, M.R., 2012. Temperature-Sensitive Mutants and Revertants in the Coronavirus Nonstructural Protein 5 Protease (3CLpro) Define Residues Involved in Long-Distance Communication and Regulation of Protease Activity. J. Virol. 86, 4801–4810. doi:10.1128/JVI.06754-11

Stobart, C.C., Sexton, N.R., Munjal, H., Lu, X., Molland, K.L., Tomar, S., Mesecar, A.D., Denison, M.R., 2013. Chimeric Exchange of Coronavirus nsp5 Proteases (3CLpro) Identifies Common and Divergent Regulatory Determinants of Protease Activity. J. Virol. 87, 12611–12618. doi:10.1128/JVI.02050-13

Sturman, L.S., Eastwood, C., Frana, M.F., Duchala, C., Baker, F., Ricard, C.S., Sawicki, S.G., Holmes, K.V., 1987. Temperature-sensitive mutants of MHV-A59. Adv. Exp. Med. Biol. 218, 159–168.

Sturman, L.S., Ricard, C.S., Holmes, K.V., 1990. Conformational change of the coronavirus peplomer glycoprotein at pH 8.0 and 37 degrees C correlates with virus aggregation and virus-induced cell fusion. J. Virol. 64, 3042–3050.

Tanaka, T., Kamitani, W., DeDiego, M.L., Enjuanes, L., Matsuura, Y., 2012. Severe Acute Respiratory Syndrome Coronavirus nsp1 Facilitates Efficient Propagation in Cells through a Specific Translational Shutoff of Host mRNA. J. Virol. 86, 11128–11137. doi:10.1128/JVI.01700-12

Targett-Adams, P., Graham, E.J.S., Middleton, J., Palmer, A., Shaw, S.M., Lavender, H., Brain, P., Tran, T.D., Jones, L.H., Wakenhut, F., Stammen, B., Pryde, D., Pickford, C., Westby, M., 2011. Small Molecules Targeting Hepatitis C Virus-Encoded NS5A Cause Subcellular Redistribution of Their Target: Insights into Compound Modes of Action. J. Virol. 85, 6353–6368. doi:10.1128/JVI.00215-11

Ulasli, M., Verheije, M.H., de Haan, C.A.M., Reggiori, F., 2010. Qualitative and quantitative ultrastructural analysis of the membrane rearrangements induced by coronavirus. Cellular Microbiology 12, 844–861. doi:10.1111/j.1462-

5822.2010.01437.x

Vagin, O., Turdikulova, S., Sachs, G., 2005. Recombinant Addition of N-Glycosylation Sites to the Basolateral Na,K-ATPase beta1 Subunit Results in Its Clustering in Caveolae and Apical Sorting in HGT-1 Cells. Journal of Biological Chemistry 280, 43159–43167. doi:10.1074/jbc.M508262200

van der Meer, Y., Snijder, E.J., Dobbe, J.C., Schleich, S., Denison, M.R., Spaan, W.J., Locker, J.K., 1999. Localization of mouse hepatitis virus nonstructural proteins and RNA synthesis indicates a role for late endosomes in viral replication. J. Virol. 73, 7641–7657.

Vennema, H., Poland, A., Foley, J., Pedersen, N.C., 1998. Feline infectious peritonitis viruses arise by mutation from endemic feline enteric coronaviruses. Virology 243, 150–157. doi:10.1006/viro.1998.9045

Verheije, M.H., Raaben, M., Mari, M., Lintelo, te, E.G., Reggiori, F., van Kuppeveld, F.J.M., Rottier, P.J.M., de Haan, C.A.M., 2008. Mouse Hepatitis Coronavirus RNA Replication Depends on GBF1-Mediated ARF1 Activation. PLoS Pathog 4, e1000088. doi:10.1371/journal.ppat.1000088.s002

Wathelet, M.G., Orr, M., Frieman, M.B., Baric, R.S., 2007. Severe Acute Respiratory Syndrome Coronavirus Evades Antiviral Signaling: Role of nsp1 and Rational Design of an Attenuated Strain. J. Virol. 81, 11620–11633. doi:10.1128/JVI.00702-07

Weismiller, D.G., Sturman, L.S., Buchmeier, M.J., Fleming, J.O., Holmes, K.V., 1990. Monoclonal antibodies to the peplomer glycoprotein of coronavirus mouse hepatitis virus identify two subunits and detect a conformational change in the subunit released under mild alkaline conditions. J. Virol. 64, 3051–3055.

Weiss, S.R., Leibowitz, J.L., 2011. Coronavirus Pathogenesis, 1st ed, Advances in Virus Research. Elsevier Inc. doi:10.1016/B978-0-12-385885-6.00009-2

Welsch, S., Miller, S., Romero-Brey, I., Merz, A., Bleck, C.K.E., Walther, P., Fuller, S.D., Antony, C., Krijnse-Locker, J., Bartenschlager, R., 2009. Composition and Three-Dimensional Architecture of the Dengue Virus Replication and Assembly Sites. Cell Host and Microbe 5, 365–375. doi:10.1016/j.chom.2009.03.007

Westaway, E.G., Mackenzie, J.M., Kenney, M.T., Jones, M.K., Khromykh, A.A., 1997. Ultrastructure of Kunjin virus-infected cells: colocalization of NS1 and NS3 with double-stranded RNA, and of NS2B with NS3, in virus-induced membrane structures. J. Virol. 71, 6650–6661.

WHO, 2014a. Global Alert and Response (GAR)Middle East respiratory syndrome coronavirus (MERS-CoV) – Saudi Arabia [WWW Document]. WHO. URL http://www.who.int (accessed 1.5.15a).

WHO, 2014b. Global Alert and Response (GAR): Middle East respiratory syndrome coronavirus (MERS-CoV) – Austria - as of October 2014 [WWW Document]. WHO. URL http://www.who.int (accessed 10.1.14b).

Xu, X., Lou, Z., Ma, Y., Chen, X., Yang, Z., Tong, X., Zhao, Q., Xu, Y., Deng, H., Bartlam, M., Rao, Z., 2009. Crystal Structure of the C-Terminal Cytoplasmic Domain of Non-Structural Protein 4 from Mouse Hepatitis Virus A59. PLoS ONE 4, e6217. doi:10.1371/journal.pone.0006217.t001

Yang, Z.Y., Huang, Y., Ganesh, L., Leung, K., Kong, W.P., Schwartz, O., Subbarao, K., Nabel, G.J., 2004. pH-Dependent Entry of Severe Acute Respiratory Syndrome Coronavirus Is Mediated by the Spike Glycoprotein and Enhanced by Dendritic Cell Transfer through DC-SIGN. J. Virol. 78, 5642–5650. doi:10.1128/JVI.78.11.5642-5650.2004

Yount, B., Denison, M.R., Weiss, S.R., Baric, R.S., 2002. Systematic Assembly of a Full-Length Infectious cDNA of Mouse Hepatitis Virus Strain A59. J. Virol. 76, 11065–11078. doi:10.1128/JVI.76.21.11065-11078.2002

Zaki, A.M., van Boheemen, S., Bestebroer, T.M., Osterhaus, A.D.M.E., Fouchier, R.A.M., 2012. Isolation of a Novel Coronavirus from a Man with Pneumonia in Saudi Arabia. N Engl J Med 367, 1814–1820. doi:10.1056/NEJMoa1211721

Zhao, Z., Thackray, L.B., Miller, B.C., Lynn, T.M., Becker, M.M., Ward, E., Mizushima, N.N., Denison, M.R., Virgin, H.W., 2007. Coronavirus replication does not require the autophagy gene ATG5. autophagy 3, 581–585.

Zheng, D., Chen, G., Guo, B., Cheng, G., Tang, H., 2008. PLP2, a potent deubiquitinase from murine hepatitis virus, strongly inhibits cellular type I interferon production. Cell Res 18, 1105–1113. doi:10.1038/cr.2008.294

Züst, R., Cervantes-Barragán, L., Kuri, T., Blakqori, G., Weber, F., Ludewig, B., Thiel, V., 2007. Coronavirus Non-Structural Protein 1 Is a Major Pathogenicity Factor: Implications for the Rational Design of Coronavirus Vaccines. PLoS Pathog 3, e109.